The University Of Sheffield.

Forever Seeking Closure:

The Roles of Phosphoinositide Metabolism during Phagocytic and Macropinocytic Cup Closure

By:
Christopher James Munn

A thesis submitted in partial fulfilment of the requirements for the degree of
Doctor of Philosophy

The University of Sheffield
Faculty of Science
Department of Biomedical Science

Submission Date
03/10/22

Acknowledgements

I would firstly like to start off by thanking my supervisor, Dr. Jason King who has given me the best support and guidance throughout the stages of this PhD project. Jason has greatly enhanced my capabilities of performing laboratory-based techniques, performing presentations to a high standard, proofreading, scientific communication, and for the support and critiquing of each chapter of my thesis. I would also like to emphasise his unfailing positivity, crucial support and understanding during periods of mental health difficulties. Jason has not only helped me improve my scientific skills but has helped me to achieve a much better work life balance and to unearth inner happiness.

Many thanks to all the members of the King lab (Dr. Catherine Buckley, Dr. Georgina Starling, Dr. Ben Phillips, James Vines, Ana Paula Guevara Cerdan, and the more recent recruits Dr. Dan Stark, Dr. Joe Tyler, Dr. Zhou Zhu, and Yousef Alhammad). Everyone in the laboratory has made me feel more than welcome and at home. I would particularly like to thank Dr. Georgina Starling for her guidance and patience in teaching me how to perform certain techniques and for generic scientific advice. I also would like to thank Dr. Ben Phillips for his support in critiquing my thesis chapters and taking the time to help and support me during my mental health difficulties throughout this PhD. I would also like to acknowledge that Dr. Ben Phillips was almost solely responsible for forever igniting my love for Pokemon Go and for fighting in endless gym battles in Weston Park! I would also love to thank James Vines for being brothers in arms at the bench and for his humour, which always helped me to smile and cheered me up after a tough day! I also want to highlight how much he has helped me to grasp the elements of coding (at a basic level), for his support, and for critiquing presentations, and how to tackle tasks such as lab ordering, other communal jobs, and problem solving various lab-based issues. I also would like to thank my advisors Dr. Kai Erdmann and Dr. Humphreys for their guidance and support during the stages of this project with their invaluable suggestions on experiments to undertake, as well as for giving me insight into how to think more outside the box and to understand how the science I was undertaking has an impact on the outside world.

I would love to offer my many thanks also to Dr. Emily Goodall for her constant support throughout this project. She has given me so much help in dealing with some difficulties encountered during the early stages of this PhD and gave me constant reassurance and the mental strength on dealing with difficult decisions. I also would love to acknowledge her understanding and eternal support towards me and my mental health difficulties. She has helped me to grow as a person and to deal with adversity as and when it presents itself. She will be sorely missed by all

DiMeN members across all institutions when she leaves later this month. Thank you on behalf of everyone for everything that you have done for us all! Thank you also to the DiMeN MRC DTP for funding this project and for all the everlasting support that everyone in the community has given me!

I would also like to offer my thanks to Dr. Darren Robinson, Dr. Nick van Hateren, and everyone also in the Wolfson Light Microscope Facility for their guidance and patience on helping me get to grips with the confocal microscopes! I have to emphasise that without their support I would not have been able to generate the high resolution confocal time-lapses that I did for this project without their support!

I would love to acknowledge all of my friends in BMS and in particular Dr. Mohamed ElGhazaly, Dr. Dan Williams, Dr. Neveen Mansour, Dr. Holly Stainton, Dr. Xiaoming Fang, Dr. Andrew Wood, Dr. Lily Tseng, Dr. Amber Shunshion, Dr. Jessica Willmott, Dr. Jack Paveley, Dr. Dan Stark, Ola Shehata, Dr. Laura Maple, Dr. Salma Srour, Nadia Baseer, Dr. Daniel McDowall, Dr. Stella Christou, Dr. Sarah Stevenson, Dr. Ben Stevenson, Dr. Patrick Shire, Dr. Jaime Canedo, Rachel Ashworth, Sam Lewin, and Pollyanna Rouse for being amazing, supportive friends, and work colleagues and for making my time at Sheffield a lovely experience! I also want to thank everyone at weekly football, most notably Keivan Razban for organising weekly games and for being a fantastic inspirational manager during the league games! I also want to additionally mention Dr. Laurence De Lussy Kubisa, Dr. Robert Smith, Sam Ford, Dr. Anna Underhill, Dr. Katie Greenin-Whitehead, Andy Pearson, Dr. Dylan Stavish, Terry Hawkins, Georgia Tagg, and Max Fontana for being fun to meet and get to know at football!

I also want to offer my thanks to all of the Sheffield DiMeN crew for all their support in relation to my mental health, being amazing friends, and the many drunken gatherings and karaoke events! Thank you Dr. Jacob Rudman, Dr. Olivier Tardy, Dr. Dan Bennison, Dr. Blanca Tardajos Ayllon, Dr. Elliot Brooks, Dr. Emily Graves, Lara Oberski, Dr. Tom Sheard, and Topher Donaldson.

I would like to offer my thanks to people of the Ceilidh society, Dr. Koen Semeijn, Meg Zoe, Oliver Hart, Felicity Powell, and Vitalie Costas for the fun events and socials!

Thank you to all members of the Sheffield walking club, with a special thanks to Dr. Andrew Wood and Dr. Antony Choi for all the beautiful walks around the Peak District, and for all the scenery and memories that I will never forget!

I would like to thank the University Health Service for literally saving my life when I was diagnosed with a late-onset variant of type I diabetes. Thank you to my diabetes nurses Carla and Juli for their patience and guidance on how to adjust and manage my condition and for giving me encouragement, particularly during the early stages! Thank you also to the University Counselling

Service for their support and patience when I was going through some mental health difficulties. I would also like to offer a special thanks to Nadine McGoldrick my cognitive-behavioural therapist for her support, advice, and implementation of methods to deal with anxiety, recognise negative thoughts, deal with difficult situations, seek validation from within and not from others, and show self-love, and self-happiness. She has helped me to change my life and mentality, which will have countless positive rippling affects beyond the confines of my PhD.

I would like to offer my thanks to all my friends and the staff at the University of Liverpool who were there for me when times were tough and we were good friends to me. Many thanks to Professor Barry Campbell, Dr. Cristiana Bercea, Dr. Jenn Dodd, Dr. Amy Ponsford, Professor Graham Kemp, Professor John Quinn, and Professor Julian Hiscox for their support and for facilitating my move to Sheffield!

I would love to give thanks to my mum, Dolores Munn, and Dad, John Gerrard Munn for their kindness, love, support, and encouragement throughout the difficult periods and for the praise and positivity throughout the good periods. They have contributed so much to my growth, strength, and resilience, I wouldn't have succeeded in life in general without them!

I would love to thank my brother Alexander Daniel Munn. Although he will never be able to understand what a PhD is nor how tough and challenging it can be he has forever been a source of love and happiness during this period. He has aided in giving me so many positive memories on growing up with him, and has always helped me forget about work, and focus on the importance of family and the love that comes with it! Again I could not have achieved this without him!

I would also love to thank my cousin, Isabella Morales, and my aunt, Cristina Morales, and all of my grandparents. Isabella has always been a source of positivity and has always encouraged me and praised me and gave me huge boosts to keep me going forward despite how tough times get! Despite my grandparents not being with me anymore they have all made such huge positive impacts on my life and have sown the seeds of success within me that have helped me get to this stage of my career.

I would love to thank all my friends from the Wirral who have been amazing and supportive to me over the years and for all the fun and joyous times! Special thanks goes to my close friends Tom Merriman, Jack Morgan, Mike Barrowman, Ellie Hotchkiss, Nikki Bradshaw, and Ellie Foxton! I would also love to thank all my friends at Monday night football (the football that will always be better than the Premier League equivalent). Thanks to Matthew Hoyle and Tony Sinclair for organising these weekly games, which have helped me to de-stress, have a lot of fun, and forget about work! Special thanks to my brothers in arms on the pitch: Tom Merriman, Jack Morgan, Matt Teale, Ethan Boyd, Phill Beattie, Tom Mountford, Martin Taylor, Rod Pugh, Tom Roberts, Alex Tingle,

Mark Joynson, Tim Bowker-Hughes, Paul Corke, John Ainsworth, Conor Sloan, Adam Sadler, Mihal Abraham, Ben Eyre-Jones, Fin, and Harry Hayward.

I would love to also acknowledge the West Kirby Originals Group: Ellie Hotchkiss, Nikki Bradshaw, Sarah Egan, Jon Egan, Luke Holland, Becci Edwards, Alisha Crummy, Jessica Lacy, Dr. Sinead Rowe, and Jenna Minehan for our socials and gatherings and for all the support and many happy memories!

Thanks to Dr. Laura Swan, and Dr. Massimiliano Stagi for their support.

Last and certainly not least thank you so much to my amazing and loving girlfriend Nixxi Ivony Lucero! Thank you so much for all your heartfelt love and support during the difficult period of the thesis write up! You have given me so much love and positivity that was invaluable to aiding me in getting through the tough times! Thank you for being such an amazing and wonderful person in every possible way and for being a true diamond with a heart of gold!

Abstract

Macro-endocytosis is the bulk uptake of extracellular material and encompasses macropinocytosis and phagocytosis. Macropinocytosis is the non-specific bulk uptake of extracellular fluid, and phagocytosis is the receptor-mediated uptake of solid particles. Both are complex and are regulated by the phosphoinositide signalling lipids (PIPs). However, how PIPs regulate the final stages of engulfment – cup closure – is poorly understood.

Cup closure requires controlled regulation of PIPs and Filamentous-actin (F-actin). $PI(4,5)P_2$, a known F-actin regulator is hydrolysed by mammalian inositol 5-phosphatase Oculocerebrorenal syndrome of Lowe (OCRL). In this thesis I use the amoeba and model phagocyte *Dictyostelium discoideum* to investigate how the OCRL homolog, *Dictyostelium discoideum* 5-phosphatase 4 (Dd5p4) regulates engulfment. *Dd5p4*$^-$ mutants displayed specific defects during cup closure with phagosomes unable to move through the actin cortex. Hydrolysis of $PI(4,5)P_2$ at the centre of phagocytic and to a lesser extent at macropinocytic cups was largely orchestrated by Dd5p4. Lattice light-sheet microscopy (LLSM) showed that *Dd5p4*$^-$ macropinosomes can be internalised by squeezing through small cortex openings, but then acquired F-actin 'comets' containing F-actin, the Actin related protein 2/3 complex (Arp2/3 complex), the Wiskott-Aldrich Syndrome protein (WASP), $PI(3,4,5)P_3$, and $PI(3,4)P_2$.

LLSM also illuminated the presence of thin membrane tubules that briefly connected newly-formed macropinosomes to the cell-surface PM. Like clathrin-coated pits (CCPs), these also required WASP to be efficiently resolved, indicating a new general role for WASP-generated actin in driving the final stages of endosomal formation.

List of Abbreviations

- 2xFYVE - 2xFab1 YOTB Vac1 and EEA1
- A.A. - Amino Acid Residues
- *Act5* - *act15* Promoter
- *Act6P* - *act6* Promoter
- *Act8* - *act8* Terminator
- ActA - Actin Assembly-inducing protein
- ADB - Adaptor-Binding Domain
- AdipoR1 - Adiponection Receptor 1
- AGC - Protein Kinases A, G, and C of the Akt Family
- Amp - Ampicillin Resistance Gene
- AmpR Promoter - Ampicillin Resistance Promoter
- AP - Apurinic/Apyrimidinic
- AP-2 - Adaptor Protein-2
- APPL1 - Adaptor Protein Containing Pleckstrin-Homology Domain, PTB Phosphotyrosine-Binding Domain and Leucine Zipper/Bin-Amphiphysin-Rvs Domain 1
- AR - Androgen Receptor
- Arf1 - ADP-ribosylation factor 1
- Arp2/3 complex - Actin related protein 2/3 complex
- ArpC4 - Arp Complex Subunit 4
- ASH - ASPM (Abnormal Spindle-Like Microcephaly-Associated Protein)/SPD2 (Spindle Pole Body 2)/Hydin
- BAR - Bin/Amphiphysin/Rvs
- BBS - Bardet–Biedl Syndrome
- Bcl-10 - B-cell lymphoma/Leukemia-10
- Bp - Base pairs
- BSR - Blasticidin Resistance cassette
- cAMP - cyclic Adenosine Monophosphate
- CAMs - Cellular Adhesion Molecules
- cAR1 - cAMP Receptor 1
- CARD9/11 - Caspase Recruitment Domain 9/11
- CAV-1 - Caveolin-1 (CAV-1)
- CBD - Clathrin-Binding Domain

- CBM - Carma1-Bcl-10-Malt1 signalling complex
- CC - Coiled-Coil domain
- CCPs - Clathrin-Coated Pits
- CCVs - Clathrin-Coated Vesicles
- CD28 - Cluster of Differentiation 28
- Cdc42 - Cell division control protein 42
- Cdo - CAM-related/down-regulated by oncogenes
- CDP-DAG - Cytidine Diphosphate-Diacylglycerol
- CHCs - Clathrin Heavy Chains
- CID - Clathrin Independent Endocytosis
- CIMPR - Cation-Independent Mannose 6-Phosphate Receptor
- CI-MPR - Clathrin and Cation-Independent Mannose 6-Phosphate Receptor
- CLC5 - Chloride Channel protein 5
- CLCs - Clathrin Light Chains
- CME - Caveolae-Mediated Endocytosis
- CME - Clathrin-Mediated Endocytosis
- CMT4H - Charcot-Marie-Tooth disease type 4H
- CMV Promoter - Cytomegalovirus Promoter
- *coaA* - *coactosin* promoter
- Cobl - Cordon-bleu
- CRISPR - Clustered Regularly Interspaced Short Palindromic Repeats
- CrkL - Crk-Like protein
- CV - Contracile Vacuole
- DAG - Diacylglycerol
- Dbs - Dbl's big sister
- DCC - Deleted in Colorectal Cancer
- DCs - Dendritic Cells
- Dd5p1 - *Dictyostelium discoideum* 5-phosphatase 1
- Dd5p2 - *Dictyostelium discoideum* 5-phosphatase 2
- Dd5p3 - *Dictyostelium discoideum* 5-phosphatase 3
- Dd5p4 - *Dicytostelium discoideum* 5-phosphatase 4
- Dd5p4^{D319G}-GFP - Dd5p4 Catalytic Mutant C-terminal-GFP
- Dd5p4-GFP - Full-Length Dd5p4 C-terminal-GFP

- Dd5p4^{W620A}-GFP - Dd5p4 F&H Mutant C-terminal-GFP
- DdGxcU - *Dictyostelium discoideum* GxcU
- DdPI3K1 - *D. discoideum* PI3K1
- DdPI3K2 - *D. discoideum* PI3K2
- DdPI3K3 - *D. discoideum* PI3K3
- DdPI3K4 - *D. discoideum* PI3K4
- DdPI3K5 - *D. discoideum* PI3K5
- DdPI3K6 - *D. discoideum* PI3K6
- DdPK5 - *D. discoideum* Protein Kinase 5
- DdPLC - *Dictyostelium discoideum* Phospholipase C
- DdPLCδ - *Dictyostelium discoideum* Phospholipase C isoform δ
- DdVps34 - *D. discoideum* Vps34
- DH - Dbl Homology domain
- DiGxcU-GFP - *Dictyostelium intermedium* GxcU-GFP
- EEs - Early Endosomes
- EFC - Extended Fes-CIP4 homology
- EGF - Epidermal Growth Factor
- EGFR - Epidermal Growth Factor Receptor
- EpsinR - Epsin-Related
- ER - Endoplasmic Reticulum
- ERBIN - ERB-B2 Interacting protein
- F&H Motif - Phenylalanine (F) & Histidine (H) Motif
- *f1 ori* - f1 phage-derived origin of replication
- FAB - F-actin-Binding domain
- F-actin - Filamentous-actin
- fAR1 - folic Acid Receptor 1
- FARP2 - FERM, ARH/Rho-GEF, and Pleckstrin domain protein 2
- FcγR - Fc gamma Receptor
- FEME - Fast Endophilin-Mediated Endocytosis
- FGD - Faciogenital Dysphasia
- *Fgd4$^{SC-/-}$* - Frabin expression specifically suppressed within SCs of mice
- FITC - Fluorescein Isothiocyanate
- FOVs - Fields Of View

- FOXO - Forkhead box O
- Frabin - FGD1- related F-actin binding protein
- FSC - Forward Scatter
- FSHR - Follicle Stimulating Hormone Receptor
- Fyn - Family Tyrosine Kinase
- GAK - Cyclin G-Associated Kinase
- GAPs - GTPase Activating Proteins
- GBD - GTPase Binding Domain
- GBD/CRIB - GTPase Binding Domain/Cdc42 and Rac Interactive Binding domain
- GDP - Guanosine Diphosphate
- GefB - Guanine nucleotide exchange factor B
- GefF - Guanine nucleotide exchange factor F
- GEFs - Guanine nucleotide Exchange Factors
- GFP-PH-Crac - Green Fluorescent Protein-Pleckstrin Homology-Cytosolic Regulator of Adenylate Cyclase
- GIPC1 - GAIP-Interacting Protein C terminus, member 1
- GPCR - G-Protein-Coupled Receptor
- Grb2 - Growth factor receptor-bound protein 2
- GST - Glutathione S-Transferase
- GTP - Guanosine Triphosphate
- GxcU - Guanine Exchange Factor for Rac U
- Hck - Haematopoietic cell kinase
- HDA1-3 - Histone Deactylases 1-3
- HGFR - Hepatocyte Growth Factor Receptor
- Hsc70 - Heat shock cognate 70 protein
- HSK TK Poly A - Herpes Simplex Virus Thymidine Kinase Poly(A) signal
- HSPC300 - Haematopoietic Stem/Progenitor Cell protein 300
- I 3-P - Inositol 3-Phosphatase
- I 4-P - Inositol 4-Phosphatase
- ICAM-1 - Intercellular Adhesion Molecule-1
- IgG - Immunoglobulin G
- IgG-RBCs - IgG-opsonised anti-Sheep Red Blood Cells
- IL-2 - Interleukin-2

- IL-2R - Interleukin-2 Receptor
- INPP4A - Inositol Polyphosphate 4-phosphatase type I
- INPP4B - Inositol Polyphosphate 4-phosphatase type II
- INPP5A - Inositol Polyphosphate-5-phosphatase A
- INPP5B - Inositol Polyphosphate-5-phosphatase B
- INPP5E - Inositol Polyphosphate-5-phosphatase E
- INPP5F - Inositol Polyphosphate-5-phosphatase F
- INPP5J - Inositol Polyphosphate-5-phosphatase J
- INPP5K - Inositol Polyphosphate-5-phosphatase K
- Ins(1,3,4,5)P_4 - Inositol 1,3,4,5-Tetrakisphosphate
- Ins(1,4,5)P_3 - Inositol 1,4,5-Trisphosphate
- IPIP27A/B - Inositol Polyphosphate phosphatase-Interacting Protein of 27 kDa A/B
- IR - Insulin Receptor
- Itk - IL-2 Inducible T-cell kinase
- J-loop - JMY-specific loop
- JMY - Junction-Mediating and regulatory protein
- JNK - c-Jun N-terminal Kinase
- KanR - Kanamycin Resistance
- Lat-A - Latrunculin-A
- LIR - LC3-Interacting Region
- LLSM - Lattice Light-Sheet Microscopy
- LmpB - Lysosomal membrane Glycoprotein B
- LS - Lowe Syndrome
- MAF - Musculoaponeurotic Fibrosarcoma
- Malt1 - Mucosa-associated lymphoid tissue lymphoma translocation protein 1
- MCCC1 - Methylcrotonyl-CoA Carboxylase subunit 1
- MDCK - Madin-Darby Canine Kidney
- mDia2 - Dia Family in mouse 2
- MDP - Membrane-Deforming Protein
- mhcA-T - *mhcA* Terminator
- MIP - Maximum Intensity Projection
- MPR - Mannose 6-Phosphate Receptor
- MRP300 - 300 kDa Mannose 6-Phosphate Receptor

- MSP - Major Sperm Protein
- MTMs - Myotubularins
- mTOR - mammalian Target Of Rapamycin
- MTRs - Myotubularin-Related Proteins
- MURC - Muscle-Restricted Coiled-coil protein
- MVB - Multi-Vesicular Body
- NA - Numerical Aperture
- Nck - Non-catalytic region of tyrosine kinase
- Neo - Neomycin resistance gene
- NeoR - Neomycin Resistance
- NF1 - Neurofibromin 1
- NHE1/6 - Na^+/H^+ Exchanger protein 1/6
- NLS - Nuclear Localisation Signal
- NMD - Nonsense-Mediated Decay
- NMDA - N-Methyl D-Aspartate
- NPF - Nucleation-Promoting Factor
- NRG1 type III/ERBB2/3 - Neuregulin-1 type III/ERB-B2 receptor tyrosine kinase 2/3
- N-WASP - Neuronal-Wiskott-Aldrich Syndrome Protein
- OCRL - Oculocerebrorenal syndrome of Lowe
- OIBP - OCRL-Interacting Bar domain Protein
- One-way ANOVA - One-way Analysis Of Variance
- Ori - Origin of replication
- $p21^{CIP1}$ - Cyclin-Dependent Kinase Inhibitor 1
- PAK1 - p21-Activated Kinase 1 (PAK1)
- PAM - Protospacer-Adjacent Motif
- PC - Primary Cilium
- PDZ - PSD-95/Discs-large/ZO-1
- PECAM-1 - Platelet Endothelial Cell-Adhesion Molecule-1
- PH - Pleckstrin Homology
- PHETA1/2 - PH domain-containing Endocytic Trafficking Adaptor 1/2
- PH-PLC-δ - Pleckstrin Homology-Phospholipase C isoform δ
- PI - Phosphatidylinositol
- PI(3)P - Phosphatidylinositol 3-Phosphate

- $PI(3,4)P_2$ - Phosphatidylinositol 3,4-Bisphosphate
- $PI(3,4,5)P_3$ - Phosphatidylinositol 3,4,5-Trisphosphate
- $PI(3,5)P_2$ - Phosphatidylinositol 3,5-Bisphosphate
- PI(4)P - Phosphatidylinositol 4-Phosphate
- $PI(4,5)P_2$ - Phosphatidylinositol 4,5-Bisphosphate
- PI(5)P - Phosphatidylinositol 5-Phosphate
- PI3KC2A - Phosphatidylinositol 3-Kinase Class 2α
- PI3KC2B - Phosphatidylinositol 3-Kinase Class 2β
- PI3KC2C - Phosphatidylinositol 3-Kinase Class 2γ
- PI3KCA - Phosphatidylinositol-4,5-Bisphosphate 3-Kinase Catalytic Subunit α
- PI3KCB - Phosphatidylinositol-4,5-Bisphosphate 3-Kinase Catalytic Subunit β
- PI3KCD - Phosphatidylinositol-4,5-Bisphosphate 3-Kinase Catalytic Subunit δ
- PI3KCG - Phosphatidylinositol-4,5-Bisphosphate 3-Kinase Catalytic Subunit γ
- PI3Ks - Phosphoinositide 3-Kinases
- PI4KIIα - Phosphatidylinositol 4-Kinase type IIα
- PID - Phosphotyrosine-Interacting Domain
- PIKfyve - Phosphatidylinositol-3-Phosphate 5-Kinase Type III
- PIO - PH domain Interacting with OCRL
- PIP_2 - $PI(4,5)P_2$
- PIP_3 - $PI(3,4,5)P_3$
- PIP5K - Phosphatidylinositol-4-Phosphate 5-Kinase
- PIP5K1A - Phosphatidylinositol 4-Phosphate 5-Kinase type-1α
- PIP5K1B - Phosphatidylinositol 4-Phosphate 5-Kinase type-1β
- PIP5K1C - Phosphatidylinositol 4-Phosphate 5-Kinase type-1γ
- PIPP - Proline-rich Inositol Polyphosphate 5-Phosphatase
- PIPs - Phosphatidylinositol Phosphates
- PIPs - Plasmanylinositol Phosphates
- PKC - Protein Kinase C
- PLC - Phospholipase C
- PLIP - Phospholipid-Inositol Phosphatase
- PM - Plasma Membrane
- PNS - Peripheral Nervous System
- PRD - Proline-Rich Domain

- PRR - Proline-Rich Region
- PSTPIP1 - Proline-Serine-Threonine Phosphatase-Interacting Protein 1
- PTB - Phosphotyrosine-Binding domain
- PTC - Premature Termination Codon
- PTEN - Phosphatase and Tensin homolog
- PTKR - Protein Tyrosine Kinase Receptor
- PTRF - Polymerase I and Transcript Release Factor
- PX - Phox homology domain
- R6C - Arginine (R) at position 6 replaced by a Cysteine (C) amino acid residue
- Rab11-FIP2 - Rab11 Family-Interacting Protein 2
- RBD - Ras-Binding Domain
- RCC1 - Regulator of Chromosome Condensation 1
- REMI - Restriction Enzyme-Mediated Integration
- RGBARG - Regulator of Chromatin Condensation 1 (RCC1), Rho-GEF, BAR, and Ras-GAP-containing protein
- Rho-GAP - Rho-GTPase-Activating Protein
- ROCK/LIM - Rho-associated Coiled-coil-containing protein Kinase/Lin11, Isl-1 and Mec-3 kinase
- RPE-1 - Retinal Pigmented Epithelial-1 cells
- RRM - RNA Recognition Motif
- RTKs - Receptor Tyrosine Kinases
- SAC1 - Suppressor of Actin 1-like
- SAC3 - Sac domain-containing phosphatase 3
- SAM - Sterile Alpha Motif
- SCAR - Suppressor of cAMP Receptor
- SCs - Schwann Cells
- SDRP - Serum Deprivation Response Protein
- SEM - Standard Error of the Mean
- Ses1/2 - Sesquipedalian1/2
- sgDNA - single-guide RNA
- SH2 - Src Homology 2
- SH3 - Src Homology 3
- SHIP1 - Src Homology 2-containing-Inositol-Phosphatase-1

- SHIP2 - Src Homology 2-containing-Inositol-Phosphatase-2
- SibA - Similar to integrin beta A
- SKICH - SKIP Carboxyl Homology domain
- SKIP - Skeletal muscle and Kidney-enriched Inositol polyphosphate Phosphatase
- SNARE - Soluble N-ethylmaleimide-sensitive factor Attachment protein Receptor
- SNX18 - Sorting Nexin-18
- SNX3 - Sorting Nexin-3
- SNX5 - Sorting Nexin-5
- SNX9 - Sorting Nexin-9
- SRBC - Sdr-Related gene product that Binds to C-Kinase
- srGAP3 - slit-robo GTPase-Activating Protein 3
- SSC - Side Scatter
- Stx17 - Syntaxin 17
- STxB - Shiga Toxin B-subunit
- SUM - Simple Up-regulation Media
- SV40 - Simian Vacuolating virus 40
- SYNJ1/2 - Synaptojanins 1/2
- TAPP1-PH-GFP - Tandem PH-domain-containing Protein 1-Pleckstrin Homology-Green Fluorescent Protein
- TCR - T-Cell antigen Receptor
- Tec - Tyrosine kinase expressed in hepatocellular carcinoma
- TfR - Transferrin Receptor
- TGN - *Trans*-Golgi Network
- TGN46 - *Trans*-Golgi Network integral membrane protein 46
- TLR9 - Toll-Like Receptor 9
- TOCA-1 - Transducer Of Cdc42-dependent Actin assembly-1
- TPIP - TPTE and PTEN homologous Inositol lipid Phosphatase
- TPTE2 - Transmembrane Phosphoinositide 3-phosphatase and Tensin homolog 2
- TRITC - Tetramethylrhodamine Isothiocyanate
- TrkA - Tropomyosin receptor kinase A
- tRNA - transfer RNA
- Trp - Tryptophan
- TRPML1 - Transient Receptor Potential channel Mucolipin-1

- UTR - Untranslated Region
- VAP - Vesicle-associated membrane protein-Associated Protein
- VASP - Vasodilator-Stimulated Phosphoprotein
- VCA - Verprolin homology and a Central and an Acidic region
- VEGFR - Vascular Endothelial Growth Factor Receptor
- VPS34 - Vacuolar Protein Sorting 34
- WAHD - WASH Homology Domain
- WASH - Wiskott-Aldrich syndrome protein and SCAR Homologue
- WASP - Wiskott-Aldrich Syndrome Protein
- WAVE1 - Wiskott Aldrich syndrome protein and Verprolin homologue 1
- WAVE2 - Wiskott Aldrich syndrome protein and Verprolin homologue 2
- WAVE3 - Wiskott Aldrich syndrome protein and Verprolin homologue 3
- WCA - WH2 and a Central and an Acidic region
- WH1 - WASP Homology 1 domain
- WH2 - WASP Homology 2 domain
- WHAMM - WASP Homolog associated with Actin, Membranes, and Microtubules
- WHD - WAVE Homology Domain
- WHDL - WAVE Homology Domain-Like
- WHIMP - WAVE Homology In Membrane Protrusions
- WIP - WASP-Interacting Protein
- WJHD - WHAMM and JMY Homology Domain
- YL2 - Yellow Laser 2
- YPD - Yeast extract Peptone Dextrose

Table of Contents

Chapter 1

Introduction

1.1 Endocytosis and the different endocytic pathways within mammals

The term endocytosis is defined as a route by which a cell internalises cell-surface extracellular lipids, proteins, and other macromolecules. These components are contained within small membrane vesicle compartments, which form as a result of plasma membrane (PM) invagination and are subsequently transferred into the cytosol (Ju et al. 2020). Several different pathways of endocytosis take place in mammals, which serve different purposes, either acquiring nutrients, coordinating signal transduction and surface membrane turnover, or stimulating immune system defences, and antigen capture. Endocytosis can be divided into two subcategories, based on the size of the vesicles that are formed; these subcategories are micro-endocytosis and macro-endocytosis. Micro-endocytic pathways include non-canonical endocytic pathways, clathrin-mediated endocytosis (CME), and clathrin independent endocytosis (CID) (Vines and King 2019, Ju et al. 2020). Macro-endocytic pathways include macropinocytosis and phagocytosis (Vines and King 2019, Ju et al. 2020). These are summarised (Fig. 1.1.).

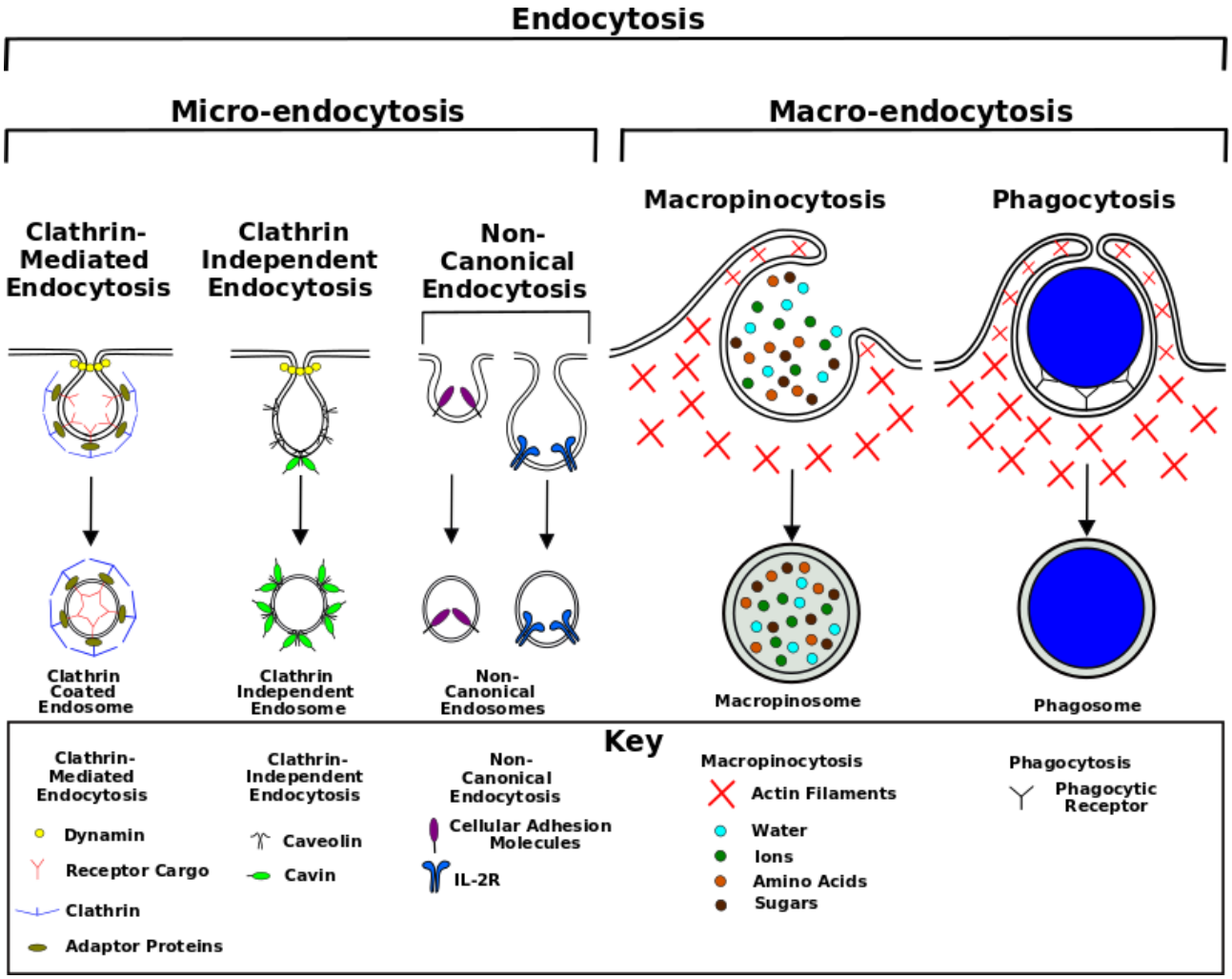

Figure 1.1. An overview of the different types of endocytic pathways in mammals. During CME, clathrin-coated pits (CCPs) form, which contains a clathrin coat (blue) connected to adaptor proteins (olive), like AP-2. The receptor cargo (red) is then internalised via dynamin activity (yellow). In CID, a well-known example being caveolae-mediated endocytosis (CME), involves the formation of a caveolin coat (black) followed by internalisation through dynamin activity, which is independent of clathrin. Non-canonical endocytic pathways that are independent of both clathrin and caveolin coat formation, involve the internalisation of cell surface cellular adhesion molecules (purple), and the interleukin-2 receptors (IL-2R) (blue). All three pathways of endocytosis are forms of micro-endocytosis. Macropinocytosis involves the non-specific bulk uptake of extracellular fluid containing sugars (brown), water (blue), amino acids (orange), and ions (green). This process is mediated via actin filament (red lines) formation and filament disassembly. Phagocytosis involves the engagement of solid particles (blue) like yeast or bacteria, with phagocytic receptors (black), which enters the cytosol following actin filament disassembly. These two pathways of endocytosis are forms of macro-endocytosis. A key indicates the components that are involved in these endocytic processes. Adapted from (Vines and King 2019, Ju et al. 2020).

1.1.1. Clathrin-mediated endocytosis (CME)

The most studied micro-endocytic pathway to date is CME. This process involves the internalisation of cell-surface receptors and their associated ligands, as well as the regulation of transmembrane transporter activities involved in glucose, amino acid, and ion transportation. CME plays crucial roles in the maintenance of intracellular signalling, cell to substrate interactions, and cellular homeostasis (Mettlen et al. 2018). This form of micro-endocytosis is a multi-step process in which assembled clathrin forms a coat, which subsequently matures at the PM. This forms a 100 nm clathrin-coated pit (CCP), within which cargo is concentrated. CCPs then progressively invaginate and through dynamin activity are detached from the PM, forming clathrin-coated vesicles (CCVs) (Fig. 1.1.). Dynamin is itself a large Guanosine Triphosphate (GTP)ase that regulates scission of the vesicle from the PM (Shpetner and Vallee 1989, Sweitzer and Hinshaw 1998, Roux et al. 2006). Following scission, CCVs lose their clathrin coat and the cargo is delivered to the early sorting endosomes (Ju et al. 2020). CME is regulated by over 50 different proteins; the most heavily investigated of these are the clathrin light chains (CLCs), the clathrin heavy chains (CHCs), and the heterotetrameric adaptor protein-2 (AP-2) made up of α, β2, μ2, and σ2 subunits (Motley et al. 2003, Huang et al. 2004, Mitsunari et al. 2005, Poupon et al. 2008, Ferreira et al. 2012, Biancospino et al. 2019).

1.1.2. Caveolae-mediated endocytosis (CME)

Caveolae-mediated endocytosis (CME) is a well-known form of CID that plays a role in the regulation of membrane tension (Sinha et al. 2011). This occurs when cargo interacts with abundant cargo receptors located in the omega-shaped caveolar bud, which is 50-100 nm in diameter (Ju et al. 2020). Interactions between cargo and the associated cargo receptors triggers PM caveolae budding, forming endocytic carriers containing both cavin-1, and the oligomeric integral membrane protein, caveolin-1 (CAV-1) (Fig. 1.1.) (Hill et al. 2008). The cytoplasmic protein family of cavins, include cavin1, which is also called the polymerase I and transcript release factor (PTRF) (Jansa et al. 1998), and cavin2, which is also called the serum deprivation response protein (SDRP) (Gustincich and Schneider 1993). Additional family members include cavin3, which is also called the sdr-related gene product that binds to c-kinase (SRBC) (Izumi et al. 1997), and cavin4, which is also called the muscle-restricted coiled-coil protein (MURC) (Ogata et al. 2008, Tagawa et al. 2008).

1.1.3. Non-canonical endocytic pathways; cellular adhesion molecule (CAM)-mediated endocytosis, and interleukin-2 receptor (IL-2R)-mediated endocytosis

CAMs like the platelet endothelial cell-adhesion molecule-1 (PECAM-1), and intercellular adhesion molecule-1 (ICAM-1), are internalised by endothelial cells without using traditional endocytic machinery. This unconventional pathway does not utilise clathrin or caveolin, and is defined as CAM-mediated endocytosis (Muro et al. 2003). The exact mechanism behind CAM-mediated endocytosis is unclear, however it is inhibited following the expression of the dominant negative mutant of dynamin 2, and the administration of amiloride, and actin depolymerisation inhibitors, Src kinases, protein kinase C (PKC), and Rho kinases (Muro et al. 2003). In addition, the Na^+/H^+ exchanger protein 1 (NHE1) and the Na^+/H^+ exchanger protein 6 (NHE6), may also regulate distinct phases of CAM-mediated endocytosis (Muro et al. 2006). This process demonstrates some similarities with macropinocytosis in these respects, although further work is required to elucidate this process in more mechanistic detail.

IL-2R-mediated endocytosis is another example of non-canonical endocytosis. The IL-2R binds interleukin-2 (IL-2), with IL-2R internalisation forming part of the signalling process within immune cells. This variant of endocytosis was termed, fast endophilin-mediated endocytosis (FEME), as endophilins collaborated with the actin cytoskeleton and dynamin activity during vesicle scission. IL-2R-mediated endocytosis is regulated by p21-activated kinase 1 (PAK1), actin polymerisation, dynamin, Rac, and phosphoinositide 3-kinases (PI3Ks), through studies in which these components were inhibited. In addition, this process was activated through inhibition of cell division control protein 42 (Cdc42) activity (Grassart et al. 2008, Boucrot et al. 2015). Ligand-induced internalisation of a range of receptors is also associated with this pathway including the dopaminergic receptors D3 and D4, and the β1-adrenergic G-protein-coupled receptor (GPCR). Other receptors include the muscarinic acetylcholine receptor 4, and the receptor tyrosine kinases like the epidermal growth factor receptor (EGFR), the vascular endothelial growth factor receptor (VEGFR), and the hepatocyte growth factor receptor (HGFR) (Boucrot et al. 2015).

1.1.4. Macropinocytosis

Macropinocytosis is the non-specific bulk uptake of extracellular fluid, which a cell uses to acquire nutrients from its extracellular environment. The characteristics of this pathway were first described back in 1937 by Warren Lewis, who outlined that both macrophages and cancer cells formed ruffles to encapsulate and internalise extracellular fluid (Lewis 1937). Unlike previously described micro-endocytic pathways and phagocytosis, the pathway of macropinocytosis was not initiated by cargo interacting with specific cell-surface receptors, nor interactions between the cell-

surface and large particles, thereby making this process non-saturable (Kerr and Teasdale 2009). Macropinocytosis is alternatively initiated by actin polymerisation at the cell-surface PM, resulting in the formation of extensions called membrane ruffles (Lim and Gleeson 2011). These extensions can form at the leading edge of migrating cells and fold backwards as cells move forwards, or these extensions can form from the dorsal surface, resulting in the formation of circular macropinocytic cups (Lim et al. 2015). Ruffles encase extracellular fluid into larger, irregularly shaped, membrane-bound vesicles, which are approximately 0.2-5 μm in diameter, called macropinosomes (Lim and Gleeson 2011). Following macropinocytic cup closure, macropinosomes then experience homotypic fusion and fission, and are transported to other cellular organelles of the endolysosomal system (Wang et al. 2014).

Macropinocytosis occurs in numerous cell types within mammals. Regulation occurs by a variety of different cell type specific stimuli and macropinocytic machinery with differences also observed in macropinosome maturation (Racoosin and Swanson 1993). In some cell types, macropinosomes can also be recycled back to the cell-surface (Norbury et al. 1995). An additional complexity of macropinocytosis is that the same machinery can be utilised for different parts of this process. A well-known example includes that of PI3Ks, which promotes cup closure within macrophages (Araki et al. 1996), however in endothelial cells PI3Ks regulates membrane ruffling (Wennstrom et al. 1994).

1.1.5. Phagocytosis

Phagocytosis involves the recognition and internalisation of particles that are larger than 0.5 μm in size into vacuoles that are PM-bound, called phagosomes (Freeman and Grinstein 2014). Microbial pathogens and apoptotic cells are ingested by phagocytes, allowing this process to maintain the clearance of billions of cells, which are turned over each day within the human body. Phagocytosis is therefore not only vital for the destruction of microbial pathogens but is also required for tissue homeostasis (Rosales and Uribe-Querol 2017). Professional phagocytes include neutrophils, macrophages, osteoclasts, monocytes, dendritic cells (DCs), and eosinophils (Rabinovitch 1995). These cells tackle any microbial pathogens and eliminate them through presentation of their antigens on their cell-surfaces to cells of the adaptive immune system and thus participate in apoptotic clearance (Flannagan et al. 2012, Gordon 2016).

This project will aim to focus on understanding the mechanisms of macropinocytosis and phagocytosis, and to elucidate how the different stages are coordinated, especially around closure. Phosphatidylinositol phosphates (PIPs) are components of the macro-endocytic machinery found to regulate both macropinocytosis and phagocytosis (Levin et al. 2015). However, it is unclear how PIPs

regulate the stages around cup closure during these macro-endocytic processes. The core of the studies undertaken in this project will therefore centre on ascertaining how PIPs regulate the stages around cup closure during both of these macro-endocytic processes.

1.2 What are phosphatidylinositol phosphates (PIPs)?

1.2.1. How are PIPs synthesised?

PIPs are known to be important regulators that govern both the processes of macropinocytosis and phagocytosis (Levin et al. 2015). PIPs themselves are a small group of low-abundance, anionic, phospholipid molecules, located on the cytoplasmic leaflet of all cellular membranes, that maintain membrane homeostasis, cell signalling, and compartmentalise membrane identity (Balla 2013). Phosphatidylinositol (PI) is synthesised in the endoplasmic reticulum (ER), specifically a highly mobile ER-derived sub-compartment, which may aid in the transport of PI to other membranes (Kim et al. 2011). PIPs were first identified back in 1953 as a very rare, and infrequent species of phospholipid, which underwent turnover following stimulation of hormonal secretion (Hokin and Hokin 1953).

1.2.2. What is the chemical structure of PIPs?

The chemical structure of PIPs includes the polar *myo*-inositol head and the hydrophobic Cytidine Diphosphate-Diacylglycerol (CDP-DAG) components. Phosphorylation takes place at the hydroxyl group of the D1 position of the *myo*-inositol head, which links the *myo*-inositol head to the DAG backbone via a phosphodiester linkage. This results in five free hydroxyl groups of the *myo*-inositol head being available for phosphorylation, however only three positions D3, D4, and D5 of the *myo*-inositol head can be phosphorylated, giving rise to seven different variants of PIPs. These seven PIPs are phosphatidylinositol 3-phosphate [PI(3)P], phosphatidylinositol 4-phosphate [PI(4)P], phosphatidylinositol 5-phosphate [PI(5)P], phosphatidylinositol 3,4-bisphosphate [$PI(3,4)P_2$], phosphatidylinositol 4,5-bisphosphate [$PI(4,5)P_2$], phosphatidylinositol 3,5-bisphosphate [$PI(3,5)P_2$], and phosphatidylinositol 3,4,5-trisphosphate [$PI(3,4,5)P_3$]. Typically, PIPs normally possess in mammals stearic acid and arachidonic acid at the *Sn*-1 and *Sn*-2 positions of the glycerol backbone respectively (Milne et al. 2008). The chemical structure of PI is illustrated (Fig. 1.2.).

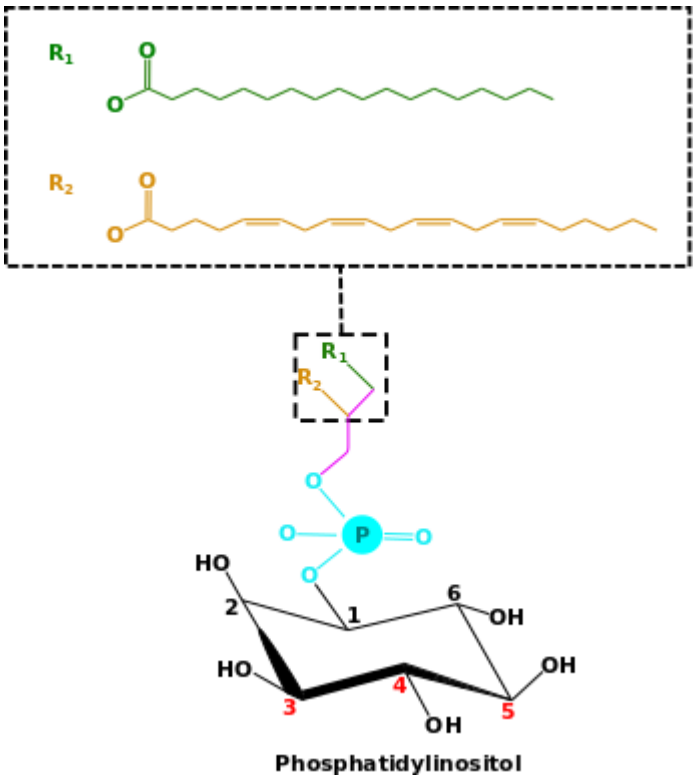

Figure 1.2. The chemical structure of PI. PI is a form of glycerophospholipid with a polar *myo*-inositol head group. Only the 2'hydrolxyl group is perpendicular to the central plane of the *myo*-inositol ring, with the other hydroxyl groups being equatorial in reference to the *myo*-inositol head group. The configuration of the PI that is illustrated is the 1-stearoyl acyl R_1 chain (green), and the 2-arachidonyl acyl R_2 chain (orange), both of which are contained within a black and dashed rectangle. Both acyl chains bind to the glycerol backbone (magenta), which binds to the phosphate (aqua blue), which is linked via a phosphodiester link to the D1 position of the *myo*-inositol ring (black). The D3, D4, and D5 positions of the *myo*-inositol ring that are phosphorylated by numerous kinases, and de-phosphorylated by numerous phosphatases are indicated in red. Adapted from (Posor et al. 2022).

1.2.3. The PIP enzymatic interconversion reactions

Each of the seven PIPs are interconverted by either the addition of a phosphate group by various kinases at the D3, D4, or D5 positions of the *myo*-inositol head group, or the removal of a phosphate at the equivalent positions by various phosphatases. These PIP enzymatic interconversion reactions are summarised (Fig. 1.3.).

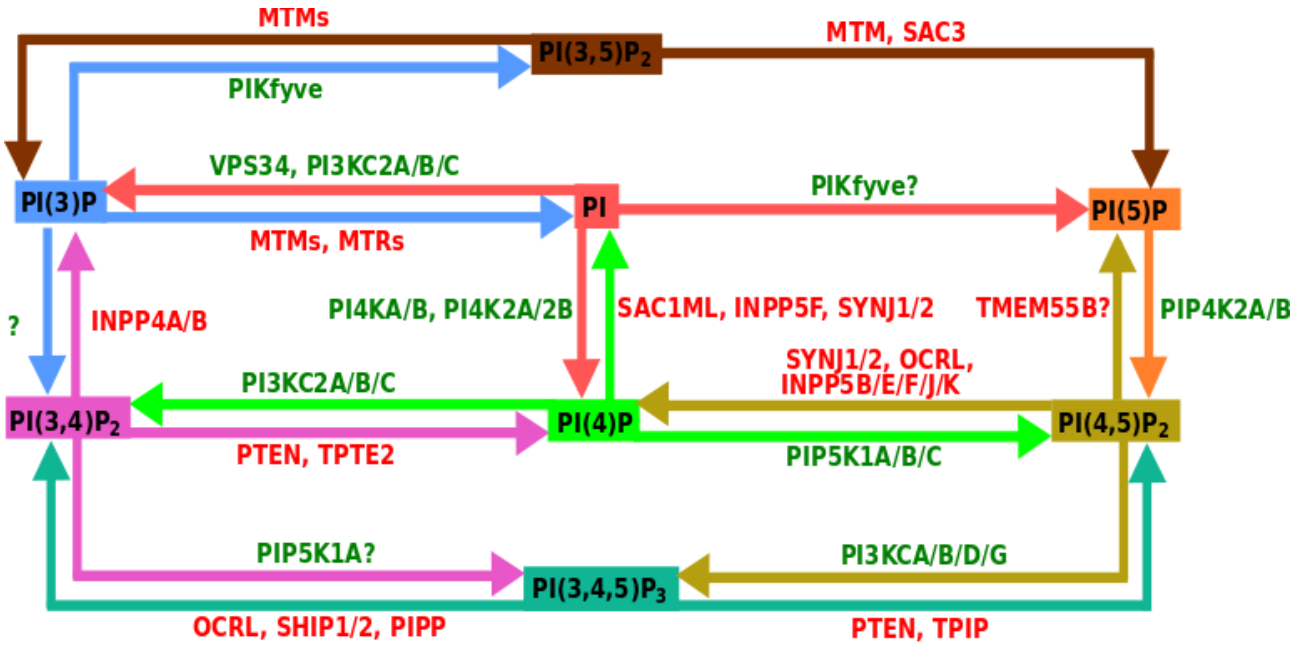

Figure 1.3. The PIP enzymatic interconversion reactions. Arrows indicate PIP interconversions, each arrow is colour-coded in reference to the PIP utilised in the enzymatic reaction. Green text shows kinases and red shows phosphatases. Phosphatidylinositol 3,5-bisphosphate [PI(3,5)P_2], myotubularins (MTMs), sac domain-containing phosphatase 3 (SAC3), phosphatidylinositol 5-phosphate [PI(5)P], phosphatidylinositol-3-phosphate 5-kinase type III (PIKfyve), Myotubularin-related proteins (MTRs), vacuolar protein sorting 34 (VPS34), phosphatidylinositol 3-kinase class 2α (PI3KC2A), phosphatidylinositol 3-kinase class 2β (PI3KC2B), phosphatidylinositol 3-kinase class 2γ (PI3KC2C), phosphatidylinositol 3-phosphate [PI(3)P], phosphatidylinositol 3,4-bisphosphate [PI(3,4)P_2], inositol polyphosphate 4-phosphatase type A (INPP4A), inositol polyphosphate 4-phosphatase type B (INPP4B), phosphatase and tensin homolog (PTEN), transmembrane phosphoinositide 3-phosphatase and tensin homolog 2 (TPTE2), phosphatidylinositol 4-phosphate [PI(4)P], synaptojanins 1/2 (SYNJ1/2), oculocerebrorenal syndrome of Lowe (OCRL), inositol polyphosphate-5-phosphatase B (INPP5B), inositol polyphosphate-5-phosphatase E (INPP5E), inositol polyphosphate-5-phosphatase F (INPP5F), inositol polyphosphate-5-phosphatase J (INPP5J), inositol polyphosphate-5-phosphatase K (INPP5K), phosphatidylinositol 4-phosphate 5-kinase type-1α (PIP5K1A), phosphatidylinositol 4-phosphate 5-kinase type-1β (PIP5K1B), phosphatidylinositol 4-phosphate 5-kinase type-1γ (PIP5K1C), phosphatidylinositol 4,5-bisphosphate [PI(4,5)P_2], phosphatidylinositol-4,5-bisphosphate 3-kinase catalytic subunit α (PI3KCA), phosphatidylinositol-4,5-bisphosphate 3-kinase catalytic subunit β (PI3KCB), phosphatidylinositol-4,5-bisphosphate 3-kinase catalytic subunit δ (PI3KCD), phosphatidylinositol-4,5-bisphosphate 3-kinase catalytic subunit γ (PI3KCG), TPTE and PTEN homologous inositol lipid phosphatase (TPIP), phosphatidylinositol 3,4,5-trisphosphate [PI(3,4,5)P_3], src homology 2-containing-inositol-phosphatase 1 (SHIP1), src homology 2-containing-inositol-phosphatase 2 (SHIP2), proline-rich inositol polyphosphate 5-phosphatase (PIPP). Adapted from (Dickson 2019, Posor et al. 2022).

1.2.4. Subcellular localisation of PIPs during endocytosis

PIPs are distinctly localised to various subcellular compartments within *H. sapiens* during the different stages of endocytosis, with combinations of PIPs localising to the same subcellular compartment in some cases. There however, have been numerous studies in other organisms such as *Entamoeba histolytica* (Nakada-Tsukui et al. 2009), *Saccharomyces cerevisiae* (Homma et al. 1998), and mice (Clarke et al. 2009), which may indicate species-to-species variation in PIP distribution during endocytosis.

PI(4)P and PI(4,5)P_2 are enriched at the PM, whilst PI(3,4,5)P_3 and PI(3,4)P_2 in contrast are formed transiently *in situ* due to extracellular stimuli or intracellular signals (Di Paolo and De Camilli 2006). The Golgi apparatus is enriched with PI(4)P, which regulates trafficking within the Golgi and the subsequent transportation to the endosomal system or the PM (De Matteis et al. 2013). PI(3)P is enriched on the membranes of early endosomes (EEs) and has been established to initiate the recruitment of numerous effector proteins that are crucial for the identity and functionality of the EE (Di Paolo and De Camilli 2006, Marat and Haucke 2016, Schink et al. 2016). Phosphorylation of PI(3)P forms PI(3,5)P_2, which amasses at the multi-vesicular bodies (MVBs) as well as the late endosomes/lysosomes as the EEs progressively mature (Marat and Haucke 2016). PI(5)P has been observed in the endomembranes such as the autophagosomes, the nucleus and the PM (Hammond and Balla 2015, Vicinanza et al. 2015, Varnai et al. 2017) and plays a role in the regulation of the actin cytoskeleton and the stress signalling pathways (Viaud et al. 2014). The localisation of all PIPs with the exception of both PI(3,4)P_2 and PI(3,5)P_2 have been observed within the nucleus (Ye and Ahn 2008). A summary of the generic subcellular distribution of PIPs during endocytosis is illustrated (Fig. 1.4.).

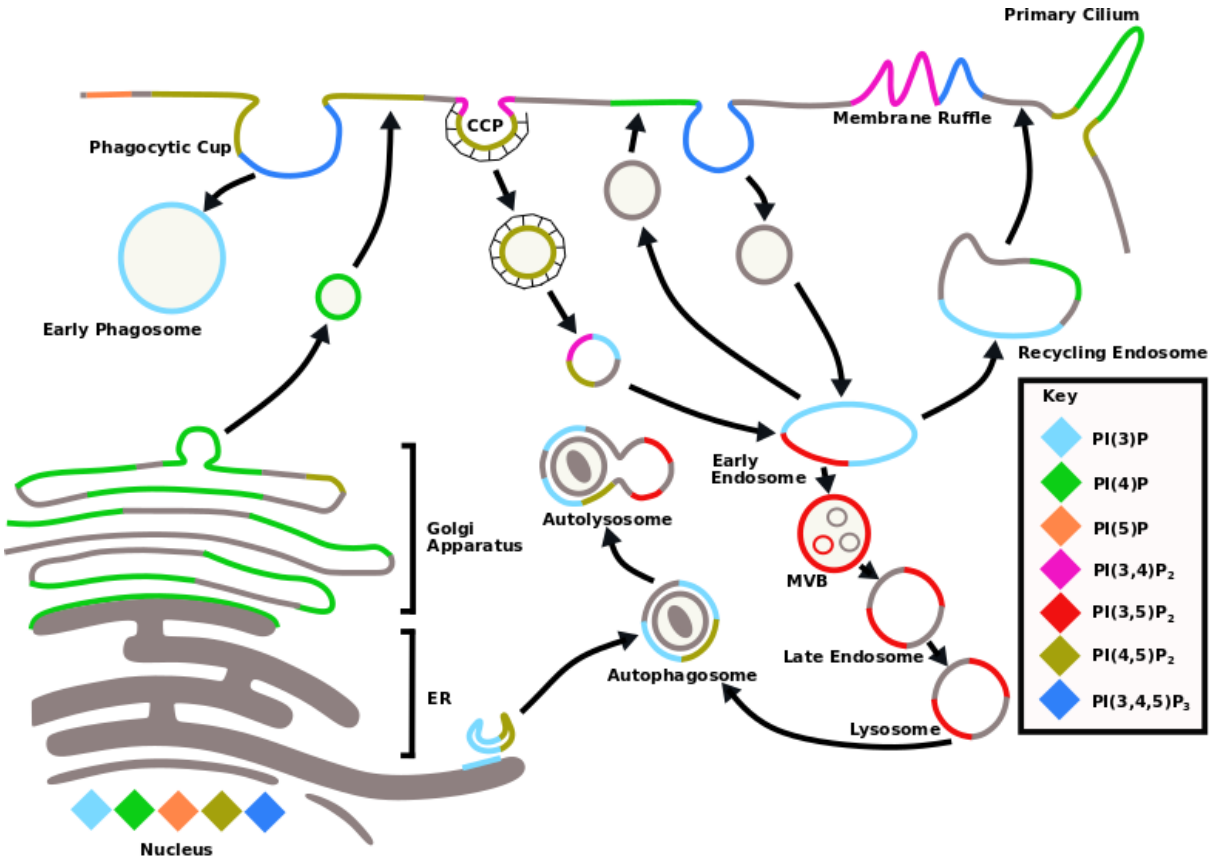

Figure 1.4. The subcellular localisation of PIPs during endocytosis. PIPs are colour-coded as indicated in the key, and are displayed as coloured lines accordingly. Multi-vesicular body (MVB). Adapted from (Nakada-Tsukui et al. 2019).

Numerous kinases and phosphatases tightly control the correct interconversion reactions that occur during each of the stages of endocytosis (Fig. 1.3. and Fig. 1.4.). This project will focus on the roles of phosphatases, which function to de-phosphorylate PIPs, specifically the inositol 5-phosphatases, which as the name suggests, removes a phosphate from the D5 position of the *myo*-inositol ring (Fig. 1.2.).

1.3 The family of inositol 5-phosphatases in mammals

Understanding PIP metabolism in this project will focus on identifying the roles that inositol 5-phosphatases play during endocytosis. A large family of inositol 5-phosphatases have been characterised, consisting of 10 different Mg^{2+}-dependent enzymes in mammals, with four members encoded in yeast. Each mammalian member has a shared 300 amino acid inositol 5-phosphatase domain, which catalyses the hydrolysis of $PI(3,4,5)P_3$, $PI(4,5)P_2$, and/or $PI(3,5)P_2$, by removal of the D5 phosphate from the *myo*-inositol ring (Astle et al. 2007). This group of 5-phosphatases belongs to the apurinic/apyrimidinic (AP) family of endonucleases and contains two unique signature motifs, (F/Y)WXGDXN(F/Y)R and P(A/S)(W/Y)(C/T)DR(I/V)L(W/Y), which are separated by 60-75 amino acids (Majerus et al. 1999). These phosphatases have been shown to regulate a wide variety of processes including phagocytosis, protein trafficking, and synaptic vesicle recycling (Ai et al. 2006, Astle et al.

2007, Horan et al. 2007). The first member to be purified and cloned was the 5-phosphatase-I, also known as inositol polyphosphate-5-phosphatase A (INPP5A) (Speed et al. 1996). INPP5A is the only member capable of recognising only the water-soluble inositol 1,4,5-trisphosphate [Ins(1,4,5)P_3], and inositol 1,3,4,5-tetrakisphosphate [Ins(1,3,4,5)P_4] substrates, and therefore primarily regulates intracellular calcium signalling, making this enzyme a type I inositol 5-phosphatase (Laxminarayan et al. 1993, 1994, Desmedt et al. 1994, Lowe 2005) (Fig. 1.5.). Type II inositol 5-phosphatases are capable of hydrolysing the water-soluble Ins(1,4,5)P_3 and Ins(1,3,4,5)P_4, as well as PI(4,5)P_2, PI(3,4,5)P_3, and sometimes PI(3,5)P_2 (Lowe 2005). These members include oculocerebrorenal syndrome of Lowe (OCRL) (Lowe 2005), the inositol polyphosphate-5-phosphatase B (INPP5B) (Jefferson and Majerus 1996, Whisstock et al. 2000, Tresaugues et al. 2014), synaptojanin 1 (SYNJ1) (McPherson et al. 1996), and synaptojanin 2 (SYNJ2) (Nemoto et al. 1997) (Fig. 1.5.). Additional members include the inositol polyphosphate-5-phosphatase J (INPP5J) (Mochizuki and Takenawa 1999) and the inositol polyphosphate-5-phosphatase K (INPP5K) (Ijuin et al. 2000) (Fig. 1.5.). The type III inositol 5-phopsphatases are only capable of hydrolysing substrates possessing a D3 phosphate (Lowe 2005) and include the src homology two domain containing inositol-5-phosphatase 1 (SHIP1) (Damen et al. 1996, Kavanaugh et al. 1996, Ono et al. 1996, Odai et al. 1997) and the src homology two domain containing inositol-5-phosphatase 2 (SHIP2) (Pesesse et al. 1997) (Fig. 1.5.). The type IV inositol 5-phosphatase only functions to hydrolyse PI(3,4,5)P_3 (Lowe 2005) and solely includes the inositol polyphosphate-5-phosphatase E (INPP5E) (Asano et al. 1999) (Fig. 1.5.). The domain composition of each member of the *H. sapiens* inositol 5-phosphatases is illustrated (Fig. 1.5.).

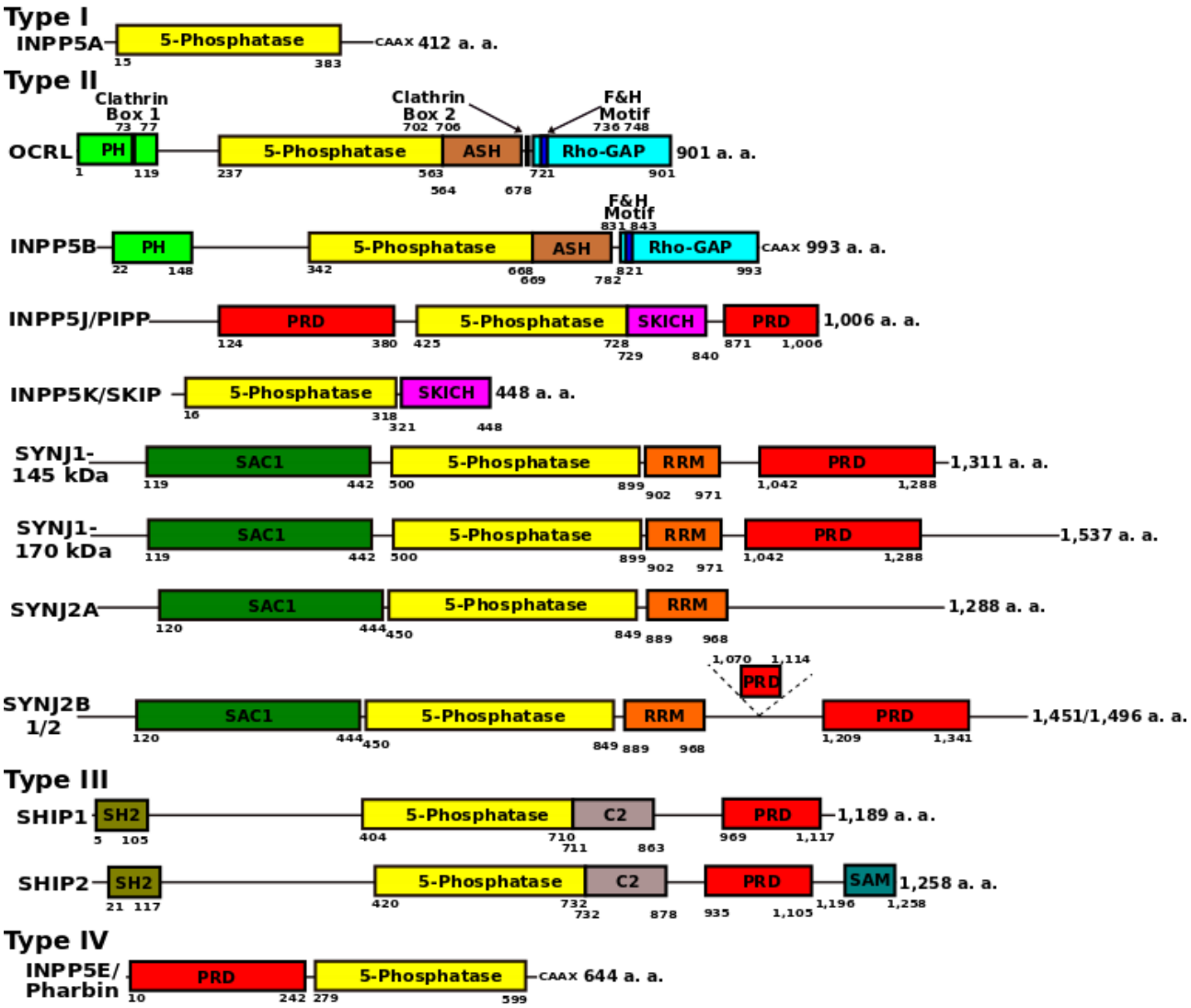

Figure 1.5. The domain composition of the inositol 5-phosphatases within *H. sapiens*. This family of enzymes are grouped into four different types based on their substrate preferences. The type I enzyme is only capable of hydrolysing the water-soluble Ins(1,4,5)P_3 and Ins(1,3,4,5)P_4, whereas type II enzymes can hydrolyse the water-soluble Ins(1,4,5)P_3 and Ins(1,3,4,5)P_4, as well as the membrane-bound PI(4,5)P_2, PI(3,4,5)P_3, and sometimes PI(3,5)P_2. Type III enzymes however, can only hydrolyse substrates that possess a D3 phosphate, whilst the type IV enzyme can only hydrolyse PI(3,4,5)P_3 to PI(3,4)P_2. The type I group consists of the 43 kDa INPP5A enzyme. Type II consists of OCRL, the 75 kDa INPP5B, INPP5J also called PIPP, INPP5K also called SKIP, with the two splice variants of SYNJ1 (145 kDa and 170 kDa), and the three splice variants of SYNJ2 (with 1288, 1451, and 1496 amino acids indicated for each slice variant). Type III contains the SHIP1 (SHIP1α full-length isoform), and SHIP2 phosphatases, with type IV consisting of INPP5E; also called Pharbin. Domain and motif positions are displayed under each protein, along with the protein size displayed to the right of each phosphatase. PRD as shown with black dashed lines comprises the larger SYNJ2B2 splice variant, which is absent in SYNJB1. C=Cysteine, A=Alanine, X=any amino acid residue. Pleckstrin Homology (PH), ASPM (abnormal spindle-like microcephaly-associated protein)/SPD2 (spindle pole body 2)/Hydin (ASH), Rho GTPase-Activating Protein (Rho-GAP), Proline-Rich Domain (PRD), Skeletal muscle and kidney-enriched inositol polyphosphate phosphatase (SKIP), SKIP Carboxyl Homology (SKICH), Suppressor of Actin 1-like (SAC1), RNA Recognition Motif (RRM), Src Homology two (SH2), and Sterile Alpha Motif (SAM). Adapted from (Paesmans et al. 2020).

1.4 OCRL type II inositol 5-phosphatase

1.4.1. Introduction to OCRL

OCRL is a type II inositol 5-phosphatase that will form the core of this project. It was discovered in 1992 that mutations within OCRL was the cause of Lowe syndrome (LS) (Attree et al. 1992). This disease was identified back in 1952 as a rare, X-linked disorder, which affected approximately 1 in 200,000 live births. Patients with LS displayed symptoms including mental retardation, renal tubular acidosis, congenital cataracts, glaucoma, hypercalciuria, and aminoaciduria (Lowe et al. 1952, Mehta et al. 2014). More recently a subset of patients were diagnosed with another X-linked disease called Dent disease, which is separate from LS whilst also bearing mutations within the *OCRL* locus (Hoopes et al. 2005). This observation was at first controversial as Dent disease was initially found to be caused by mutations within the *chloride channel protein 5* (*CLC5*) locus, which encodes an endosomal chloride and proton antiporter (Fisher et al. 1994). Patients with Dent disease that harboured mutations within *OCRL* were classified as having Dent-2 disease, whilst patients harbouring mutations within *CLC5* were classified as having Dent-1 disease (Bokenkamp et al. 2009). Both the X-linked LS and Dent-2 diseases displayed impairment of proximal tubular cells within the kidney due to defects in the endocytic trafficking of megalin, which may cause the low molecular weight proteinuria that is observed in both diseases (Mehta et al. 2014). Dent-2 disease affects the same organs and also displays similar manifestations in comparison to LS, however, the neurological and ocular defects in Dent-2 disease are usually milder in comparison to those observed in patients with LS. In addition, renal tubular acidosis is less frequently found in patients with Dent-2 disease (Bockenhauer et al. 2008, Bokenkamp et al. 2009).

The complete *OCRL* locus itself comprises of 24 coding exons, and is found on chromosome Xq25-26 (De Matteis et al. 2017). The gene as well as the exons that comprise each protein domain is illustrated (Fig. 1.6.).

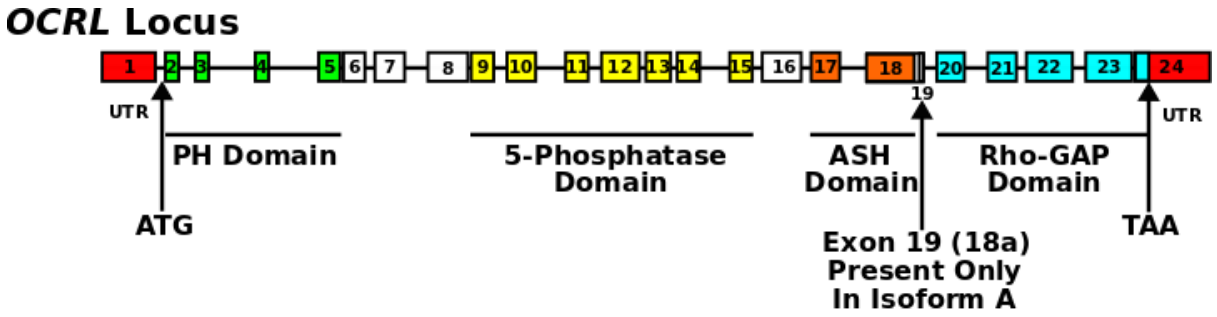

Figure 1.6. The *OCRL* locus within *H. sapiens*. Numbered boxes from 1-24 indicate each exon. Each exon is colour-coded from 5' to 3' as follows: red for the UTR, light green for exons encoding the PH domain, white for exons encoding unstructured regions/loops, yellow for exons encoding the 5-phosphatase domain, orange for exons encoding the ASH domain, and blue for exons encoding the Rho-GAP domain. Labelling below the gene indicates the start (ATG) and stop (TAA) codons, and the coverage across the locus, which corresponds to each protein domain. Exon 19 (18a) is absent in OCRL isoform B but is present in OCRL isoform A. Untranslated Region (UTR). Adapted from (Shrimpton et al. 2009, De Matteis et al. 2017).

There are two isoforms of OCRL expressed in humans: OCRL isoform A and OCRL isoform B (Nussbaum et al. 1997). Isoform B lacks exon 19, also known as exon 18a, which encodes 8 amino acids found in OCRL isoform A (Fig. 1.6.). OCRL Isoform A displays a ubiquitous expression profile, whilst OCRL isoform B is present in all different tissues apart from the brain. OCRL isoform A also establishes interactions with clathrin at a higher affinity in comparison to OCRL isoform B, suggesting that isoform A plays a role in the regulation of intracellular membrane trafficking within the proximal tubule and the endocytosis of low-molecular weight proteins (Choudhury et al. 2009). This would suggest that OCRL isoform A is likely to be involved in the regulation of CME in neurons of the brain (Choudhury et al. 2009). OCRL isoform B may in contrast participate in processes that are not clathrin-mediated or participate in signalling, the regulation of actin dynamics, or play a housekeeping role in order to maintain the correct PIP homeostasis on both endosome and Golgi membranes (Lowe 2005).

Pathogenic mutations arise across *OCRL*, with the majority of disease-causing mutations leading to LS located between exons 8-24, which encode the catalytic 5-phosphatase, ASH, and Rho-GAP domains (Fig. 1.6.). Most of the disease-causing mutations that result in Dent-2 disease reside between exons 1-7, which encodes the PH domain (Fig. 1.6.) (Hichri et al. 2011, Staiano et al. 2015, De Matteis et al. 2017, Zaniew et al. 2018). The OCRL protein itself exhibits numerous cellular functions due to the four protein domains that are encoded.

1.4.2. The domain structure of OCRL

OCRL is a multi-domain protein, which is 110 kDa in size and has a similar domain organisation to the INPP5B enzyme (Fig. 1.5.). The N-terminal OCRL PH domain is atypical as it lacks

the basic PIP binding pocket, which prevents binding to PIPs and PIP-containing liposomes (Mao et al. 2009). An isolated loop from the PH domain structure, which bears a clathrin-binding motif, functions to recruit OCRL to CCPs (Choudhury et al. 2009, Mao et al. 2009). This domain is linked to the central 5-phosphatase domain via a flexible linker, which bears the FEDNF motif, which binds the clathrin adaptor AP-2 (Ungewickell et al. 2004).

The central catalytic 5-phosphatase domain has a preference for the de-phosphorylation of $PI(4,5)P_2$, however OCRL also displays significant catalytic activity *in vitro* against $PI(3,4,5)P_3$ and can also de-phosphorylate $PI(3,5)P_2$ to PI(3)P (Zhang et al. 1995, Schmid et al. 2004). This phosphatase can also de-phosphorylate the water soluble $Ins(1,4,5)P_3$, and $Ins(1,3,4,5)P_4$, however this has only been seen *in vitro* (Schmid et al. 2004).

C-terminal to the 5-phoshatase domain is the ASPM (abnormal spindle-like microcephaly-associated protein)/SPD2 (spindle pole body 2)/Hydin (ASH) domain (Ponting 2006). The ASH domain possesses an immunoglobulin-like fold, which is highly similar to the major sperm protein (MSP) and the vesicle-associated membrane protein-associated protein (VAP), with this domain often observed within proteins associated with the centrosomal region of the cell or the cilia (Ponting 2006). The OCRL ASH domain establishes interactions with a variety of Rab proteins including Rab5, which ensures the correct subcellular localisation of OCRL to the EE for example (Hyvola et al. 2006). OCRL interacts with Rab proteins in a very atypical manner in comparison to other effectors, which normally bind via α-helical structures. OCRL however, in addition to a single α-helix, establishes interactions via an immunoglobulin G (IgG)-like beta strand structure within the ASH domain, which may allow OCRL to form interactions with numerous different Rab proteins (Hou et al. 2011).

The final domain is the OCRL C-terminal Rho-GAP domain, which is directly adjacent to, and is stabilised by the ASH domain. These domains function as a single unit called the ASH-Rho-GAP domain of OCRL. The Rho-GAP domain alone however, is catalytically inactive due to the lack of the catalytic arginine (Erdmann et al. 2007, Pirruccello et al. 2011). The OCRL Rho-GAP domain, like the PH domain, also contains a clathrin motif located on the loop of the Rho-GAP domain. Crucially both of these clathrin motifs are absent in the otherwise highly similar INPP5B phosphatase (Fig. 1.5.) (Jefferson and Majerus 1995, Ungewickell et al. 2004, Erdmann et al. 2007). The OCRL ASH-Rho-GAP domain is responsible for establishing the vast majority of the protein-protein interactions, and plays an important role in OCRL membrane recruitment. The Rho-GAP domain binds to Cdc42 and Rac1, which targets OCRL to regions at which actin is assembled (Faucherre et al. 2003, Lichter-Konecki et al. 2006, Erdmann et al. 2007). It is within the Rho-GAP domain that a conserved 11-13 amino acid residue phenylalanine & histidine (F&H) motif is located, which will be a focal point for

this project. This F&H motif can bind to the F&H motifs of other proteins like the early endocytic adaptor, the Adaptor Protein containing Pleckstrin-homology domain, PTB phosphotyrosine-binding domain and Leucine zipper/bin-amphiphysin-rvs domain 1 (APPL1), and the later Sesquipedalian1/2 (Ses1/2) endocytic adaptors, which are alternatively called the Inositol Polyphosphate phosphatase-Interacting Protein of 27 kDa A/B (IPIP27A/B), and also the PH domain-containing Endocytic Trafficking Adaptor 1/2 (PHETA1/2). These F&H motif-based interactions display a crucial functional link between OCRL and endocytic trafficking and signalling (Erdmann et al. 2007, Swan et al. 2010, Noakes et al. 2011, Pirruccello et al. 2011).

1.4.3. The subcellular localisation and functional roles of OCRL in membrane trafficking

Mammalian OCRL is present on various vesicular structures peppered throughout the endosomal system, and the Golgi apparatus, membrane ruffles, and late-stage CCPs (Olivosglander et al. 1995, Dressman et al. 2000, Faucherre et al. 2003, 2005, Ungewickell et al. 2004, Choudhury et al. 2005, Vicinanza et al. 2011, Nandez et al. 2014). This enzyme displays a broad distribution due to the numerous protein-protein interactions that it establishes (Mehta et al. 2014). A key part to understanding how OCRL can influence endocytosis around the stage of closure first requires an understanding as to what roles OCRL participates in within the cell.

1.4.3.1. The functional roles of OCRL in membrane trafficking

Most of the work that has unearthed some of the functional roles of OCRL have pointed towards the regulation of membrane trafficking (Choudhury et al. 2005, Erdmann et al. 2007, Choudhury et al. 2009, Mao et al. 2009, Cui et al. 2010, Noakes et al. 2011, Vicinanza et al. 2011, van Rahden et al. 2012, Luscher et al. 2019). The functional roles of OCRL in membrane trafficking will be discussed in more detail within each subcellular compartment.

1.4.3.2. OCRL and the early endosomes (EEs)

OCRL localises to the early and recycling endosomes (Ungewickell et al. 2004, Choudhury et al. 2005, Erdmann et al. 2007, Noakes et al. 2011). OCRL establishes localisation with the EEs via interactions with Rab5 (Shin et al. 2005). This association is crucial to ensure that low levels of $PI(4,5)P_2$ are constantly maintained for unperturbed endocytic trafficking to occur (Ungewickell et al. 2004, Choudhury et al. 2005, Vicinanza et al. 2011). OCRL only displays enzymatic phosphatase activity when it is present together with its preferred $PI(4,5)P_2$ substrate (Schmid et al. 2004). The lack of functional OCRL prevents $PI(4,5)P_2$ hydrolysis on the EE, resulting in $PI(4,5)P_2$ and Rac-dependent stimulation of actin polymerisation (Vicinanza et al. 2011). This results in the

dysregulation of the trafficking of various receptors (Vicinanza et al. 2011). The different receptors affected include receptors destined for the Golgi like the mannose 6-phosphate receptor (MPR), receptors destined to be degraded like the EGFR, and receptors that move through the EE to the PM for recycling, like megalin (De Matteis et al. 2017). $PI(4,5)P_2$ facilitates endosomal actin accumulation through the activation of the nucleation-promoting factor (NPF), Neuronal-Wiskott-Aldrich Syndrome protein (N-WASP), and the inhibition of cofilin, a protein that cuts actin filaments (Prehoda et al. 2000, Gorbatyuk et al. 2006, Vicinanza et al. 2011).

1.4.3.3. OCRL and the Golgi complex

A collection of investigations have shown that cells lacking OCRL activity or cells expressing OCRL dominant-negative constructs displayed defective trafficking to the *trans*-Golgi network (TGN) from endosomes (Choudhury et al. 2005, Cui et al. 2010, Vicinanza et al. 2011, van Rahden et al. 2012). OCRL is localised to the TGN via Rab1 and Rab6 interactions, but an understanding of how OCRL functions within the TGN remains elusive (Olivosglander et al. 1995, Dressman et al. 2000). OCRL wild-type and OCRL catalytic mutant overexpression within HeLa cells induced clathrin and cation-independent mannose 6-phosphate receptor (CI-MPR) redistribution (Choudhury et al. 2005, van Rahden et al. 2012) from the TGN to EEs causing them to become enlarged. This thereby suggested a defect in trafficking in the retrograde transportation of CI-MPR to the TGN. The overexpression of OCRL may cause endocytic defects as a result of interfering with the ability of OCRL to associate with various trafficking components (Choudhury et al. 2005). A similar observation was made when investigating retrograde trafficking following the application of the Shiga toxin B, which was also decreased due to overexpression of catalytically inactive OCRL (Hyvola et al. 2006). Interestingly, cells which lacked functional OCRL also resulted in CI-MPR (Vicinanza et al. 2011, van Rahden et al. 2012), and the *trans*-Golgi network integral membrane protein 46 (TGN46) (van Rahden et al. 2012) redistribution to enlarged endosomes, suggesting that OCRL orchestrates the cycling of components between the endosomes and the TGN. OCRL may coordinate this stage in collaboration with Rab31, as both proteins co-localised and interacted at the EEs and the TGN, which was crucial for the transportation of MPRs (Rodriguez-Gabin et al. 2010).

1.4.3.4. OCRL and the lysosomes

OCRL is also reported to be on lysosomes, however this only occurs when the lysosomes themselves are overloaded (De Leo et al. 2016). Lysosomes obtain their cargo through either late endosome-lysosome fusion, autophagosome-lysosome fusion, macropinocytosis or phagocytosis (Mizushima et al. 2008, Luzio et al. 2009, Kaushik and Cuervo 2012). In the event of sustained

autophagic flux, the rate at which autophagosomes fuse with lysosomes is elevated and the efficiency of membrane fusion maintained. The delivery of autophagic cargo to the lysosome initiates the lysosome cargo response via activation of the Toll-like receptor 9 (TLR9), which identifies the presence of mitochondrial DNA within autophagosomes (Bao et al. 2016, De Leo et al. 2016). TLR9 activation results in the eventual recruitment of lysosomal enzymes, which generate $PI(4,5)P_2$, and includes phosphatidylinositol 4-phosphate 5 kinase 1α (PIP5K1α), and phosphatidylinositol 4-phosphate 5 kinase 1β (PIP5K1β) (Choi et al. 2015). The generation of $PI(4,5)P_2$ is crucial for the recycling of the components of the fusion machinery, like the autophagosomal Soluble N-ethylmaleimide-sensitive factor Attachment protein Receptor (SNARE) protein, Syntaxin 17 (Stx17) (Itakura et al. 2012). $PI(4,5)P_2$ levels within the lysosomes must be tightly controlled however, which gives functional relevance to TLR9 signalling in the recruitment of OCRL to the autolysosomes (De Leo et al. 2016). In OCRL deficient cells, elevated lysosomal $PI(4,5)P_2$ reduces the efficiency of autophagosome-lysosome fusion via the direct inhibition of the lysosomal calcium channel, Transient Receptor Potential channel Mucolipin-1 (TRPML1), also called Mucolipin-1 (Dong et al. 2010, Zhang et al. 2012). The TRPML1 receptor is activated by $PI(3,5)P_2$, which causes calcium release to allow the efficient fusion of the autophagosome with the lysosome. In cells in which OCRL is deficient, the uncontrolled increase in $PI(4,5)P_2$ levels inhibits TRPML1 and prevents the fusion of autophagosomes with lysosomes (Vergarajauregui et al. 2008, De Leo et al. 2016). Kidney biopsy samples from patients with LS highlight the importance of OCRL in this pathway, as patient cells displayed a very high number of autophagosomes (De Leo et al. 2016). The prevention of autophagic flux may thereby render the proximal tubular cells non-viable (Kimura et al. 2011, De Leo et al. 2016).

1.4.3.5. OCRL and the primary cilium (PC)

The PC functions as a central platform for signalling in the kidney proximal tubular cells (Raghavan and Weisz 2015), and other cell types (Goetz and Anderson 2010, Satir et al. 2010), and recognises a plethora of chemical, mechanical, and environmental stimuli. The trafficking of vesicles dictates the formation and maintenance of PC through the precise targeting of cilium specific proteins and lipids. The PC retrieves cargo from two separate routes: the first via the TGN, which involves the release of vesicles with Rab8 and Rab11 (Knoedler et al. 2010), and the second from endosomes through vesicles with Rab5 (Kaplan et al. 2012). OCRL is a known effector of Rab8, meaning that cells lacking OCRL have a reduction in the trafficking of ciliary signalling molecules and constituents (Coon et al. 2012, Luo et al. 2012, 2014). Another component shown to be important in PC functionality is the Bardet-Biedl Syndrome (BBS) complex, which is comprised of seven

different proteins. This complex functions with Rab8 to modulate ciliary function and transport carriers loaded with receptors and channels. The PC is a dynamic organelle, which undergoes a series of cycles of assembly and disassembly during the cell cycle. OCRL may be involved in the generation of cilia as it localises to where the PC originates, at the basal body. In addition, the lack of OCRL in some cell types like fibroblasts results in the formation of smaller cilia, however in other cell types like the Madin-Darby canine kidney (MDCK) cells instead display an increase in the length of the cilia (Luo et al. 2012, 2013, Rbaibi et al. 2012, Montjean et al. 2015). The explanation behind the phenotypic variability amongst different cell types lacking OCRL remains poorly understood, meaning that further studies need to ascertain the cell type specific influences that the loss of functional OCRL exerts.

1.4.3.6. OCRL and cytokinesis

Defects in cytokinesis have been reported in both *Drosophila melanogaster* and mammalian cell lines lacking functional OCRL (Dambournet et al. 2011, El Kadhi et al. 2011). In *D. melanogaster* lacking the orthologue of OCRL, abortive cleavage furrow formation and ingression was noted, leading to failure of cell division and a progressive increase in the number of bi-nucleated cells (El Kadhi et al. 2011). Within cells that possessed functional OCRL, high levels of $PI(4,5)P_2$ were normally observed at both the cleavage furrow and the midbody. In cells lacking functional OCRL, $PI(4,5)P_2$ was seen to accumulate on enlarged endosomes, causing the endosomal mis-targeting of both actin and the associated cytokinesis machinery. The cytokinesis defects that were seen in *D. melanogaster* cells could therefore be attributed to the dysregulation of both $PI(4,5)P_2$ and actin (El Kadhi et al. 2011). Interestingly, within mammals the cytokinesis defects are much more subtle in cells lacking functional OCRL, with the dysregulation of actin also observed within these cells (Dambournet et al. 2011). The enzymatic activity of OCRL is recruited to the midbody via interactions with Rab35, which provides a direct method of regulating $PI(4,5)P_2$ levels and therefore actin, which is required for the more efficient completion of abscission and cytokinesis (Dambournet et al. 2011). In mammalian cells the depletion of $PI(4,5)P_2$ at the midbody was reduced in cells from patients with LS, however the completion rate of abscission was unaltered. The time taken to achieve complete abscission in cells from patients with LS was however, increased by approximately 2-fold and consequently stalled cytokinesis at abscission in these cells (Dambournet et al. 2011). Interestingly, the abscission kinetic defects could be rescued by the treatment of LS patient cells with the F-actin depolymerising agent, Latrunculin-A (Lat-A), at a minimal dose that did not perturb the activity of wild-type cells. This may therefore provide a therapeutic avenue to treat the cytokinesis defects that are observed in patients with LS (Dambournet et al. 2011).

1.4.3.7. OCRL and cell adhesion and migration

OCRL localises to lamellipodia, which indicates that this enzyme might also play a role in the regulation of migration; indeed fibroblasts lacking functional OCRL displayed migration defects that were not rescued by INPP5B (Coon et al. 2009). Cell adhesion was also established to be adversely affected in cells lacking functional OCRL (Coon et al. 2009). Both the activities of cofilin, and Rac1, which are crucial for the regulation of actin dynamics within lamellipodia, were found to be considerably decreased within OCRL deficient cells (van Rahden et al. 2012). OCRL targeting to the PM was also partly facilitated by Rac1, which functions to coordinate actin cytoskeleton dynamics, the progression of the cell cycle, and transcriptional regulation (Gu et al. 2003, Wang et al. 2003). Stimulation of cells with the epidermal growth factor (EGF) mediates the association of Rac1 with OCRL, which is then translocated to PM ruffles (Faucherre et al. 2003, 2005). Loss of functional OCRL resulted in PI(4,5)P_2 accumulation at ruffles and increased the induction of actin polymerisation and the formation of actin comets (Allen 2003, Nandez et al. 2014), causing a reduction in cell migration and adhesion (Coon et al. 2009).

1.4.3.8. OCRL and phagocytosis

OCRL plays a crucial role in the regulation of phagocytic engulfment. This was first seen in the social amoeba, *Dicytostelium discoideum*, when the loss of the OCRL homolog, *Dicytostelium discoideum* 5-phosphatase 4 (Dd5p4), resulted in the phagocytic engulfment failure of yeast (Loovers et al. 2007). Subsequent studies indicated that mammalian OCRL also played a role in the regulation of phagocytosis as shown within RAW264.7 macrophages eating latex beads (Bohdanowicz et al. 2012) and RAW264.7 murine macrophages engulfing IgG-opsonised anti-Sheep Red Blood Cells (IgG-RBCs) (Marion et al. 2012). OCRL was established to be recruited to phagosomes and functioned to catalyse the hydrolysis of PI(4,5)P_2 to PI(4)P at the stage of phagocytic cup closure and promote actin remodelling to facilitate phagosome closure, whilst simultaneously halting the generation of PI(3,4,5)P_3, and thereby reducing Akt kinase activity. OCRL is itself transported to the phagosomes via vesicles that originated from either the TGN or the endosomes, and is retained at the phagosomal membrane through interactions with the APPL1 endocytic adaptor and Rab5 (Bohdanowicz et al. 2012, Marion et al. 2012).

OCRL has also been proposed to play an important role during the phagocytosis of various pathogenic bacterial species like *Listeria monocytogenes* and *Yersinia pseudotuberculosis*, which causes Listeriosis and Far East scarlet-like fever respectively (Kuehbacher et al. 2012, Sarantis et al. 2012). In both studies, OCRL was established to be exploited and recruited to the bacterial phagosome, which coincided with the depletion of PI(4,5)P_2 and the actin disassembly that was

needed for closure. This may suggest that various other bacterial pathogens may also exploit OCRL in order to gain entry into host cells. Other bacterial infections such as *Chlamydia* utilise OCRL at the post-closure stage during infection (Moorhead et al. 2010). OCRL localises to the surface of bacterial non-acidified vacuole inclusions formed by *Chlamydia*, which together with the host proteins ADP-ribosylation factor 1 (Arf1) and Phosphatidylinositol 4-Kinase type IIα (PI4KIIα) collectively regulate PI(4)P metabolism at the inclusion to facilitate infection (Moorhead et al. 2010).

1.4.3.9. A summary of the subcellular localisation of OCRL

Building on from the cellular functions of OCRL that have been described a visual summary of the subcellular distribution of OCRL is illustrated (Fig. 1.7.).

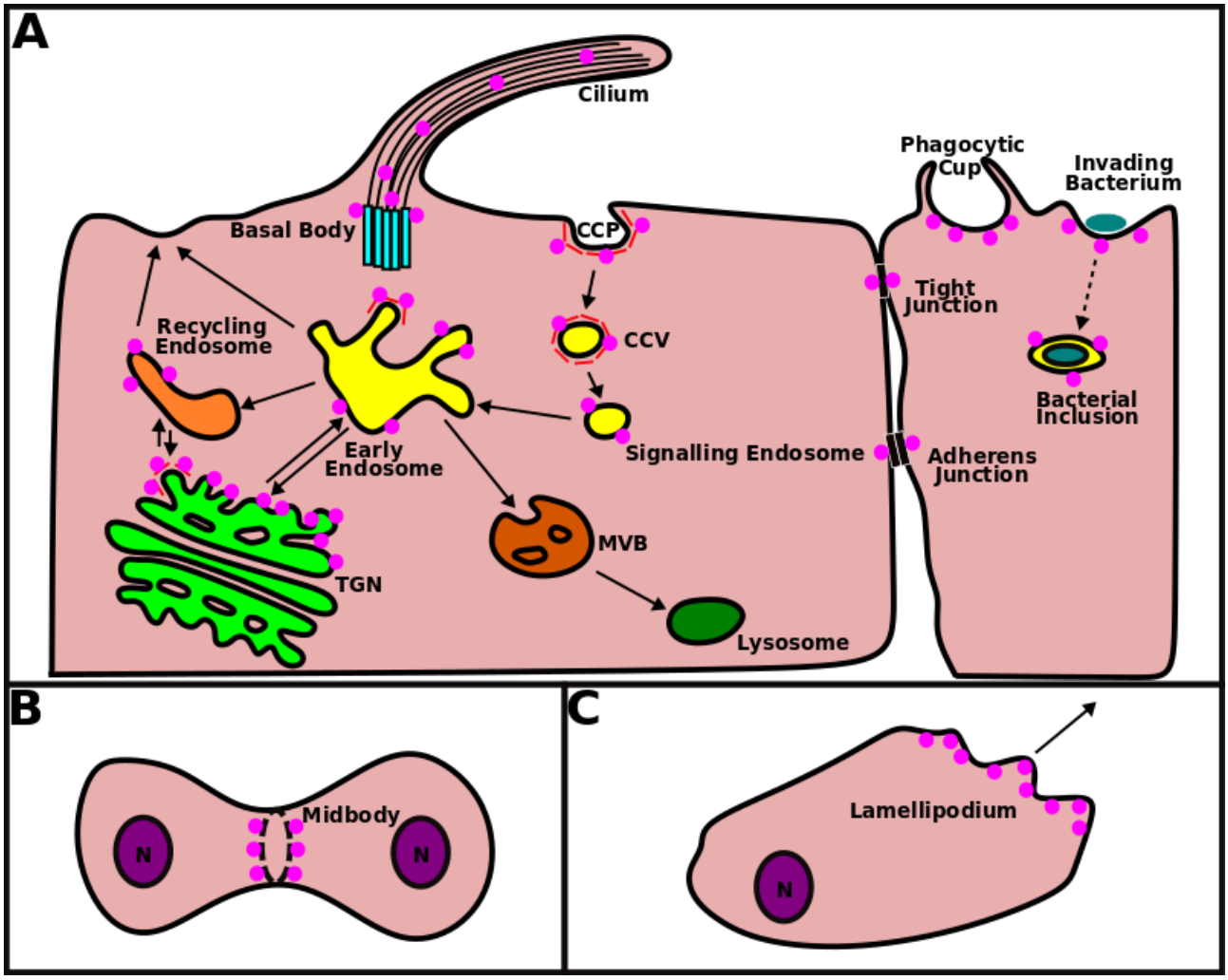

Figure 1.7. The subcellular localisation of OCRL. (A) OCRL (magenta ovals) localises to various subcellular compartments during endocytosis. OCRL is present in abundance at the TGN, CCPs, CCVs, the EE, signalling endosomes, and recycling endosomes. OCRL is associated with the PC and could be associated with the cilia themselves. In epithelia that are in the process of maturing, OCRL transiently localises with adherens and tight junctions. OCRL recruitment to phagocytic cups occurs progressively towards cup closure and is crucial for the successful closure of the phagocytic cup, and endocytic signalling events, which occur following cup closure. OCRL recruitment to phagosomes that form due to invading pathogenic bacteria including *Listeria* or *Yersinia* also localises to various intracellular bacterial inclusions formed by infection with bacteria like *Chlamydia* or *Legionella*. (B) OCRL in association with the midbody within cells during the process of cytokinesis. (C) OCRL localises to the lamellipodia within migrating fibroblasts. Subcellular organelles are each displayed as different colours with arrows indicating the direction of flow of endocytic events. *Trans*-Golgi network (TGN), Primary cilium (PC), Nucleus (N), Early endosome (EE). Adapted from (Mehta et al. 2014).

1.4.3.10. A summary of the impact of the lack of functional OCRL within proximal tubular cells

Following on from a detailed understanding of the functional roles of OCRL, an understanding of how the loss of functional OCRL affects endocytic events is required. A schematic, which displays the molecular defects of the endolysosomal system and the PC within the proximal tubular cells of patients with LS in comparison to healthy proximal tubular cells is illustrated (Fig. 1.8.A-B.).

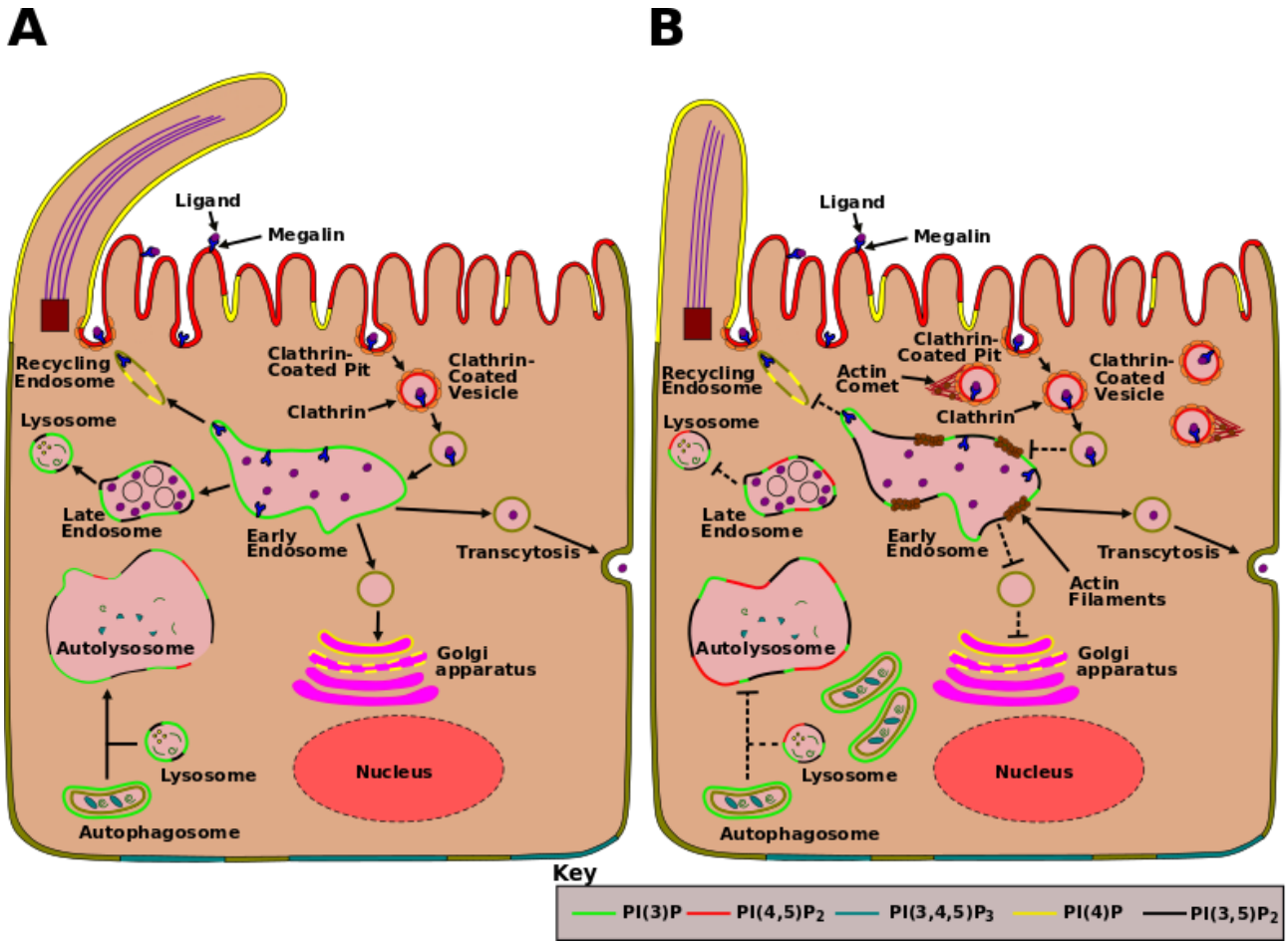

Figure 1.8. Comparison of healthy proximal tubular cells to equivalent cells from patients with LS. (A) The endolysosomal system within healthy proximal tubular cells. (B) Proximal tubular cells of LS patients lacking functional OCRL, with defects observed in the endolysosomal system and the PC. In cells from LS patients, a hallmark defect is the failed removal of clathrin, which results in an increase of CCVs, which are incapable of losing their clathrin coat and the associated actin machinery due to the severe reduction in PI(4,5)P_2 (red) depletion, causing actin comets to form. The reduced levels of PI(4,5)P_2 depletion fails to trigger actin disassembly and instead triggers actin polymerisation on the intracellular membranes of the EE. The stimulation of actin polymerisation hinders the trafficking of receptors via the EEs, preventing receptor recycling to the PM, reduced retrograde trafficking to the Golgi apparatus, and a decrease in the sorting of cargo to the lysosomes. In addition, without OCRL, PI(4,5)P_2 builds on the membranes of the autolysosomes causing defects in autophagic flux and the increase in the number of autophagosomes per cell. The lack of functional OCRL affects the PC, causing them to be shorter than normal. Fibroblasts from individuals with LS displayed clear signs of defects in ciliogenesis. PIPs are colour-coded as shown in the key, with each subcellular compartment clearly labelled and indicated (Bothwell et al. 2010, 2011, Ramirez et al. 2012, Oltrabella et al. 2015, Inoue et al. 2017). Adapted from (De Matteis et al. 2017).

1.4.4. How do actin comets form in cells lacking functional OCRL?

One of the key phenotypes observed upon the loss of OCRL is the excessive polymerisation of actin on various compartments, which gives rise to actin comets. In mammals, these actin comets formed during CME in which vesicles failed to lose their clathrin coat in the absence of OCRL enzymatic activity (Nandez et al. 2014). Actin comets are concentrated, highly dynamic bundles of

actin that propel organelles within the cytoplasm as a result of actin polymerisation occurring at the organelle interface and the depolymerisation of actin occurring at the opposite end (Suchy and Nussbaum 2002, Nandez et al. 2014, Dong et al. 2016). The formation of actin comets is however, not restricted to CME as comets have also been observed to form during phagocytosis in response to infection by the gram-positive *Listeria monocytogenes* bacterium (Kocks et al. 1992, 1995). To induce comet formation and thus bacterial movement within the cytosol the *L. monocytogenes* surface protein, Actin Assembly-inducing protein (ActA), mimics the activity of members of the WASP family of proteins within eukaryotes, resulting in the recruitment of the components of the actin nucleation machinery (Kocks et al. 1992, 1995). The recruitment of this machinery subsequently stimulates actin polymerisation and the formation of actin comets, which propels the parasite within the cytosol and aids in the infection of neighbouring cells (Kocks et al. 1992, 1995).

In 2017 a mechanism in mammals that resulted in the stimulation of actin polymerisation and thereby comet formation was elucidated, which involved PIP dysregulation and high membrane curvature (Daste et al. 2017). PIP dysregulation arose in part due to the loss of OCRL activity preventing the hydrolysis of the remaining $PI(4,5)P_2$ and inhibited the un-coating of CCVs. $PI(4,5)P_2$ is itself a well-known regulator of actin assembly (Yamaguchi et al. 2009), meaning that hydrolysis of $PI(4,5)P_2$ is crucial in order to facilitate CCV un-coating and actin disassembly. Initially $PI(4,5)P_2$ is hydrolysed to PI(4)P by the inositol 5-phosphatases Synaptojanin p-170 and later by the Synaptojanin p-145 isoform during CME (Perera et al. 2006). The resulting PI(4)P is then phosphorylated to $PI(3,4)P_2$ by PI3KC2A (Posor et al. 2013), which is then de-phosphorylated to PI(3)P by INPP4A phosphatase activity (Fig. 1.9.A.) (Ivetac et al. 2005). The generation of PI(3)P and $PI(4,5)P_2$ due to lack of OCRL activity collectively recruit the sorting nexin-9 (SNX9) adapter protein (Daste et al. 2017). In addition to the generation of PI(3)P from the de-phosphorylation of $PI(3,4)P_2$ by INPP4A phosphatase activity in OCRL deficient cells, a second source of PI(3)P arises from the phosphorylation of PI to PI(3)P by the kinase activity of the Vps34 class III PI3K (Fig. 1.9.B.) (Daste et al. 2017). In cells lacking functional OCRL, the transient coincidence of both $PI(4,5)P_2$ and PI(3)P is far more sustained causing defects in the SNX9 actin assembly pathway (Fig. 1.9.B.). Membrane curvature functions as an additional requirement for this actin assembly pathway as it enhances the enzymatic activities of Synaptojanin (Chang-Ileto et al. 2011), the class II PI3K (Hubner et al. 1998), and INPP4A (Daste et al. 2017), resulting in greater levels of PI(3)P generation. The elevated $PI(4,5)P_2$ due to OCRL deficiency, the increase in membrane curvature, and PI(3)P production collectively recruits and enhances the activity of SNX9 (Fig. 1.9.B.) (Daste et al. 2017). Binding of both $PI(4,5)P_2$ and PI(3)P were shown to occur through the combined activities of the SNX9 phox homology (PX)-Bin/Amphiphysin/Rvs (BAR) domains (Daste et al. 2017). In addition, the PX-BAR SNX9 domains

preferentially interact with membranes of high membrane curvature (Pylypenko et al. 2007). SNX9 has been shown to directly bind to OCRL at later stage CCPs (Nandez et al. 2014). SNX9 however, is recruited to CCPs just before OCRL, with the recruitment of OCRL itself being coincidental with the temporal recruitment of cyclin G-Associated Kinase (GAK) to CCPs (Taylor et al. 2011). GAK like its homologue, auxilin, functions as a cofactor for the Heat shock cognate 70 protein (Hsc70) and therefore participates in clathrin un-coating after fission (Fotin et al. 2004, Massol et al. 2006). SNX9 functions to regulate actin polymerisation during CME via activating the NPF, N-WASP (Yarar et al. 2008), which together with the presence of elevated $PI(4,5)P_2$ in OCRL depleted cells further aids in the activation of N-WASP (Rohatgi et al. 1999). Activation of N-WASP in this model however, also required the presence of activated Cdc42 for the polymerisation of actin to be stimulated (Fig. 1.9.B.) (Gallop et al. 2013, Daste et al. 2017). Cdc42 activity is unique in this model as it is regulated by $PI(4,5)P_2$ alone and is not influenced by increases in membrane curvature (Daste et al. 2017). The combined activities of SNX9 and Cdc42 result in the activation of N-WASP and consequently Actin-related protein 2/3 (Arp2/3)-mediated actin polymerisation, causing comet formation (Fig. 1.9.B.) (Daste et al. 2017). The use of class III PI3K inhibitors such as the Vps34-IN1, which specifically inhibits the kinase activity of Vps34, has been suggested as a therapeutic route to prevent comet formation in *OCRL*$^{-/-}$ mutant patient cells and to thus alleviate LS disease symptoms (Bago et al. 2014, Daste et al. 2017). A summary of the proposed mechanism of comet formation driven by SNX9, $PI(4,5)P_2$, and PI(3)P is displayed (Fig. 1.9.A-B.).

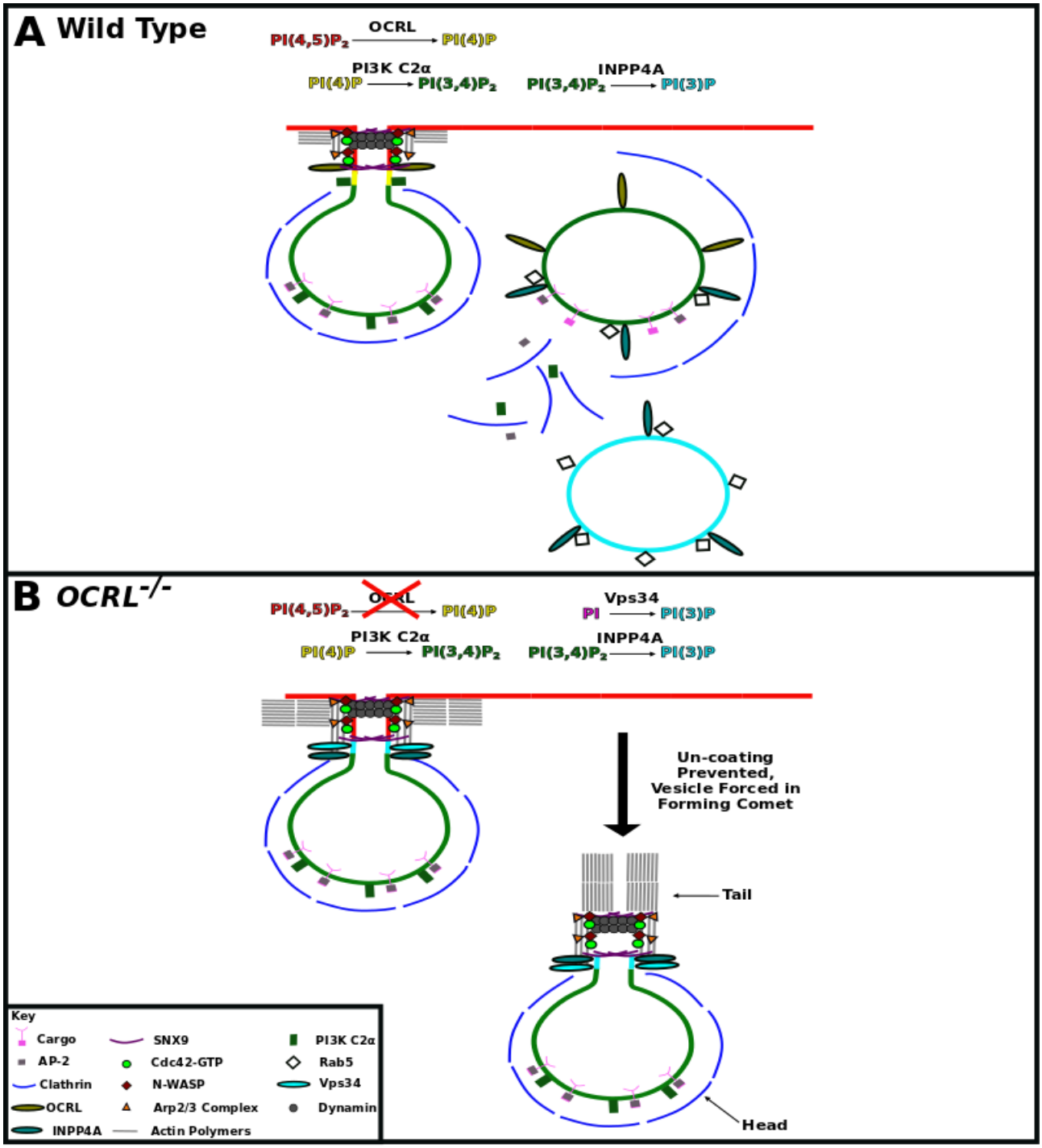

Figure 1.9. The mechanism of comet formation during CME in mammals. (A) Wild-type Retinal Pigmented Epithelial-1 (RPE-1) cells were used in which OCRL was deficient as this recapitulated the actin comet phenotype observed in patient fibroblasts. The presence of later stage PI(4,5)P_2 (red) at the neck of growing vesicles recruits the actin regulators SNX9 and Dynamin. The remaining PI(4,5)P_2 is de-phosphorylated to PI(4)P (yellow) by OCRL initiating clathrin un-coating and disassembly. The resulting PI(4)P is then phosphorylated to PI(3,4)P_2 (green) by PI3K C2α, after which PI(3,4)P_2 is then hydrolysed to PI(3)P (light blue) by INPP4A as the vesicle is internalised. (B) *OCRL*$^{-/-}$ mutant cells in which later stage PI(4,5)P_2 hydrolysis is prevented, stopping the disassembly of clathrin and actin regulators, resulting in the vesicle being propelled into the cell with the actin machinery still intact. INPP4A is recruited to the neck as part of the source of PI(3)P, with Vps34 kinase activity generating PI(3)P from PI phosphorylation. The abundance of both PI(4,5)P_2, and PI(3)P result in enhanced SNX9 activity, further preventing machinery disassembly. This collectively results in comet formation in *OCRL*$^{-/-}$ mutants, with membrane curvature being crucial for enhanced PIP enzymatic activity. PIPs are colour-coded, with a key showing all components involved in comet formation. Adapted from (Posor et al. 2015, Daste et al. 2017).

1.5 The OCRL F&H interactors in mammals

Mammalian OCRL is able to function at various stages of endocytosis by establishing interactions with endocytic adaptors and a Cdc42 Rho-GEF. These interactors include APPL1, and Ses1/2, as well as the FGD1- related F-actin binding protein (Frabin). These protein-protein interactions occur between the C-terminal Rho-GAP F&H motif of OCRL and the F&H motifs of APPL1, Ses1/2, and Frabin (Erdmann et al. 2007, Swan et al. 2010, Noakes et al. 2011, Pirruccello et al. 2011, Luscher et al. 2019).

1.5.1. The roles of APPL1 in the regulation of endocytosis in mammals

The early endocytic APPL1 adaptor regulates numerous signalling events. The N-terminal BAR domain of APPL1 (Fig. 1.10.A.) has been linked to the induction or sensing of membrane curvature (Takei et al. 1999, Habermann 2004). The centrally located PH domain and the C-terminal phosphotyrosine-binding domain (PTB) domain (Fig. 1.10.A.), have been shown to interact with a variety of phospholipids (Li et al. 2007) and can bind all PIPs, except $PI(4,5)P_2$ (Li et al. 2007, Chial et al. 2008). The N-terminal BAR domain grants APPL1 the ability to form homodimers with itself and heterodimers with APPL2 (Chial et al. 2008). Both the BAR and PH domains are important for interactions with the small GTPases, Rab5 and Rab21 (Pereira-Leal and Seabra 2001, Zhu et al. 2007). The C-terminal PTB domain links APPL1 to signalling receptors like the Tropomyosin receptor kinase A (TrkA) (Lin et al. 2006), the EGFR (Miaczynska et al. 2004), and the Adiponection Receptor 1 (AdipoR1) (Mao et al. 2006). Additional receptors include the Follicle Stimulating Hormone Receptor (FSHR), the Insulin Receptor (IR), Deleted in Colorectal Cancer (DCC) (Liu et al. 2002), N-Methyl D-Aspartate (NMDA) receptors (Husi et al. 2000), and the Androgen Receptor (AR) (Yang et al. 2003). APPL1 also establishes interactions with the GAIP-Interacting Protein C terminus member 1 (GIPC1), via its PSD-95/Discs-large/ZO-1 (PDZ) domain (Varsano et al. 2012). GIPC1 acts to load cargo onto vesicles through its interaction with the actin motor protein, myosin VI (Katoh 2013). The APPL1 paralogue, APPL2, has a very similar domain structure, however, it lacks the F&H motif and also possesses a C-terminal Phosphotyrosine-Interacting Domain (PID), in place of the C-terminal APPL1 PTB domain (Pirruccello and De Camilli 2012). A summary of the key APPL1 interactors involved in trafficking and endocytosis, and the domain structures of APPL1 and APPL2 is illustrated (Fig. 1.10.A-B.).

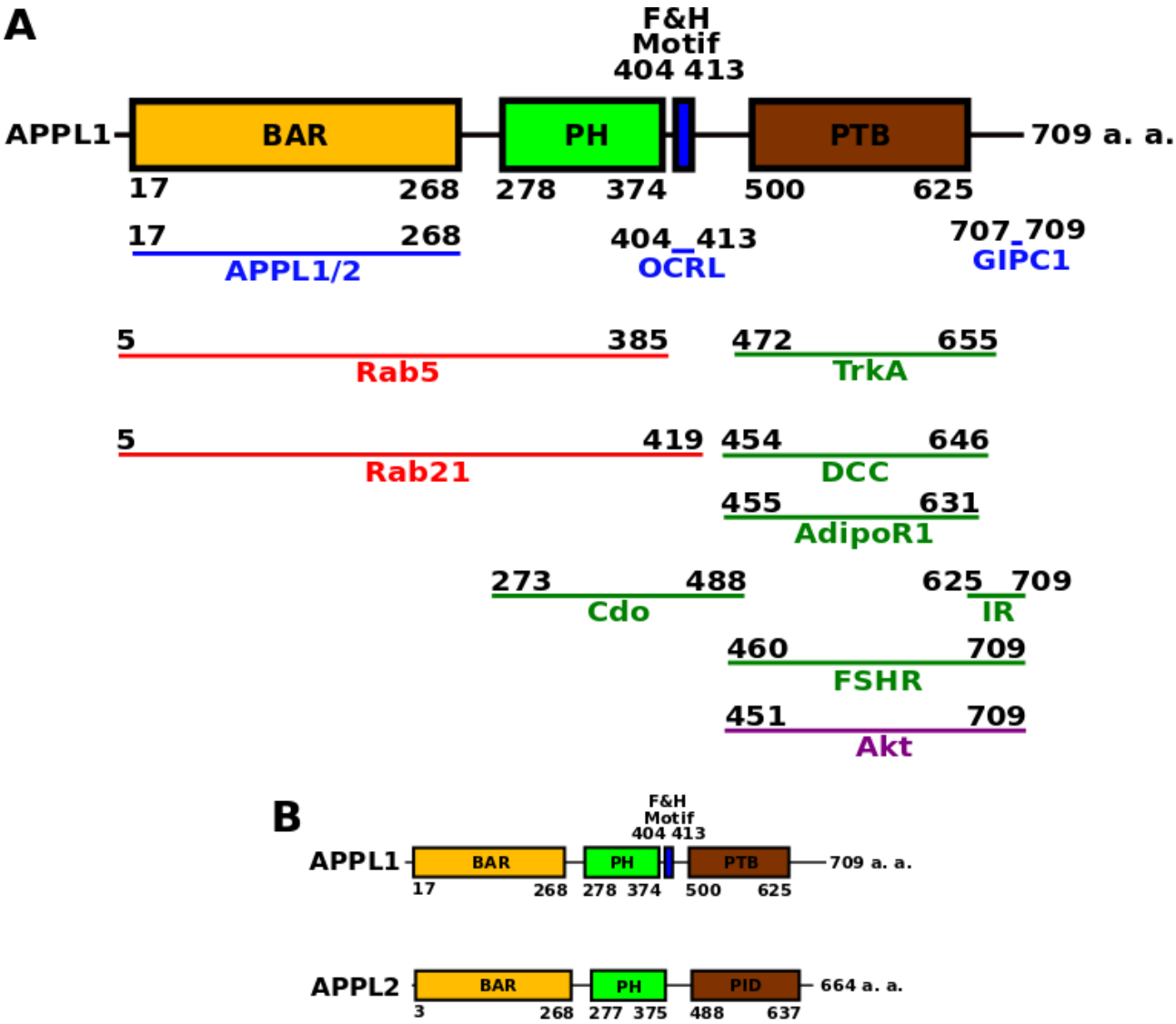

Figure 1.10. The binding sites of proteins that interact with APPL1 and the domain comparison with APPL2. (A) Schematic and interaction sites of the various APPL1-binding proteins. The labelled amino acid positions of each interaction site with the colour-coded APPL1 interacting proteins are labelled as follows: red for trafficking proteins, blue for proteins involved in both signalling and trafficking, green for receptor proteins, and purple for signalling proteins. CAM-related/down-regulated by oncogenes (Cdo). Adapted from (Diggins and Webb 2017). (B) Domain organisation of APPL1 and APPL2. Adapted from (Pirruccello and De Camilli 2012, Luscher et al. 2019).

APPL1 itself establishes interactions with Rab5, which recruits APPL1 to the early phagosome (Fig. 1.10.). APPL1 establishes interactions via its F&H motif with the F&H motifs of OCRL and INPP5B, resulting in the recruitment of these inositol 5-phosphatases via active Rab5 to the early phagosome. This recruitment results in the hydrolysis of PI(4,5)P_2 and the disassembly of actin (Bohdanowicz et al. 2012). The absence of either APPL1 or Rab5 prevented the hydrolysis of PI(4,5)P_2 through the prevention of OCRL and INPP5B recruitment, indicating that both were crucial to facilitate PI(4,5)P_2 hydrolysis and the subsequent disassembly of actin on the membranes of phagosomes (Bohdanowicz et al. 2012).

The functionality of APPL1 is not just restricted to endosomes however, as APPL1 participates in establishing links between receptor trafficking in EEs and signalling to the nucleus, via APPL1-Rab5 interactions. Upon Rab5-GTP hydrolysis APPL1 dissociates from EEs, and translocates to the nucleus, where it regulates gene transcription through interacting with histone deacetylases 1-3 (HDA1-3) (Miaczynska et al. 2004, Banach-Orlowska et al. 2009, Joshi et al. 2013).

1.5.2. The roles of Ses1 and Ses2 in the regulation of endocytosis in mammals

In mammals, Ses1 and Ses2 interact with OCRL via F&H motifs present in their C termini. Ses1 and Ses2 both localise at later endocytic stages than the earlier APPL1 endocytic adaptor (Swan et al. 2010, Noakes et al. 2011). The binding between OCRL and Ses1 has been shown to cause minor structural changes to the Rab-binding loop of OCRL, which facilitates binding with the Rab8a protein and thus endocytic trafficking to the PC (Coon et al. 2012, Shalaby et al. 2018). These later mammalian endocytic adaptors have also been established to participate in receptor recycling, such as the transferrin receptor (TfR) to the cell surface (Noakes et al. 2011). Ses1/2 are also important in the regulation of trafficking of the cation-independent mannose 6-phosphate receptor (CIMPR) and the Shiga toxin B-subunit (STxB) between the endosomes and the TGN (Noakes et al. 2011). Ses1/2 has also been shown to be crucial for the recruitment of OCRL to coordinate $PI(4,5)P_2$ homeostasis and thus results in the recruitment of the cytokinesis machinery required for successful cytokinesis to occur (Carim et al. 2019). In Zebrafish the disruption of Ses1/2 resulted in endocytic defects and disrupted ciliogenesis within renal tissues, with these proteins also being shown to play a role in craniofacial development (Ates et al. 2020). The phenotypes that were observed in Zebrafish were also consistent with the clinical features displayed by a patient that possessed a *de novo* mutation where an Arginine (R) at position 6 was replaced by a Cysteine (C) amino acid residue (R6C) within the Ses1 protein (Ates et al. 2020). Expression of the R6C Ses1 mutant within Zebrafish worsened the craniofacial deficits, which suggested that the R6C allele was dominant negative. The symptoms of the patient bearing the R6C allele included global developmental delay and coarse facial features, which did not match the symptoms of patients with LS, which thus indicated that Ses1 possessed OCRL-independent functions *in vivo* (Ates et al. 2020).

1.5.3. The Faciogenital dysphasia (FGD) family, Frabin, and the roles they play in mammalian endocytosis

Frabin is one of a group of seven closely related proteins, called the faciogenital dysphasia (FGD) proteins, the members of which include FGD1-6 and the FERM, ARH/Rho-GEF, and Pleckstrin domain, protein 2 (FARP2), which all function as Cdc42 Rho-GEFs. Of the seven FGD proteins, three

of them are associated with disease, the first being FGD1, which is mutated in the Aarskog-Scott syndrome (Pasteris et al. 1994). The second is FGD4/Frabin, which is mutated in the Charcot Marie Tooth 4H peripheral neuropathy (Delague et al. 2007). The third is FGD6, the mutations of which presents as a major risk factor for the development of macular degeneration (Huang et al. 2016). Pull-downs have identified putative F&H motifs in three members, FGD4/Frabin, FGD5, and FGD6. This investigation revealed however, that only FGD4/Frabin interacted with endogenous OCRL (Luscher et al. 2019). The domain structures of the three F&H motif-containing FGD family members is illustrated (Fig. 1.11.).

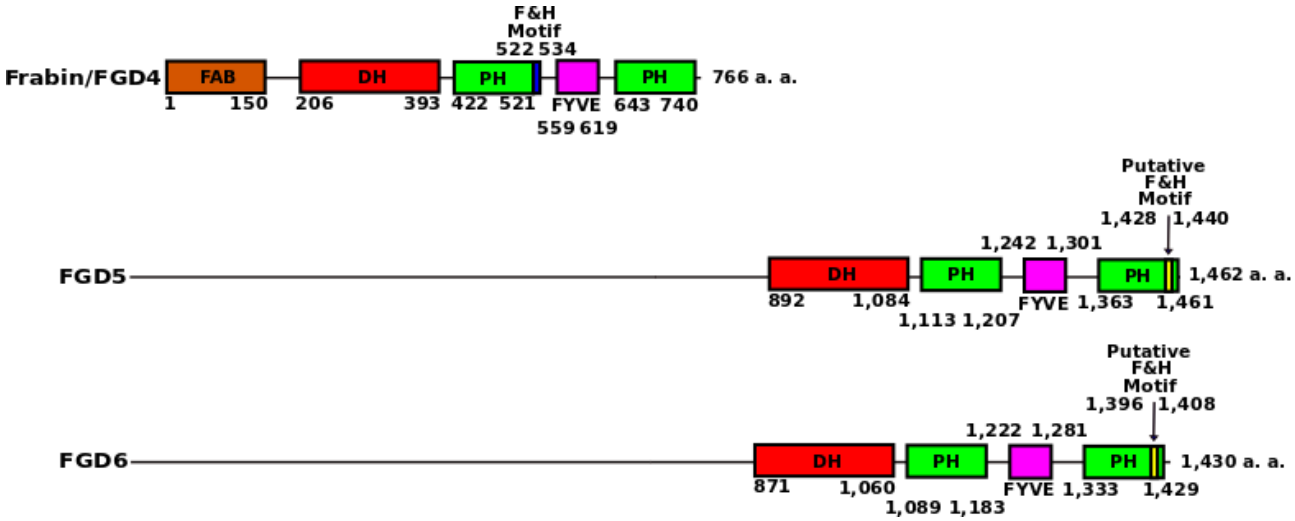

Figure 1.11. The domain organisation of the three F&H motif-containing FGD family members in *H. sapiens*. FGD4/Frabin was only able to interact with endogenous OCRL, via its F&H motif (dark blue) in the PH 1 domain. The putative F&H motifs (yellow) located in the PH 2 domains of both FGD5 and FGD6 were incapable of interacting with endogenous OCRL. The amino acid positions of each colour-coded domain are displayed. Adapted from (Luscher et al. 2019).

In mice, the loss of Frabin resulted in increased demyelination in Schwann cells (SCs), with Frabin found to be crucial for the maintenance of myelin (Horn et al. 2012). Aberrant myelination *in vitro* in the dorsal root ganglia neurons/SCs co-cultures were observed within a conditional null allele mouse model in which Frabin expression was specifically suppressed within SCs (*Fgd4*$^{SC-/-}$) (El-Bazzal et al. 2022). Aberrant myelination was also seen *in vivo* in distal sciatic nerves from *Fgd4*$^{SC-/-}$ mice (El-Bazzal et al. 2022). The defects in myelination were found to be the result of the upregulation of various interactors of the Neuregulin-1 type III (NRG1 type III)/ERB-B2 receptor tyrosine kinase 2/3 (ERBB2/3) signalling pathway, which ensures the correct physiological levels of myelination in the peripheral nervous system (PNS) (El-Bazzal et al. 2022). A new Frabin-binding partner found to be involved in endocytic trafficking was also identified via a yeast 2-hybrid screen, and was called the Sorting Nexin-3 (SNX3) protein (El-Bazzal et al. 2022). The loss of Frabin activity

was also outlined to result in endocytic defects, which may have caused defects in NRG1 type III/ERBB2/3 signalling and consequently myelination (El-Bazzal et al. 2022). The possible effectors of the de-regulated NRG1 type III/ERBB2/3 signalling pathway were also identified, which included the ERB-B2 Interacting protein (ERBIN), Rab11 Family-Interacting Protein 2 (Rab11-FIP2), and the transcription factor Musculoaponeurotic Fibrosarcoma (MAF) (El-Bazzal et al. 2022). The MAF transcription factor is itself activated following signalling via the NRG1 type III/ERBB2/3 signalling pathway and has been documented to play an important role within PNS myelination via regulating the biosynthesis of cholesterol, a fundamental component of myelin membranes (Kim et al. 2018). Interestingly, following treatment with Niacin there was a reduction in NRG1 type III/ERBB2/3 signalling and an observed decrease in the number of myelin outfoldings in the nerves of mice with Charcot-Marie-Tooth disease type 4H (CMT4H), which outlined that the myelination defects arose from overstimulation of the NRG1 type III/ERBB2/3 signalling pathway (El-Bazzal et al. 2022). Frabin has also been established to regulate Cdc42 activity in peripheral nerves, with the activity of Cdc42 being important for myelin maintenance. This Cdc42 Rho-GEF has also been shown to regulate endocytosis, as loss of Frabin activity reduced TfR uptake in the rat SC line, RT4 (Horn et al. 2012). Frabin also functions to induce filopodia formation and the activation of c-Jun N-terminal Kinase (JNK) via the activation of Cdc42 within fibroblast cells (Obaishi et al. 1998, Umikawa et al. 1999, Ono et al. 2000). Frabin also induces the formation of lamellipodia, via the indirect activation of Rac within fibroblasts (Ono et al. 2000). A detailed model of Frabin activity in conjunction with the small GTP-binding proteins and actin regulators involved in the formation of filopodia and lamellipodia is illustrated (Fig. 1.12.) (Nakanishi and Takai 2008).

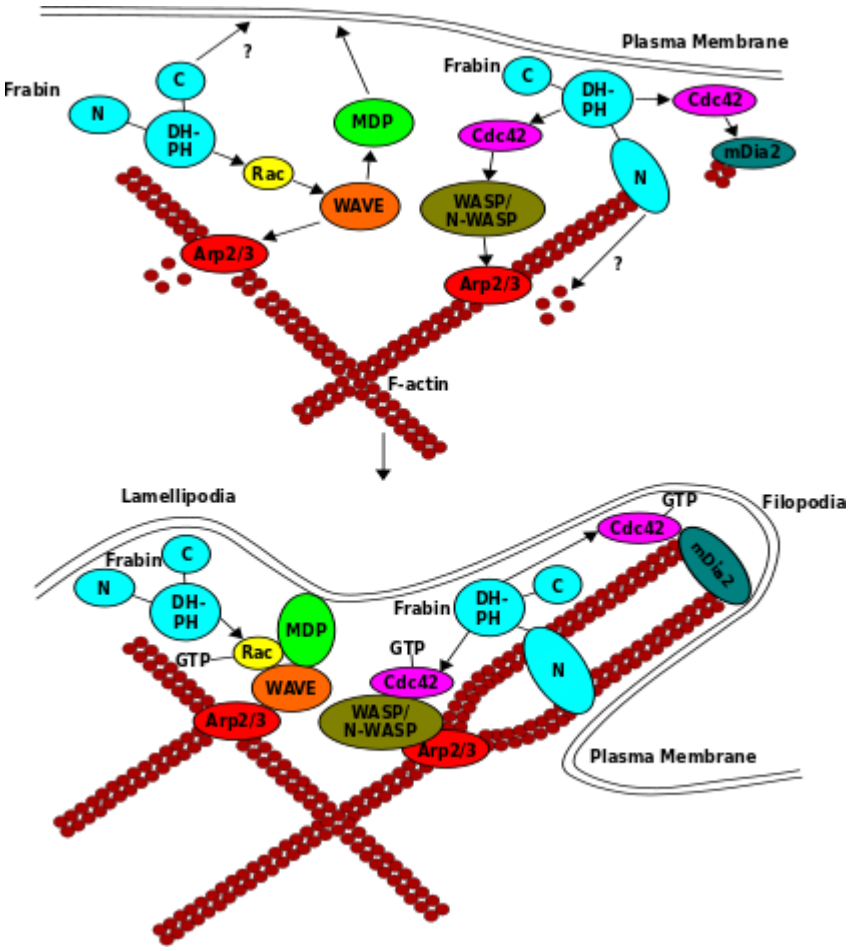

Figure 1.12. The model of Frabin activity, which coordinates changes in cell shape. Frabin recruitment through the N-terminal F-actin-binding (FAB) domain localises Frabin to pre-existing, specific actin structures. Frabin then reorganises components of the actin cytoskeleton, using its N-terminal FAB and Dbl Homology (DH) domains, in a manner that is Cdc42-independent. Frabin also activates Cdc42 via its DH and first PH domains in close proximity to structures of actin, WASP, N-WASP, and the Arp2/3 complex, which thus generates branched F-actin. Frabin activity causes F-actin to come together as bundles. Actin polymerisation via mDia2 is stimulated via Frabin DH-PH domain activation of Cdc42. The sum of Cdc42-dependent and Cdc42-independent activities induced actin reorganisation, which stimulates the formation of filopodia. The C-terminal region of Frabin functions to recruit proteins to specific membrane structures, causing membrane deformation and the formation of outward membrane protrusions. In close proximity to membrane structures, Frabin activates Rac, which results in the generation of branched F-actin via the WAVE and Arp2/3 complexes, as well as the formation of outward membrane protrusions via the WAVE complex and the membrane-deforming protein (MDP). The simultaneous reorganisation of the PM and the actin cytoskeleton, results in lamellipodia formation. Dia family in mouse 2 (mDia2), N-terminal region of Frabin includes the FAB domain (N), DH-PH are the DH and first PH domains of Frabin (DH-PH), and the C-terminal region encompasses the FYVE and the second PH domains (C). Adapted from (Nakanishi and Takai 2008).

1.6 The family of actin regulators, the WASP family

The formation of comets in cells lacking functional OCRL was a result of the enhanced activation of N-WASP, which drove increased levels of Arp2/3-mediated polymerisation, forming actin comets (Suchy and Nussbaum 2002, Allen 2003, Nandez et al. 2014, Daste et al. 2017). The

actin cytoskeleton plays a vital role in all eukaryotic cells. The polymerisation of actin gives the essential locomotive forces, which aids to facilitate processes that centre on membrane deformation, such as the trafficking of vesicles, migration, and neuron growth (Luo 2002, Pollard and Cooper 2009, Blanchoin et al. 2014). The generation of an actin dimer is the rate-limiting step during actin polymerisation, which then spontaneously gives rise to the formation of a new actin filament. The efficient polymerisation of actin filaments requires the presence of a regulator, which oversees and facilitates nucleation (Pollard 2016). A well-known facilitator of nucleation is the Arp2/3 complex, which consists of seven protein subunits (Pollard 2007).

The Arp2/3 complex functions by interacting with the side of an already existing actin filament, and creates a completely new, branched actin filament (Machesky et al. 1994, Blanchoin et al. 2000, Zhang et al. 2016, Cioni et al. 2018, Cao et al. 2022, Yang et al. 2022, Zagelbaum et al. 2022). The Arp2/3 complex exists in a resting, inactive state, and requires activation via a group of activating proteins known as NPFs (Higgs and Pollard 2001, Goley and Welch 2006, Rotty et al. 2013). Chief amongst these are the Wiskott-Aldrich Syndrome protein (WASP) family, which dictates a wide array of signalling events that lie upstream of Arp2/3-mediated actin polymerisation in important cellular processes.

In mammals there are nine WASP family protein members, which are grouped into five different categories on the basis of their sequence similarity (Kollmar et al. 2012, Alekhina et al. 2017). These include WASP (Derry et al. 1994), N-WASP (Miki et al. 1996, 1998a), Wiskott Aldrich Syndrome protein and verprolin homologues 1-3 [WAVE1-3, also known as the suppressor of cAMP receptor (SCAR)] (Suetsugu et al. 1999). Additional members include the Wiskott-Aldrich Syndrome protein and SCAR Homologue (WASH) (Linardopoulou et al. 2007), the WASP Homolog associated with Actin, Membranes and Microtubules (WHAMM) (Campellone et al. 2008), the Junction-mediating and regulatory protein (JMY) (Shikama et al. 1999, Zuchero et al. 2012), and the very recently identified WAVE Homology In Membrane Protrusions (WHIMP) (Kabrawala et al. 2020).

A hallmark of all WASP family members is the highly conserved C-terminal catalytic Verprolin homology and a Central and an Acidic domain (VCA), which interacts with and activates the Arp2/3 complex (Machesky and Insall 1998, Miki et al. 1998b, Higgs et al. 1999). The Verprolin homology domain is in more accurate terms called the WASP Homology 2 (WH2) motif and binds to nascent monomers of actin and is required to recruit actin to the Arp2/3 complex (Paunola et al. 2002, Dominguez 2007). This consequently gives the alternative acronym, WH2 and a Central and an Acidic domain (WCA). The WH2 motif is also present in a wide variety of other regulators of actin including Cordon-bleu (Cobl) (Husson et al. 2011), the *Drosophila* Spire protein (Quinlan et al. 2005), the WASP-interacting protein (WIP) (Vaduva et al. 1999), and the bacterial effector proteins; VopF

of *Vibrio cholera*, and VopL of *Vibrio parahaemolyticus* (Pernier et al. 2013). The CA region of the V(W)CA domain is responsible for binding the Arp2/3 complex. Two separate CA regions bind to two different locations on the Arp2/3 complex and causes conformational changes converting it from its inactive to active state, and thus initiating actin polymerisation (Marchand et al. 2001, Panchal et al. 2003, Padrick et al. 2008, 2011, Shaaban et al. 2020, Zimmet et al. 2020). The C region possesses an affinity for both the Arp2/3 complex and actin, and may also play a part in the transfer of a monomer of actin to the Arp2/3 complex (Marchand et al. 2001, Kelly et al. 2006). The A region of WASP is a low complexity region, which is highly abundant in acidic amino acid residues. An important feature of this region is the presence of the Tryptophan (Trp) residue located two positions away from the C-terminus, which facilitates the binding and enhances the activation of the Arp2/3 complex (Marchand et al. 2001). A summary of the domain organisation of each individual WASP family member in mammals is illustrated (Fig. 1.13.).

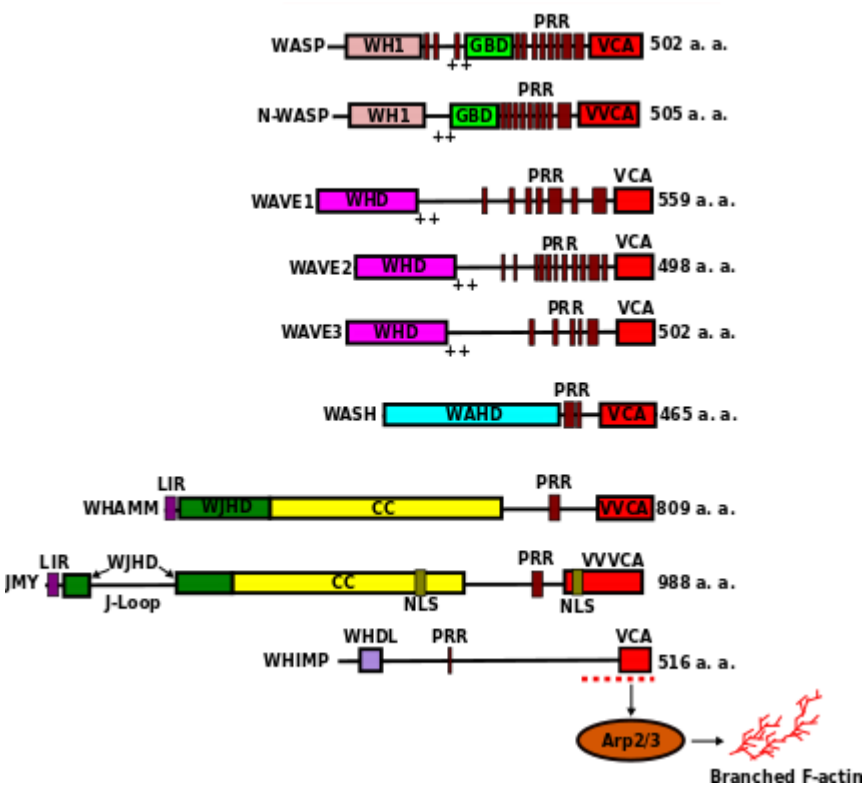

Figure 1.13. The domain composition of each member of the WASP family in mammals. Colour-coded domains and motifs are labelled, along with the displayed protein sizes showing the number of amino acids to the right of each protein. WHAMM and JMY Homology Domain (WJHD), WASP Homology 1 domain (WH1), GTPase Binding Domain (GBD), Proline-Rich Region (PRR), Verprolin-Central-Acidic domain (VCA), WAVE Homology Domain (WHD), WASH Homology Domain (WAHD), LC3-Interacting Region (LIR), JMY-specific loop (J-loop), Coiled-Coil domain (CC), Nuclear Localisation Signal (NLS), WAVE Homology Domain-Like (WHDL). "+ +" indicates positively charged amino acid residues. Adapted from (Kramer et al. 2022).

As WASP and N-WASP appear to be important in the formation of comets in cells lacking functional OCRL, an understanding of where these proteins localise within mammals (Fig. 1.14.) and how they are activated (Fig 1.15.) will aid to illustrate the importance of these proteins in regulating actin dynamics within different parts of the cell.

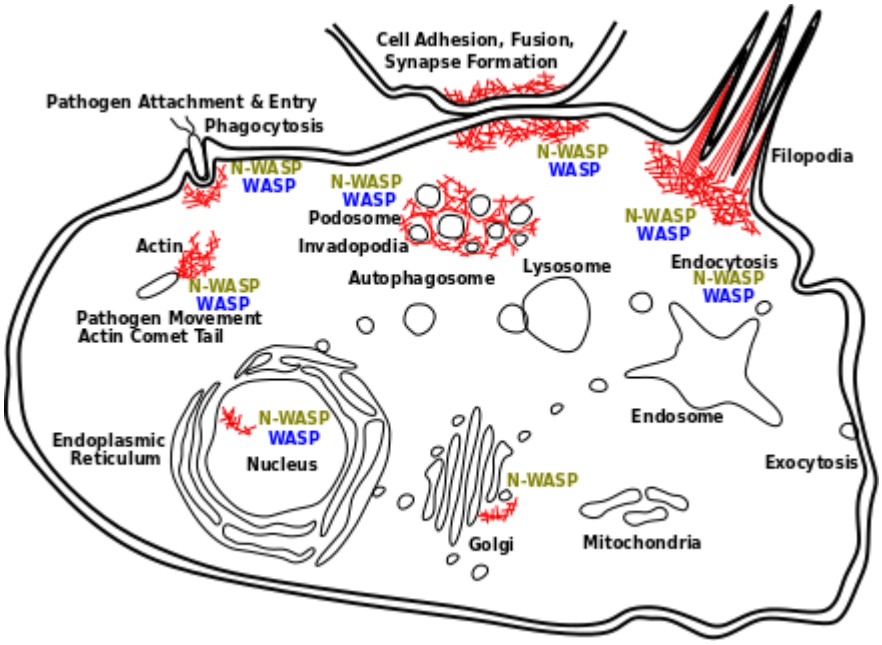

Figure 1.14. The subcellular localisation and function of WASP and N-WASP in mammals. WASP and N-WASP are colour-coded and where they localise within the cell are indicated along with the F-actin filaments only associated with the activities of these proteins displayed in red. Adapted from (Kramer et al. 2022).

In mammals, WASP exists in two different conformations, one being an inactive auto-inhibited state, and the other being an active form. In the auto-inhibited state, WASP is present in the cytoplasm, which is maintained via interactions with WIP. In response to cellular activation, WASP is recruited to regions of membrane signalling, and establishes protein-protein interactions with various adaptor proteins through the WASP PPR region and/or through associations of Non-catalytic region of tyrosine kinase (Nck) or the Crk-Like protein (CrkL) with WIP (Anton et al. 1998, Sasahara et al. 2002).

WASP is activated by release from the auto-inhibited state and exposure of the VCA domain by one or more signals, depending on the microenvironment to which this complex is recruited. These signals include: PI(4,5)P_2 binding to the B domain, binding of Cdc42-GTP to the GBD, Y291 phosphorylation, interactions of the Transducer Of Cdc42-dependent Actin assembly-1 (TOCA-1) with the PPR and Cdc42-GTP, and interactions of various adaptor proteins, including Nck and the Growth factor receptor-bound protein 2 (Grb2) to the PPR of WASP. Y291 phosphorylation of WASP is orchestrated by the Src Homology Three (SH3) domain-containing Src kinases, such as the Haematopoietic cell kinase (Hck), and the Family tyrosine kinase (Fyn). This phosphorylation acts to

maintain the active conformation of WASP obtained through PI(4,5)P_2 and Cdc42-GTP binding (Guinamard et al. 1998, Baba et al. 1999, Cory et al. 2002, Torres and Rosen 2003, Bodour et al. 2004). The V domain of WASP forms interactions with G-actin; the C-terminal A domain however, establishes interactions with the Arp2/3 complex to which G-actin is relayed over, leading to the initiation of localised elongation and/or branching of actin filaments (Oda et al. 1998, Blundell et al. 2009). A summary of the mechanism of WASP activation from the auto-inhibited state to the active state is shown (Fig. 1.15.).

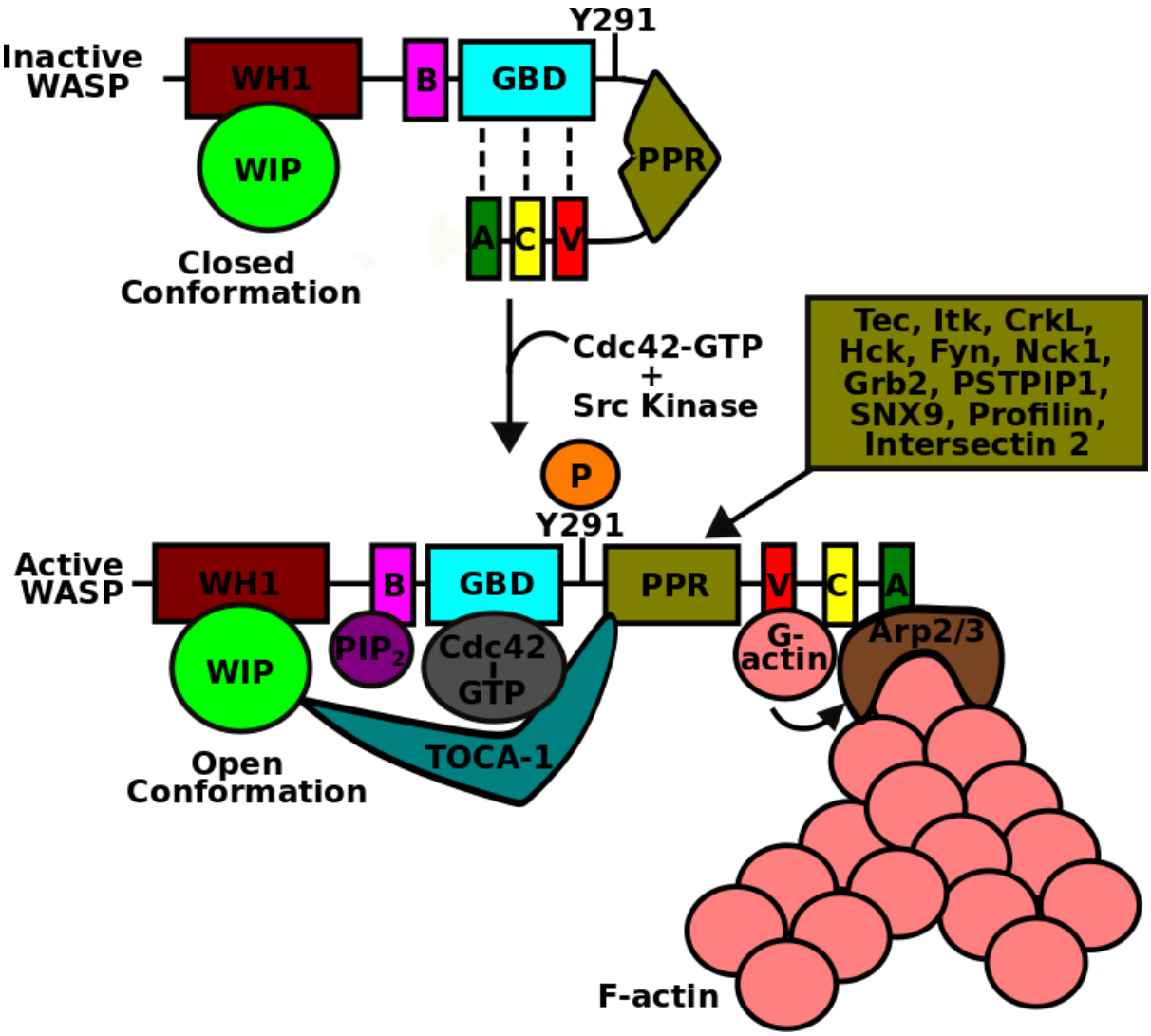

Figure 1.15. Mechanism of WASP activation in mammals. Inactive WASP exists in a closed, auto-inhibited conformation, in which the GBD (aqua blue) forms interactions (dashed black lines) with the VCA domain (red, yellow, and green respectively). Binding of Cdc42-GTP (grey) to the GBD, PI(4,5)P_2 (dark purple) to the B domain (magenta), phosphorylation (orange) of Y291, binding of TOCA-1 (teal) to the PPR (olive), Cdc42-GTP, and WIP (light green), or binding of the SH3 domain-containing adaptors (olive box) to the PPR releases the VCA domain, causing WASP activation. Active WASP can establish interactions with the Arp2/3 complex (brown), resulting in F-actin (pink) polymerisation. Proteins, which interact with the WASP PPR are indicated in an olive-coloured box. Phosphatidylinositol 4,5-bisphosphate (PIP_2), Transducer of Cdc42-dependent actin assembly-1 (TOCA-1), Tyrosine kinase expressed in hepatocellular carcinoma (Tec), IL-2 inducible T-cell kinase (Itk), Proline-serine-threonine phosphatase-interacting protein 1 (PSTPIP1), Tyrosine at position 291 (Y291), Phosphate (P). Adapted from (Massaad et al. 2013, Sun et al. 2019, Ngoenkam et al. 2021).

1.7 *Dictyostelium discoideum* as a model organism

1.7.1. An introduction to *D. discoideum*

In mammalian cells, OCRL and its paralog, INPP5B, function to deplete PI(4,5)P_2. As the domain structures are very similar and they both possess an F&H motif separating the functions of one enzyme from the other would prove to be complex and problematic. I therefore used the

simpler organism, *D. discoideum*, which only expresses a single OCRL homolog, Dd5p4, which has a similar domain organisation and amino acid sequence in comparison to human OCRL and human INPP5B, and also possesses an F&H motif (Fig. 1.16.A-B.) (Loovers et al. 2003, Luscher et al. 2019, Paesmans et al. 2020). It should be noted however, that Dd5p4 in *D. discoideum* lack both the PH and ASH domains, and also the clathrin boxes that are present in human OCRL (Fig. 1.16.A-B.) (Loovers et al. 2003).

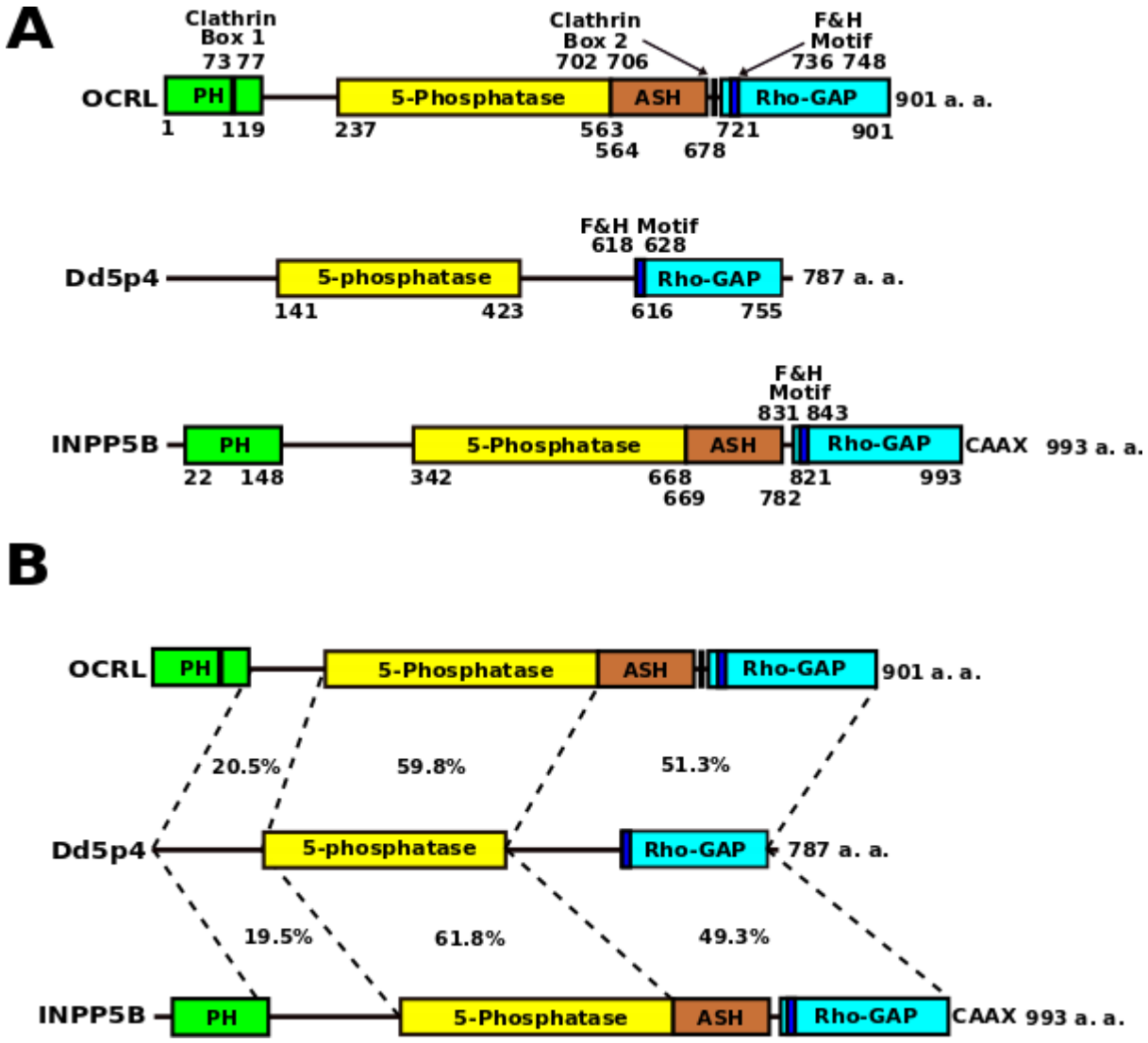

Figure 1.16. The domain organisation and sequence comparison between Dd5p4 and human OCRL and human INPP5B inositol 5-phosphatases. (A) Domain organisation of Dd5p4 compared to human OCRL and human INPP5B. The amino acid positions of each colour-coded domain and motif are indicated. (B) The amino acid sequence of Dd5p4 compared to human OCRL and human INPP5B. The amino acid % sequence similarity of each region are indicated between dashed black lines. Adapted from (Loovers et al. 2003, Luscher et al. 2019, Paesmans et al. 2020).

This OCRL homolog, Dd5p4, displayed clear defects in both phagocytosis and macropinocytosis, however the mechanistic causes behind these defects were poorly understood

(Loovers et al. 2007). I therefore aimed to use this system to investigate the roles of Dd5p4 in the regulation of both phagocytosis and macropinocytosis.

D. discoideum is a useful and highly robust model organism, and was used exclusively in this project to investigate Dd5p4 and the roles it played in endocytosis. This organism is a free-living, professional phagocyte, which performs greater levels of endocytosis, specifically, phagocytosis and macropinocytosis than both mammalian neutrophils and macrophages (Cardelli 2001). *D. discoideum* are also highly capable of performing rapid chemotaxis in response to folate release by various bacterial species, which is similar to what is utilised by mammalian phagocytes (Devreotes and Zigmond 1988, King and Insall 2009, Nichols et al. 2015).

D. discoideum was originally isolated from the soil back in 1932 (Raper and Thom 1932) as wild-type *D. discoideum* strains, which could only grow through the phagocytosis of bacteria. Two independent mutant axenic strains were later isolated in 1970 and 1971 from the Ddb parental strain and were dubbed as Ax2 and Ax3 respectively (Watts and Ashworth 1970, Loomis 1971). Both axenic strains exhibited upregulated macropinocytosis as a result of a mutation in the *axeB* gene located on chromosome 3, which resulted in the loss of Neurofibromin 1 (NF1) activity and enabled axenic growth within liquid culture (Watts and Ashworth 1970, Loomis 1971, Bloomfield et al. 2015). An additional axenic strain was also derived from the Ax3 strain and this strain was called Ax4 (Knecht et al. 1986). Both the axenic Ax3 and Ax4 strains share an inverted duplication that covers a large area of chromosome 2 (Eichinger et al. 2005), with the Ax2 strain lacking this inverted duplication. The mutation however, within the *axeB* locus is identical between the Ax2 and Ax4 axenic strains (Bloomfield et al. 2015). These axenic strains are highly attractive to use for research purposes due to this organism being easy to culture, both in the axenic setting and on bacteria, the genetic tractability, and the haploid genome, which has been completely sequenced (Cardelli 2001, Eichinger et al. 2005). Crucially, numerous mechanistic molecules involved in both macropinocytosis and phagocytosis are highly conserved between *D. discoideum* and the professional mammalian phagocytes (Cardelli 2001, Dunn et al. 2018). This makes *D. discoideum* a highly attractive model organism to use for studying cellular trafficking, and the functions of the innate immune system (Steinert et al. 2003, Dunn et al. 2018).

Most of the small GTPases and actin related proteins, which regulate actin dynamics including SCAR/WAVE, WASP, and WASH are conserved in *D. discoideum* and display the same functional roles during macropinocytosis and phagocytosis (Annesley and Fisher 2009). Despite these similarities however, there are some differences; *D. discoideum* does not possess any homologues of either Cdc42 or the Rho proteins, even though this organism encodes 14 different Rac homologues. Interestingly, in *D. discoideum* some Rac proteins possess divergent functional

roles, which indicate that some of these functionally divergent Rac proteins could potentially fulfil the roles of Cdc42 and the Rho proteins (Wilkins and Insall 2001). As an example, RacG has been proposed to perform a similar function to that of Cdc42 (Somesh et al. 2006).

Whilst the GPCR effectors are themselves highly conserved within *D. discoideum*, the receptors themselves display differences from their mammalian counterparts. Well-known examples include that of the Fc gamma Receptor (FcγR) and the receptor tyrosine kinases both of which are absent in *D. discoideum* (Insall 2005). *D. discoideum* instead possesses a family called the Sib protein family, which shares domain organisation with the mammalian integrin-β and can establish interactions with talin (Cornillon et al. 2006). *D. discoideum* also possesses homologues of the mammalian scavenger receptors, a notable example includes the Lysosomal membrane glycoprotein B (LmpB), which has been proposed to be a phagocytic receptor (Dunn et al. 2018). Interestingly, GPCRs within this organism have been implicated in coordinating both phagocytosis and chemotaxis, a fairly recent example includes the seven-transmembrane folic acid receptor 1 (fAR1) (Pan et al. 2016).

D. discoideum are professional phagocytes that frequently engulf pathogens, undergo constitutive macropinocytosis, and are easy to modify at the genetic level. This collectively makes *D. discoideum* a fantastic and highly robust model organism to use to tackle various unanswered questions of how PIPs and actin govern phagocytosis and macropinocytosis. Importantly, *D. discoideum* possesses a single orthologue of OCRL, Dd5p4, which avoids the problems in mammals whereby the disruption of OCRL could be masked by the highly similar INPP5B, which thus makes *D. discoideum* an ideal model organism to use (Loovers et al. 2003, 2007, Luscher et al. 2019). Dd5p4 is itself one of five inositol 5-phosphatases that are encoded by *D. discoideum* (Loovers et al. 2003) and will be subsequently compared to the other inositol 5-phosphatases expressed in this model organism.

1.7.2. **An overview of the inositol 5-phosphatases in *D. discoideum***

Five inositol 5-phosphatases have so far been discovered within *D. discoideum*, which include *Dictyostelium discoideum* 5-phosphatase 1 (Dd5p1), *Dictyostelium discoideum* 5-phosphatase 2 (Dd5p2), *Dictyostelium discoideum* 5-phosphatase 3 (Dd5p3), Dd5p4, and the Phospholipid-Inositol Phosphatase (PLIP) (Loovers et al. 2003, Merlot et al. 2003). Dd5p1 shares a lot of sequence similarity with the SHIP2 phosphatase, however Dd5p1 lacks the N-terminal Src Homology two (SH2) domain, whilst Dd5p2 is unique in that it possesses both a Regulator of Chromosome Condensation 1 (RCC1) domain along with the 5-phosphatase catalytic domain (Fig. 1.17.). Dd5p3 displays homology with the mammalian Synaptojanin, with Dd5p3 possessing a Sac1

domain, whilst Dd5p4 displays homology with mammalian OCRL and mammalian INPP5B (Fig. 1.17.) (Loovers et al. 2003). The PLIP enzyme, however does not behave as a classical inositol 5-phosphatase, as PLIP does not possess the classical conserved motifs I and II. The protein sequence of PLIP displays a greater degree of sequence similarity with that of PTEN, but has a substrate preference for PI(5)P *in vitro* (Merlot et al. 2003). A summary of the domain organisation of these five inositol 5-phosphatases in *D. discoideum* is displayed (Fig. 1.17.).

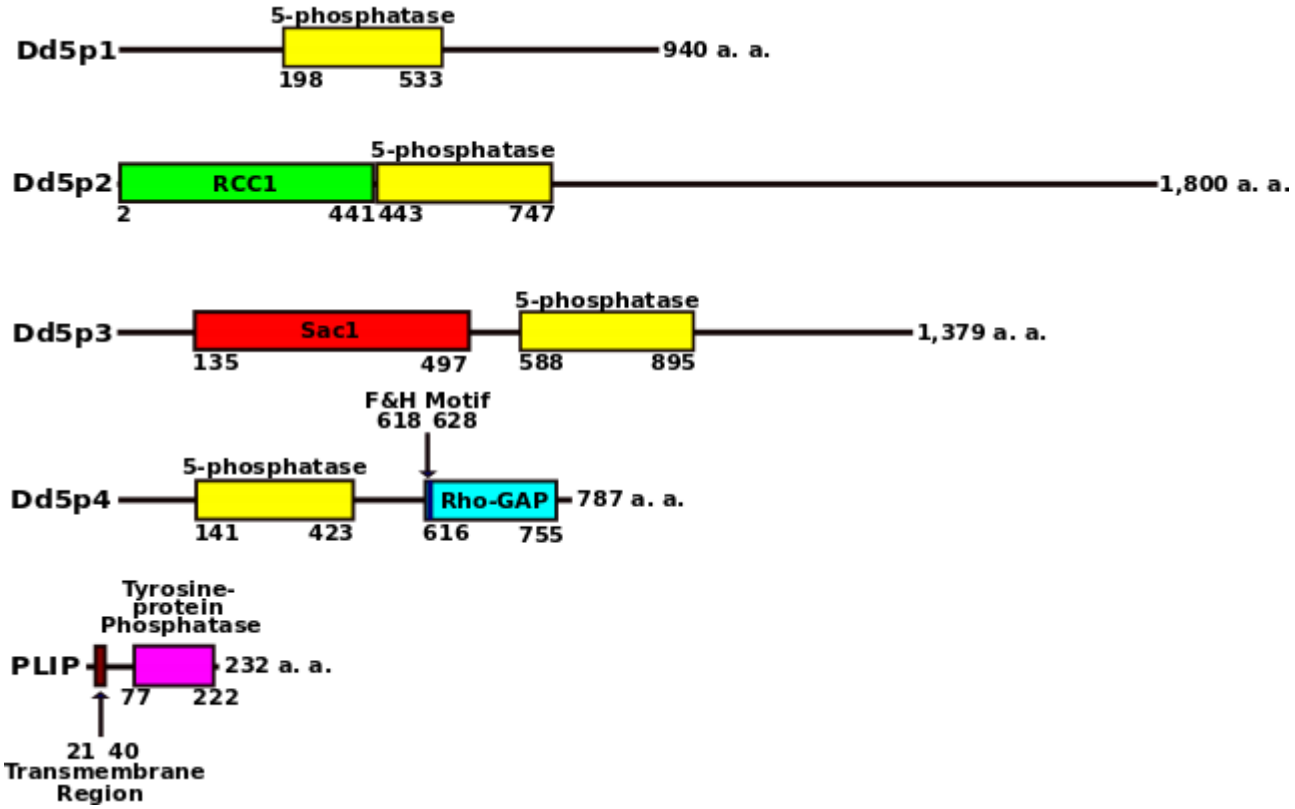

Figure 1.17. The domain structures of the *D. discoideum* Dd5p1-Dd5p4 and the PLIP inositol 5-phosphatases. The amino acid positions of each colour-coded domain and motif are indicated. Adapted from (Loovers et al. 2003).

The catalytic preference of Dd5p1 has so far not been determined due to difficulties in being able to express significant levels of this inositol 5-phosphatase (Loovers et al. 2003). In reference to the water-soluble inositol phosphates Dd5p2, Dd5p3, and Dd5p4 are able to de-phosphorylate Ins(1,4,5)P_3 and Ins(1,3,4,5)P_4, with Dd5p3 displaying the greatest preference for de-phosphorylating Ins(1,4,5)P_3 to Ins(1,4)P_2, and Dd5p2 for de-phosphorylating Ins(1,3,4,5)P_4 to Ins(1,3,4)P_3 (Loovers et al. 2003). PI(4,5)P_2 is de-phosphorylated to PI(4)P by Dd5p2-Dd5p4, and PI(3,4,5)P_3 is de-phosphorylated to PI(3,4)P_2 by Dd5p4, and in particular by Dd5p2, but not by Dd5p3 (Loovers et al. 2003).

Dd5p4 can hydrolyse both PI(4,5)P_2 and PI(3,4,5)P_3 (Loovers et al. 2003). The conversion of one Dd5p4 substrate, PI(4,5)P_2, to the other substrate, PI(3,4,5)P_3, occurs at membrane ruffles and

indicates that PI3Ks play a crucial role in the regulation of endocytosis within this model organism. The *D. discoideum* PI3Ks will thus be subsequently covered and compared to their mammalian counterparts.

1.7.3. An overview of the PI3Ks and the comparison between mammals and *D. discoideum*

PI3Ks function to phosphorylate the D3 position of the *myo*-inositol ring of PIPs and thus make them function as ligands and regulators for a variety of proteins. There are eight PI3Ks that are encoded within *H. sapiens* (Fig. 1.18.A.) (Engelman et al. 2006), and seven that are encoded within *D. discoideum* (Fig. 1.18.B.) (Takeda et al. 2007). This family of enzymes are divided into three main classes within mammals based on their sequence homology and substrate preferences (Table 1.1.) (Fig. 1.18.A.) (Cantley 2002, Fox et al. 2020). In mammals the PI3K Class I enzymes can be further subdivided based on their regulatory subunits. The PI3K Class IA enzymes possess either the p85α, p85β, p55α, p55γ, or p50α regulatory subunits and are normally activated by growth factor receptor tyrosine kinases (RTKs) (Tsolakos et al. 2018), whereas Class IB PI3K enzymes possess either the p101 or p84 regulatory subunits and are typically activated by GPCRs (Table 1.1.) (Vadas et al. 2013).

Table 1.1. The Classification of Mammalian PI3Ks.

PI3Ks Enzyme Class	Catalytic Subunits	Regulatory Subunits	PIP Substrates
IA	p110α, p110β, p110δ	p85α, p85β, p55α, p55γ, p50α	PI, PI(4)P, PI(4,5)P_2
IB	p110γ	p101, p84	PI, PI(4)P, PI(4,5)P_2
II	PI3KC2α, PI3KC2β, PI3KC2γ		PI, PI(4)P
III	Vps34	P150	PI

Table adapted from (Fox et al. 2020).

In mammals Class I PI3Ks are crucial for the generation of PI(3,4,5)P_3 and thus the activation of the kinase activity of Akt, which governs numerous pathways such as the mammalian Target Of Rapamycin (mTOR) pathway (Burgering and Coffer 1995, Franke et al. 1995, Nobukuni et al. 2005) and the Forkhead box O (FOXO) pathway (Biggs et al. 1999, Brunet et al. 1999, Kops et al. 1999). This allows Class I PI3Ks to regulate the processes of cell survival (Brunet et al. 1999), proliferation (Fruman et al. 1999), growth, and metabolism (Foukas et al. 2006). The localisation of the kinase activities of these Class I PI3Ks is also crucial in the regulation of cortical F-actin dynamics, which

underlies the phagocytosis of large particles and chemotaxis (Wennstrom et al. 1994, Leverrier et al. 2003, Tamura et al. 2009). Class II PI3Ks, such as PI3KC2α plays a role in CME in which it interacts with clathrin via its N-terminal clathrin box motif (Gaidarov et al. 2001) leading to the generation of a local pool of PI(3,4)P_2, which is required for CCP maturation (Posor et al. 2013). The generation of PI(3,4)P_2 results in the recruitment of the curvature-inducing SNX9 protein and also the Sorting Nexin 18 (SNX18) protein in some other cell types, which results in the constriction of the membrane at the neck of CCPs, forming a template for the next stage of Dynamin GTPase-mediated membrane scission and subsequent vesicle release (Posor et al. 2013, Schoeneberg et al. 2017). To further support the role of PI(3,4)P_2 in membrane fission PI(3,4)P_2 functions to enhance the activity of the flat BAR domain protein called the FCH and double SH3 Domains 2 (FCHSD2), which results in the stimulation of branched actin filament formation at the flat membrane that encircles the CCP (Almeida-Souza et al. 2018). PI3KC2β appears to also play a role in CME, although the precise location of clathrin binding within the N-terminal region of this protein has not been specified (Wheeler and Domin 2001, Aung et al. 2019), PI3KC2γ however, lacks the ability to bind to clathrin (Fig. 1.18.A.) (Rozycka et al. 1998). The sole Class III PI3K member, Vps34, functions in collaboration with numerous other protein complexes to stimulate the production of PI(3)P within various subcellular compartments. Vps34 regulates processes such as phagocytosis (Berger et al. 2010), macropinocytosis (Filippakis et al. 2018), endosomal sorting (Zhou et al. 2010, Morel et al. 2013, Rostislavleva et al. 2015), and autophagy (Itakura et al. 2008, Sun et al. 2008).

In *D. discoideum*, six of the seven PI3Ks are Class I enzymes, whilst additionally possessing a single Class III Vps34 kinase. The first three Class I PI3Ks that were identified in *D. discoideum* are known as *D. discoideum* PI3K1 (DdPI3K1) encoded by *pikA*, *D. discoideum* PI3K2 (DdPI3K2) encoded by *pikB*, and *D. discoideum* PI3K3 (DdPI3K3), which is encoded by *pikC* (Zhou et al. 1995). These three Class I PI3Ks function as the major PI(3,4,5)P_3 producers during cyclic Adenosine Monophosphate (cAMP)-stimulated chemotaxis in *D. discoideum* (Takeda et al. 2007) with DdPI3K1 and DdPI3K2 also playing a crucial role in the generation of PI(3,4,5)P_3 during macropinocytic cup formation (Hoeller et al. 2013). Both DdPI3K1 and DdPI3K2 kinases also preferentially bind to activated RasG and RasS over other Ras proteins, whilst DdPI3K3 on the other hand preferentially binds to activated RasB, RasD, RasG, and Rap1, with minimal binding occurring with RasS (Hoeller et al. 2013). The fourth *D. discoideum* PI3K known as *D. discoideum* PI3K4 (DdPI3K4), which is encoded by *pikF* (Takeda et al. 2007), has been shown to play a role in the generation of vesicles after macropinocytic cup closure (Hoeller et al. 2013). DdPI3K4 exhibited a strong binding preference to activated RasG, whilst also being able to establish less potent interactions with activated RasB, RasD, RasS, and Rap1 (Hoeller et al. 2013). The fifth *D. discoideum* PI3K, *D. discoideum* PI3K5 (DdPI3K5) is encoded by *pikG*, which

has weaker binding preferences for RasB, RasD, RasG, and Rap1 (Hoeller et al. 2013). The sixth *D. discoideum* PI3K, *D. discoideum* PI3K6 (DdPI3K6), which is encoded by *pikH* is unique compared to the other PI3Ks in this organism as it lacks the Ras-Binding Domain (RBD) and instead has a PH domain in its place (Fig. 1.18.B.) (Takeda et al. 2007). The DdPI3K6 kinase domain also shares some homology with the Class III Vps34 kinase domain (Takeda et al. 2007). The Class III *D. discoideum* Vps34 (DdVps34) kinase encoded by *pikE* is a putative homologue of the *S. cerevisiae* Vps34 kinase, which has been shown to be important for the growth of *D. discoideum* on bacteria but not in liquid culture (Zhou et al. 1995). The comparison of the domain organisations of the catalytic subunits of *H. sapiens* and *D. discoideum* PI3Ks is displayed (Fig. 1.18.A-B.).

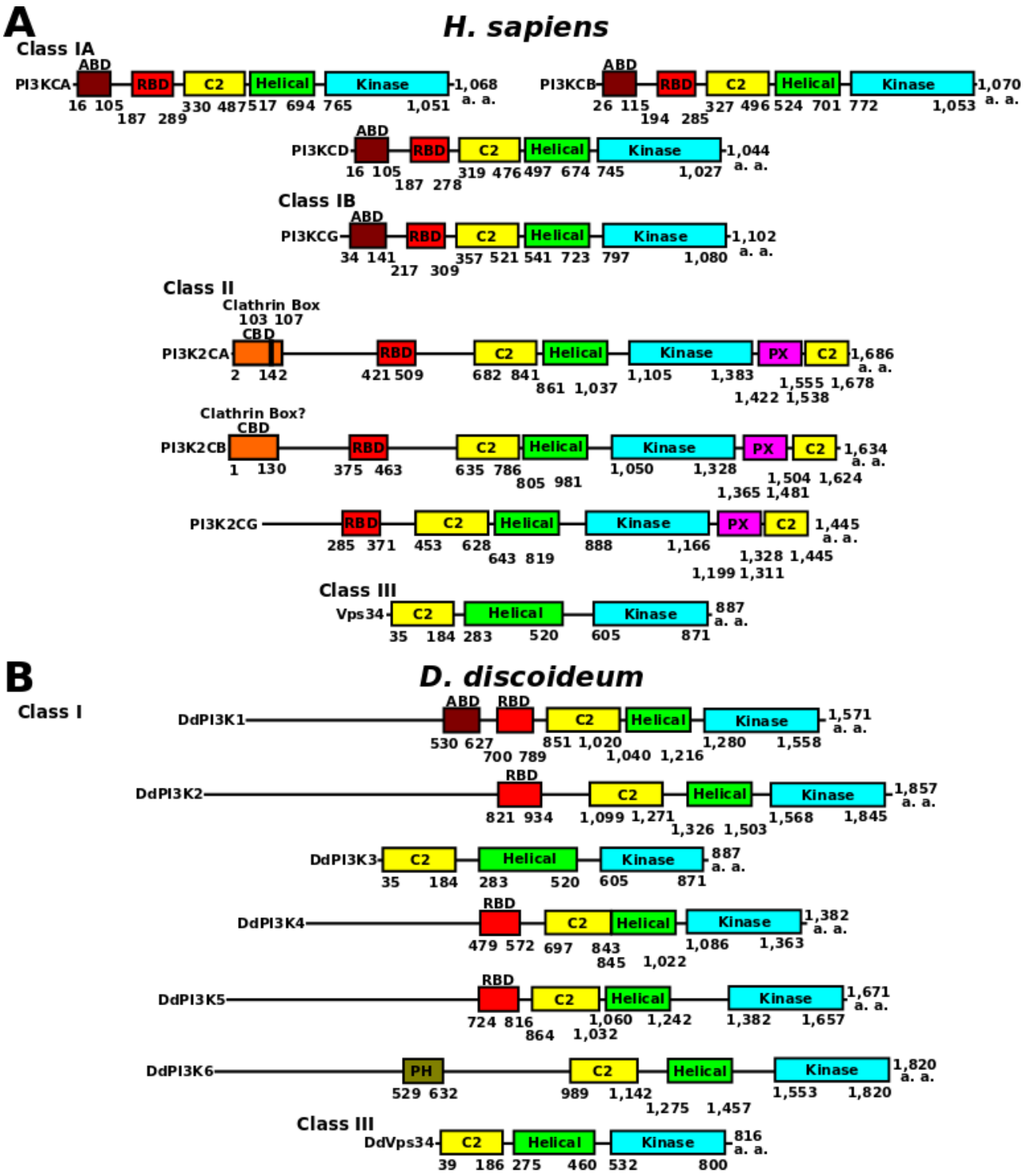

Figure 1.18. The domain organisation of the catalytic subunits of the PI3Ks in *H. sapiens* and *D. discoideum*. (A) Domain organisation and the classes of PI3Ks in *H. sapiens*. Each individual domain and motif is indicated by coloured rectangles as well as the positions of each located within each protein. (B) Domain organisation and the classes of PI3Ks in *D. discoideum*. Adaptor-Binding Domain (ABD), Clathrin-Binding Domain (CBD). Adapted from (Takeda et al. 2007, Vanhaesebroeck et al. 2010, Bilanges et al. 2019).

1.7.4. A comparison between *D. discoideum* and mammalian PIPs

PIPs within *D. discoideum*, just like in mammals, are crucial in governing the processes of phagocytosis and macropinocytosis. These lipids are very similar in *D. discoideum* to those observed in mammals, except that the lipid ligated to the *sn*-1 part of the glycerol backbone is attached

through an ether bond, in place of an ester bond, which is present in mammals (Fig. 1.19.A-B.). In *D. discoideum*, these lipids are known as Plasmanylinositol Phosphates (PIPs), whilst in mammals they are known as Phosphatidylinositol Phosphates (Fig. 1.19.A-B.). Plasmanylinositol phosphates in this social amoeba most often exist with a C16:0-ether, C18:1-acyl glycerol backbone (Clark et al. 2014). The molecular structure comparisons of phosphatidylinositol phosphates and plasmanylinositol phosphates is illustrated (Fig. 1.19.A-B.).

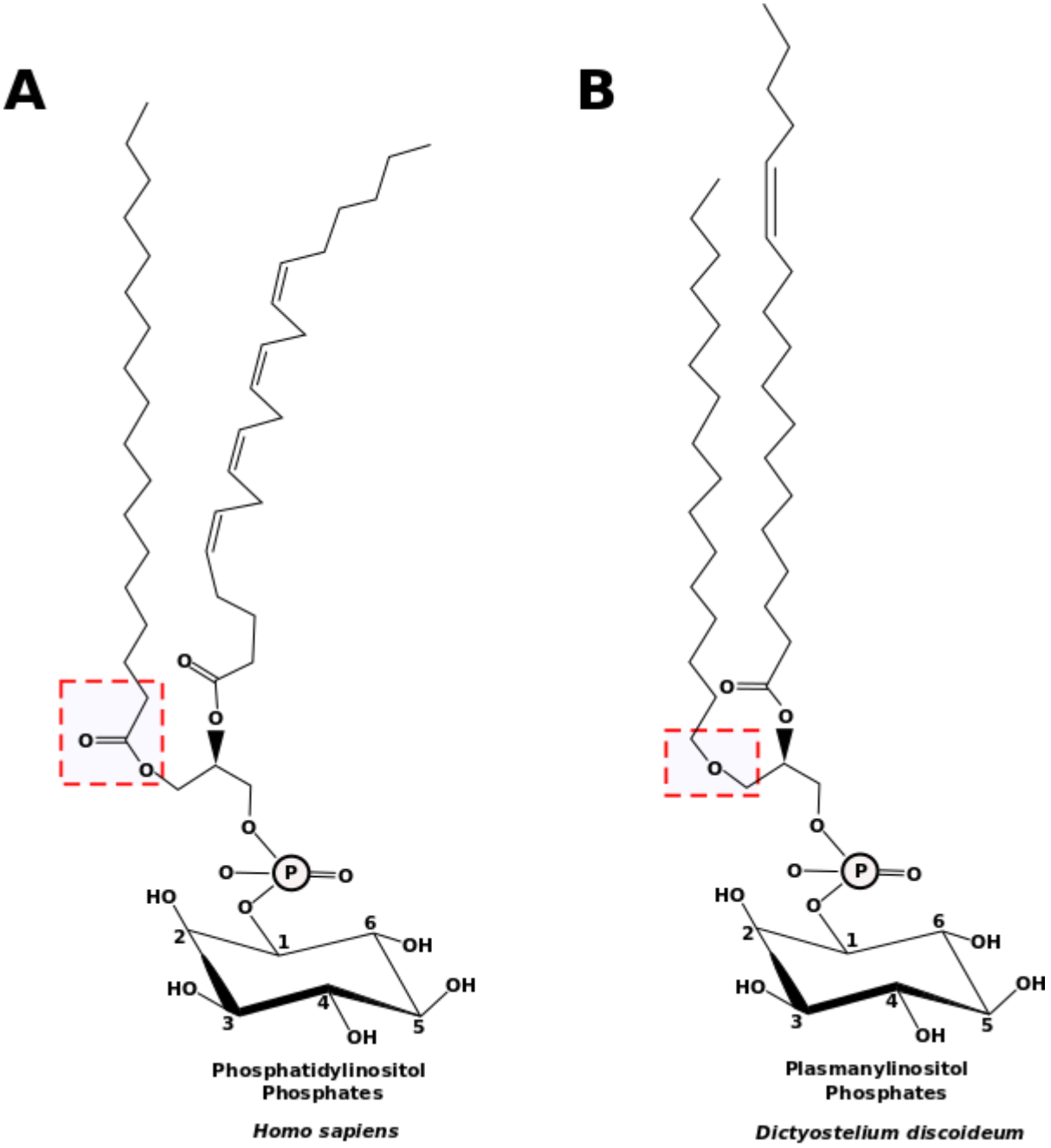

Figure 1.19. The molecular structure of phosphatidylinositol phosphates *H. sapiens* and plasmanylinositol phosphates in *D. discoideum*. (A) *H. sapiens* phosphatidylinositol phosphates have the lipid tail joined at the *sn*-1 position of the glycerol backbone by an ester linkage indicated by a red dashed box. The ester linkage itself has the chemical composition by which a carbon atom links to an oxygen atom by a double bond, another oxygen by a single bond, and another carbon (or alkyl group) by a single bond. (B) *D. discoideum* plasmanylinositol phosphates have the lipid tail joined at the *sn*-1 position of the glycerol backbone by an ether linkage indicated by a red dashed box. The ether linkage itself has the chemical composition by which an oxygen atom is linked by two single bonds to two carbon atoms (or alkyl groups). Adapted from (Clark et al. 2014, Posor et al. 2022).

The differences in chemical structure between phosphatidylinositol phosphates and plasmanylinositol phosphates does not appear to have any effect on downstream signalling events as most interactions occur with the *myo*-inositol head group not the lipid chains. *D. discoideum* has itself been used extensively in the study of PIP signalling events (Dormann et al. 2004, Kortholt et

al. 2007, King et al. 2009, Calvo-Garrido et al. 2014). In this project, the PIPs acronym will refer to plasmanylinositol phosphates, unless otherwise stated.

1.8 The stages of endocytosis in *D. discoideum*

1.8.1. The construction of phagocytic and macropinocytic cups

The creation of both phagocytic and macropinocytic cups centres on the localised polymerisation of actin at the PM through utilising the equivalent actin machinery that creates both pseudopods and lamellipodia during cell migration (Swanson 2008, King and Kay 2019). The creation of a cup is more complex than a migratory protrusion however, with the protrusive activity limited to a ring shape, which surrounds a static interior domain. In phagocytosis, this occurs around a solid particle or object, driven by the localised activation of receptors, and the formation of cups *de novo*. In contrast however, macropinocytic cups self-organise with an almost identical geometry in the absence of any spatial external cues (Veltman et al. 2016). The creation of cups can therefore take place spontaneously through the intrinsic dynamics of the underlying signalling. Unlike phagocytic cups, macropinocytic cups do not always form *de novo* in *D. discoideum* and instead a cup can split creating more macropinocytic cups (Veltman et al. 2016). The formation of cups in *D. discoideum* has been proposed to occur by which the cup interior is outlined by the spontaneous localised activation of Ras (Veltman et al. 2016).

1.8.2. Cup protrusion and membrane extension

The creation of a cup shaped protrusion requires coordinated alterations in both the PM and the actin cytoskeleton over both space and time. The machinery that is utilised to generate phagocytic and macropinocytic cups are very similar overall. A feature that is common in both mechanisms of cup formation includes the protrusion of the membrane and the polymerisation of actin that creates the force that is needed to push the membrane forwards.

1.8.3. Driving protrusions at the tips of macropinocytic and phagocytic cups

$PI(3,4,5)P_3$ is a universal organiser of cups and is synthesised by PI3Ks, which are activated by Ras (Swanson 2008). The Ras superfamily of small GTPases function as essential regulators of actin polymerisation during the formation of phagocytic and macropinocytic cups (Swanson 2008). Generally, small GTPases can adopt one of two forms, either the Guanosine Diphosphate (GDP)-bound inactive form or the GTP-bound active form. The inactive GDP-bound state is converted into the active GTP-bound form via guanine nucleotide exchange factors (GEFs), which facilitates the removal of GDP. The active form is transformed into the inactive form through GTP hydrolysis, which

is orchestrated by the GTPase activating proteins (GAPs). In *D. discoideum* the activities of RasG and RasS have been shown to be crucial in macropinocytosis through binding via their RBDs and activating the PI3K1/2 kinases needed for ruffle formation, resulting in the generation of PI(3,4,5)P_3, which forms a patch of Ras/PI(3,4,5)P_3 (Hoeller et al. 2013). RasS may be activated by the GEF called the Guanine nucleotide exchange factor B (GefB) (Wilkins et al. 2000, King and Insall 2003), whilst RasG is activated by the Guanine nucleotide exchange factor F (GefF) (Williams et al. 2019). These Ras proteins may be inactivated by the GAP activity of NF1, which is localised throughout the cup and is crucial during cup formation as NF1 GAP activity is required to restrict the size of cups via the local inhibition of Ras signalling, and thus controls both macropinocytosis and phagocytosis (Bloomfield et al. 2015). The Rac1 GTPase overlaps with the activity of Ras in the cup interior (Veltman et al. 2016). Rac1A, Rac1B, and Rac1C are direct activators of SCAR once recruited to the periphery of PI(3,4,5)P_3 patches, resulting in Arp2/3-mediated actin polymerisation (Dumontier et al. 2000, Veltman et al. 2016). It is crucial to note that Rac overlaps with SCAR and not WASP at the rim in *D. discoideum* in order to activate SCAR alone (Veltman et al. 2016), whilst WASP is localised to the periphery of PI(3,4,5)P_3 patches at the rim and is activated by PI(4,5)P_2 and PI(3,4,5)P_3 (Myers et al. 2005, Veltman et al. 2016). These studies collectively suggest that these mechanisms must be in place to restrict the localisation of active SCAR and active WASP only to the rim of cups during their formation in order to generate the correct cup shape.

The activities of Ras and Rac are themselves controlled and coordinated during cup formation by the multi-domain protein called the RCC1, Rho-GEF, BAR, and Ras-GAP-containing protein (RGBARG) (Buckley et al. 2020). This protein dictates the shape of cups at the tip by expanding the profile of active Rac at the tips of cups whilst suppressing the activity of Ras within the cup interior (Buckley et al. 2020).

1.8.4. Signalling events at the base of cups and during cup closure

The closure of both phagocytic and macropinocytic cups involves the fusion of membranes from the cup rim in order to seal the contents to be internalised. PI3K4, which generates PI(3,4,5)P_3 has been shown to be crucial for successful cup closure, as *PI3K4*$^-$ mutant cells had a three-fold reduction in being able to successfully close their cups compared to control cells (Hoeller et al. 2013). Interestingly, in the context of phagocytosis, the complete absence of PI3K1-PI3K5 still allowed the phagocytosis of beads that were 1 µm in diameter and bacteria, which suggested that PI3Ks were not essential for the phagocytic engulfment of small particles (Hoeller et al. 2013). Phagocytosis of larger particles did however, require PI3K for successful phagocytic engulfment in macrophages through the termination of actin assembly (Schlam et al. 2015). It has been shown

that the enzymatic activity of the inositol 5-phosphatase, Dd5p4, was crucial for the successful completion of phagocytic cup closure, suggesting that PI(3,4,5)P_3 and PI(4,5)P_2 hydrolysis may be important for this process (Loovers et al. 2007). Dd5p4 hydrolysis of PI(4,5)P_2 is one method by which PI(4,5)P_2 is depleted at the base of the cup. Other routes occur via phosphorylation of PI(4,5)P_2 to PI(3,4,5)P_3 by PI3K4 (Hoeller et al. 2013), and the degradation of PI(4,5)P_2 to Ins(1,4,5)P_3 and DAG through *Dictyostelium discoideum* phospholipase C (DdPLC) activity (Drayer et al. 1994). PI(4,5)P_2 depletion at closure is essential for the removal of the inhibition of *D. discoideum* cofilin, which thus allows severing of actin filaments and thus the transportation of material through the cortex (Aizawa et al. 1995, Gorbatyuk et al. 2006). Dd5p4, which has been mentioned previously will form the core of this PhD project and will be discussed in more detail in the introduction section of chapter three.

1.9 The Dd5p4 F&H interactors in *D. discoideum*

The first Dd5p4 F&H interactor, the OCRL-Interacting Bar domain Protein (OIBP), will be referred in this project as the early APPL1-like endocytic adaptor as this was related in its domain structure to mammalian APPL1 (Luscher et al. 2019). The second Dd5p4 F&H interactor, the PH domain Interacting with OCRL (PIO), will be referred in this project as the later Ses1/2-like endocytic adaptor as it was related in its domain structure to mammalian Ses1/2 (Luscher et al. 2019). In mammals, Frabin was identified as another OCRL F&H interactor, however in *D. discoideum* there were four Frabin-like proteins that were expressed with only the Guanine exchange factor for Rac U (GxcU) having an F&H motif, which could bind to the OCRL homologue, Dd5p4 (Luscher et al. 2019). The Dd5p4 F&H interactors will be discussed in more detail in the introduction section of chapter four.

1.10 An overview of the WASP proteins in *D. discoideum*

In *D. discoideum* there are three WASP orthologues, which localise to CCPs and were found to be associated with actin polymerisation; WasA, WasB, and WasC (Myers et al. 2005, Chung et al. 2013, Jeon and Jeon 2020). The domain composition of each of these proteins is illustrated (Fig. 1.20.).

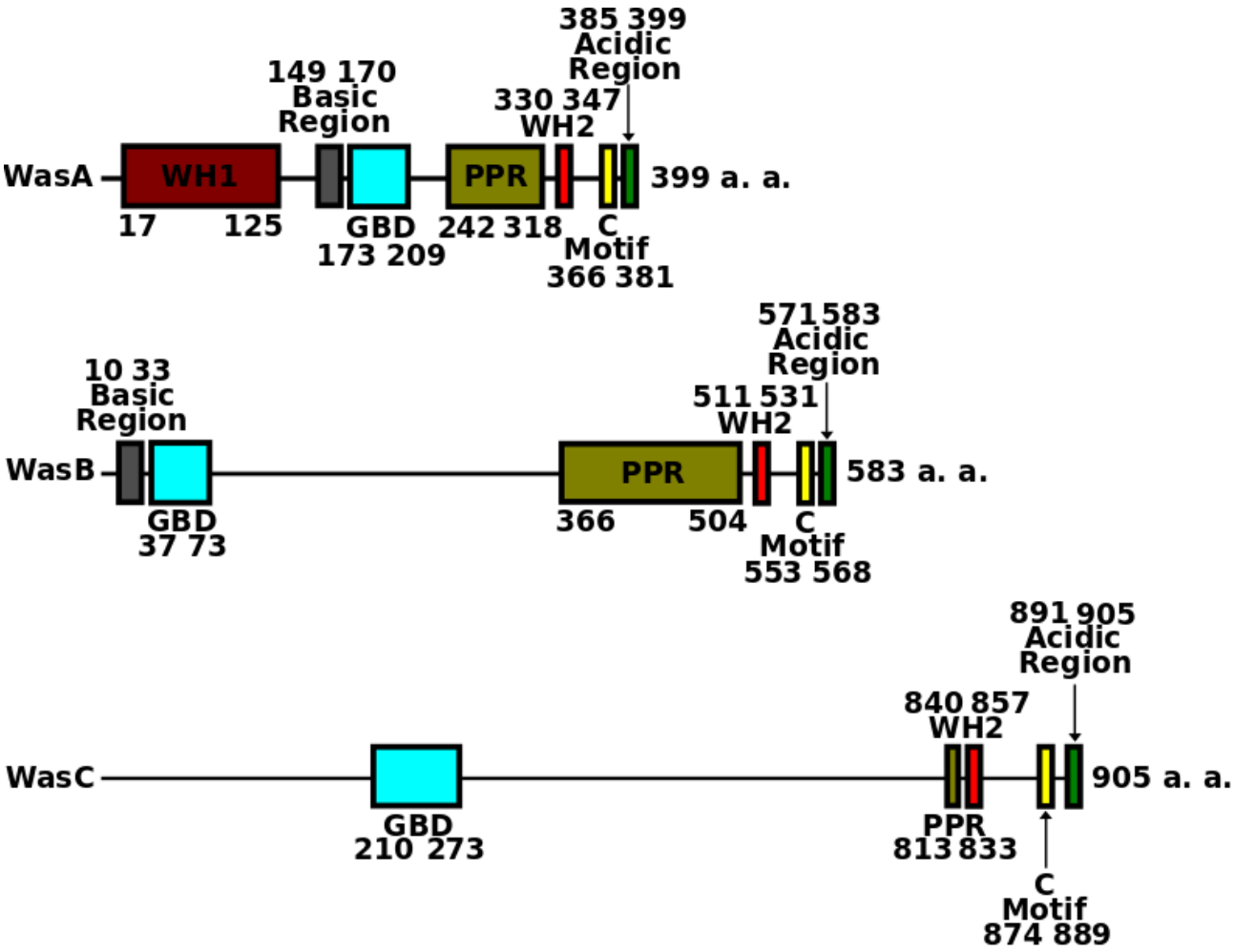

Figure 1.20. The domain composition of the three *D. discoideum* WASP proteins. WasA has an N-terminal WH1 domain (maroon), which is not present in any of the other WASP proteins. A basic region (grey) is located near to the centre of WasA, with an N-terminal basic region located in WasB, these bind to negatively charged PIPs. All proteins possess a GTPase binding domain/Cdc42 and Rac interactive binding domain (GBD/CRIB), within which the CRIB motif is located, which binds Rac proteins, including RacC. PPRs (olive) are in all proteins with WasC having a very limited PPR. C-terminal catalytic VCA domains are located in all three WASP proteins, which encompass the WH2 domain (red), the C motif (yellow), and the acidic region (green). This region binds to actin and the Arp2/3 complex, and leads to Arp2/3 complex activation. Each individual domain/motif are indicated by coloured rectangles as well as the positions of each located within each protein. Adapted from (Miki et al. 1998b, Marchand et al. 2001, Kelly et al. 2006, Dominguez 2007, Veltman and Insall 2010).

The roles of WasA in *D. discoideum* will be covered in more detail in the introduction and discussion sections of chapter five. WasB and WasC, despite both lacking the WH1 domain (Fig. 1.20.) could both still localise to CCPs and thus play a role in CME (Veltman and Insall 2010). This stated that both WasB and WasC possessed all the regulatory sequences that were required for localisation to CCPs (Veltman and Insall 2010).

This PhD project was to be split into three sections: chapter three will focus on how Dd5p4 regulates PIP and F-actin dynamics during endocytosis and to understand how actin comets were

formed, chapter four will seek to explore how the Dd5p4 F&H interactors governed endocytosis, with chapter five investigating the roles of the WASP proteins during endocytosis.

1.11 Project aims

1.11.1. Aims of chapter three

- Are the same *Dd5p4*$^-$ endocytic defects that were observed in the Ax3 strain also seen in the Ax2 strain?
- How crucial are the Dd5p4 catalytic and Dd5p4 F&H motifs for the successful completion of phagocytosis?
- How are the dynamics of macropinocytosis altered in *Dd5p4*$^-$?
- How is the time taken to enwrap yeast and internalise phagosomes altered in *Dd5p4*$^-$? What is the cause of phagocytic failure and what is the phagocytic failure rate of these mutants?
- How are the levels of $PI(4,5)P_2$ depletion across the cups altered in *Dd5p4*$^-$ at different stages towards cup closure during phagocytosis and macropinocytosis?
- How are the dynamics of $PI(3,4,5)P_3$ $PI(3,4)P_2$, $PI(4,5)P_2$, PI(4)P, and PI(3)P on macropinosomes altered after cup closure in *Dd5p4*$^-$?
- How are the temporal dynamics of macropinocytic PIPs and F-actin altered during the early stages of macropinocytosis in *Dd5p4*$^-$?
- How do F-actin 'comets' arise in *Dd5p4*$^-$ and what specific PIPs and actin regulators are localised to these comets?

1.11.2. Aims of chapter four

- Do single mutants of the Dd5p4 F&H interactors display reduced levels of phagocytosis?
- Is the time taken to enwrap yeast and internalise phagosomes altered in the single mutants of the Dd5p4 F&H interactors? What is the phagocytic failure rate?
- How does the severity of the *GxcU*$^-$ phagocytic defects compare to that of *Dd5p4*$^-$?
- What is the phagocytic phenotype of the *Dd5p4*$^-$ *GxcU*$^-$ double mutants? Is the time taken to enwrap yeast and internalise phagosomes altered? What is the phagocytic failure rate?
- How are the dynamics of macropinosomes altered in all mutants of the Dd5p4 F&H interactors?
- Are the lengths of macropinocytic cups altered in *GxcU*$^-$ mutants?
- Is there evidence of altered localisation of *D. intermedium* GxcU-GFP in *Dd5p4*$^-$, *GxcU*$^-$, and *Dd5p4*$^-$ *GxcU*$^-$ in the Ax2 genetic background? How does this compare with previous studies in Ax3?

1.11.3. Aims of chapter five

- How does WasA regulate macropinocytosis at cup closure?
- How are the tether dynamics in the *WasA*$^{-}$ single mutants altered after macropinocytic cup closure?
- How was the bulk uptake of fluid altered in the *WasA*$^{-}$ single mutants? How was the bulk uptake of fluid altered in the *WasA*$^{-}$ *WasB*$^{-}$ double mutants?
- How were the dynamics of macropinosomes altered in the *WasA*$^{-}$ single and *WasA*$^{-}$ *WasB*$^{-}$ double mutants?
- Do the *WasA*$^{-}$ single mutants and the *WasA*$^{-}$ *WasB*$^{-}$ double mutants display reduced levels of phagocytosis?
- Was the time taken to enwrap yeast in *WasA*$^{-}$ single and *WasA*$^{-}$ *WasB*$^{-}$ double mutants altered? Was the time taken to internalise phagosomes altered in these WASP mutants? Did the *WasA*$^{-}$ *WasB*$^{-}$ double mutants display a more severe phagocytic failure rate than the *WasA*$^{-}$ single mutants?

Chapter 2

Materials and Methods

2.1. *Dictyostelium discoideum* cell culture

Adhered *D. discoideum* cells were grown in 9 cm Sterilin Petri dishes (Thermo Scientific) in filter sterilised HL-5 nutrient-rich media (peptone, yeast extract, KH_2PO_4, Na_2HPO_4) with glucose (Formedium) at 22°C. *D. discoideum* are free-living unicellular organisms so regulation of N_2 and CO_2 levels was not necessary (http://dictybase.org/techniques/media/dicty_growth.html). Typically cells became confluent after 2-3 days, after which cells were re-suspended and 2 mL of cell suspension was typically transferred to 8 mL of fresh HL-5 media in a new Petri dish. Transformed cells were grown under the appropriate antibiotic selection by supplementation of either 50 µg/mL Hygromycin B (Invitrogen), 20 µg/mL G418 (Sigma), or 10 µg/mL Blasticidin (Melford). For cell based experiments, cells were normally grown to 80-90% confluence unless otherwise indicated.

2.2. Axenic *Dictyostelium discoideum* transformation

Cells were transformed by electroporation. Approximately one third of a confluent dish (~ 6 x 10^6 cells) were pelleted at 2,000 rpm for 2 minutes. The supernatant was aspirated and cells re-suspended in 0.4 mL of ice cold E-buffer (10 mM KH_2PO_4 pH 6.1, 50 mM sucrose) and were transferred to 2 mm gap electroporation cuvettes containing DNA (0.5 µg for extra-chromosomal plasmids, and 20 µg for linearised knockout constructs) that were kept on ice. Cuvettes were electroporated with a Bio-Rad Gene Pulser II with a 5 Ω resistor connected at 1.2 kV, 3 µF capacitance, with the resistance being set to ∞, with a time constant of approximately 0.3 ms being typically recorded. Following electroporation cells were immediately transferred to Petri dishes containing 10 mL of HL-5 and 10 µg/mL Doxycycline hydrochloride (Fisher) to prevent infections. Electroporated cells were left to recover at 22°C for approximately 24 hours, after which the relevant antibiotic selection was applied and cells were left for ~ 1 week in order for large colonies to form, which would then be cultured as normal.

2.3. Cloning

All the gene sequences that were utilised in this project were obtained from dictybase (http://www.dictybase.org/). All the restriction enzymes and buffers that were used were obtained from NEB. Dd5p4 gene constructs were designed to be compatible with the pDM extra-chromosomal series of vectors (gifted by Douwe Veltman) to allow the C-terminal tagging of the Dd5p4 gene as well as variants of Dd5p4 bearing point mutations. Both the early series of pDM vectors (Veltman et al. 2009) under the influence of an *actin 6* promoter and the more recent series of pDM vectors under the influence of a *coactosin* (*coaA*) promoter (Paschke et al. 2018), were constructed to ensure selection during growth on bacteria. pDM vectors were cleaved by the BglII

and SpeI restriction enzymes in order to allow the insertion of the gene of interest. pDM1045 was utilised for generating Dd5p4 C-terminal fusions with the details of the plasmids created indicated as shown (Table 2.1.).

N-terminal GFP fusions of wild type Dd5p4, and Dd5p4^{W620A} were cloned by PCR from clones in TOPO (gifted by Dr. Laura Swan) using the PrimeSTAR max DNA polymerase (Takara Europe). A BglII restriction site was incorporated into the forward primer and a SpeI restriction site was incorporated into the reverse primer. Plasmid DNA for each construct was used as a template and added to 2x PrimeSTAR max mix, each primer (fw-5'-AGTAGATCTATGGGTGATATTCAAAATACAG-3', rv-5'-GCGACTAGTATTAATTAAATCTTTTGAAATTAAAAAATG-3') (see Table 2.2. for all primers used in this project), and H_2O. The PCR protocol that was utilised was as follows: 95^{o}C for 30 seconds, followed by 35 cycles of 98^{o}C for 10 seconds, 57^{o}C for 15 seconds, and elongation at 72^{o}C for 50 seconds for 10 seconds per Kb.

Dd5p4 PCR products were subsequently run on a 1% agarose gel (Geneflow Ltd), the DNA bands were subsequently excised and the DNA extracted using the Zymo DNA gel extraction kit (Cambridge Bioscience) as per the manufacturer's instructions. The Dd5p4 PCR inserts and the pDM1045 vector backbone were separately digested using BglII and SpeI restriction enzymes. The digested Dd5p4 inserts and pDM1045 vector were run on a 1% agarose gel after which the DNA bands were excised and subsequently extracted using the Zymo DNA gel extraction kit. Extracted DNA were ligated using the T4 DNA ligase (NEB) for 5 hours at room temperature. For ligation reactions a 3:1 ratio of insert to vector was used in order to maximise colony yield. Ligations were then heat shocked at 42^{o}C for 45 seconds into DH5α *E. coli* (lab made) and were plated onto ampicillin (Santa Cruz Biotechnology) LB plates. The next day colonies were picked, and the ligated plasmid DNA isolated using minipreps (Geneflow) as per the manufacturer's instructions, restriction enzyme diagnostic digests were then performed in order to confirm plasmid identity. Dr. Jason King performed cloning of the extra-chromosomal plasmids; PkgE-PH-mCherry TAPP1-PH-GFP co-expression vector (pJSK697), RFP-PH-PkgE GFP-2xFYVE co-expression vector (pJSK698), GFP-WasA RFP-LifeAct co-expression vector (pJSK702), TAPP1-PH-GFP mCherry-LifeAct co-expression vector (pJSK703), GFP-2xFYVE mCherry-LifeAct co-expression vector (pJSK704), PkgE-PH-mCherry Nodulin-GFP co-expression vector (pJSK706), and Nodulin-GFP mCherry-LifeAct co-expression vector (pJSK707) (see Table 2.1. for the complete list of plasmids). Plasmid DNA was then used to transform Ax2 and *Dd5p4*$^{-}$ mutant cells (see section 2.2.).

2.4. Generation of knockouts by homologous recombination

APPL1-like^{-}, *Ses1/2-like*$^{-}$, and *WasA*$^{-}$ single mutants were generated through the incorporation of a Blasticidin resistance cassette into each respective locus by homologous recombination. The Blasticidin knockout cassette cloned by Dr. Laura Swan was targeted to the *APPL1-like* or *Ses1/2-like* loci through performing PCRs on the upstream and downstream regions of the *APPL1-like* or *Ses1/2-like* genes. KpnI restriction enzyme sites were then incorporated into the 5' end of the upstream fragment and the 3'end of the downstream fragment, with these fragments subsequently ligated either side of a Blasticidin resistance gene in the pKOSG-IBA-dicty1 vector backbone (IBA Lifesciences). The provision of these knockout plasmids by Dr. Laura Swan gave the incentive to generate these mutants by homologous recombination. The provided knockout plasmids for *APPL1-like* (DDB_G0275301) and *Ses1/2-like* (DDB_G0280015) would introduce a 2,833 bp deletion into the central region of these genes (See Table 2.3. for the complete information on all the strains used for this project). Prior to *D. discoideum* transformation the knockout cassette was separated from the pKOSG-IBA-dicty1 vector backbone through restriction enzyme digestion with KpnI, and the resulting DNA precipitated. 1/10 of the total volume of 3 M NaAc together with two volumes of 100% ethanol was applied and was incubated at room temperature for 5 minutes before samples were centrifuged at 14,680 rpm for 5 minutes. The resulting supernatant was subsequently removed and the pellet washed and vortexed in 70% (v/v) ethanol and further centrifuged at 14,680 rpm for 1 minute and the residual ethanol removed and the DNA diluted to 1 mg/mL in E-buffer for subsequent *D. discoideum* transformation. 20 µg of the linearised DNA was electroporated into Ax2 cells as described in section 2.2. The next day the electroporated cells were re-suspended and seeded into 4x 96-well plates in the presence of 10 µg/mL Blasticidin. After 14 days colonies formed and were then screened by PCR in order to identify knockout clones (see section 2.6.).

WasA (DDB_G0293834) was disrupted using the same method as the Blasticidin knockout cassette that was targeted specifically to the *WasA* locus was kindly provided by our collaborators (Davidson et al. 2018). The Blasticidin knockout cassette was separated from the pAD94 vector (Davidson et al. 2018) by overnight digestion with SpeI and BglII. The digested knockout cassette was then precipitated and *D. discoideum* Ax2 cells were subsequently transformed and after 24 hours electroporated cells were plated as above and were left to growth for 14 days. The provision of an anti-WASP primary polyclonal antibody by our collaborators (Davidson et al. 2018) meant that screening for mutants via Western blotting was instead performed (see section 2.7.).

2.5. Extraction of genomic DNA

Extraction of gDNA for genotype screening was performed by pelleting ~ 1 x 10^6 cells at 2,000 rpm for 2 minutes. The media was then aspirated and the cell pellet re-suspended in 100 µL of lysis buffer (10 mM Tris-HCl pH 8.0, 50 mM KCl, 2.5 mM $MgCl_2$, 0.45% NP40, 0.45% Tween 20). 2 µL of 20 mg/mL molecular biology grade Proteinase K (NEB) was then added and samples were left at room temperature for 5 minutes after which Proteinase K was heat inactivated at 95°C for 10 minutes.

2.6. Screening of *APPL1-like*$^-$ and *Ses1/2-like*$^-$ knockout mutant clones via PCR

The introduction of the Blasticidin resistance gene into the central region of either the *APPL1-like* or the *Ses1/2-like* loci gave the incentive to screen for mutants containing the Blasticidin resistance gene using PCRs as there were differences in size between the wild-type locus and the mutated locus that could be observed on an agarose gel.

5 µL of extracted gDNA (see section 2.5.) from colonies were thus utilised as a template for PCRs to screen for *APPL1-like*$^-$ and *Ses1/2-like*$^-$ mutants. PCRs were performed using the DreamTaq Hot Start Green PCR Master Mix (2X) (Thermo Fisher), with the standard protocol being followed. Pairs of primers were designed across each targeted locus, with two additional primer pairs also being designed to screen each homology arm together with the Blasticidin resistance gene. For the *APPL1-like* gene the complete Blasticidin resistance gene screen
(fw-5'-GTAAAGCAGCAATTAGAATCACATC-3', rv-5'-GGATTTTTATCATCAAATGGATTTGGTG-3'),
the 5' homology arm and the Blasticidin resistance gene screen
(fw-5'-GTAAAGCAGCAATTAGAATCACATC-3', rv-5'-GTCGTCCATCAATTGTTCACAG-3'),
and the 3' homology arm and the Blasticidin resistance gene screen
(fw-5'-CGCTTCAATATGTACTGCCGAA-3', the Bsr primer rv-5'-GCATTTGAAATTGGTTGTGGTG-3').
For the *Ses1/2-like* gene the complete Blasticidin resistance gene screen
(fw-5'-TTTAAAGGCAACTCAAAAAGGTTTGG-3', rv-5'-AGGAGGACATTGATGGTGATGTAG-3'),
the 5' homology arm and the Blasticidin resistance gene screen
(fw-5'-TTTAAAGGCAACTCAAAAAGGTTTGG-3', rv-5'-GTCGTCCATCAATTGTTCACAG-3'),
and the 3' homology arm and the Blasticidin resistance gene screen
(fw-5'-CGCTTCAATATGTACTGCCGAA-3' Bsr primer rv-5'-CGAACTCATAATTACACCTAAGCG-3').
See Table 2.2 for the complete list of the primers that were used. The PCR products were subsequently run on a 1% agarose gel to diagnose the presence of the KO based on DNA fragment size.

2.7. Screening of *WasA*$^{-}$ mutant clones via Western blot

The provision of a rabbit anti-WASP primary polyclonal antibody, which has been shown to bind to *D. discoideum* WasA (Davidson et al. 2018) meant that Western blotting could be used as an alternative to PCRs for screening for *WasA*$^{-}$ single mutant clones.

1 mL of confluent cells (1 x 10^6 cells per mL) for each potential *WasA*$^{-}$ colony were thus re-suspended and subsequently spun down at 2,000 rpm for 2 minutes. Cells were then re-suspended and lysed in 50 µL of 4x Laemelli sample buffer (0.5 M Tris-HCl pH 8.0, 10% SDS, 10% glycerol, 5% β-mercaptoethanol, and 0.05% bromophenol blue) and samples were subsequently boiled at 100^{o}C for 5 minutes. Samples were then subsequently loaded onto an SDS-PAGE gel and were run at 200 V. Proteins were then transferred onto hybond C 0.45 µm nitrocellulose membranes (Amersham Biosciences) and were subsequently probed by a rabbit anti-WASP primary polyclonal antibody (gifted by Professor Robert Insall) at a 1:5,000 dilution, followed by a 1:20,000 dilution of goat anti-rabbit IgG (H+L) secondary antibody, DyLight^{TM} 800 (Thermo Fisher Scientific SA5-35571) and was subsequently visualised on the LI-COR Odyssey SA. Alexa-680 labelled Streptavidin at a dilution of 1:20,000 was utilised as a loading control against the mitochondrial protein 3-methylcrotonyl-CoA carboxylase α (MCCC1) (DDB_G0287377) (Davidson et al. 2013).

2.8. Generation of *GxcU*$^{-}$, *Dd5p4*$^{-}$ *GxcU*$^{-}$, and *WasA*$^{-}$ *WasB*$^{-}$ mutants using Clustered Regularly Interspaced Short Palindromic Repeats (CRISPR)

Due to the lack of the provision of Blasticidin knockout constructs from our collaborators and a restricted time frame an alternative, more rapid, and fairly recently optimised approach was used to generate *GxcU*$^{-}$, *Dd5p4*$^{-}$ *GxcU*$^{-}$ and *WasA*$^{-}$ *WasB*$^{-}$ mutants as a suitable alternative to homologous recombination. To this end Clustered Regularly Interspaced Short Palindromic Repeats (CRISPR) was performed (Sekine et al. 2018).

A single-guide RNA (sgRNA) 20-nucleotide targeting sequence, which was upstream of the protospacer-adjacent motif (PAM) NGG was designed through importing the genomic *GxcU* (DDB_G0291996) or *WasB* (DDB_G0272811) loci into **http://www.rgenome.net/cas-designer/**. The following rules were then applied to choose an appropriate guide: no TTTT sequences to prevent polIII transcription termination; %GC > 20%; out-of-frame score >65; no other binding sites with 0 or 1 mismatch. The resulting oligonucleotides were generated for GxcU (primers: fw-5'-AGCATTCAAGATAGAATGACGACA-3', rv-5'-AAACTGTCGTCATTCTATCTTGAA-3') and WasB (primers: fw-5'-AAACGAGTGGAGACAATTATTTCA-3', rv-5'-AGCATGAAATAATTGTCTCCACTC-3'). In conjunction, sequencing primers were also designed to amplify the target loci for genotype screening for GxcU (primers: fw-5'-GGTTAATAAAACCAATAGAGATAAAGTTGCA-3', rv-5'-

CCAAACGAATTCTCACTGGTAACT-3') and WasB (primers: fw-5'-TTGACTCTCATAATCCAAGTAAG-3', rv-5'-TATAAATGAATTGAACAGTTTCTGG-3'). Annealing of GxcU or WasB guide oligonucleotides was performed by adding 0.5 µL of 100 µM of each oligonucleotide to 1 uL of 10x annealing buffer (400 mM Tris-HCl pH 8.0, 200 mM $MgCl_2$, 500 mM NaCl) and 8 µL of dH_2O in a final reaction volume of 10 µL, which was then heated to 95°C for 5 minutes and was left to slowly cool to room temperature. Ligated oligonucleotides were annealed into the pTM1285 all-in-one vector using the Golden gate assembly method, which involved adding 0.4 µL of 10x T4 DNA ligase buffer (NEB) (50 mM Tris-HCl pH 7.5, 10 mM $MgCl_2$, 1 mM ATP, 10 mM DTT), 0.6 µL of 25 ng/µL pTM1285 all-in-one vector, 1 µL of annealed GxcU targeting oligonucleotides, 0.2 µL of T4 DNA ligase (NEB), 0.15 µL of BpiI (Thermo) and 1.65 µL of dH_2O in a final reaction volume of 4 µL. The reaction mixture was subjected to 5 cycles of 37°C for 5 minutes --> 16°C for 15 minutes. To the same mixture 0.4 µL of 10x G buffer (Thermo) (10 mM Tris-HCl pH 7.5, 10 mM $MgCl_2$, 50 mM NaCl, 0.1 mg/mL BSA) and 0.1 µL of BpiI was added and the contents subjected to 37°C for 60 minutes followed by 80°C for 5 minutes. Only circularised plasmids would successfully confer ampicillin resistance to DH5α *E. coli* that were heat transformed and plated on ampicillin resistant LB plates. Correct ligations were then verified by bacterial colony PCRs by picking 4x colonies and a smear from each transferred into separate 20 µL PCR reaction mixtures each consisting of 10 µL DreamTaq Hot Start Green PCR Master Mix (2X), 0.5 µL of 10 µM gene-specific forward targeting primer, 0.5 µL of 10 µM of the end of the sgRNA (primer rv-5'-AAGCTTAAAAAAAGCACCGACTCGGTGCC-3') and 9 µL of dH_2O. The PCR protocol that was used was as follows: initial denaturation at 95°C for 2 minutes, with 30 cycles of denaturation at 95°C for 15 seconds, annealing at 55°C for 15 seconds, and elongation at 72°C for 10 seconds. The resulting PCR products were then screened on a 2% agarose gel, and a colony that was positive for the gene-targeting sgRNA was grown in 250 mL of LB with 50 µg/mL ampicillin at 37°C and was shaken at 200 rpm for approximately 16 hours overnight. The plasmid DNA was extracted using the ZymoPure Kit, see manufacturer's instructions. The GxcU targeting sgRNA were then electroporated into Ax2 cells to generate *GxcU*$^-$ single mutants, and *Dd5p4*$^-$ mutants to generate *Dd5p4*$^-$ *GxcU*$^-$ double mutants. The WasB targeting sgRNA was electroporated into *WasA*$^-$ single mutants to generate *WasA*$^-$ *WasB*$^-$ double mutants. Electroporation was performed as described in section 2.2., this was done three times in parallel to test different antibiotic concentrations in conjunction with a negative control at the transient G418 selection stage. 24 hours after electroporation cells were split into 3x dishes and were administered either a final concentration of 10, 15, or 20 µg/mL G418 for 72 hours, after which selection was removed and the cells left to grow for a further 72 hours in fresh HL-5 liquid media lacking G418. After this stage, colonies were washed twice using fresh HL-5 and were re-suspended in 1 mL 1x KK_2 (10 mM KH_2PO_4 pH 6.1) and serial dilutions of 1:1, 1:10, and 1:100 for each G418

concentration were prepared and 200 µL of LB *Klebsiella aerogenes* suspension were spread on SM agar plates, after which 10 µL of each dilution in duplicate were applied. Plates were stored at room temperature for ~ 4-5 days for colonies to grow.

2.9. Screening for *GxcU*$^-$, *Dd5p4*$^-$ *GxcU*$^-$, and *WasA*$^-$ *WasB*$^-$ CRISPR mutants

Potential *D. discoideum* mutant colonies were picked and the gDNA extracted as described in section 2.5. The region of the *GxcU* or *WasB* loci harbouring potential mutations were screened by PCR using DreamTaq Hot Start Green PCR Master Mix (2X). 5 µL of template gDNA of each sample was applied to 25 µL of DreamTaq Hot Start Green PCR Master Mix (2X), 2 µL of 10 µM of the GxcU or WasB forward sequencing primers, 2 µL of 10 µM of the GxcU or WasB reverse sequencing primers and 16 µL of dH_2O, giving a final reaction volume of 50 µL. The PCR protocol used was as follows: initial denaturation at 95°C for 3 minutes, with 35 cycles of denaturation at 95°C for 30 seconds, annealing at 55°C for 30 seconds, and elongation at 68°C for 30 seconds. PCR samples were run on a 2% agarose gel and DNA from the bands extracted using the Zymoclean gel extraction kit, see manufacturer's instructions. Sample genotypes were then determined using the GxcU or WasB sequencing primers via DNA sequencing, with samples that only possessed deletions at the PAM site that were not a multiple of three being classified as mutants to be utilised in this project. Deletions that were not a multiple of three would give rise to frameshifts and the generation of a Premature Termination Codon (PTC) within the expressed transcript causing Nonsense-Mediated Decay (NMD) of the resulting mRNA transcript and the consequent degradation of the aberrant peptide products (Losson and Lacroute 1979, Maquat et al. 1981, Lieber 2010, Lykke-Andersen and Bennett 2014).

2.10. Axenic growth curves

To measure the growth rate of cells in HL-5 nutrient-rich liquid media, 1 mL of 5 x 10^3 cells/mL were seeded into a 24-well plate in duplicate. Cells were counted using a haemocytometer twice a day for 72 hours. Average cell counts for each time point were then calculated and the generation times were calculated using the exponential decay (growth curve) curve-fitting function of Graph Pad Prism 8.

2.11. Macropinocytosis assay (Kay & Williams, 2018)

To measure bulk fluid uptake, cells were firstly seeded in duplicate for each time point to be tested in nutrient-rich HL-5, with the cell densities for each genotype firstly optimised by eye following overnight growth, 1 x 10^4 cells per 50 µL for each well were seeded for Ax2 control cells,

and 1.5 x 10^4 cells were seeded per 50 µL for each well for the slower growing *Dd5p4*$^-$ mutant cells in a 96-well plate and were left to grow overnight. Alternatively as overnight growth was later established to not be necessary for this experimental set up Ax2 control cells, *WasA*$^-$, and *WasA*$^-$ *WasB*$^-$ mutant clones were each instead seeded in nutrient-rich HL-5 at a higher density of 3 x 10^4 cells per 50 µL per well. The cells were then left to settle for approximately 1 hour to allow them to attach to the bottom of the 96-well plate prior to incubation with Tetramethylrhodamine isothiocyanate (TRITC) dextran (molecular mass 40 kDa, Sigma). Duplicate wells were then incubated with 50 µL of 1 mg/mL TRITC dextran made up in HL-5 for the time points indicated. The dextran was then poured away and the plate washed only once in ice-cold 1x KK_2 buffer (10 mM KH_2PO_4 pH 6.1) as this was sufficient to remove most of the TRITC dextran that bound to the surface of the cells (Williams and Kay 2018). 100 µL of 5 mM ice-cold NaN_3 was added to each well and the cells were left on ice for 10-15 minutes to detach and to prevent additional endocytosis or exocytosis from taking place without compromising cell viability (Glynn and Clarke 1984, Maselli et al. 2002, Williams and Kay 2018). TRITC dextran fluorescence was sampled and quantified using the Attune Flow Cytometer autosampler using the yellow laser 2 (YL2), with the laser strength set to 400, forward scatter (FSC) and side scatter (SSC) were set to 500 and 360 respectively. The flow rate was set to 25 µL per minute with the final and acquisition volumes being set to 100 µL and 60 µL respectively. The average fluorescence intensity of the dye that was taken up via macropinocytosis was then calculated.

The fluorescence output obtained from each sample reading was calculated and displayed by the Attune NxT Flow Cytometer Software. The fluorescence output at time point 0 (background fluorescence) was subtracted from each time point of the same experimental setup. The average of each duplicate for each of the three independent biological repeats was calculated and the data displayed as a line graph with statistical comparisons being made between the average fluorescence output of the 2 hour time point of the Ax2 control and the 2 hour time point of the mutant cell lines.

2.12. Preparation of *Saccharomyces cerevisiae* for labelling and microscopy

Wild type *Saccharomyces cerevisiae* (KAY447) were grown in Yeast extract Peptone Dextrose (YPD) (ThermoFisher) at 37°C for three days by Dr. Stella Christou until they were in the stationary phase for a predominately non-budded population. The composition of YPD per 100 mL: 1 g of yeast extract, 2 g of peptone, 0.2 g of Adenine Sulphate (all Formedium), 5 mL of 40% glucose, and 95 mL of H_2O. These yeast were subsequently used for fluorescent labelling and phagocytosis assays. Cells were centrifuged at 3,000 rpm for 1 minute and subsequently washed 3x in 1x KK_2 and counted giving a final cell density of 1 x 10^9 cells per 1,000 µL in 1x PBS pH 7.0. Cells were heat killed at 90°C

for 30 minutes and were stored at -20°C until needed. Labelling of yeast particles was adapted from a protocol that was used for staining *Staphylococcus aureus* (Renshaw lab). Alexa Fluor™ 594 NHS Ester (Succinimidyl Ester) (Fischer Scientific), and Alexa Fluor™ 405 NHS Ester (Succinimidyl Ester) (Life Technologies) were separately dissolved in DMSO giving a final concentration of 10 mM (stored in the dark at -20°C). Frozen aliquots of yeast were thawed and centrifuged at 13,400 rpm for 3 minutes at room temperature, the supernatant aspirated and 1 mL of 1x PBS pH 8.5 was used to re-suspend and combine multiple yeast aliquots. 6 µL of 10 mM NHS-dye was applied and re-suspended immediately to avoid clumps and were vortexed. All samples containing the fluorescent dye were covered in foil and were incubated for 30 minutes at 37°C and were shaken at 100 rpm. Samples were given 1 mL of 1x PBS pH 8.5, vortexed and centrifuged at 13,400 rpm for 3 minutes. The pellet was then washed twice in 25 mM Tris-HCl pH 8.5, before re-suspension in 1 mL of 1x KK_2 pH 6.1, cells were then stored at -20°C until needed.

2.13. Fluorescence microscopy – general

Investigation of probe localisation and general fluorescence microscopy involved all cells being seeded at 80-90% confluence within a 35 mm Petri dish with a 14 mm glass micro well (Mattek P35G-1.5-14-C) and were allowed to adhere for at least 1 hour unless otherwise stated prior to live-cell imaging. Cells were imaged in HL-5 unless otherwise stated, with the exception being cells that stably expressed the TAPP1-PH-GFP probe [$PI(3,4)P_2$]. Cells, which expressed this probe were seeded in SIH minimal media (L-Arginine, L-Asparagine, L-Aspartic Acid, L-Cysteine, L-Glutamic Acid, Glycine, L-Histidine, L-Isoleucine, L-Leucine, L-Lysine, L-Methionine, L-Proline, L-Threonine, L-Tryptophan, L-Phenylalanine, Valine, NH_4Cl, KH_2PO_4, $CaCl_2$, Glucose, $FeCl_3$, Vitamins, $MgCl_2$, Micro Elements) (Formedium) prior to live-cell imaging. This was undertaken to reduce the number of macropinosomes per cell and allowed $PI(3,4)P_2$ lifetime quantification on macropinosomes to be less problematic. Cells were visualised on a Perkin-Elmer Ultraview VoX spinning disk confocal microscope that operates on an Olympus Ix81 body using either the UplanSApo 60x or 100x oil immersion objectives. Cells were visualised with either 488 nm or 594 nm lasers and images were captured using a Hamamatsu C9100-50 EM-CCD camera using Volocity 6.3 software. The acquired images were analysed or processed using ImageJ. Time-lapse movies and stills consisting of multiple *z*-slices were acquired on a Zeiss Axiovert LSM880 Airyscan confocal microscope with a 63x Plan Apochromat oil objective. Macropinocytic events were visualised using a 488 nm argon laser and/or a 561 nm diode laser. The 488 nm and/or the 561 nm laser were used in conjunction with the 405 nm laser to visualise Alexa Fluor 405 NHS Ester (Succinimidyl Ester)-labelled dead *S. cerevisiae* during

phagocytic events. Images were Airyscan processed utilising the Zeiss microscope software and were analysed using ImageJ 1.52p.

2.14. Phagocytosis by cells in suspension

D. discoideum were seeded at 1 x 10^6 cells per mL in 3 mL of HL-5 in 15 mL Falcon tubes. 7.5 x 10^6 Alexa Fluor™ 594-labelled *S. cerevisiae* were then applied giving a 2.5:1 ratio of *S. cerevisiae* to *D. discoideum*. Cells were left for 30 minutes on a roller at 10 rpm at room temperature after which, 2 mL of cell suspension were subsequently transferred to microscope imaging dishes and were left to settle for 5-6 minutes. 100 µL of 0.4% trypan blue solution (ThermoFisher) was applied and gently mixed to quench the fluorescence of any yeast that had not been internalised. Cells were then imaged using a Zeiss Axiovert 100 widefield microscope with a Hamamatsub Orca ER camera running µManager software (Edelstein et al., 2010, Edelstein et al., 2014) using a Plan Apochromat 63x DIC. The number of yeast per *D. discoideum* were manually quantified using ImageJ 1.52p.

Nine Fields Of View (FOV) were randomly selected for each independent biological repeat, per cell line, and were analysed by counting only the internalised fluorescent *S. cerevisiae* and all the non-fluorescent *D. discoideum* using the ImageJ cell counter. The sum total of internalised *S. cerevisiae* was divided by the sum total of *D. discoideum* to give the ratio of *S. cerevisiae* to *D. discoideum* as shown below:

$$\textit{S. cerevisiae} \text{ to } \textit{D. discoideum} \text{ Ratio} = \frac{\text{(Total Number of Internalised Fluorescent } \textit{S. cerevisiae}\text{)}}{\text{(Total number of Non-fluorescent } \textit{D. discoideum}\text{)}}$$

2.15. Observation of nascent macropinosomes with Fluorescein Isothiocyanate (FITC) dextran

Cells were seeded based on their growth rate in HL-5 in microscope dishes at 2 x 10^5 cells per mL for Ax2 cells and 4 x 10^5 cells per mL for the slower growing *Dd5p4*$^-$ mutants, cells were left to grow overnight. Alternatively as overnight growth was later established to not be necessary for this experimental set up all other mutants and control cells were instead seeded at 5 x 10^5 per mL in 2 mL in imaging dishes and were left to settle for 1 hour prior to live-cell imaging. HL-5 media was carefully poured away and 50 µL of 0.4 mg/mL FITC dextran (molecular mass 70 kDa, Sigma) in HL-5 was applied gently to the centre of the imaging dishes. After 5 minutes stills were taken on the Airyscan microscope using the 63x immersion oil objective and the 488 nm argon laser.

As macropinocytosis is a highly variable process by nature some cells from some cell lines displayed a great degree of variability in which some contained few to no macropinosomes, some contained more macropinosomes, whilst some contained a number of macropinosomes that lay

between these two extremes. To account for this natural variability and to get a better representation of the overall population 20 cells were selected in total which consisted of some that possessed few macropinosomes, some that had more macropinosomes, and some that had a moderate number of macropinosomes. Some cell lines however, displayed little variability in their macropinosome numbers between cells so 20 cells were instead randomly selected in this case from the population. The macropinosome volume of all FITC dextran-containing macropinosomes were calculated within these selected cells by measuring the diameter of macropinosomes at their largest size through *z* in still images using ImageJ, and the following formula:

Macropinosome Volume (μm^3) = 4/3 x π x r^3 (when r = the macropinosome radius µm)

This formula was applied to only macropinosomes, which were spherical and not distorted. The same 20 cells that were used to measure volume were also utilised to measure the number of FITC dextran-containing macropinosomes per cell.

2.16. Time-lapse microscopy of phagocytosis

Cells were seeded at 1 x 10^6 per mL in 2 mL within imaging dishes, and were left to settle for 1 hour prior to live-cell imaging. 1% agarose was heated and dissolved in HL-5 and was left to polymerise prior to imaging in cell culture dishes. For 2.5:1 ratio of *S. cerevisiae* to *D. discoideum* 5 x 10^6 of re-suspended Alexa Fluor 405 NHS Ester labelled yeast were gently applied to the centre of the imaging dish and were left to settle for 10 minutes. HL-5 media was carefully aspirated from the edge of the imaging dishes and the 1% agarose disc that was cut using a cryovial lid was gently applied to the centre of each dish, with excess media carefully removed using blue roll. After 2 minutes of experimental setup, time-lapses of a single *z*-slice across three FOV were taken using the definite focus system on the Zeiss Axiovert LSM880 Airyscan confocal microscope with a 63x Plan Apochromat oil objective.

2.17. Lattice Light-Sheet Microscopy (LLSM) cell preparation

Dr. Jason King and our collaborators at the University of Warwick super-resolution microscopy facility seeded sub-log phase cells in 6-well plates on the afternoon of the day prior to live-cell imaging at 0.75 x 10^5, 1.5 x 10^5, and 4 x 10^5 cells per well in 3 mL of filtered HL-5 for each genotype. On the morning of the day of imaging the filtered HL-5 of wells that were 10-20% confluent were removed and replaced with 3 mL of simple up-regulation media (SUM) (4 mM of arginine, 3.7 mM of glutamic acid, 8.5 mM of lysine, 55 mM of glucose, 20 mM KH_2PO_4, 2 mM

$MgSO_4$, 0.1 mM of $CaCl_2$, pH 6.5) to reduce the levels of auto-fluorescence at least two hours before imaging (Williams and Kay 2018). Cells were then detached and re-suspended by pipetting and were transferred to two coverslips for each well and were left to settle prior to live-cell imaging.

2.18. LLSM live-cell imaging

LLSM super-resolution imaging was performed by our collaborators at the University of Warwick super-resolution microscopy facility using a 3i lattice light-sheet instrument, which possessed a 0.71 Numerical Aperture (NA) long working distance water-immersion excitation objective as well as a 1.1 NA water-immersion emission objective, with a sum magnification of 62.5x. Images were obtained using two separate Hamamatsu OCRA-Flash v3 sCMOS cameras (each possessed a single channel). Live-cells were visualised using 488 nm laser (set between 1-2% laser power), and the 561 nm laser (set between 5-10% laser power), which depended on the fluorescent probes that were utilised. 3D volumes were recorded and a step size of 0.3 µm was utilised (following de-skewing this was altered to 0.163 µm) with a 10 ms exposure across 120 imaging planes. This experimental setup resulted in a 2.883 s time resolution per volume with this rate of acquisition lasting between 3-5 minutes in duration.

2.19. Graphical display of data and statistical analyses performed - general

All data were analysed and the averages calculated using Microsoft Excel. All graphs unless otherwise stated were displayed as Super-plots (Lord et al. 2020) and were constructed using GraphPad Prism 8. Data from each clone of each genotype was separately plotted from three independent biological repeats, each performed on separate days unless otherwise stated. Individual data points of repeat 1 were displayed as small red circles, individual data points of repeat 2 were displayed as small green rectangles, and the individual data points of repeat 3 were displayed as small blue diamonds. The averages of each independent biological repeat were displayed as larger triangles, which were red for repeat 1, green for repeat 2, and blue for repeat 3. All error bars were ± the standard error of the mean (SEM).

Unpaired *t* tests with Welch's correction were carried out comparing the replicate average values between the cell lines when both populations displayed a normal distribution without the standard deviations being equal. In the setting when one or both populations that were compared did not display a normal distribution the Mann Whitney U non-parametric test was alternatively utilised. When using this non-parametric test the ranks of the individual data points from each independent biological repeat were compared. The *P* values of non-significant statistical

comparisons were indicated with significant statistical comparisons being displayed as stars based on the strength of the statistical difference; *(P<0.05), **(P<0.01), ***(P<0.001), ****(P<0.0001).

2.20. Quantification of macropinocytic cup dynamics

The number of macropinocytic cups or patches before closure, per cell, at a single time point, regardless of the stage of cup progression towards closure were calculated. The length of each macropinocytic cup from stills were measured using ImageJ at their largest size through *z*. Time-lapses were used to quantify the number of macropinosomes that were generated from each individual macropinocytic cup until the macropinocytic cup being analysed had faded completely. For each of the three parameters that were measured 30 macropinocytic cups were measured at random, per cell line, per independent biological repeat.

2.21. Quantification of the kinetics of phagocytic engulfment and phagocytic failure rate

The time taken in seconds for the PM of the cell to fully enwrap around the yeast regardless of whether phagocytic engulfment was successful or not was calculated between Ax2 control cells and mutant cell lines. In cells stably expressing RFP-PH-PkgE [PI(3,4,5)P_3-probe] the time taken to enwrap was the period from which the yeast first made direct contact with the PI(3,4,5)P_3-labelled PM to the point at which the PI(3,4,5)P_3 labelled PM fully encircled the yeast. The time taken to internalise the phagosome in cells stably expressing RFP-PH-PkgE GFP-2xFYVE during successful phagocytic engulfment events were also calculated. The time taken in seconds to successfully internalise the phagosome was measured from the point at which the PI(3,4,5)P_3 labelled membrane had completely enwrapped the yeast to the stage at which GFP-2xFYVE [PI(3)P-probe] fully encircled the phagosome. The time taken to internalise the phagosome included the time in which neither PI(3,4,5)P_3, or PI(3)P encircled the phagosome and also included the number of PI(3,4,5)P_3 'flashes' prior to successful internalisation, with each flash of PI(3,4,5)P_3 representing an internalisation attempt.

The phagocytic failure rate was quantified by tallying up the total number of successful attempts and the total number of failed attempts, with the failure rate being calculated as follows:

$$\text{Phagocytic Failure Rate} = \frac{\text{(Total Number of Failed Phagocytic Engulfment Events)}}{\text{(Total Number of Successful + Failed Phagocytic Engulfment Events)}}$$

Only the replicate averages of each individual biological repeat were plotted. Successful phagocytosis was classified as an event in which the yeast were successfully transitioned to a PI(3)P-

positive compartment. Only phagocytic engulfment events, which were conclusive within the time constraints of each time-lapse were quantified. Failure rate and engulfment kinetics were quantified across all FOV for which the total number of events was fewer than 50 across all FOV in order for valid statistical comparisons to be made between each cell line.

2.22. Quantification of the PI(3,4,5)P_3, PI(4,5)P_2, and PI(4)P enrichment profiles across phagocytic and macropinocytic cups at different stages towards cup closure

The PIP profiles of both phagocytic and macropinocytic cups were measured approximately 50% towards closure, and just before the cup closed. ImageJ was used to free-hand draw across each individual cup at each stage towards closure during time-lapses from cup tip to cup tip. 10 cups, per independent biological repeat, per cell line were quantified. Cups that were labelled with Nodulin-GFP [PI(4,5)P_2] and P4M-GFP [PI(4)P] were each separately normalised over 1,000 points against the respective PIP levels of the non-protruding PM and the cytosol. The linescan point value corresponds to the fluorescent signal at that particular point across the phagocytic/macropinocytic cup. The formula used to calculate the fold enrichment of PI(4,5)P_2 or PI(4)P is shown:

$$\text{PI(4,5)}P_2\text{/PI(4)P Fold Enrichment} = \frac{\text{(Linescan Point Value - Cytosolic Signal)}}{\text{(Non-Protruding Membrane - Cytosolic Signal)}}$$

To calculate the fold enrichment of RFP-PH-PkgE [PI(3,4,5)P_3]:

$$\text{PI(3,4,5)}P_3\text{ Fold Enrichment} = \frac{\text{Linescan Point Value}}{\text{Non-Protruding Membrane}}$$

The scripts were written by James Vines (see chapter seven, section 7.1.-7.2.). The complete profiles were displayed as line graphs in which the Ax2 average data values were displayed as black connecting lines, with Ax2 error bars shown in dark grey, *Dd5p4*$^-$ average data values were displayed as red connecting lines, with *Dd5p4*$^-$ error bars outlined in light-red/pink. The central enrichment profiles, which consisted of the central 101 points from position 450 to 550 of the 1,000 points of the full enrichment profiles were taken and plotted as bar charts, with Ax2 shown in black and *Dd5p4*$^-$ in red. Statistical comparisons were made between the average fold enrichment central profiles for each cup between Ax2 and *Dd5p4*$^-$ mutant cells.

2.23. Quantification of PIP timings during macropinocytosis from Airyscan confocal microscopy

The GFP-PH-PkgE [PI(3,4,5)P_3] was utilised to measure the time taken from macropinocytic cup formation to the formation of a macropinosome. This measurement encompassed the time frame at which a macropinocytic cup had started to form to when the first macropinosome was generated from that same cup during time-lapses.

The lifetime of each PIP after closure on the membranes of macropinosomes was quantified by calculating the time interval between which the macropinosome first emerged from the macropinocytic cup to the time at which the PIP signal on the macropinosome was lost during time-lapses.

The ratio of the non-protruding PM PI(4,5)P_2 intensity levels to the cytosolic PI(4,5)P_2 signal was quantified using the following equation:

$$\text{PI(4,5)}P_2 \text{ Non-Protruding Plasma Membrane / Cytosolic Ratio} = \frac{\text{(Non-Protruding Signal - Extracellular Signal)}}{\text{(Cytosolic Signal - Extracellular Signal)}}$$

10 cells, per cell line, per independent biological repeat, were quantified at random for this analyses.

2.24. Processing of LLSM images and quantification of PIP and F-actin dynamics during macropinocytosis from LLSM

LLSM images were deconvolved and processed by Kirsty Tinsley (a Master's student) and Scott Brooks (University of Warwick) in order to enhance the resolution and contrast of image stacks. The PIP and F-actin dynamics during the early stages of macropinocytosis were also quantified by Kirsty Tinsley from LLSM images that were obtained from our collaborators in the University of Warwick, which made up a single biological repeat. Profiles of the intensity signals over time of each fluorescent probe was measured and quantified using ImageJ. The average intensities around the entire macropinocytic cups were measured over time until the intensity signal was lost. PI(4,5)P_2 levels were normalised against both the non-protruding PM and intracellular signals to outline the levels of PI(4,5)P_2 depletion, with PI(4,5)P_2 levels quantified through *z*. The intensity signals of PI(3,4,5)P_3, PI(3,4)P_2, and F-actin were each normalised to the corresponding intracellular signal in contrast, and were quantified using maximum intensity projections (MIPs). Mann Whitney U statistical tests were performed to compare the intensity levels of certain fluorescent probes at certain time points within Ax2 and *Dd5p4*$^-$ mutant cell lines as normal data distributions were not displayed.

2.25. Quantifying tether dynamics in Ax2 and *WasA*$^{-}$ single mutants from LLSM images

The lifetime of tethers in seconds were quantified from LLSM time-lapse images just after macropinocytic cup closure. This covered the point at which the tether first appeared linking the macropinosome to the PM, until the time point in which the tether signal disappeared. The end point of tethers also marked the point at which the macropinosome was able to move more freely following scission away from the PM. ImageJ was used to measure the maximum length of the tether from one end to the other. The Super-plot that was displayed from these data analyses were from a single biological repeat with Ax2 individual data points indicated as small green circles and *WasA*$^{-}$ individual data points indicated as small red circles. The replicate average of each cell line was displayed as a single, larger, dark-blue triangle, with statistical comparisons being made between the individual data points of the Ax2 and *WasA*$^{-}$ single mutant cell lines using Mann Whitney U statistical tests.

2.26. Table 2.1. List of plasmids that were used in this project

Plasmid ID	Gene ID	Description	Insert	Vector	Selection (*E. coli*)	Selection (*D. discoideum*)
CJM2	DDB_G0267462	Dd5p4-GFP Expression	Dd5p4 gene PCR * BglII/SpeI	pDM1045 * BglII/SpeI	Ampicillin	Hygromycin B
CJM4	DDB_G0267462	$Dd5p4^{D319G}$-GFP Expression	Dd5p4 gene PCR * BglII/SpeI	pDM1045 * BglII/SpeI	Ampicillin	Hygromycin B
CJM6	DDB_G0267462	$Dd5p4^{W620A}$-GFP Expression	Dd5p4 gene PCR * BglII/SpeI	pDM1045 * BglII/SpeI	Ampicillin	Hygromycin B
pD631	DDB_G0285161	PH-Crac-GFP Expression	pDM612 * BamHI/XbaI	pDM450 * BglII/SpeI	Ampicillin	Hygromycin B
pJSK698	N/A	GFP-2xFYVE/ RFP-PH-PkgE co-expression vector	pPI84 * NgoMIV	pJSK418 * NgoMIV	Ampicillin	Hygromycin B
Nodulin-GFP	N/A	Nodulin-GFP expression (Gift from Peter N. Devreotes)	N/A	N/A	Ampicillin	Hygromycin B
P4M-GFP	N/A	P4M-GFP expression	P4M	pDM323	Ampicillin	G418
pPI304	N/A	LifeAct-mCherry/PH-PkgE-GFP co-expression vector	LifeAct & PkgE-PH	pDM1209	Ampicillin	G418
pTH219	N/A	TAPP1-PH expression	TAPP1-PH cDNA from *H. sapiens* * SacI/NheI	pDM323 * SacI/NheI	Ampicillin	G418
pJSK418	N/A	GFP-2xFYVE expression	pJSK408 * BclI/XbaI	pDM448 * BglII/SpeI	Ampicillin	Hygromycin B
pJSK696	N/A	GFP-TAPP1/ RFP-PH-PkgE co-expression vector	TAPP1-PH cDNA from *H. sapiens* * NgoMIV	pPI84 * NgoMIV	Ampicillin	G418

Plasmid ID	Gene ID	Description	Insert	Vector	Selection (*E. coli*)	Selection (*D. discoideum*)
pJSK697	DDB_G0293834	GFP-WasA RFP-PH-PkgE co-expression vector	pPI84 * NgoMIV	pDM608 * NgoMIV	Ampicillin	Hygromycin B
pJSK706	N/A	Nodulin-GFP/PkgE-PH-mCherry co-expression vector	Nodulin-GFP expression (Gift from Peter N. Devreotes) *NgoMIV	pPI84 * NgoMIV	Ampicillin	Hygromycin B
pJSK703	N/A	TAPP1-PH-GFP/ LifeAct-mCherry co-expression vector	pTH219 * NgoMIV	pPT782 * NgoMIV	Ampicillin	G418
pJSK707	N/A	Nodulin-GFP/ LifeAct-mCherry co-expression vector	Nodulin-GFP expression (Gift from Peter N. Devreotes) *NgoMIV	pPT782 * NgoMIV	Ampicillin	Hygromycin B
pJSK704	N/A	GFP-2xFYVE/ mCherry-LifeAct co-expression vector	pPT782 * NgoMIV	pJSK418 * NgoMIV	Ampicillin	Hygromycin B
pJSK702	DDB_G0293834	GFP-WasA/RFP-LifeAct co-expression vector	pPT782 * NgoMIV	pDM608 * NgoMIV	Ampicillin	Hygromycin B
pLP147	DDB_G0292878	GFP-WASH/ RFP-actin expression	pLP122	pDM616	Ampicillin	Hygromycin B
pPT782	DDB_G0279175	Hspc300-GFP RFP-Actin expression	pDM580	pDM557	Ampicillin	Hygromycin B
pDM608	DDB_G0293834	GFP-WasA ArpC4-mRFP Mars2 expression	pDM601 * NgoMIV	pDM482 * NgoMIV	Ampicillin	Hygromycin B

Plasmid ID	Gene ID	Description	Insert	Vector	Selection (*E. coli*)	Selection (*D. discoideum*)
DiGxcU-GFP	DDB_G0291996	*D. intermedium* GxcU-GFP expression	*D. intermedium* GxcU	pDM323	Ampicillin	G418
pDM641	DDB_G0269102	GFP-ArpC4 LifeAct-mRFPmars2 co-expression vector	pDM623 * NgoMIV	pDM528 * NgoMIV	Ampicillin	Hygromycin B

2.27. Table 2.2. List of primers used in this project

Primer Code	Full Name	Sequence (5'-3')
dd5p4_5' BglII	Dd5p4 5' BglII Full Length Forward Primer	AGTAGATCTATGGGTGATATTCAAAATACAG
dd5p4_3' SpeI	Dd5p4 3' SpeI Full Length Reverse Primer	GCGACTAGTATTAATTAAATCTTTTGAAATTAAAAAATG
oCJM1	APPL1-like Upstream WT/KO Forward Primer	GTAAAGCAGCAATTAGAATCACATC
oCJM2	APPL1-like 3' Arm Primer	GGATTTTTATCATCAAATGGATTTGGTG
oCJM3	pKOSG-dicty Blasticidin Resistance Cassette Reverse Primer	GTCGTCCATCAATTGTTCACAG
BSR Fw	Blasticidin Resistance Cassette Forward Primer	CGCTTCAATATGTACTGCCGAA
oCJM5	APPL1-like Downstream WT/KO Forward Primer	GCATTTGAAATTGGTTGTGGTG
oCJM11	Ses1/2-like Upstream WT/KO Forward Primer	TTTAAAGGCAACTCAAAAAGGTTTGG
oCJM14	Ses1/2-like 3' Arm Primer	AGGAGGACATTGATGGTGATGTAG
oCJM8	Ses1/2-like Downstream WT/KO Forward Primer	CGAACTCATAATTACACCTAAGCG
gxcU_CRISPR fw	GxcU CRISPR PAM Site Sense Forward Primer	AGCATTCAAGATAGAATGACGACA

Primer Code	Full Name	Sequence (5’-3’)
gxcU_CRISPR rv	GxcU CRISPR PAM Site Anti-Sense Reverse Primer	AAACTGTCGTCATTCTATCTTGAA
wasB antisense	WasB CRISPR PAM Site Anti-Sense Reverse Primer	AAACGAGTGGAGACAATTATTTCA
wasB sense	WasB CRISPR PAM Site Sense Forward Primer	AGCATGAAATAATTGTCTCCACTC
gxcU_seq5'	GxcU CRISPR Sequencing Forward Primer	GGTTAATAAAACCAATAGAGATAAAGTTGCA
gxcU_seq3'	GxcU CRISPR Sequencing Reverse Primer	CCAAACGAATTCTCACTGGTAACT
WasB_SeqFw_Imp	WasB CRISPR Sequencing Forward Primer Improved	TTGACTCTCATAATCCAAGTAAG
WasB_SeqRv_Imp	WasB CRISPR Sequencing Reverse Primer Improved	TATAAATGAATTGAACAGTTTCTGG
PCR CRISPR Screen Reverse Primer	PCR CRISPR Screen Reverse Primer (King Lab Communal Use)	AAGCTTAAAAAAAGCACCGACTCGGTGCC

2.28. Table 2.3. List of cell strains that were used in this project

Name	Parental Strain	Genotype	Source	Strain ID	Clone No.
Ax2	Ax1 (DBS0237979)	*axeA2*, *axeB2*, *axeC2*	Robert Kay	DBS0235521	N/A
***Dd5p4*$^-$**	Ax2 (DBS0235521)	Blasticidin Resistant	Arjan Kortholt (van Haastert Lab)	*Dd5p4*$^-$ (Swan)	N/A
***GxcU*$^-$**	Ax2 (DBS0235521)	11 bp CRISPR Deletion in *GxcU* Locus	Chris Munn – King Lab	JSK25	1
***GxcU*$^-$**	Ax2 (DBS0235521)	2 bp CRISPR Deletion in *GxcU* Locus	Chris Munn – King Lab	JSK26	2
***Dd5p4*$^-$ *GxcU*$^-$**	*Dd5p4*$^-$ (Swan)	Blasticidin Resistant, 7 bp CRISPR Deletion in *GxcU* Locus	Chris Munn – King Lab	JSK22	1
***Dd5p4*$^-$ *GxcU*$^-$**	*Dd5p4*$^-$ (Swan)	Blasticidin Resistant, 2 bp CRISPR Deletion in *GxcU* Locus	Chris Munn – King Lab	JSK23	2
***APPL1-like*$^-$**	Ax2 (DBS0235521)	Blasticidin Resistant	Chris Munn – King Lab	JSK11	1
***APPL1-like*$^-$**	Ax2 (DBS0235521)	Blasticidin Resistant	Chris Munn – King Lab	JSK17	2
***Ses1/2-like*$^-$**	Ax2 (DBS0235521)	Blasticidin Resistant	Chris Munn – King Lab	JSK10	1
***Ses1/2-like*$^-$**	Ax2 (DBS0235521)	Blasticidin Resistant	Chris Munn – King Lab	JSK16	2
***WasA*$^-$**	Ax2 (DBS0235521)	Blasticidin Resistant	Chris Munn – King Lab	JSK27	1
***WasA*$^-$**	Ax2 (DBS0235521)	Blasticidin Resistant	Chris Munn – King Lab	JSK28	2
***WasA*$^-$ *WasB*$^-$**	*WasA*$^-$ Clone 1 (JSK27)	Blasticidin Resistance, 2 bp CRISPR Deletion in *WasB* Locus	Chris Munn – King Lab	JSK33	1

Name	Parental Strain	Genotype	Source	Strain ID	Clone No.
***WasA*$^{-}$ *WasB*$^{-}$**	*WasA*$^{-}$ Clone 1 (JSK27)	Blasticidin Resistance, 2 bp CRISPR Deletion in *WasB* Locus	Chris Munn – King Lab	JSK34	2

Chapter 3

The role of Dd5p4 in PIP metabolism, phagosome, and macropinosome formation, and dynamics

3.1. Introduction

OCRL, an inositol 5-phosphatase expressed in mammals has been shown to play vital roles in endocytic trafficking (Ponting 2006, Erdmann et al. 2007, Mao et al. 2009, Swan et al. 2010, Pirruccello and De Camilli 2012). To gain greater understanding of the function of this enzyme in endocytosis the single orthologue, Dd5p4, in *D. discoideum* was studied. Dd5p4 is one of five inositol 5-phosphatases found in *D. discoideum* (Loovers et al. 2003, Merlot et al. 2003). Dd5p4 catalyses the hydrolysis of $P(3,4,5)P_3$ to $PI(3,4)P_2$ and $PI(4,5)P_2$ to PI(4)P, with equal preference through the removal of the D5 phosphate of the *myo*-inositol ring. Dd5p4 possesses two domains in the form of a 5-phosphatase catalytic domain, and a catalytically inactive C-terminal Rho-GAP domain (Loovers et al. 2003). Dd5p4 has been linked with the regulation of both macropinocytosis and phagocytosis, with the loss of Dd5p4 being shown to cause growth defects in both axenic culture and on bacteria, with both domains being shown to be crucial for growth (Loovers et al. 2007). Previous work has suggested that Dd5p4-null mutants were able to establish contacts with yeast at normal frequencies, but were unable to extend their membranes beyond half the circumference of yeast particles (Loovers et al. 2007). Use of the Green Fluorescent Protein-Pleckstrin Homology-Cytosolic Regulator of Adenylate Cyclase (GFP-PH-Crac) probe, indicated that $PI(3,4,5)P_3$ and $PI(3,4)P_2$ levels were unaltered in these mutants. The absence of active 5-phosphatase activity was shown to hinder phagocytosis, which suggested that mechanistic failure was due to the prevention of $PI(3,4,5)P_3$ or $PI(4,5)P_2$ de-phosphorylation, which was necessary for extension around yeast and for cup closure. Failed events were stated to occur as a result of phagocytosis stalling halfway through enwrapping yeast, with the particle being subsequently released (Loovers et al. 2007). Quantification of phagocytic and macropinocytic $PI(3,4,5)P_3$ and $PI(3,4)P_2$ levels showed a reduction in Ax3 control cells, but was not fully elucidated in Ax3 Dd5p4-null cells as they were unable to stably express the Tandem PH-domain-containing Protein 1-Pleckstrin Homology-Green Fluorescent Protein (TAPP1-PH-GFP) $PI(3,4)P_2$-binding probe (Dormann et al. 2004, Loovers et al. 2007). This investigation thus had a relatively low coverage of PIP metabolism within Dd5p4-null cells during phagocytosis and macropinocytosis. This gave the incentive to establish if and how $PI(3,4,5)P_3$ and $PI(3,4)P_2$ dynamics, as well as those of other PIPs, were affected in the absence of Dd5p4 enzymatic activity, in an attempt to elucidate why loss of Dd5p4 severely hindered phagocytosis and macropinocytosis.

Dd5p4 has also been shown to interact with endocytic adaptor proteins via an F&H motif, located in the Rho-GAP domain. Interactions with orthologues of the endocytic adaptors APPL1, Ses1/2, and a Cdc42 Rho-GEF, Frabin, have been documented (Swan et al. 2010, Pirruccello et al. 2011, Luscher et al. 2019). Dd5p4 functions in coordination with these endocytic adaptor proteins to influence membrane deformation at numerous stages of endocytosis (Luscher et al. 2019). The

details however, of the mechanism by which Dd5p4 regulates macropinocytosis and phagocytosis via PIP metabolism and dynamics currently remains elusive.

Following on from these findings, part of this project also aimed to investigate the mechanistic actions of Dd5p4 and how this enzyme influences PIP metabolism during macropinocytic and phagocytic cup formation. PIP metabolism after closure was also investigated to understand why loss of Dd5p4 hindered phagocytosis of yeast and altered macropinosome dynamics.

3.2. Results

3.2.1. Loss of Dd5p4 hindered the phagocytosis of yeast

The loss of Dd5p4 has previously been shown to inhibit phagocytosis of yeast and hinder growth of *D. discoideum* in liquid media in the Ax3 genetic background (Loovers et al. 2007). Studies for this project however, were conducted using the Ax2 strain as this had the lowest frequency of genetic duplications and was the least genetically unstable in comparison to other axenic strains that have been used (Bloomfield et al. 2008). All studies in the King Lab centred predominantly on the Ax2 parental strain, as a result *Dd5p4*$^{-}$ in the Ax2 genetic background were provided by our collaborators.

To study if phagocytic defects were observed in the Ax2 genetic background, *Dd5p4*$^{-}$ phagocytic levels were compared to Ax2 control cells. Cells were shaken for 30 minutes with fluorescently labelled yeast, prior to live-cell imaging to quantify phagocytic engulfment. The fluorescence of yeast that were not engulfed was quenched by the addition of trypan blue. Ax2 had a higher level of yeast uptake (Fig. 3.1.A.) in comparison to *Dd5p4*$^{-}$ (Fig. 3.1.B.). Quantification of the yeast to *Dictyostelium* ratio in the Ax2 genetic background (Fig. 3.1.C.) were consistent with the observations made in the Ax3 genetic background (Loovers et al. 2007).

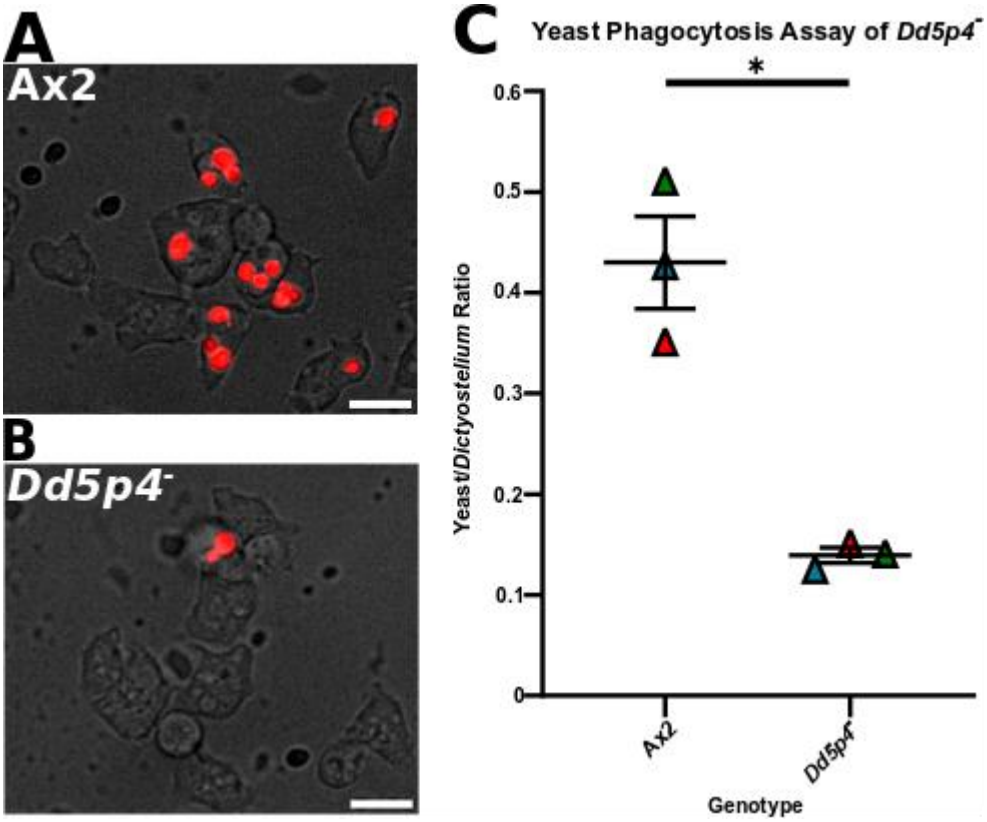

Figure 3.1. *Dd5p4*⁻ have a phagocytic defect. (A-B) Confocal images of Ax2 and *Dd5p4*⁻ respectively, taking up fluorescently labelled yeast following 30 minutes of shaking. (C) Quantification of the yeast to *Dictyostelium* ratio across both cell lines. All cells across nine FOV were analysed per cell line, per biological repeat. The data shown is the average ratio calculated from three independent, colour-coded biological repeats, ± SEM. Scale bars are 10 microns. Significance was determined using a Welch's t test. * $P < 0.05$.

3.2.2. Dd5p4 catalytic activity but not F&H interactions were crucial for phagocytosis

It has been shown in Ax3 Dd5p4-null mutants, that the stable expression of *H. sapiens* OCRL mostly restored growth in axenic culture, whereas partial phagocytic restoration was observed on bacteria. The 5-phosphatase and Rho-GAP domains were both found to be critical for Dd5p4 functionality (Loovers et al. 2007). Understanding whether the stable expression of Dd5p4, and two other Dd5p4 constructs each bearing one of two critical point mutations in the 5-phosphatase or the Rho-GAP domains were able to rescue the phagocytic defects of *Dd5p4*⁻ in the Ax2 background became apparent. The 5-phosphatase domain point mutation abolished Dd5p4 enzymatic activity, whereas the Rho-GAP domain point mutation located in the F&H motif abolished interactions with the Dd5p4 F&H interactors (Pirruccello et al. 2011, Luscher et al. 2019). The location of these point mutations within Dd5p4 are indicated (Fig. 3.2.A.).

To test whether the Dd5p4-GFP (full-length), Dd5p4^{D319G}-GFP (catalytic mutant) and Dd5p4^{W620A}-GFP (F&H mutant) constructs were dominant negative, each were firstly stably expressed in Ax2 control cells and the levels of yeast phagocytosis were quantified (Fig. 3.2.B-E. and J.). The stable expression of full-length Dd5p4, the catalytic mutant, and the F&H mutant did not

affect the levels of phagocytosis in comparison to the levels of phagocytosis in the non-transfected Ax2 control cells (Fig. 3.2.J.). The stable expression of the same constructs in *Dd5p4*$^{-}$ indicated that the stable expression of full-length (WT) does rescue phagocytosis in *Dd5p4*$^{-}$ (Fig. 3.2.G. and K.). The F&H mutant also fully rescued phagocytosis (Fig. 3.2.I. and K.), whereas the stable expression of the catalytic mutant did not rescue the phagocytosis of yeast (Fig. 3.2.H. and K.). The loss of Dd5p4 catalytic activity would suggest that PI(3,4,5)P_3 and/or PI(4,5)P_2 degradation was critical for the phagocytosis of yeast to be successfully completed (Fig. 3.2.K.).

In mammals, OCRL has been shown to localise to the base of nascent phagocytic cups (Marion et al. 2012), however attempts to visualise Dd5p4 localisation within *D. discoideum* have thus far been unsuccessful (Loovers et al. 2007, Luscher et al. 2019). I thereby attempted to stably express full-length Dd5p4-GFP in Ax2 control cells in the presence of fluorescently labelled blue yeast in an attempt to visualise Dd5p4 protein localisation. The GFP signal was predominantly cytosolic however, and yielded no definitive localisation at the base of phagocytic cups (Fig. 3.2.L.).

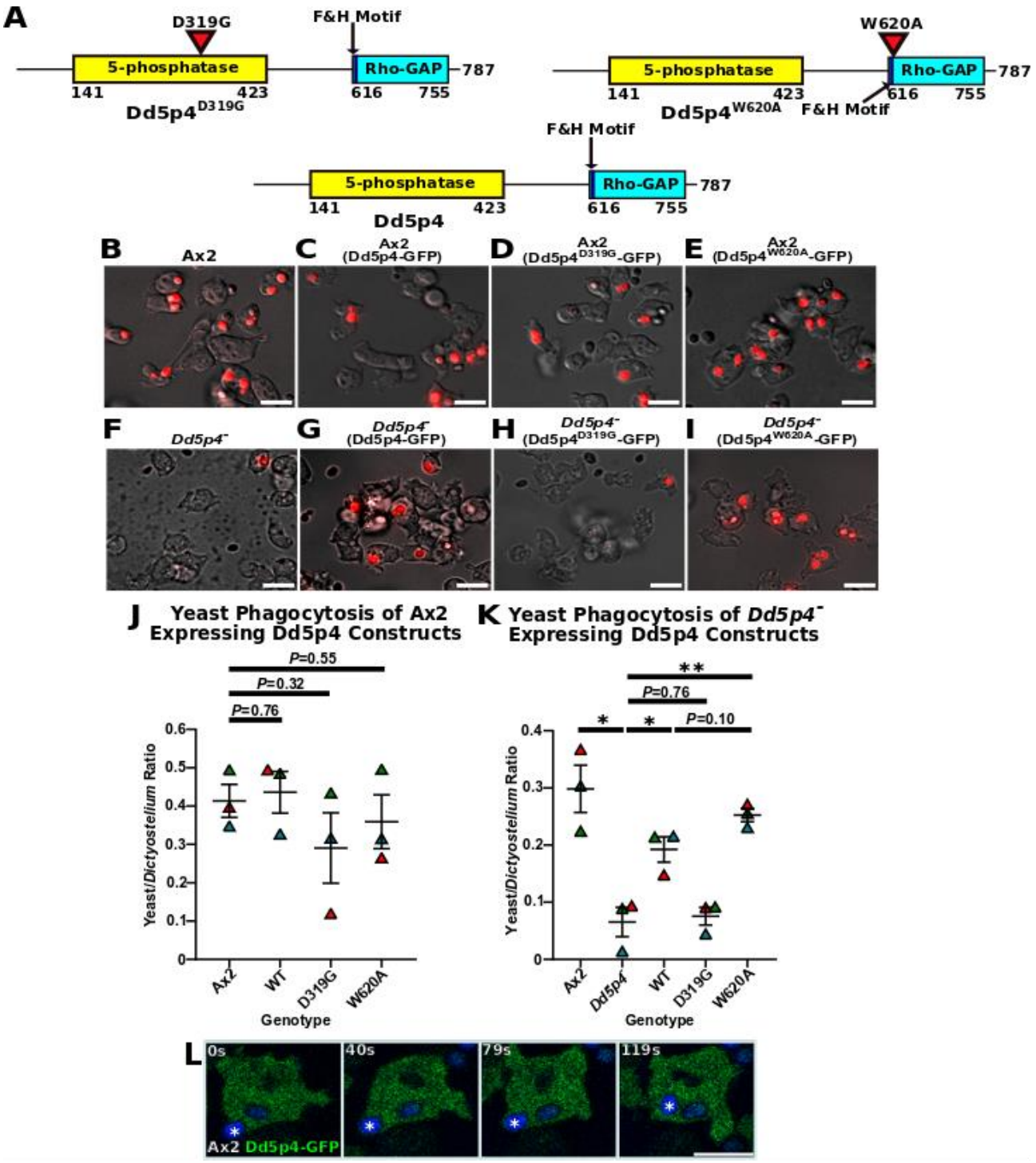

Figure 3.2. Dd5p4 catalytic activity but not F&H interactions were crucial for phagocytosis. (A) Domain structure of Dd5p4 together with the location of the catalytic and F&H point mutations, both indicated by red inverted triangles. (B-E) Confocal images of internalised fluorescently labelled red yeast in Ax2, and Ax2 cells stably expressing Dd5p4-GFP (WT), Dd5p4^{D319G}-GFP (D319G), and Dd5p4^{W620A}-GFP (W620A). (F-I) Images of internalised yeast in *Dd5p4*$^{-}$ mutant cells stably expressing the same constructs. (J) Quantification of yeast phagocytosis in the Ax2 control cells stably expressing Dd5p4 constructs. (K) Equivalent quantification in the *Dd5p4*$^{-}$ mutant background. All cells across nine FOV were analysed per cell line, per biological repeat. (L) Time-lapse of Ax2 cells stably expressing Dd5p4-GFP engulfing fluorescently labelled blue yeast. Yeast of interest are indicated by white stars. The graphs (J-K) show the average of the means from three independent, colour-coded biological repeats, ± SEM. Scale bars are 10 microns. Statistical significance was determined using Welch's *t* tests. * $P < 0.05$, ** $P < 0.01$.

3.2.3. Loss of Dd5p4 increased the generation time and altered macropinosome dynamics

It has been shown that loss of Dd5p4 hindered growth in liquid culture in the Ax3 genetic background, indicating that there were defects in macropinocytosis (Loovers et al. 2007). I therefore started by testing whether Dd5p4 loss led to macropinocytic defects in Ax2 control cells. Cells were seeded and counted at defined time intervals, up to 72 hours after seeding. The generation time in Ax2 was determined to be 10.8 hours, whilst the loss of Dd5p4 activity resulted in an increase to 12.5 hours (Fig. 3.3.A.). This finding is comparable to, but less severe than the observations made in the Ax3 genetic background (Loovers et al. 2007).

The mechanism of how loss of Dd5p4 activity impeded macropinocytosis was unknown, which gave the incentive to investigate how, and at which stage, Dd5p4 regulated this process. To investigate whether Dd5p4 regulated the dynamics of macropinosomes, the number of macropinosomes formed per cell and the volume of newly formed macropinosomes were quantified. Cells were administered pH-sensitive FITC dextran to visualise early, non-acidified macropinosomes and were observed by confocal microscopy (Fig. 3.3.B.). The loss of Dd5p4 activity greatly increased the number of macropinosomes, with a 2.5-fold increase per cell compared to Ax2 control cells (Fig. 3.3.C.). The volume of macropinosomes were also decreased in *Dd5p4*$^{-}$ mutants by 3-fold compared to those observed in Ax2 control cells (Fig. 3.3.D.).

Due to *Dd5p4*$^{-}$ having different fluid acquisition dynamics compared to Ax2 cells, I then quantified the sum total fluid acquired by these mutants. This would address whether alterations in macropinosome dynamics that were observed in *Dd5p4*$^{-}$ mutants would cause differences in the total fluid uptake compared to Ax2 control cells. To that end, macropinocytosis assays were performed comparing bulk uptake of TRITC dextran at different time points by flow cytometry (Fig. 3.3.E.). Loss of Dd5p4 activity did not alter the bulk uptake of TRITC dextran at the 2 hour time point in comparison to Ax2 control cells (Fig. 3.3.E.). This would suggest that *Dd5p4*$^{-}$ compensates for the smaller macropinosomes that are generated by forming more macropinosomes, resulting in the sum nutrient acquisition being unaltered (Fig. 3.3.B-E.). This finding would also suggest that there were no defects in fluid uptake, meaning that this was therefore not responsible for the growth defects that have been observed in these mutants (Fig. 3.3.A. and E.). It could be possible that forming numerous, smaller macropinosomes may somehow constitute a growth defect in *Dd5p4*$^{-}$ mutant cells (Fig. 3.3.A-D.).

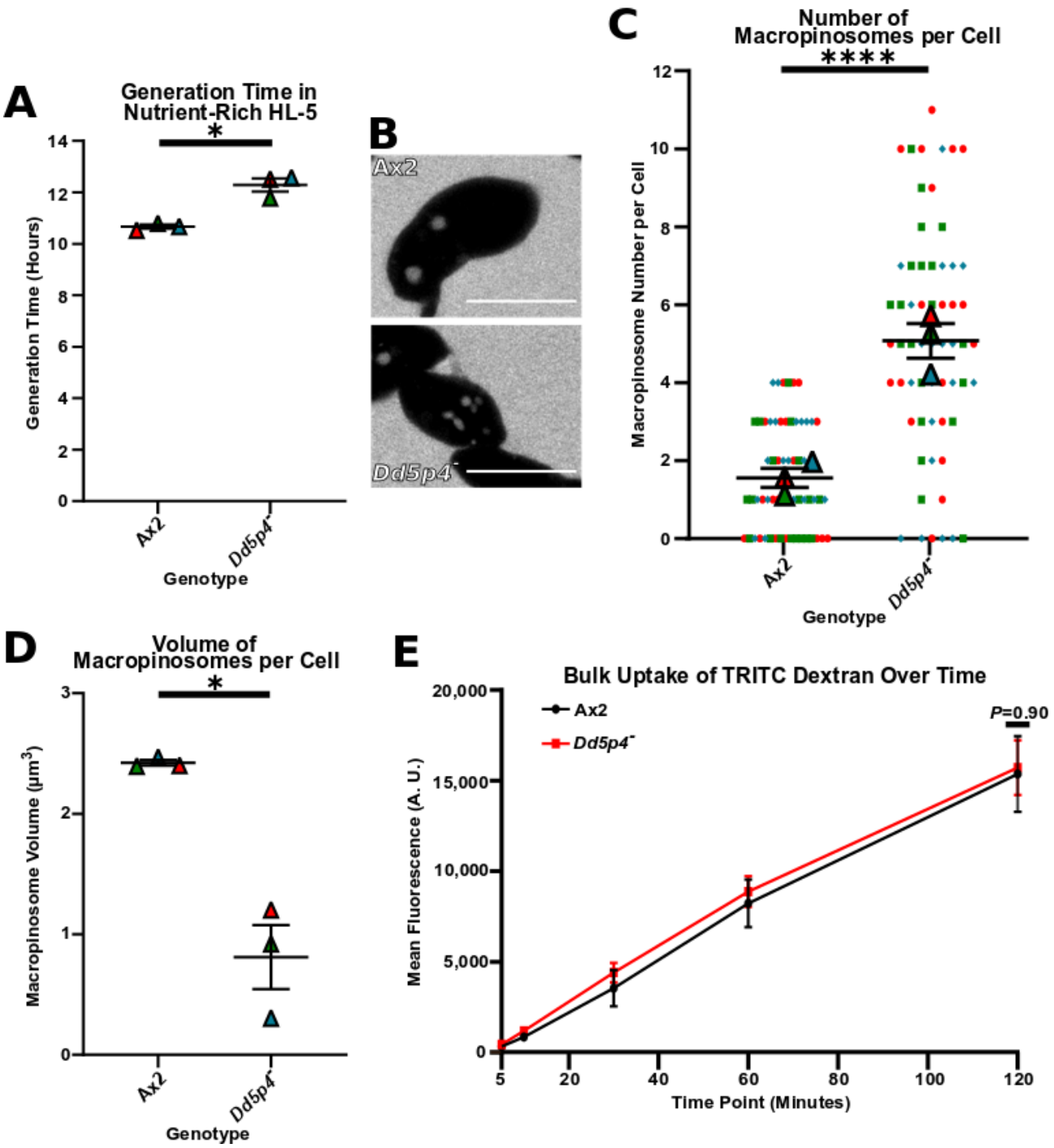

Figure 3.3. Loss of Dd5p4 increased the generation time and altered macropinosome dynamics. (A) The generation times of Ax2 and *Dd5p4*$^-$ cells cultured in HL-5 nutrient-rich media. Cells were seeded in duplicate and were counted at regular time intervals for up to 72 hours after seeding. Significance was determined using a Welch's *t* test. (B) Confocal images of Ax2 and *Dd5p4*$^-$ cells following application of FITC dextran for 5 minutes. (C) Quantification of the number of macropinosomes per cell. Significance was determined using a Mann Whitney U test. (D) Quantification of the average macropinosome volume. Individual data points were omitted in D to make the replicate averages more clearly visible. Significance was determined using a Welch's *t* test. 20 cells were selected per cell line, per biological repeat, and macropinosome dynamics were quantified. The data from each of the three biological repeats are colour-coded in A, C, and D. (E) Quantification of the mean fluorescence of Ax2 and *Dd5p4*$^-$ cells following incubation with TRITC dextran over time. Both Ax2 and *Dd5p4*$^-$ cells in this experimental setup were seeded in duplicate for each time point that was tested. Statistical comparisons were compared at the 2 hour time point and were determined using a Welch's *t* test. All data shown are from three independent biological repeats, ± SEM. Scale bars are 10 microns. * $P < 0.05$, **** $P < 0.0001$.

3.2.4. Numerous, smaller cups and macropinosomes were formed in *Dd5p4*$^-$ cells

In order to investigate how the absence of Dd5p4 activity influenced macropinocytosis, the dynamics of macropinocytic cups were next investigated. *Dd5p4*$^-$ cells were established to form smaller macropinosomes (Fig. 3.3.D.), which gave the incentive to establish whether this was due to smaller macropinocytic cups being formed, or smaller macropinosomes budding off from normal-sized macropinocytic cups. Studies were performed using a well-characterised PH-Crac probe, which binds PI(3,4,5)P_3 and PI(3,4)P_2, and acts as a marker for macropinocytic cups (Insall et al. 1994, Parente et al. 1998, Dormann et al. 2004) (Fig. 3.4.A-B.). Various features of macropinocytic cups were therefore measured starting with the number of macropinocytic cups formed per cell at a single time point. Using 3D acquisitions of Ax2 (Fig. 3.4.A.) and *Dd5p4*$^-$ (Fig. 3.4.B.) stably expressing the GFP-PH-Crac probe, the number of cups formed through *z* per cell was quantified. The absence of Dd5p4 activity increased the number of cups formed, with a cup frequency 3-fold higher compared to Ax2 control cells (Fig. 3.4.C.). Quantification of macropinocytic cup size indicated that *Dd5p4*$^-$ cells had smaller cups relative to Ax2 (Fig. 3.4.D.). *Dd5p4*$^-$ cups had an average length of 4.5 µm, a 25% reduction when compared to an average of 6 µm in Ax2 control cells (Fig. 3.4.D.). Another feature of macropinocytosis that was investigated was the number of macropinosomes generated per macropinocytic cup, as sometimes numerous macropinosomes formed from a single cup. This was quantified using time-lapses of Ax2 and *Dd5p4*$^-$ stably expressing GFP-PH-Crac. In *Dd5p4*$^-$, 5 macropinosomes on average were formed from each cup in comparison to Ax2 cells in which 2 macropinosomes per cup were generated (Fig. 3.4.E.). In summary, cells lacking Dd5p4 activity displayed numerous, small-sized macropinocytic cups, with numerous macropinosomes forming from each macropinocytic cup compared to Ax2 control cells.

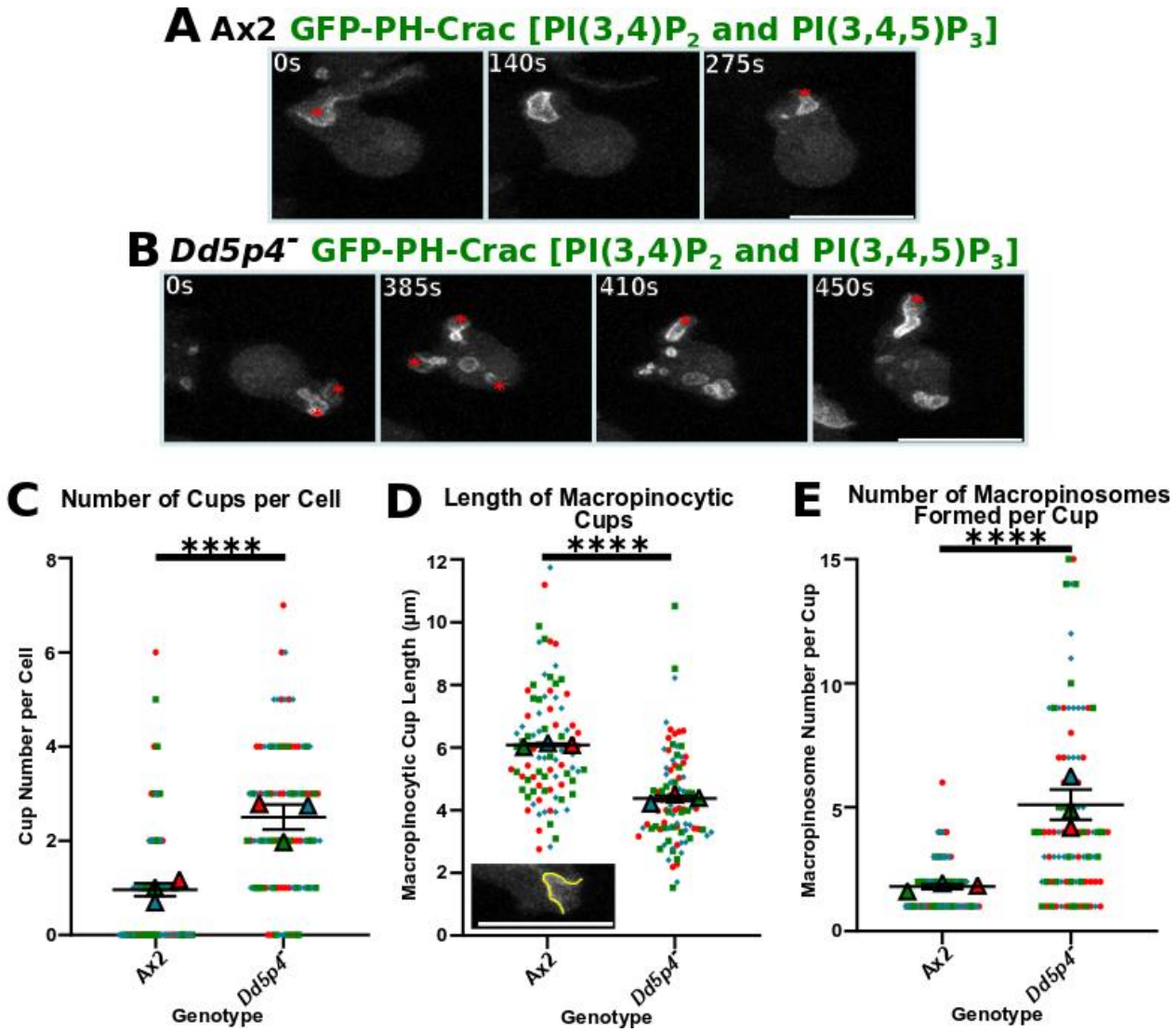

Figure 3.4. Multiple, smaller-sized macropinocytic cups, and macropinosomes were formed in *Dd5p4*⁻ cells. (A-B) Confocal images of Ax2 and *Dd5p4*⁻ respectively stably expressing GFP-PH-Crac. Red stars show macropinocytic cups. (C) Quantification of the macropinocytic cup numbers per cell. (D) Quantification of macropinocytic cup lengths. Cups were quantified at their largest size through *z* (an example measurement is shown with a yellow line). (E) Analysis of the number of macropinosomes generated from each macropinocytic cup. 30 cups were selected at random, per cell line, per biological repeat for all the data quantification that was performed. All the data shown are from three independent, colour-coded biological repeats, ± SEM. Scale bars are 10 microns. Significance was determined using Mann Whitney U tests. **** $P < 0.0001$.

3.2.5. *Dd5p4*⁻ phagocytic defects were due to failure in phagosome internalisation

The observations above suggest a role for Dd5p4 in organising macropinocytic cup structures. I therefore next turned to explore the roles that Dd5p4 may play during phagocytosis in more detail using confocal microscopy. To understand why *Dd5p4*⁻ cells were not able to successfully engulf yeast I first explored the speed in which yeast were enwrapped. $PI(3,4,5)P_3$ formation from $PI(4,5)P_2$ phosphorylation by the PI3K class I enzymes is a hallmark of phagocytic cup formation (Marshall et al. 2001). $PI(3,4,5)P_3$ was visualised using the specific and characterised

probe, which is a putative pseudogene, which is similar to the protein kinases A, G, and C (AGC) of the Akt family. The gene product is known as *D. discoideum* Protein Kinase 5 (DdPK5), which will be named from this point on as PkgE (acronym meaning unknown) (Ruchira et al. 2004, Goldberg et al. 2006, and van Haastert lab, unpublished data). The PkgE PI(3,4,5)P_3-binding probe was used to visualise if *Dd5p4*$^-$ mutants responded to initial contacts with yeast. The time taken for the PI(3,4,5)P_3-labelled PM to fully encircle the yeast was also measured to test if loss of Dd5p4 activity altered the rates of this process.

Dd5p4 functions to convert PI(3,4,5)P_3 patches to PI(3,4)P_2, and PI(4,5)P_2 to PI(4)P (Marshall et al. 2001, Loovers et al. 2003). In Ax2, phagosomes only acquire PI(3)P after phagocytic cup closure. I therefore used 2xFab1 YOTB Vac1, and EEA1 (2xFYVE) as a reporter (Gillooly et al. 2000, Calvo-Garrido et al. 2014) to unequivocally identify the completion of phagocytic engulfment as it was not always clear from previous time-lapses (Ellson et al. 2001, Vieira et al. 2001, Desale and Chinnathambi 2021).

Cells were stably transfected with the RFP-PH-PkgE GFP-2xFYVE dual expression probe, and were administered fluorescent blue yeast for 10 minutes in an imaging dish. An agarose disc was then applied to improve visualisation (Fig. 3.5.A-B. and D-G.).

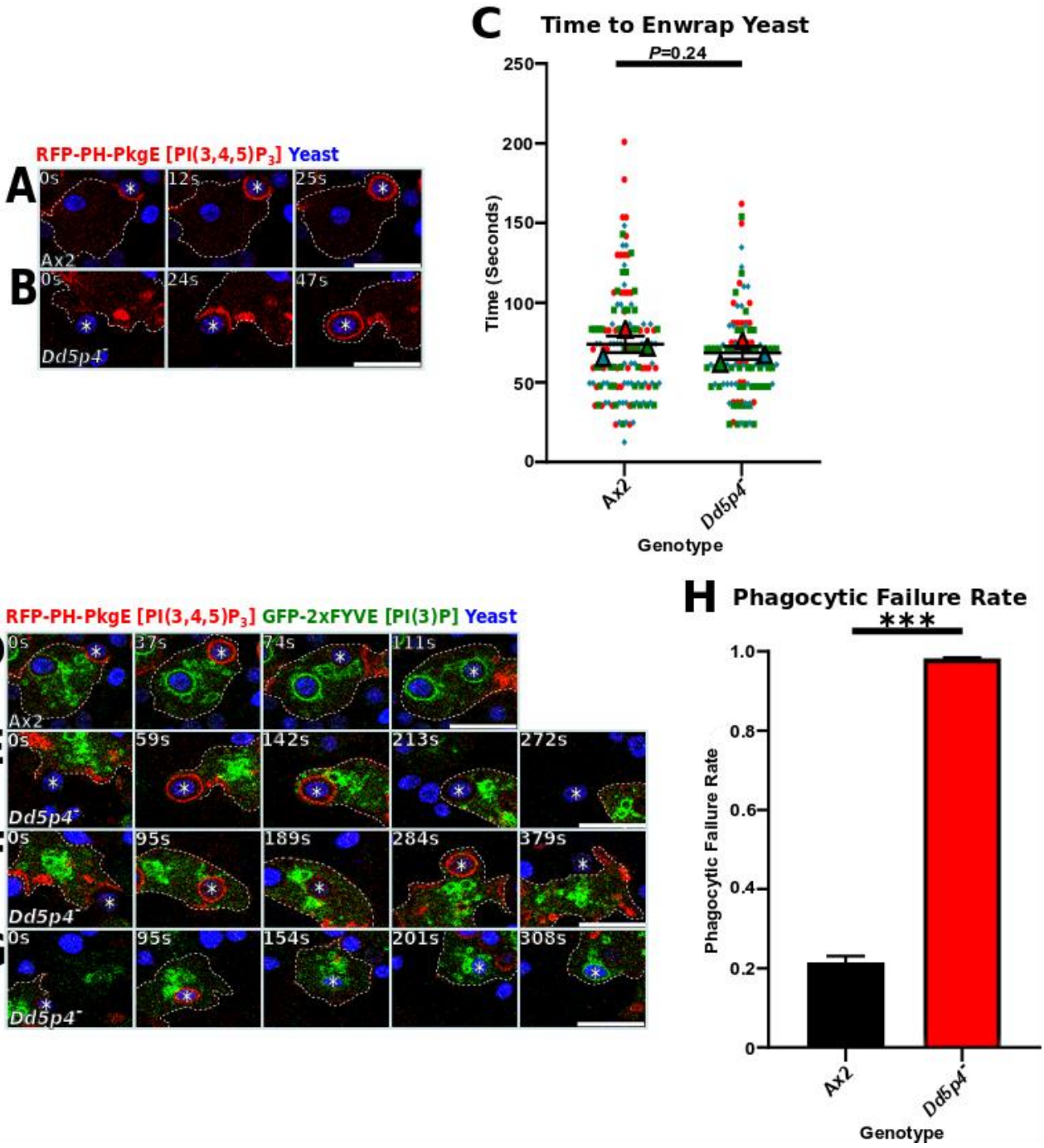

Figure 3.5. *Dd5p4*⁻ cells have a severe phagocytic defect due to phagosome internalisation failure. (A-B) Confocal images of Ax2 and *Dd5p4*⁻ respectively stably expressing RFP-PH-PkgE engulfing fluorescent blue yeast. (C) Quantification of the time taken for the PI(3,4,5)P_3-labelled PM (red with no white dashed lines) to fully enwrap yeast. The data shown are the individual points and averages from each of the three independent biological, colour-coded repeats. Non-significance was determined using a Mann Whitney U test. (D) Confocal time-lapse of Ax2 cells stably expressing the PI(3,4,5)P_3 probe together with GFP-2xFYVE engulfing fluorescent blue yeast. (E-G) Confocal time-lapses of *Dd5p4*⁻ stably expressing the equivalent probes engulfing fluorescent blue yeast. The cell peripheries are indicated by white dashed lines, with the time intervals indicated in white. Yeast of interest are indicated by white stars. (H) Quantification of the phagocytic failure rate. Successful events occurred when PI(3,4,5)P_3 (red) was converted to PI(3)P (green). The data shown is the average failure rate across all three independent biological repeats for each cell line. Significance was determined using a Welch's *t* test. All error bars are ± SEM. Scale bars are 10 microns. *** $P < 0.001$.

In Ax2 cells, PI(3,4,5)P_3 forms upon contact with yeast and encircles the yeast with the PI(3,4,5)P_3 being removed after phagocytic cup closure. Upon successful internalisation, PI(3)P was formed and encircled the early phagosome, accompanied by the abrupt movement away from the initial point of contact (Fig. 3.5.D.). In *Dd5p4*$^-$, the cells were able to make contact with yeast and PI(3,4,5)P_3 was able to encircle the yeast successfully, however the phagosome remained close to the initial site of contact. After this period PI(3,4,5)P_3 disappeared and shortly after the yeast were released from the cell, indicating phagocytic engulfment failure (Fig. 3.5.E.). The *Dd5p4*$^-$ failed phagocytic events also exhibited, albeit at a reduced frequency, multiple flashes of PI(3,4,5)P_3 prior to the eventual particle release, indicating multiple failed attempts at phagocytic engulfment (Fig. 3.5.F.). On very rare occasions *Dd5p4*$^-$ cells were successfully able to internalise the phagosome and this was demonstrated through the formation of PI(3)P (Fig. 3.5.G.). This would suggest that these mutants failed to internalise the phagosome almost exclusively as a result of unsuccessful phagocytic engulfment at the final stages of internalisation. This stage would be explored in more detail later to ascertain the exact cause of phagocytic engulfment failure. *Dd5p4*$^-$ cells overall exhibited a very severe phagocytic defect, with 98% of all phagocytic engulfment events failing compared to 20% for Ax2 control cells (Fig. 3.5.H.).

3.2.6. PI(4,5)P_2 depletion was reduced at the centre of *Dd5p4*$^-$ phagocytic cups

PI(3,4,5)P_3 and PI(4,5)P_2 are both Dd5p4 substrates, which are hydrolysed to form PI(3,4)P_2 and PI(4)P respectively (Loovers et al. 2003). This gave the incentive to investigate PI(3,4,5)P_3, PI(4,5)P_2, and PI(4)P levels across phagocytic and macropinocytic cups to test if Dd5p4 loss affected the levels of these PIPs during the different stages towards cup closure (Fig. 3.6.A-L.). PkgE was used to visualise PI(3,4,5)P_3 levels across both phagocytic and macropinocytic cups. The previously well-characterised Pleckstrin Homology-Phospholipase C isoform δ (PLC-δ) probe, which was shown to bind to PI(4,5)P_2 (Drayer and Vanhaastert 1992), only displayed cytosolic localisation when stably expressed in *D. discoideum*, making this probe unsuitable. An alternative PI(4,5)P_2-specific probe, Nodulin, which bound to PI(4,5)P_2 at the PM when stably expressed in *D. discoideum* was used instead (Ghosh et al. 2015). The product of PI(4,5)P_2 hydrolysis, PI(4)P, was also investigated using the *D. discoideum* optimised P4M probe, which bound to a pool of PI(4)P present at the PM (Hammond et al. 2014).

The profiles of PI(4,5)P_2, PI(4)P, and PI(3,4,5)P_3 were first visualised across phagocytic cups at different stages towards cup closure (Fig. 3.6.A-L.). Cells were seeded and left to settle for one hour before being administered fluorescently labelled blue yeast for 10 minutes.

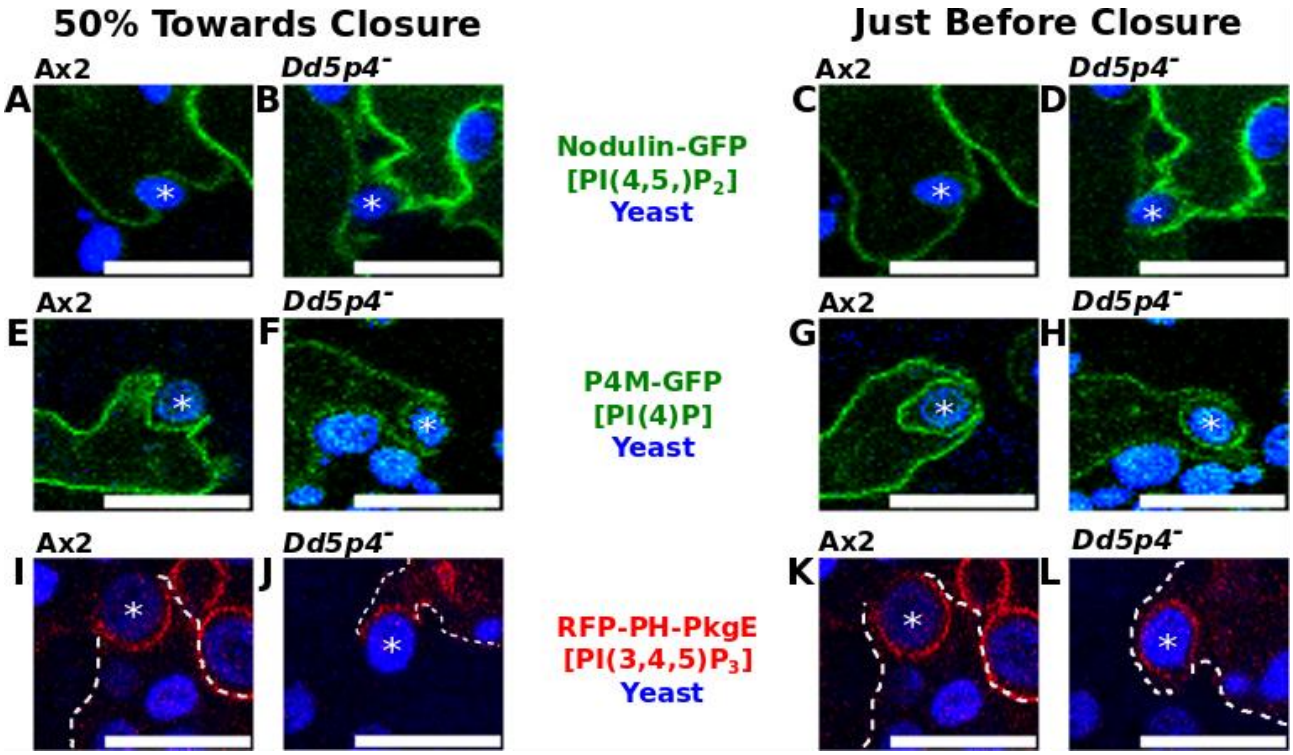

Figure 3.6. PI(4,5)P_2 depletion was reduced at the centre of *Dd5p4*$^-$ phagocytic cups. (A-B) Confocal images of Ax2 and *Dd5p4*$^-$ cells respectively stably expressing Nodulin-GFP [PI(4,5)P_2] 50% towards phagocytic cup closure. (C-D) Cells stably expressing the same probe showing the same cups just before phagocytic cup closure. (E-F) Ax2 and *Dd5p4*$^-$ cells stably expressing P4M-GFP [PI(4)P] 50% towards phagocytic cup closure. (G-H) Cells stably expressing the same probe showing the same cups just before phagocytic cup closure. (I-J) Ax2 and *Dd5p4*$^-$ cells stably expressing RFP-PH-PkgE [PI(3,4,5)P_3] 50% towards phagocytic cup closure. (K-L) Cells stably expressing the same probe showing the same cups just before phagocytic cup closure. Yeast during the different stages of engulfment are highlighted by white stars. White dashed lines indicate cell peripheries. Scale bars are 10 microns.

To quantify and determine how Dd5p4 regulated PI(4,5)P_2, PI(4)P, and PI(3,4,5)P_3 dynamics across phagocytic cups at different stages towards phagocytic cup closure, the fluorescence intensity was normalised and the fold enrichment for each PIP was calculated, and averaged across multiple cups, from cup tip to cup tip (Fig. 3.7.A-L.).

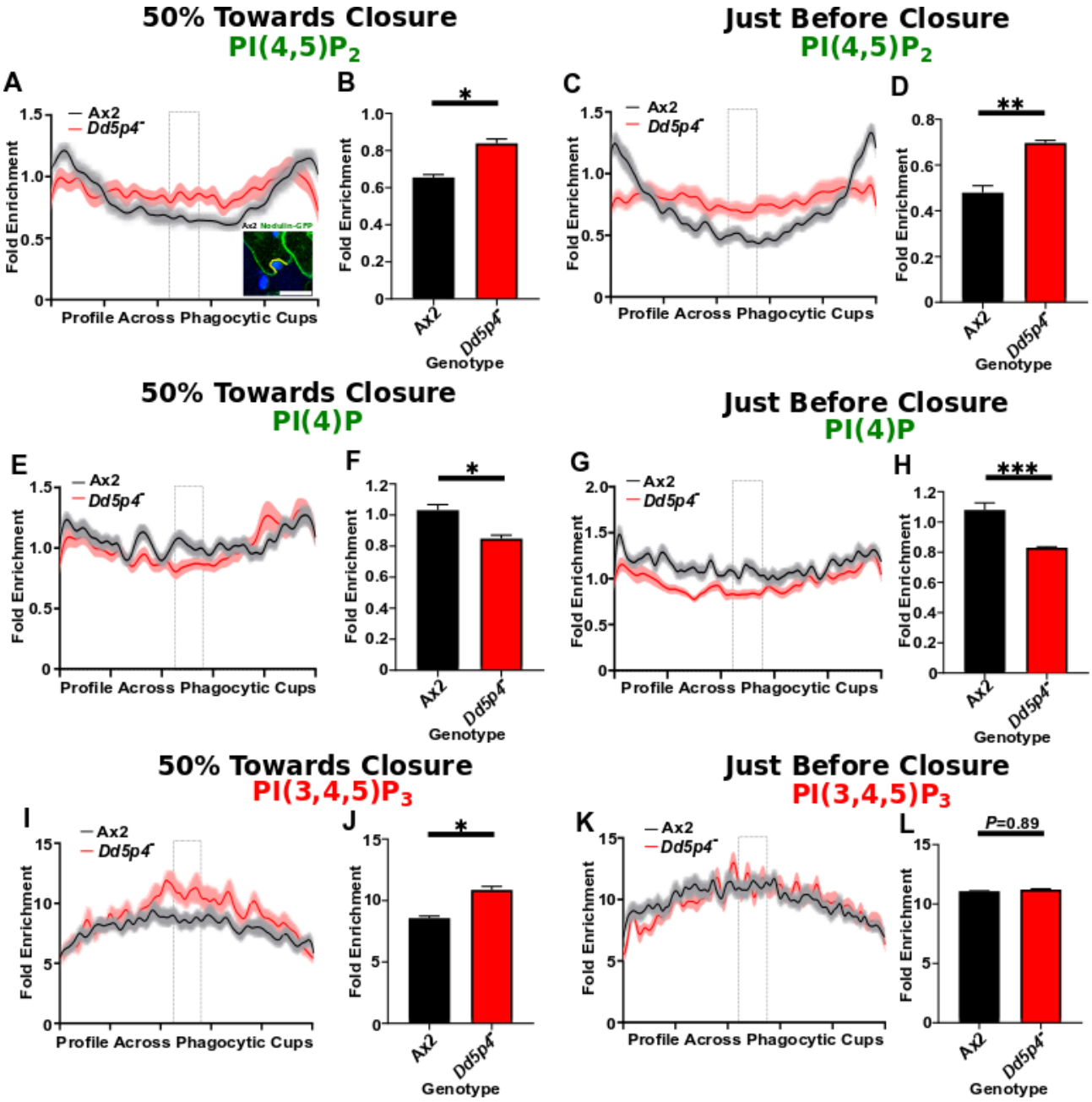

Figure 3.7. PI(4,5)P_2 depletion was reduced at the centre of *Dd5p4*$^-$ phagocytic cups. (A) PI(4,5)P_2 enrichment in cells stably expressing Nodulin-GFP 50% towards phagocytic cup closure, an example cup and the quantified region is shown in yellow. (B) Central 10% of PI(4,5)P_2 profiles in (A), indicated by a light-grey, dashed rectangle. (C-D) Equivalent graphs of PI(4,5)P_2 enrichment just before phagocytic cup closure. Data was normalised to non-protruding PM and intracellular PI(4,5)P_2 levels. (E) PI(4)P enrichment from cells stably expressing P4M-GFP 50% towards phagocytic cup closure. (F) Central 10% of PI(4)P profiles in (E) indicated by a dashed rectangle. (G-H) Equivalent graphs of PI(4)P enrichment just before phagocytic cup closure. Data was normalised to non-protruding PM and intracellular PI(4)P. (I) PI(3,4,5)P_3 enrichment from cells stably expressing RFP-PH-PkgE 50% towards phagocytic cup closure. (J) Central 10% of PI(3,4,5)P_3 profiles in (I) indicated by a dashed rectangle. (K-L) Equivalent graphs of PI(3,4,5)P_3 enrichment just before phagocytic cup closure. Data was normalised to non-protruding PM PI(3,4,5)P_3. 10 phagocytic cups per stage towards phagocytic cup closure were quantified, per cell line, per biological repeat for all the displayed data. Macro was written by James Vines. All the data shown are from three independent biological repeats, ± SEM. Scale bar is 10 microns. Significance and non-significance was determined using Welch's *t* tests of the central profile averages. * $P < 0.05$, ** $P < 0.01$, *** $P < 0.001$.

In Ax2 cells, PI(4,5)P_2 was depleted progressively at the base of phagocytic cups at both time points towards cup closure, however in *Dd5p4*$^-$ cells PI(4,5)P_2 depletion was reduced, causing a more uniform PI(4,5)P_2 profile across phagocytic cups in these mutants (Fig. 3.7.A-D.). This would suggest that Dd5p4 directs its catalytic activity progressively towards phagocytic cup closure at the centre of cups to de-phosphorylate PI(4,5)P_2 to PI(4)P.

In Ax2 cells, the fold enrichment of PI(4)P was shown across phagocytic cups to be similar overall to that observed in *Dd5p4*$^-$, with the exception of the centre of *Dd5p4*$^-$ cups, in which less PI(4)P was observed at both time points towards phagocytic cup closure (Fig. 3.7.E-H.). These observations did not quite show the inverse pattern to the PI(4,5)P_2 enrichment profiles in Ax2 cells (Fig. 3.7.A-D.), in which PI(4)P levels were expected to be reduced at the tips and elevated at the centre of phagocytic cups due to increased PI(4,5)P_2 to PI(4)P hydrolysis.

In Ax2 cells, the PI(3,4,5)P_3 fold enrichment was observed to be very similar overall to the PI(3,4,5)P_3 fold enrichment in *Dd5p4*$^-$ mutants at both time points towards phagocytic cup closure (Fig. 3.7.I-L.). Ax2 cells did, however, display less PI(3,4,5)P_3 at the centre of phagocytic cups halfway towards cup closure compared to the PI(3,4,5)P_3 levels in *Dd5p4*$^-$ mutants (Fig. 3.7.J.). The lack of any major changes in the PI(3,4,5)P_3 fold enrichment overall suggested that PI(4,5)P_2 hydrolysis was the main target of Dd5p4 enzymatic activity.

3.2.7. PI(4,5)P_2 depletion was moderately reduced at the centre of *Dd5p4*$^-$ macropinocytic cups

The profiles of PI(4,5)P_2, PI(4)P, and PI(3,4,5)P_3 were next visualised across macropinocytic cups at different stages towards macropinocytic cup closure. This was undertaken to observe if there were any differences in PIP dynamics between phagocytosis and macropinocytosis (Fig. 3.6.A-L. and Fig. 3.8.A-L.). Cells were seeded and left to settle for one hour prior to confocal imaging.

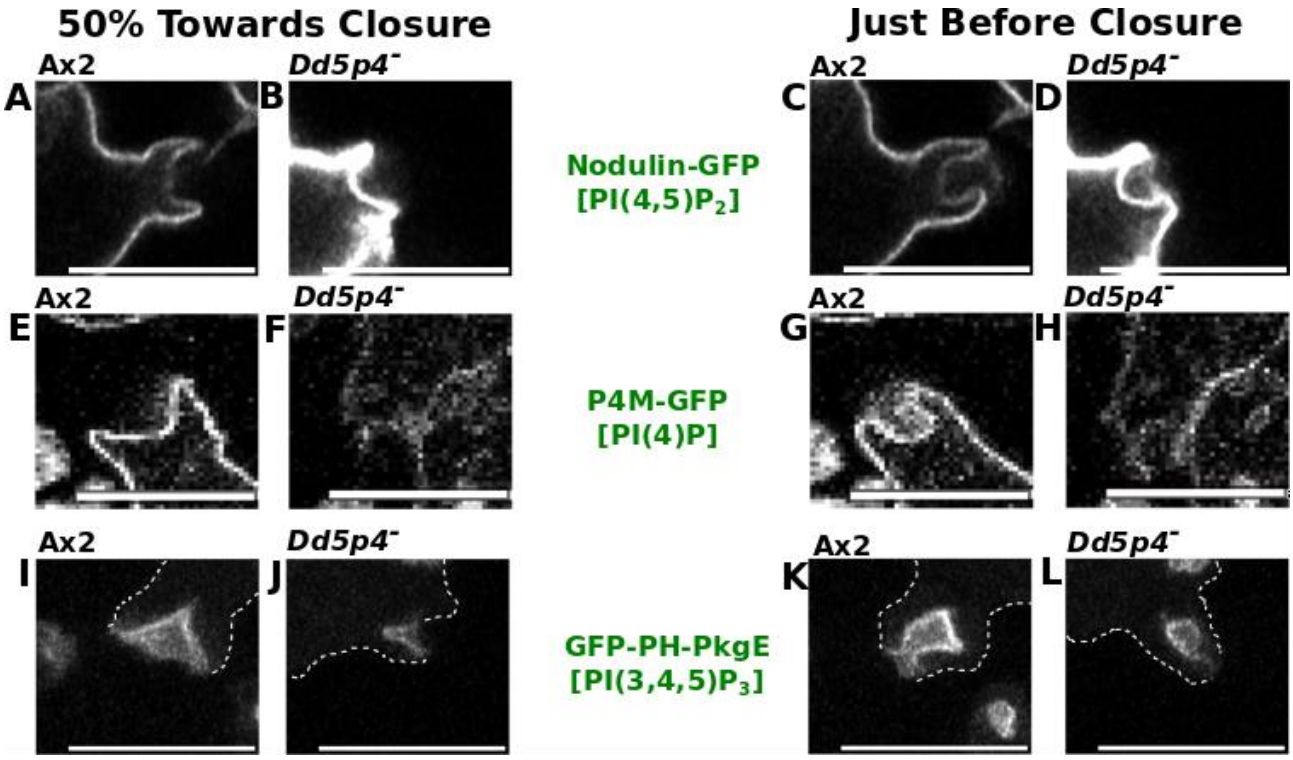

Figure 3.8. PI(4,5)P_2 depletion was moderately reduced at the centre of *Dd5p4*$^-$ macropinocytic cups. (A-B) Confocal images of Ax2 and *Dd5p4*$^-$ cells respectively stably expressing Nodulin-GFP [PI(4,5)P_2] 50% towards macropinocytic cup closure. (C-D) Cells stably expressing the same probe showing the same cups just before macropinocytic cup closure. (E-F) Ax2 and *Dd5p4*$^-$ cells respectively stably expressing P4M-GFP [PI(4)P] 50% towards macropinocytic cup closure. (G-H) Cells stably expressing the same probe showing the same cups just before macropinocytic cup closure. (I-J) Ax2 and *Dd5p4*$^-$ cells stably expressing RFP-PH-PkgE [PI(3,4,5)P_3] 50% towards macropinocytic cup closure. (K-L) Cells stably expressing the same probe showing the same cups just before macropinocytic cup closure. White dashed lines indicate cell peripheries. Scale bars are 10 microns.

The macropinocytic PIP dynamics across cups appeared to be very similar to those observed in cells stably expressing the equivalent probes during the different stages of cup closure (Fig. 3.6.A-L. and Fig. 3.8.A-L.).

The analysis performed during the different stages of phagocytic cup closure to quantify PIP dynamics was also applied to macropinocytic cups of cells stably expressing the equivalent probes. This generated a profile of each PIP across macropinocytic cups for each cell line, at different stages towards cup closure (Fig. 3.9.A-L.).

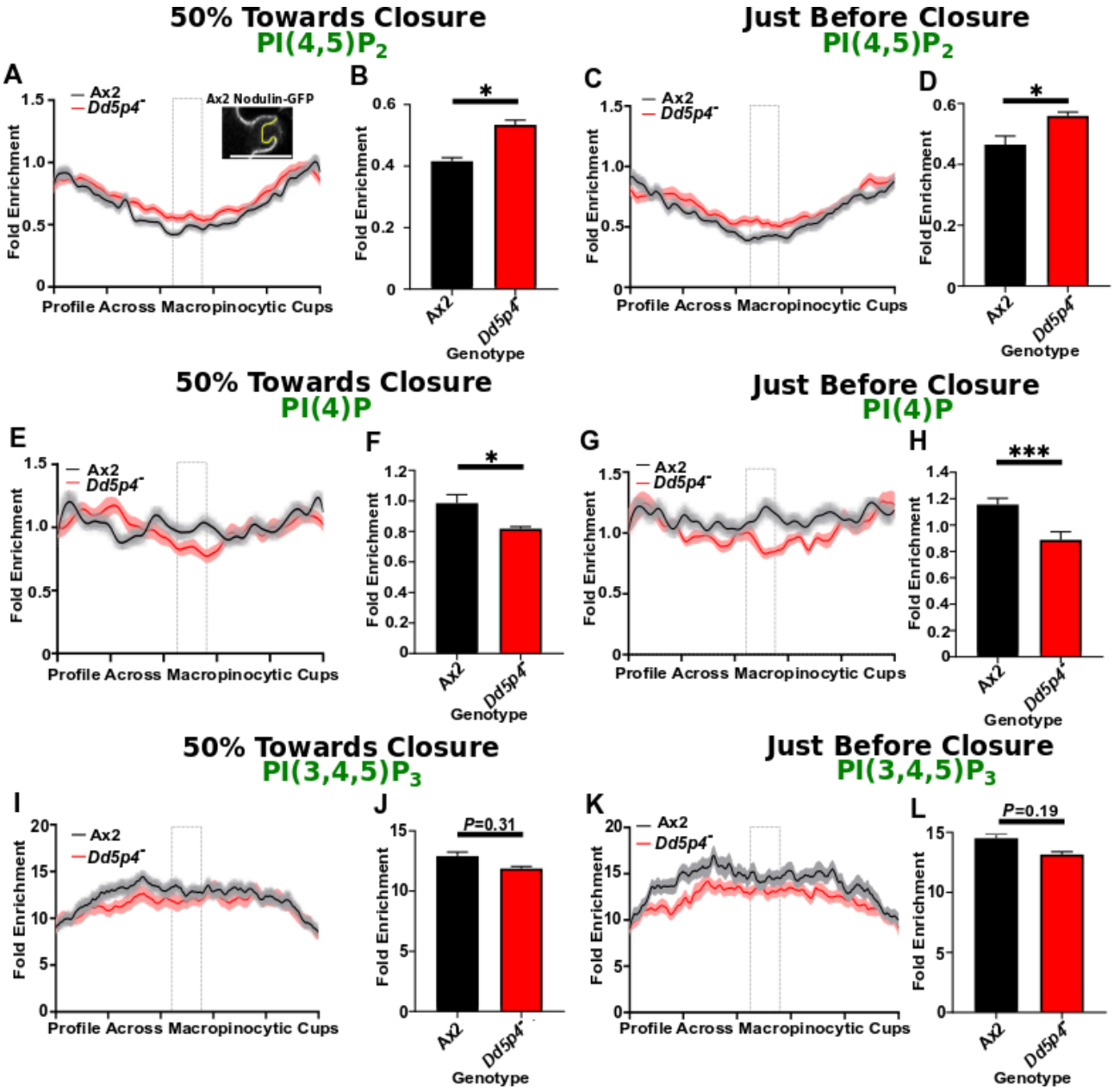

Figure 3.9. PI(4,5)P_2 depletion was moderately reduced at the centre of *Dd5p4*$^-$ macropinocytic cups. (A) PI(4,5)P_2 enrichment from cells stably expressing Nodulin-GFP 50% towards macropinocytic cup closure, an example cup and the quantified region is shown in yellow. (B) Central 10% of PI(4,5)P_2 profiles in (A), indicated by a light-grey, dashed rectangle. (C-D) Equivalent graphs of PI(4,5)P_2 enrichment just before macropinocytic cup closure. Data was normalised to non-protruding PM and intracellular PI(4,5)P_2 levels. (E) PI(4)P enrichment from cells stably expressing P4M-GFP 50% towards macropinocytic cup closure. (F) Central 10% of PI(4)P profiles in (E) shown by a light-grey, dashed rectangle. (G-H) Equivalent graphs of PI(4)P enrichment just before macropinocytic cup closure. Data was normalised to non-protruding PM and intracellular PI(4)P. (I) PI(3,4,5)P_3 enrichment from cells stably expressing RFP-PH-PkgE 50% towards macropinocytic cup closure. (J) Central 10% of PI(3,4,5)P_3 profiles in (I) shown by a light-grey, dashed rectangle. (K-L) Equivalent graphs of PI(3,4,5)P_3 enrichment just before macropinocytic cup closure. Data was normalised to non-protruding PM PI(3,4,5)P_3. 10 macropinocytic cups per stage towards macropinocytic cup closure were quantified, per cell line, per biological repeat, for all the displayed data. Macro was written by James Vines. All the data shown are from three independent biological repeats, ± SEM. Scale bar is 10 microns. Significance and non-significance was determined using Welch's *t* tests of central profile averages. * $P < 0.05$, *** $P < 0.001$.

PI(4,5)P_2 was hydrolysed in both Ax2 cells and, to a slightly lesser degree in *Dd5p4*$^-$ mutant cells across the full profile of macropinocytic cups, with a significant reduction of PI(4,5)P_2 depletion observed in the centre of *Dd5p4*$^-$ macropinocytic cups at both stages towards macropinocytic cup closure (Fig. 3.9.A-D.). The differences in PI(4,5)P_2 dynamics between the two cell lines were of lesser magnitude overall than what was observed for phagocytosis (Fig. 3.7.A-D.).

The macropinocytic profiles of PI(4)P, and PI(3,4,5)P_3, were both found to be very similar to the equivalent profiles displayed during phagocytic cup closure in both cell lines (Fig. 3.7.E-L. and Fig. 3.9.E-L.). In summary, the effects on PIP metabolism across cups were more pronounced in phagocytosis, and indicated a localised role for Dd5p4 in PI(4,5)P_2 hydrolysis progressively in the interior of macro-endocytic cups towards closure.

3.2.8. PI(3,4,5)P_3 and PI(3,4)P_2 dynamics after cup closure were altered in *Dd5p4*$^-$ during macropinocytosis

Following on from the studies assessing PIP dynamics halfway towards and immediately before cup closure, I then moved onto testing if the dynamics of PIPs after closure were altered in *Dd5p4*$^-$ mutants. PI(3,4,5)P_3 and PI(3,4)P_2 dynamics were therefore investigated using GFP-PH-PkgE and TAPP1-PH-GFP probes respectively. In cells stably expressing these probes, the time taken for macropinosomes to form from macropinocytic cups, and the post-closure lifetimes of PI(3,4,5)P_3, and PI(3,4)P_2 were all quantified (Fig. 3.10.A-I.) (Dowler et al. 2000, Ruchira et al. 2004, Goldberg et al. 2006, and van Haastert lab, unpublished data). Quantification of PI(3,4,5)P_3, and PI(3,4)P_2 dynamics during phagocytosis was not possible, as phagocytic events almost always failed in *Dd5p4*$^-$ mutant cells.

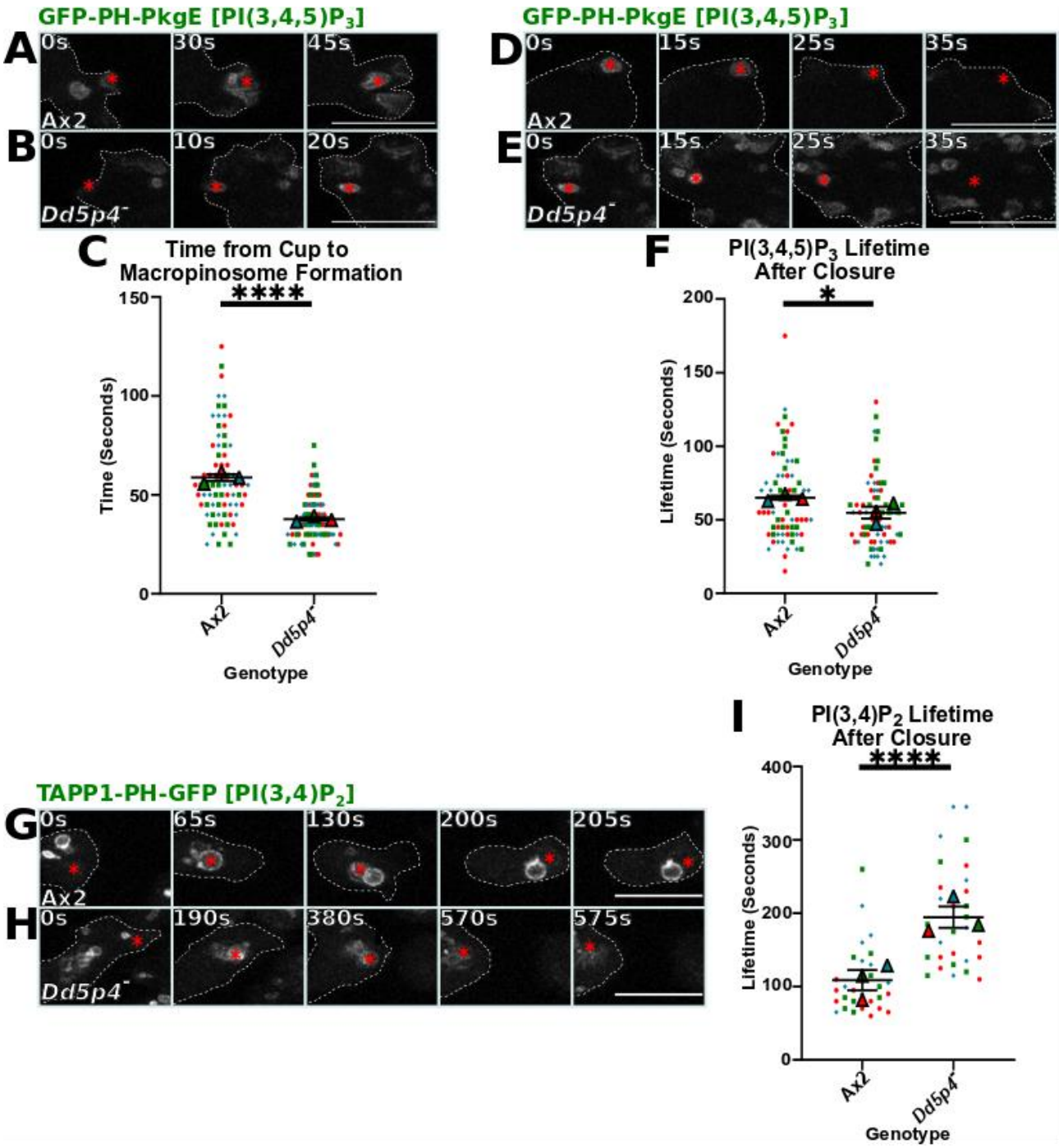

Figure 3.10. Macropinosome generation, and the lifetime of $PI(3,4,5)P_3$ and $PI(3,4)P_2$ were altered in *Dd5p4*$^-$. (A-B) Representative images of Ax2 and *Dd5p4*$^-$ stably expressing GFP-PH-PkgE. (C) Quantification of the time taken for macropinosome generation from the initial macropinocytic cup formation stage. (D-E) Cells stably expressing the same probe. (F) Quantification of the $PI(3,4,5)P_3$ lifetime on macropinosomes after cup closure. 25 macropinocytic cups and macropinosomes, per independent biological repeat, per cell line were quantified. (G-H) Ax2 and *Dd5p4*$^-$ cells stably expressing TAPP1-PH-GFP at and after macropinocytic cup closure. Macropinocytic cups and macropinosomes of interest over time are highlighted by red stars. Cell peripheries are outlined by white dashed lines. (I) Quantification of the lifetime of $PI(3,4)P_2$ on macropinosomes after cup closure. 10 TAPP1-PH-GFP-labelled macropinosomes, per independent biological repeat, per cell line were quantified. All the data shown are from three independent, colour-coded biological repeats, ± SEM. Scale bars are 10 microns. Significance was determined using Mann Whitney U tests. * $P < 0.05$, **** $P < 0.0001$.

The absence of Dd5p4 activity significantly reduced the time taken for a macropinosome to form from the initiation of a PI(3,4,5)P_3 patch (Fig. 3.10.A-C.). In Ax2 cells, the average time taken from the formation of a macropinocytic cup to the generation of the first macropinosome was 65 seconds, whereas in *Dd5p4*$^-$ this process took only 35 seconds (Fig. 3.10.C.). This suggests that either Dd5p4 is involved in the regulation of the temporal dynamics between cup and macropinosome formation, or that the macropinocytic cups simply close sooner due to their smaller sizes.

It was initially hypothesised that in *Dd5p4*$^-$ cells, as less PI(3,4,5)P_3 would have been de-phosphorylated to PI(3,4)P_2 then the lifetime of PI(3,4,5)P_3 on macropinosomes in *Dd5p4*$^-$ would have been expected to have increased. Analysis however, of the lifetime of PI(3,4,5)P_3, which encompassed the emergence of PI(3,4,5)P_3-labelled macropinosomes after closure to PI(3,4,5)P_3 degradation was measured in *Dd5p4*$^-$ and was compared to Ax2 control cells, which instead indicated that the lifetime of PI(3,4,5)P_3 was significantly reduced in these mutants (Fig. 3.10.F.).

Building on from this surprising discovery, the product of PI(3,4,5)P_3 hydrolysis, PI(3,4)P_2, was next analysed. If this followed on from the previous discovery of the decrease in the PI(3,4,5)P_3 lifetime on macropinosomes in *Dd5p4*$^-$ (Fig. 3.10.F.), then the lifetime of PI(3,4)P_2 on macropinosomes would have been expected to have increased. Many PI(3,4)P_2-labelled macropinosomes were indeed observed in both Ax2 control cells and in particular *Dd5p4*$^-$ mutant cells (Fig. 3.10.G-H.). Analysis of the lifetime of PI(3,4)P_2, which encompassed the emergence of the PI(3,4)P_2-labelled macropinosomes following closure to PI(3,4)P_2 degradation did display a significant increase in the lifetime by approximately 2-fold in *Dd5p4*$^-$ compared to Ax2 control cells (Fig. 3.10.I.).

These findings collectively may suggest that the decreased lifetime of PI(3,4,5)P_3 on macropinosomes in *Dd5p4*$^-$ mutant cells may occur due to the activity of another inositol 5-phosphatase, which may de-phosphorylate PI(3,4,5)P_3 to PI(3,4)P_2. The inositol 5-phosphatase, Dd5p2, which is encoded in *D. discoideum*, has a preference for the hydrolysis of PI(3,4,5)P_3 (Loovers et al. 2003), and may somehow be upregulated in the absence of Dd5p4 enzymatic activity in *Dd5p4*$^-$ mutant cells. The upregulation of Dd5p2 enzymatic activity may explain the increase in the lifetime of PI(3,4)P_2 on the macropinosomes of *Dd5p4*$^-$ mutant cells as more PI(3,4,5)P_3 could be hydrolysed to PI(3,4)P_2 in comparison to Ax2 control cells (Fig. 3.10.F. and I.) (Loovers et al. 2003).

3.2.9. PI(4)P dynamics after closure were altered in *Dd5p4*$^-$ during macropinocytosis

PI(4,5)P_2, PI(4)P, and PI(3)P were next investigated to test if Dd5p4 regulated the dynamics of these PIPs after macropinocytic cup closure. To this end, the PI(4,5)P_2, PI(4)P, and PI(3)P dynamics were dissected using the respective PIP-binding probes; Nodulin-GFP, P4M-GFP, and GFP-2xFYVE

(Fig. 3.11.A-I.) (Gillooly et al. 2000, Calvo-Garrido et al. 2014, Hammond et al. 2014, Ghosh et al. 2015).

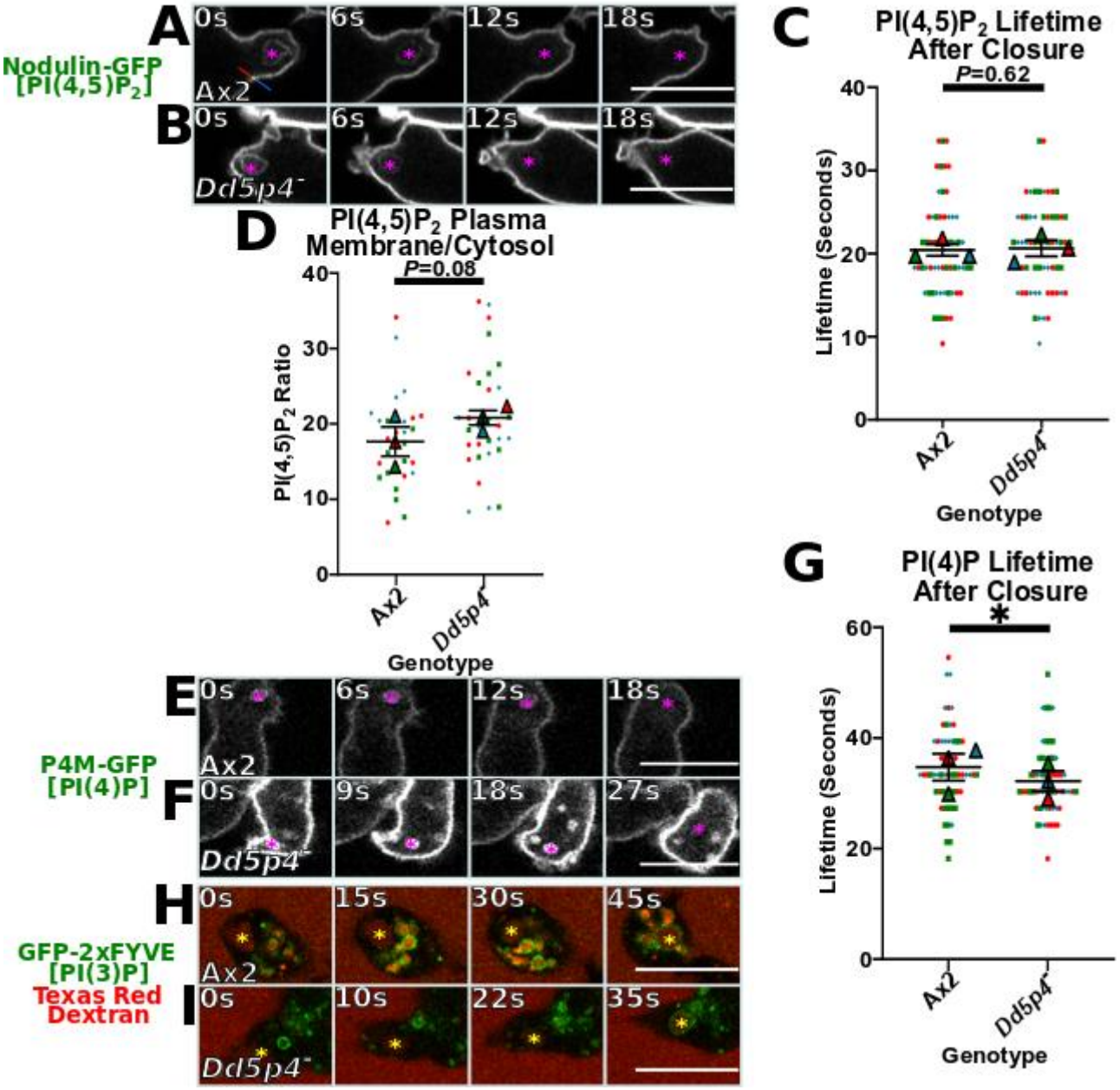

Figure 3.11. PI(4)P dynamics were altered after cup closure in *Dd5p4*⁻. (A-B) Film strips of Ax2 and *Dd5p4*⁻ stably expressing Nodulin-GFP during macropinocytosis. (C) Lifetime quantification of $PI(4,5)P_2$ on macropinosomes after closure to the loss of $PI(4,5)P_2$ in Ax2 and *Dd5p4*⁻. 20 macropinosomes, per cell line, per biological repeat were analysed. (D) Quantification of the non-protruding $PI(4,5)P_2$ PM to cytosolic ratio (example shown at time 0 seconds in A, red marks the $PI(4,5)P_2$ intracellular signal, yellow the PM signal, and blue the extracellular signal). Values were normalised through subtraction of the average extracellular signal (blue) from both the average PM (yellow) and average cytosolic signals (red), with the normalised $PI(4,5)P_2$ PM divided by the normalised cytosolic signal. 10 cells were measured at random, per cell line, per biological repeat. (E-F) Film strips of Ax2 and *Dd5p4*⁻ stably expressing P4M-GFP during macropinocytosis. Macropinosomes of interest are indicated by magenta stars. (G) Quantification of the lifetime of PI(4)P from macropinosome formation after cup closure to the loss of PI(4)P. 20 macropinosomes, per cell line, per biological repeat were analysed. (H-I) Film strips of Ax2 and *Dd5p4*⁻ stably expressing GFP-2xFYVE taking up Texas red dextran. Probes and their respective PIPs to which they bind are indicated. Macropinosomes of interest are indicated by yellow stars. All the data shown are from three independent, colour-coded biological repeats, ± SEM. Scale bars are 10 microns. Significance and non-significance was determined using Mann Whitney U tests. * $P < 0.05$.

The loss of Dd5p4 activity did not alter the time taken to deplete PI(4,5)P_2 on macropinosomes after cup closure when compared to Ax2 control cells (Fig. 3.11.A-C.). This would suggest that PI(4,5)P_2 could be degraded via alternative inositol 5-phosphatases, such as Dd5p1-Dd5p3 (Loovers et al. 2003). Another explanation could be that PI(4,5)P_2 may be degraded by the enzymatic activity of phospholipase C to generate Ins(1,4,5)P_3 and DAG after macropinocytic cup closure (Swanson 1989, Egami et al. 2014).

Dd5p4 has been shown to exhibit its enzymatic activity at the centre of macropinocytic cups causing PI(4,5)P_2 to be de-phosphorylated to form PI(4)P (Fig. 3.9.A-D.). In addition to the centre of cups, Dd5p4 activity was also tested by measuring PI(4,5)P_2 levels at non-protruding PM regions. Non-protruding PI(4,5)P_2 was measured and normalised to cytosolic PI(4,5)P_2 to test if Dd5p4 was affecting PI(4,5)P_2 levels at non-protruding membranes. The absence of Dd5p4 activity did not alter the PI(4,5)P_2 PM to cytosol ratio (Fig. 3.11.D.). This suggested that Dd5p4 did not exhibit its catalytic activity towards PI(4,5)P_2 found on non-protruding membranes. Dd5p4 might therefore only be recruited to the central regions of macropinocytic and phagocytic cups to ensure controlled and targeted PI(4,5)P_2 hydrolysis during the early stages of these macro-endocytic processes.

The absence of Dd5p4 however, decreased the lifetime of PI(4)P on macropinosomes after cup closure when compared to Ax2 control cells (Fig. 3.11.G.). This finding may suggest that the decrease in the lifetime of PI(4)P in *Dd5p4*$^-$ macropinosomes could be due to the loss of Dd5p4 activity somehow causing the upregulation of the kinase activity of PI3K4 and thus the phosphorylation of PI(4)P to PI(3,4)P_2 on macropinosomes after cup closure (Hoeller et al. 2013). This may also simultaneously explain the increase in the lifetime of PI(3,4)P_2 that has been observed on macropinosomes in *Dd5p4*$^-$ mutant cells (Fig. 3.10.I.).

PI(3,4)P_2 is subsequently de-phosphorylated by an unknown inositol 4-phosphatase in *D. discoideum* to generate PI(3)P, a marker of successful internalisation of the early macropinosome (Christoforidis et al. 1999). However, the majority of PI(3)P that forms on early macropinosomes results from the phosphorylation of PI to PI(3)P by Vps34 kinase activity (Herman and Emr 1990, Schu et al. 1993, Kihara et al. 2001). To test whether there was a delay in the emergence of PI(3)P following macropinosome internalisation in *Dd5p4*$^-$, cells were administered Texas red dextran and the time taken for PI(3)P formation was visualised following macropinosome internalisation (Fig. 3.11.H-I.). No delay in PI(3)P formation appeared to be observed in *Dd5p4*$^-$ compared to Ax2 control cells, meaning that PI(3)P appeared to be presented on early macropinosomes without delay in these mutants following macropinosome internalisation (Fig. 3.11.H-I.).

3.2.10. Investigating the temporal dynamics of macropinocytic PIPs using LLSM

To more clearly measure in 3D the high resolution temporal dynamics of crucial PIPs throughout cup formation and early maturation in Ax2 and *Dd5p4*$^{-}$ cells during the early stages of macropinocytosis, LLSM was used. Use of this state-of-the-art microscopy would also validate the changes observed previously in PIP metabolism during this investigation. The PI(3,4,5)P_3 (PkgE-PH-mCherry), PI(3,4)P_2 (TAPP1-PH-GFP), and PI(4,5)P_2 (Nodulin-GFP) intensity profiles, as well as Filamentous-actin (F-actin) intensity profiles were also plotted. The PIP intensity profiles alone comparing Ax2 to *Dd5p4*$^{-}$ during early the stages of macropinocytosis were first plotted from LLSM images by Master's student, Kirsty Tinsley (Fig. 3.12.A-D. and Fig. 3.13.A-D.).

Interestingly, the stable expression of the PI(3,4,5)P_3 and PI(3,4)P_2 binding probes showed a transition of PI(3,4,5)P_3 after cup closure to PI(3,4)P_2 in Ax2 control cells. The formation of PI(3,4)P_2 on the large macropinosome also subsequently resulted in its fragmentation into smaller macropinosomes (Fig. 3.12.A.). In *Dd5p4*$^{-}$, PI(3,4,5)P_3 conversion to PI(3,4)P_2 was unperturbed (Fig. 3.12.B.), indicating that another Dd5p inositol 5-phosphatase was likely orchestrating this reaction (Fig. 3.7.I-L., Fig. 3.9.I-L. and Fig. 3.10.D-F.), most likely Dd5p2 (Loovers et al. 2003). Macropinosome fragmentation was also observed following PI(3,4)P_2 formation within *Dd5p4*$^{-}$ cells (Fig. 3.12.B.).

PI(3,4,5)P_3 levels during the early stages of macropinocytosis displayed statistical significance at cup closure, at which *Dd5p4*$^{-}$ exhibited lower levels of PI(3,4,5)P_3 compared to the Ax2 control cells (Fig. 3.12.C.). This provided a different observation in comparison to my previous observations, which showed that *Dd5p4*$^{-}$ mutants displayed a significant reduction in the PI(3,4,5)P_3 lifetime after cup closure in these mutants in comparison to Ax2 control cells (Fig. 3.10.F.). This reduction may have also occurred due to Dd5p2 enzymatic activity (Loovers et al. 2003) at cup closure in these mutants being somehow upregulated, potentially resulting in faster PI(3,4,5)P_3 hydrolysis on the macropinosomes of *Dd5p4*$^{-}$ after cup closure (Fig. 3.10.F. and Fig. 3.12.C.).

PI(3,4)P_2 levels during the early stages of macropinocytosis were almost identical before cup closure, with there being a significant increase in PI(3,4)P_2 levels at cup closure in *Dd5p4*$^{-}$ mutant cells (Fig. 3.12.D.). After cup closure PI(3,4)P_2 remained on macropinosomes for much longer in *Dd5p4*$^{-}$ cells compared to Ax2 control cells (Fig. 3.12.D.). These observations supported those I made previously on PI(3,4)P_2 dynamics after cup closure during macropinocytosis (Fig. 3.10.G-I.).

When comparing the profiles of both PI(3,4,5)P_3 and PI(3,4)P_2 of both cell lines PI(3,4,5)P_3 levels decreased as PI(3,4)P_2 levels increased after cup closure, which illustrated that with or without Dd5p4 activity, cells were still able to hydrolyse PI(3,4,5)P_3 to PI(3,4)P_2, most likely via Dd5p2 enzymatic activity (Fig. 3.12.A-D.) (Loovers et al. 2003).

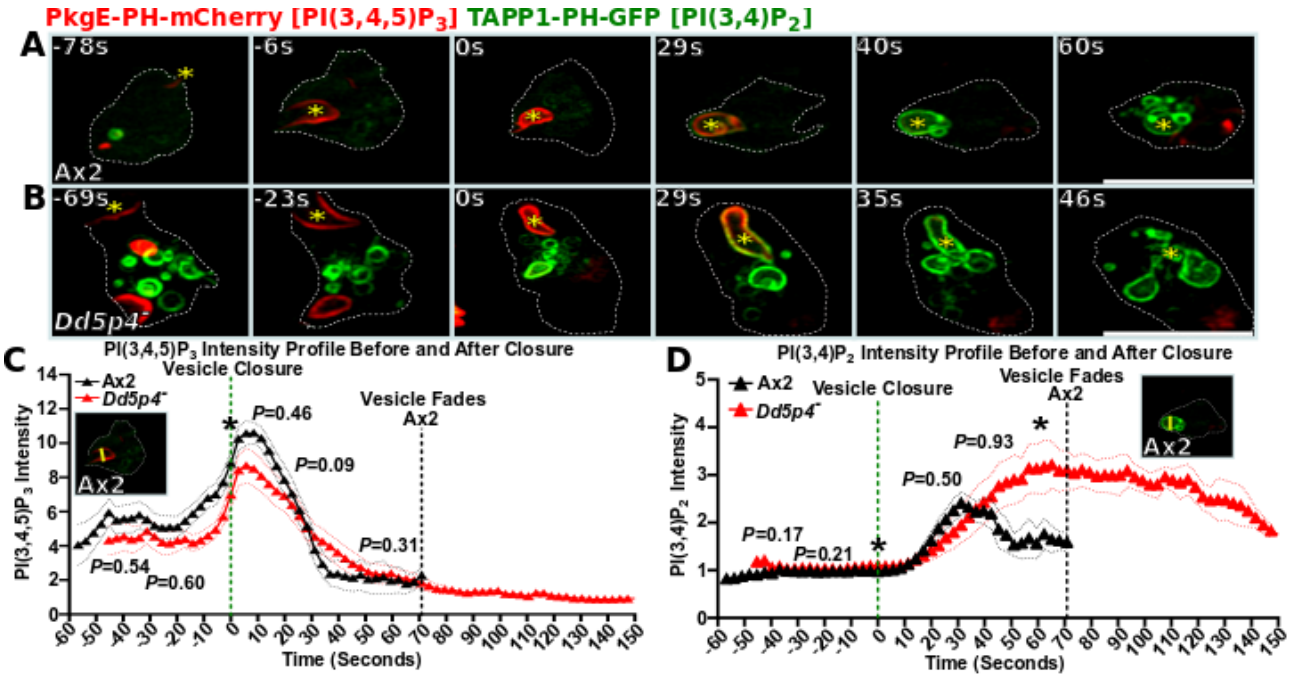

Figure 3.12. Macropinocytic PI(3,4,5)P_3 and PI(3,4)P_2 lifetimes were reduced at closure and increased after closure respectively in *Dd5p4*$^-$. (A-B) LLSM images of Ax2 and *Dd5p4*$^-$ stably expressing the PkgE-PH-mCherry TAPP1-PH-GFP dual expression probe. Yellows stars indicate cups and macropinosomes of interest. Probes and their respective PIPs are indicated. Cell peripheries are indicated by white dashed lines. (C-D) Average PI(3,4,5)P_3 and PI(3,4)P_2 profiles of cells at different stages of macropinocytic cup closure. PI(3,4,5)P_3 and PI(3,4)P_2 measurements were normalised against intracellular background intensity. Example measurements in Ax2 before cup closure (C) and after cup closure (D) are shown by yellow lines for each PIP within inset images. Green dashed lines show the point of vesicle closure at 0 seconds, with black dashed lines revealing PIP degradation in Ax2 cells. Sample size N=9, SEM error bars are shown as dotted lines (black for Ax2 and red for *Dd5p4*$^-$) from a single biological repeat. Scale bars are 10 microns. Mann Whitney U statistical tests were conducted for each PIP at time points -40 s, -20 s, 0 s, 20 s, 40 s, and 60 s between Ax2 and *Dd5p4*$^-$ cell lines. Data adapted from analyses carried out by Kirsty Tinsley. * $P < 0.05$.

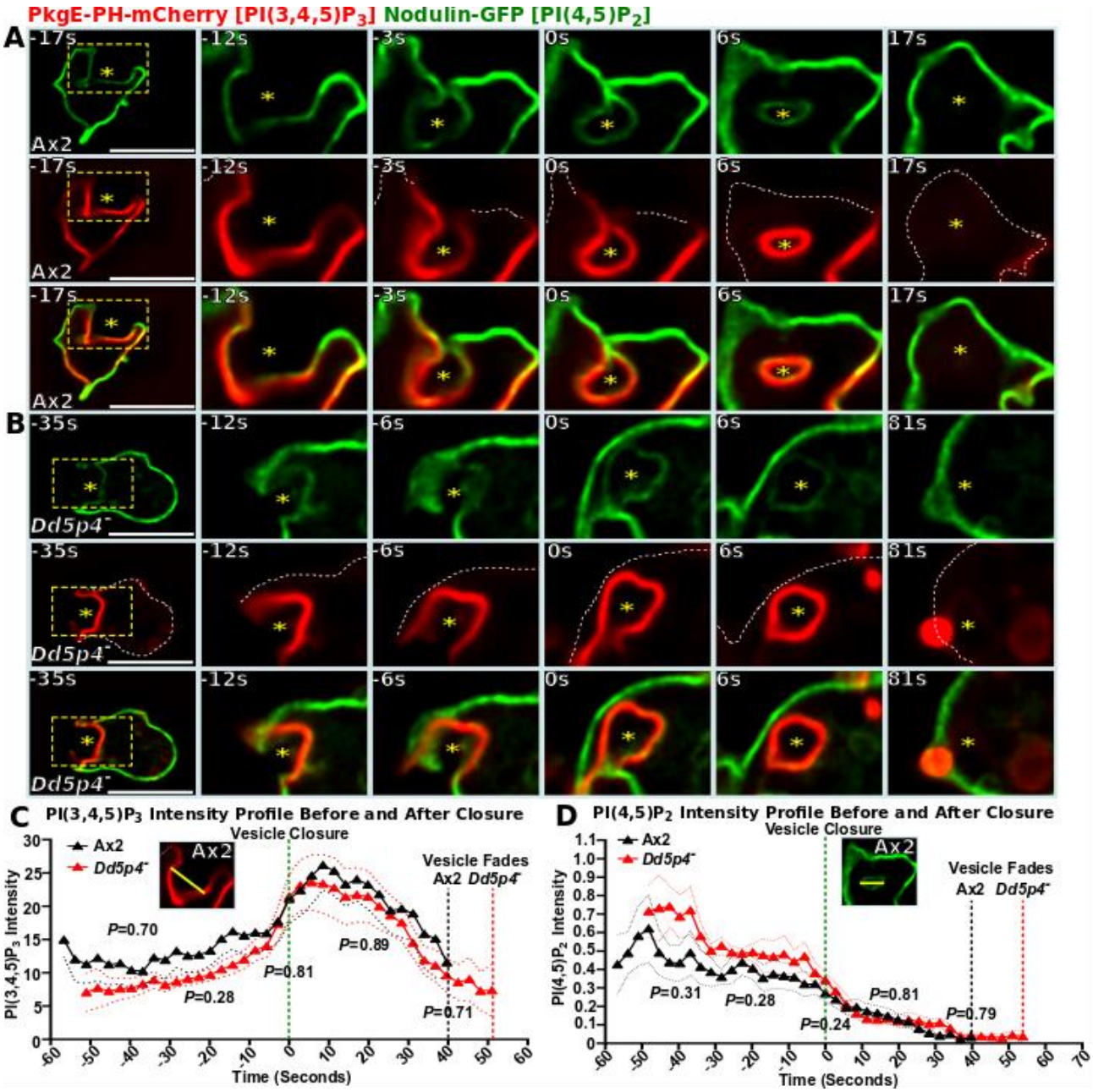

Figure 3.13. Macropinocytic PI(3,4,5)P_3 and PI(4,5)P_2 dynamics were unaffected in *Dd5p4*$^-$. (A-B) LLSM images of Ax2 and *Dd5p4*$^-$ cells stably expressing the PkgE-PH-mCherry Nodulin-GFP dual expression probe. Yellows stars indicate macropinocytic cups and macropinosomes of interest, with yellow dashed boxes showing zoomed in areas of interest. Probes and their respective PIPs are indicated. Cell peripheries are indicated by white dashed lines. (C) PI(3,4,5)P_3 and (D) PI(4,5)P_2 profiles of equivalent cells at different stages of cup closure. PI(3,4,5)P_3 measurements were normalised against intracellular background intensity, with PI(4,5)P_2 being additionally normalised to non-protruding PM levels. Example measurements in Ax2 before cup closure (C) and after cup closure (D) are shown by yellow lines for each PIP within inset images. Green dashed lines show the point of vesicle closure at 0 seconds, with black and red dashed lines revealing PIP degradation in Ax2 and *Dd5p4*$^-$ respectively. Sample size N=9, SEM error bars are shown as dotted lines (black for Ax2 and red for *Dd5p4*$^-$) from a single biological repeat. Scale bars are 10 microns. Mann Whitney U statistical tests were conducted for each PIP at time points -40 s, -20 s, 0 s, 20 s, and 40 s between Ax2 and *Dd5p4*$^-$ cell lines. Data adapted from analyses carried out by Kirsty Tinsley.

Interestingly, when analysing the macropinocytic PI(3,4,5)P_3 profile from cells stably expressing this probe together with the PI(3,4)P_2 probe differences were observed at cup closure in that Ax2 control cells displayed higher PI(3,4,5)P_3 levels than the *Dd5p4*$^-$ mutant (Fig. 3.12.C.). This differed to the macropinocytic PI(3,4,5)P_3 profile from cells stably expressing the PI(3,4,5)P_3 probe together with the PI(4,5)P_2 probe in which no statistical differences were observed at any of the tested time points (Fig. 3.13.C.). The differences in macropinocytic PI(3,4,5)P_3 profiles were most likely due to the macropinosomes being labelled for longer with both the PI(3,4,5)P_3 and PI(3,4)P_2 probes making the macropinosomes visible for longer time periods. This is shown by the loss of the PI(3,4,5)P_3 signal occurring about 70 seconds after closure in Ax2 control cells (Fig. 3.12.A-D.). In contrast, macropinosomes that were labelled with both the PI(3,4,5)P_3 and PI(4,5)P_2 probes were visible for shorter time periods as both probes faded at about the same time after cup closure. This is shown by the Ax2 PI(3,4,5)P_3 signal fading just 40 seconds after cup closure (Fig. 3.13.A-D.).

In parallel with PI(3,4,5)P_3, PI(4,5)P_2 temporal dynamics were simultaneously measured and were largely unaffected in the absence of Dd5p4 activity, which suggested that Dd5p4 did not contribute to the catabolism of PI(4,5)P_2 during macropinocytosis (Fig. 3.13.A-D.). This observation mirrored what I have previously shown after cup closure (Fig. 3.11.A-C.).

When comparing the profiles of both PI(3,4,5)P_3 and PI(4,5)P_2 of both cell lines the PI(4,5)P_2 levels decreased before closure as PI(3,4,5)P_3 levels increased after cup closure, which illustrates that with or without Dd5p4 activity cells are able to remove PI(4,5)P_2 most likely through phosphorylation to PI(3,4,5)P_3 by the PI3K class I enzymes such as PI3K4 (Fig. 3.13.A-D.) (Hoeller et al. 2013).

3.2.11. F-actin was not dismantled at cup closure causing comets to form in *Dd5p4*$^-$ during macropinocytosis

As most of the PIP dynamics were largely unaffected by the absence of Dd5p4 activity, another crucial feature of macropinocytosis was next investigated: F-actin. F-actin was visualised using LifeAct (Paschke et al. 2018), together with either PI(3,4)P_2 or PI(4,5)P_2 probes, as these PIPs are known to regulate actin dynamics (Miki et al. 1996, Zhou et al. 1998). Intensity profiles of F-actin and the associated PIPs were plotted from LLSM images by Master's student, Kirsty Tinsley (Fig. 3.14.A-H.).

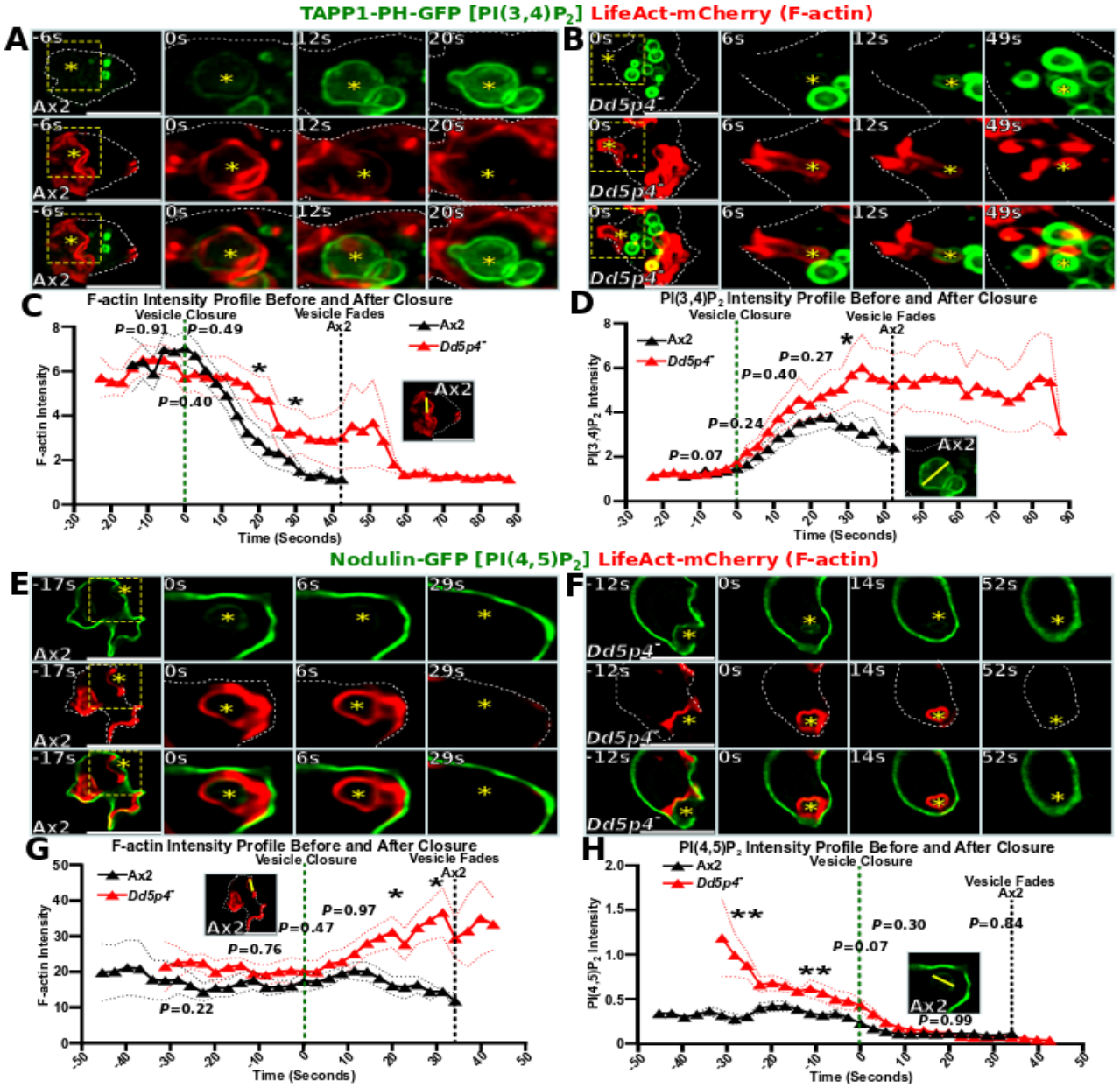

Figure 3.14. F-actin is not dismantled at cup closure in *Dd5p4*⁻ cells. (A-B) Ax2 and *Dd5p4*⁻ stably expressing TAPP1-PH-GFP LifeAct-mCherry. Time-lapses are available for Ax2 (S1) and *Dd5p4*⁻ (S2). (C-D) F-actin and associated PI(3,4)P_2 profiles of cells during early macropinocytosis, with measurements normalised against the intracellular background. (E-F) Ax2 and *Dd5p4*⁻ stably expressing Nodulin-GFP LifeAct-mCherry. Yellows stars indicate cups and macropinosomes of interest, and yellow dashed boxes show zoomed in areas. Probes and their respective PIPs are shown. Cell peripheries are indicated by white dashed lines. Example measurements in Ax2 before (C) and after cup closure (D) are shown by yellow lines for F-actin and PI(3,4)P_2. (G-H) F-actin and the associated PI(4,5)P_2 profiles during early macropinocytosis. Both measurements were normalised against the intracellular background intensity, with PI(4,5)P_2 also being normalised to non-protruding PM levels. Example measurements in Ax2 before (G) and after cup closure (H) are shown by yellow lines for F-actin and PI(4,5)P_2. Green dashed lines show vesicle closure (0 seconds), with black dashed lines revealing PIP degradation in Ax2 cells. Sample size N=9, SEM error bars are shown as dotted lines (black for Ax2 and red for *Dd5p4*⁻) from a single biological repeat. Scale bars are 10 microns. Mann Whitney U statistical tests were conducted for PI(3,4)P_2 and the associated F-actin at time points -10 s, -0 s, 10 s, 20 s, and 30 s between Ax2 and *Dd5p4*⁻ cell lines. Mann Whitney U statistical tests were also conducted for PI(4,5)P_2 and the associated F-actin at time points -25 s, -10 s, 0 s, 10 s, 20 s, and 30 s between Ax2 and *Dd5p4*⁻ cell lines. Data adapted from analyses carried out by Kirsty Tinsley. * $P < 0.05$, ** $P < 0.01$.

In Ax2, F-actin was seen to be abundant around the outline of the macropinocytic cup towards and just after cup closure, whilst PI(3,4)P_2 levels, which was used as an internal control, were negligible at these stages (-6-0 seconds, Fig. 3.14.A.). Interestingly, following cup closure PI(3,4)P_2 levels increased and peaked at 12-20 seconds after closure whilst F-actin levels decreased after cup closure (Fig. 3.14.A.). This would suggest that the emergence of PI(3,4)P_2 coincided with F-actin disassembly after cup closure in Ax2 control cells. In *Dd5p4*$^-$, however, the F-actin marking the membrane of what appeared to be a macropinosome was squeezed into the cell 0-6 seconds after cup closure (Fig. 3.14.B.), this was not observed in Ax2 cells. This provided a possible explanation as to why phagocytosis could not occur, but macropinocytosis could still take place. The squeezing of the macropinosome into the cytosol would suggest that the actin cortex opening may be restricted, which could potentially explain why larger yeast particles were unable to enter the cytosol in these *Dd5p4*$^-$ mutants. Failure of yeast to enter through a possibly restricted cortex may have prevented advancement to early maturation as the yeast were in almost all cases unable to enter the cytosol in *Dd5p4*$^-$ (Fig. 3.5.D-H., and Fig. 3.14.B.). Macropinosomes however, are far more malleable, and could squeeze through the possibly restricted cortex openings in order to enter the cytosol in these mutants. In *Dd5p4*$^-$, the removal of F-actin appeared to be delayed upon the formation of PI(3,4)P_2 and persisted forming an F-actin 'comet', which lasted for up to at least 49 seconds after cup closure (Fig. 3.14.B.). These comets seemed to form as a result of the macropinosome and the associated F-actin being forced and propelled away from the PM following cup closure in *Dd5p4*$^-$. This collectively provided a possible explanation as to why cups and macropinosomes in *Dd5p4*$^-$ mutant cells were smaller in comparison to Ax2 control cells.

In reference to PI(4,5)P_2 levels, this PIP was included as an internal control. Similar patterns were observed in F-actin dynamics in association with PI(4,5)P_2 levels at, and just after cup closure within Ax2 and *Dd5p4*$^-$ cells (Fig. 3.14.E-H.).

A comparison of the F-actin profiles however, between the F-actin associated with PI(3,4)P_2 and the F-actin associated with PI(4,5)P_2 displayed some differences (Fig. 3.14.C. and G.). These differences generally centred on the F-actin signal being present for longer time periods in association with PI(3,4)P_2 in comparison to the F-actin associated with PI(4,5)P_2 (Fig. 3.14.C. and G.). The differences in these F-actin intensity profiles were due to the macropinosomes being labelled for longer periods with both the F-actin and PI(3,4)P_2 probes, which therefore made them visible for longer durations (Fig. 3.14.C-D.). In contrast, macropinosomes that were labelled with both the F-actin and PI(4,5)P_2 probes were visible for shorter time periods as both probes labelled the macropinosomes for a shorter duration (Fig. 3.14.G-H.).

3.2.12. Understanding what formed F-actin comets in *Dd5p4*$^{-}$ during macropinocytosis

In mammalian cells, endocytic comets were found to be caused by PIPs (Suchy and Nussbaum 2002, Nandez et al. 2014, Daste et al. 2017). This gave an incentive to systematically dissect which PIPs were present on the comets, and could have been involved in comet formation in *D. discoideum Dd5p4*$^{-}$ cells using LLSM (Fig. 3.15.A. and C-E.).

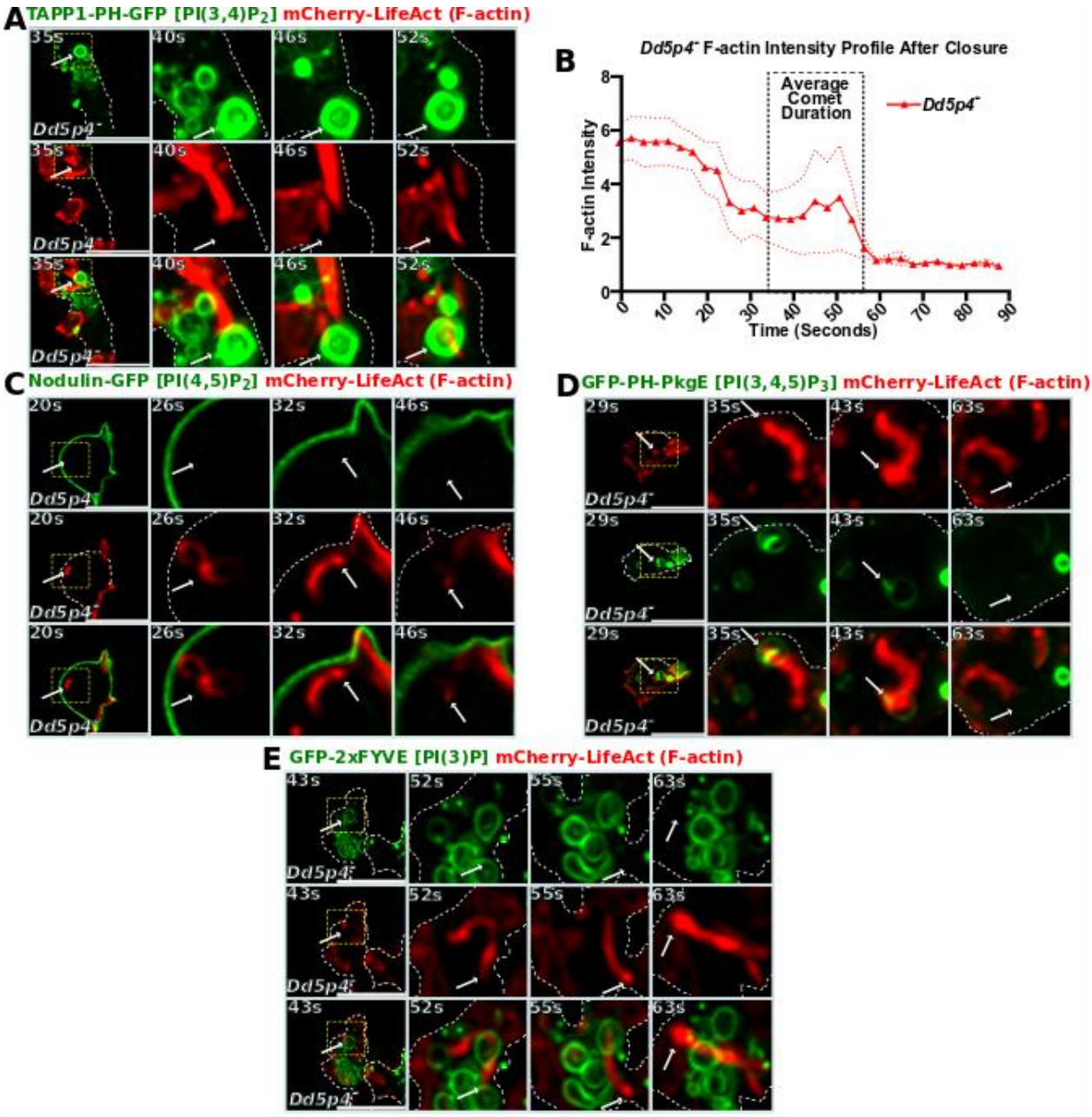

Figure 3.15. F-actin 'comets' formed in *Dd5p4*⁻ with PI(3,4,5)P_3 and PI(3,4)P_2 localised to the head. LLSM images of *Dd5p4*⁻ cells stably expressing the TAPP1-PH-GFP mCherry-LifeAct dual expression probe over time after cup closure (A). A time-lapse is available for *Dd5p4*⁻ stably expressing these probes (S3). (B) The F-actin profile of *Dd5p4*⁻ that was associated with PI(3,4)P_2 found on the comets. This particular F-actin profile was used as macropinosomes were labelled for longer during early macropinocytosis, which aided in the quantification of comet dynamics. Measurements were normalised against the intracellular background. A rectangle outlined with black, dashed lines shows the comet duration after cup closure. Sample size N=9, SEM error bars are shown as red dotted lines for *Dd5p4*⁻ from a single biological repeat. Data adapted from analyses carried out by Kirsty Tinsley. (C) Representative images showing *Dd5p4*⁻ cells stably co-expressing Nodulin-GFP and mCherry-LifeAct over time after cup closure, a time-lapse is available for *Dd5p4*⁻ stably expressing these probes (S4). (D) LLSM images showing *Dd5p4*⁻ stably expressing GFP-PH-PkgE and mCherry-LifeAct over time after cup closure, a time-lapse is available for *Dd5p4*⁻ stably expressing these probes (S5). (E) LLSM images displaying *Dd5p4*⁻ stably expressing GFP-2xFYVE and mCherry-LifeAct over time after cup closure, a time-lapse is available for *Dd5p4*⁻ stably expressing these probes (S6). White arrows indicate comets and yellow dashed boxes show zoomed in areas of interest. Probes and their respective binding partners are indicated. Cell peripheries are indicated by white dashed lines. Scale bars are 10 microns.

The first PIP, PI(3,4)P_2, which has been shown to be involved in the regulation of actin dynamics was screened (Zhou et al. 1998). PI(3,4)P_2 was found to be present at the heads of F-actin 'comets' in *Dd5p4*$^-$ cells indicating that this may possibly play a role in the formation of comets in these mutants (Fig. 3.15.A.). In *Dd5p4*$^-$, these comets formed approximately 34 seconds after cup closure and lasted for approximately 22 seconds prior to F-actin removal (Fig. 3.15.B.).

PI(4,5)P_2, another PIP involved in the regulation of actin dynamics, was next screened to see if this PIP localised on the comets (Miki et al. 1996). Surprisingly, however, PI(4,5)P_2 was not present on the comets in *Dd5p4*$^-$ cells, and therefore did not appear to contribute to comet formation (Fig. 3.15.C.).

Interestingly, the next PIP, PI(3,4,5)P_3, was found to be present at the head of comets, albeit at fairly low levels, in *Dd5p4*$^-$ cells. PI(3,4,5)P_3 was also degraded whilst present at the heads of these comets in these mutant cells (Fig. 3.15.D.).

The final PIP, which was screened was PI(3)P, which was not present on the comets, thus indicating that PI(3)P did not drive comet formation in these mutants (Fig. 3.15.E.).

In conclusion, it was shown that F-actin 'comet' heads contained both PI(3,4)P_2 and PI(3,4,5)P_3, although how or if they contributed to comet formation remains to be determined.

The formation of F-actin 'comets' in *Dd5p4*$^-$ cells, together with comet-head localised PI(3,4)P_2, suggested that differential actin regulation was taking place (Fig. 3.15.A-B.). To this end, different regulators of actin were screened to gain further insight into how these comets were formed in *Dd5p4*$^-$ (Fig. 3.16.A-D.). Key *D. discoideum* orthologues of actin regulators were investigated, such as the regulator of actin polymerisation, the Arp2/3 complex (Arp Complex subunit 4, ArpC4) (Welch et al. 1997, Mullins et al. 1998, Insall et al. 2001, Stradal and Scita 2006). Activators of the Arp2/3 complex were also screened, which included: SCAR (the SCAR regulatory complex subunit, Haematopoietic Stem/Progenitor Cell protein 300, HSPC300) (Machesky and Insall 1998, Pollitt and Insall 2009), WASP (WasA) (Miki et al. 1996, Myers et al. 2005), and WASH (Derivery et al. 2009, Gomez et al. 2012, King et al. 2013, Ryder et al. 2013).

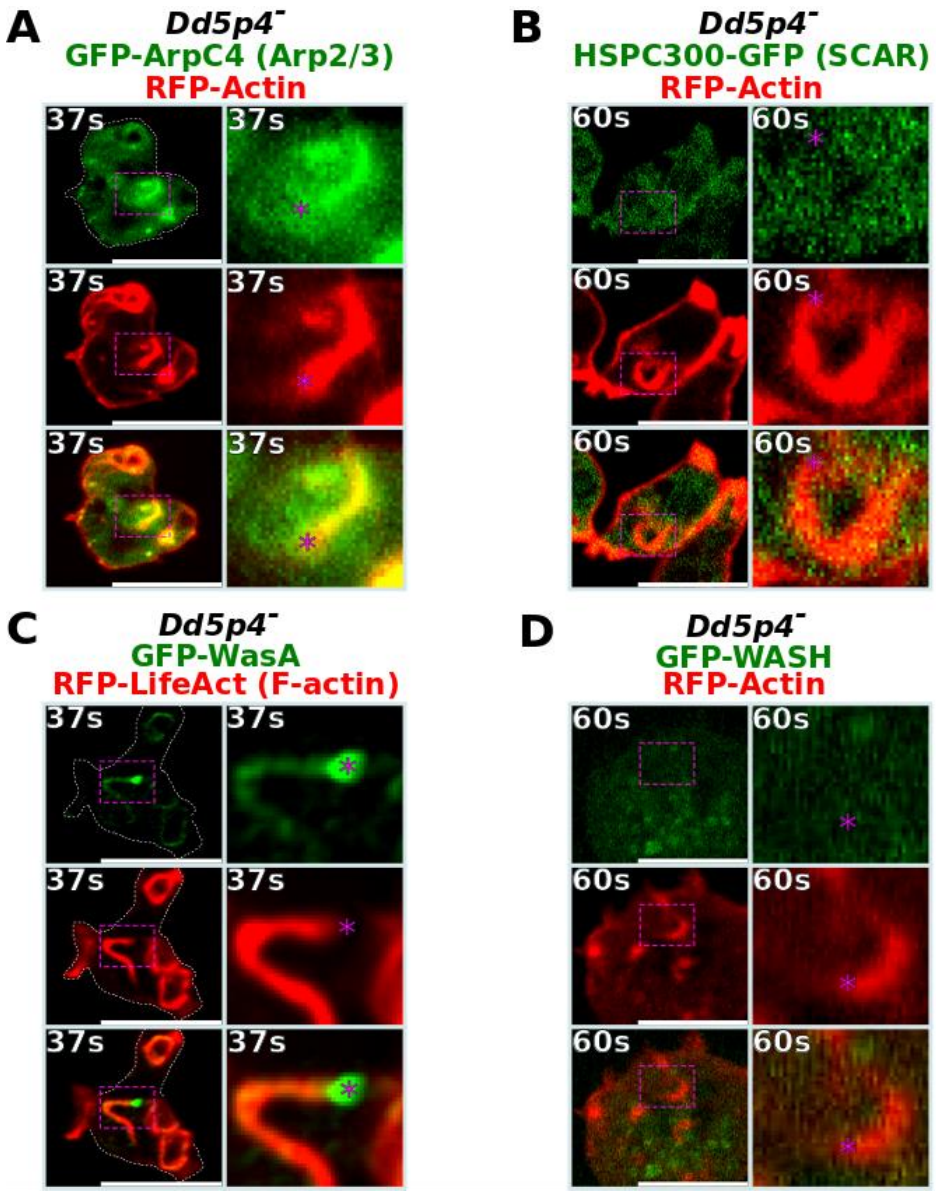

Figure 3.16. The Arp2/3 complex, and the Arp2/3 complex regulator WasA, were both found on *Dd5p4*⁻ comets. *Dd5p4*⁻ cells stably expressing (A) GFP-ArpC4 RFP-Actin, a time-lapse is available for *Dd5p4*⁻ stably expressing these probes (S7), (B) HSPC300-GFP RFP-Actin, a time-lapse is available for *Dd5p4*⁻ stably expressing these probes (S8), (C) GFP-WasA RFP-LifeAct, a time-lapse is available for *Dd5p4*⁻ stably expressing these probes (S9), and (D) GFP-WASH RFP-Actin, a time-lapse is available for *Dd5p4*⁻ stably expressing these probes (S10), after cup closure. The spinning disc was used to visualise probes in association with F-actin in A-B, and D. LLSM was used to visualise WasA in association with F-actin as shown in C. Magenta stars indicate the comets of interest, and magenta dashed boxes show zoomed in areas of interest. Fluorescent probes are indicated. Scale bars are 10 microns.

Screening of the actin regulators in *Dd5p4*⁻ cells showed that ArpC4 was present predominantly at the comet tails, with traces also observed at the comet heads indicating that activation of the Arp2/3 complex resulted in the creation of comets (Fig. 3.16.A.). The Arp2/3 complex regulators, SCAR and WASH, did not localise to the comets (Fig. 3.16.B. and D.), whereas WasA localised to the heads of comets predominantly, with traces also observed on the comet tails (Fig. 3.16.C.). This suggested that loss of Dd5p4 activity resulted in increased WasA activity, which

despite being predominantly localised to the heads seemed to enhance the activity of the Arp2/3 complex, which predominantly localised at the comet tails, potentially resulting in comet formation (Fig. 3.16.A. and C.). The traces of active WasA on the comet tails may however, be sufficient to stimulate the activation of the Arp2/3 complex and thus comet formation, although further work would need to be done to clarify this. I have previously shown however, that PI(3,4,5)P_3 was present on the heads of comets in *Dd5p4*$^-$ (Fig. 3.15.D.). This observation may provide a possible explanation for the localisation and activation of WasA at the heads of the comets as PI(3,4,5)P_3 binding to the WasA B domain has been demonstrated to be important for the recruitment and activation of WasA (Fig. 3.15.D. and Fig. 3.16.C.) (Myers et al. 2005).

In summary, I have shown that Dd5p4 activity was important for the regulation of actin dynamics at cup closure during both macropinocytosis and phagocytosis. The loss of Dd5p4 activity during macropinocytosis reduced the levels of F-actin disassembly at cup closure causing macropinosomes to squeeze through potentially restricted cortex openings. The forced separation of macropinosomes from the PM resulted in F-actin 'comets' in *Dd5p4*$^-$ mutants. PI(3,4)P_2, a known regulator of actin dynamics, was found to be associated with these comets, along with PI(3,4,5)P_3, which may recruit and activate WasA and thus lead to the activation of the Arp2/3 complex. The loss of Dd5p4 activity somehow also potentially caused traces of active WasA to be observed on the comet tails, which may have been sufficient to activate the Arp2/3 complex on the tails of the comets, and thus increase the polymerisation of F-actin. The reduced F-actin disassembly at cup closure during macropinocytosis in *Dd5p4*$^-$ gave a possible mechanistic explanation as to why phagocytic engulfment almost always failed; possibly smaller openings in the cortex, which were potentially insufficient to allow larger yeast particles to enter the cytosol of these *Dd5p4*$^-$ mutants.

3.3. Discussion

The inositol 5-phosphatase, Dd5p4, in *D. discoideum* has been shown to be crucial for successful phagocytosis and macropinocytosis to occur (Loovers et al. 2007). Previous work had suggested that Dd5p4-null mutants were able to establish contacts with yeast at normal frequencies, but were unable to extend their membranes beyond half the circumference of yeast particles (Loovers et al. 2007). Phagocytosis was shown to be hindered through the absence of Dd5p4 phosphatase activity, which led to the suggestion that phagocytic failure was caused by failure in PI(3,4,5)P_3 de-phosphorylation to PI(3,4)P_2, which was necessary for extension around the yeast and for cup closure (Loovers et al. 2007). This investigation, however, had a relatively low coverage of PIP metabolism within these mutants, whilst investigating both macropinocytosis and phagocytosis. This gave the incentive to investigate if and how the metabolism of PI(3,4,5)P_3 and

$PI(3,4)P_2$, as well as other PIPs involved in cup formation, closure, and post-closure, during phagocytosis and macropinocytosis were affected in cells lacking Dd5p4 activity.

3.3.1. Dd5p4 activity during cup formation

In this project I have shown that the dynamics of macropinocytic $PI(3,4,5)P_3$, $PI(3,4)P_2$, PI(4)P, and F-actin, along with phagocytic $PI(3,4,5)P_3$, and PI(4)P, were surprisingly largely unaltered during cup formation in *Dd5p4*$^-$ mutants. However, $PI(4,5)P_2$, a Dd5p4 substrate, was found to be altered during phagocytic and macropinocytic cup formation in *Dd5p4*$^-$ (Fig. 3.7.A-D. and Fig. 3.9.A-D.). I have demonstrated that in *Dd5p4*$^-$ mutant cells, that both macropinocytic and, in particular, phagocytic $PI(4,5)P_2$ depletion was decreased towards cup closure, however cup formation was not prevented. This suggested that Dd5p4 was not required for the formation of phagocytic or macropinocytic cups (Fig 3.7.A-D. and Fig. 3.9.A-D.). Macropinocytic cups were however, seen to be smaller, and more numerous in *Dd5p4*$^-$ mutant cells, in comparison to those observed in Ax2 control cells (Fig. 3.3.B-D.). I have also shown that across phagocytic cups towards closure, progressive $PI(4,5)P_2$ depletion was observed at the base of Ax2 cups, but little depletion was observed at the base of *Dd5p4*$^-$ phagocytic cups. This suggested that Dd5p4 depletes $PI(4,5)P_2$ progressively towards closure at the base of phagocytic cups (Fig. 3.7.A-D.). Across macropinocytic cups before closure in *Dd5p4*$^-$ mutant cells, $PI(4,5)P_2$ depletion was also reduced at the cup base, albeit with smaller differences in comparison to macropinocytic $PI(4,5)P_2$ levels at the base of Ax2 macropinocytic cups (Fig. 3.9.A-D.). This suggested that Dd5p4 localised to the base of cups to hydrolyse $PI(4,5)P_2$ to PI(4)P during macro-endocytic cup formation. I was however, unable to confirm this as stable expression of Dd5p4-GFP displayed cytosolic localisation within Ax2 control cells with no clear distinct localisation of this protein to the base of macro-endocytic cups (Fig. 3.2.L.). Macropinocytic cups in general, however, were smaller in comparison to phagocytic cups, which could have potentially caused smaller $PI(4,5)P_2$ gradients across macropinocytic cups. This could have explained the striking differences observed when comparing $PI(4,5)P_2$ gradients across macropinocytic cups to $PI(4,5)P_2$ gradients across phagocytic cups (Fig. 3.7.A-D. and Fig. 3.9.A-D.).

3.3.2. Dd5p4 activity at cup closure

In this investigation I have demonstrated a potential mechanism in which the dynamics of macropinocytosis were altered and phagocytosis was impaired in cells lacking Dd5p4 activity. The use of LLSM demonstrated that F-actin dynamics were altered at macropinocytic cup closure in *Dd5p4*$^-$ mutants compared to Ax2 control cells (Fig. 3.14.A-H.). F-actin disassembly is crucial for the entry of material into cells through the actin cortex in *D. discoideum* (Hacker et al. 1997, Schwarz et

al. 2000, Isik et al. 2008, Inaba et al. 2017). *Dd5p4*$^{-}$ mutant cells, however, were unable to disassemble their F-actin coat upon macropinocytic cup closure, and instead macropinosomes appeared to be squeezed into the cytosol, which was not observed in Ax2 control cells (Fig. 3.14.A-B.). These observations may have suggested that in *Dd5p4*$^{-}$ mutants the actin cortex openings could potentially have been restricted in comparison to those in Ax2 cells, which may have provided a possible explanation as to the formation of numerous, smaller cups, and macropinosomes, as well as the high phagocytic failure rate in *Dd5p4*$^{-}$ mutants. A summary of the possible differences in cortex sizes in Ax2 control cells and *Dd5p4*$^{-}$ mutant cells during phagocytosis and macropinocytosis is shown (Fig. 3.17.A-B.).

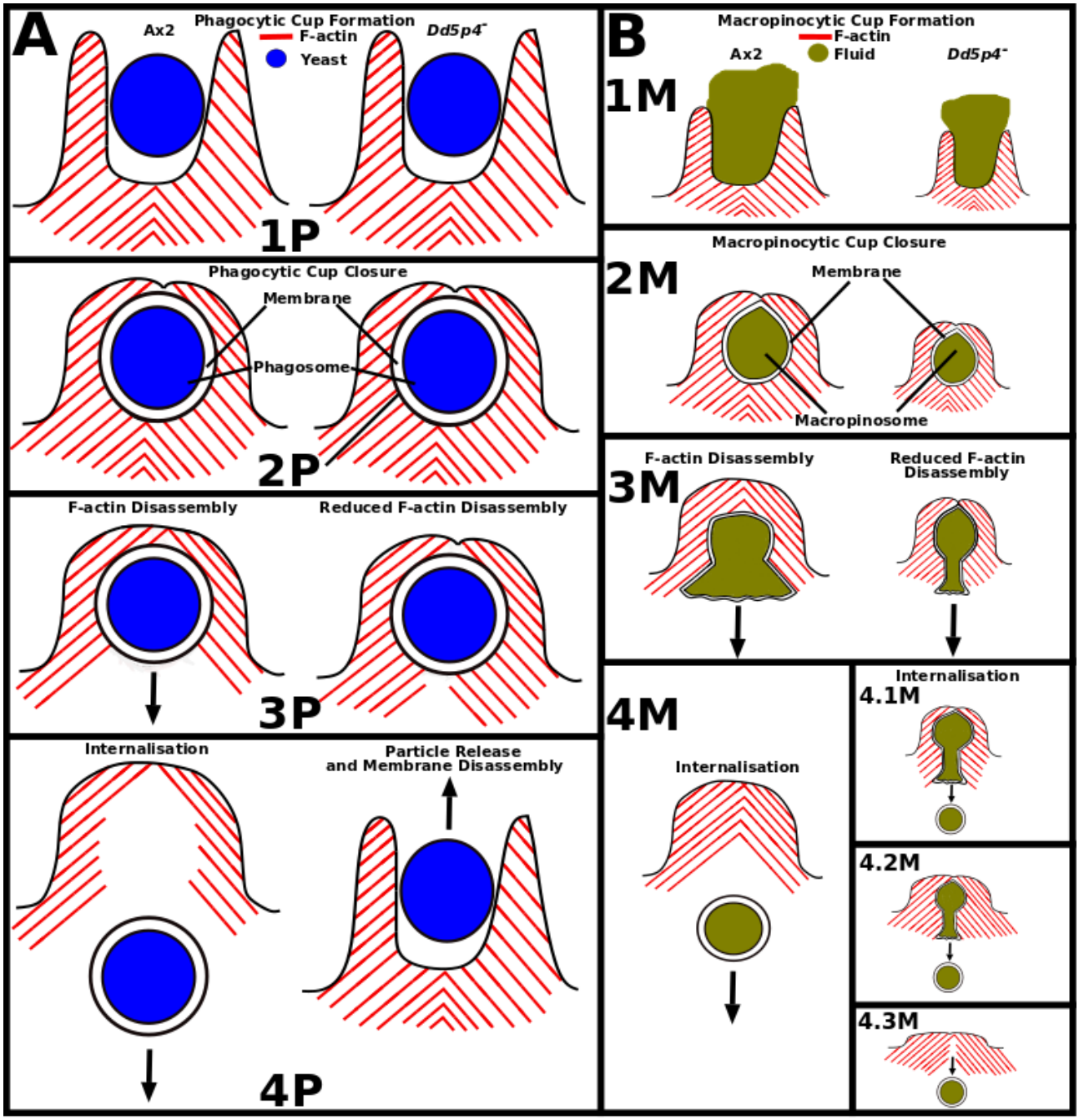

Figure 3.17. A comparison of the potential F-actin dynamics between phagocytosis and macropinocytosis in Ax2 and *Dd5p4*$^-$. (A) Ax2 and *Dd5p4*$^-$ during phagocytosis with both forming contact (1P) and being fully capable of enwrapping yeast, with the membrane encircling the newly formed phagosome (2P). The cortex opening possibly could be much wider in Ax2, as Dd5p4 hydrolyses PI(4,5)P_2 causing F-actin disassembly, this could be reduced in *Dd5p4*$^-$ (3P). The possible smaller cortex openings in *Dd5p4*$^-$ may have resulted in particle release as the yeast may not have been able to move through the cortex, this was unperturbed in Ax2 cells (4P). (B) Equivalent cells during macropinocytosis with both cell lines forming macropinocytic cups, with the mutant forming smaller cups (M1-M2). As in phagocytosis, F-actin disassembly may have been reduced in *Dd5p4*$^-$ cells resulting in potentially smaller cortex openings causing the macropinosomes to squeeze through (3M), forming numerous, smaller macropinosomes (4.1M-4.3M). In Ax2 cells, unperturbed F-actin disassembly at the base of macropinocytic cups (M3) may have resulted in larger, less-numerous macropinosomes entering through the possibly larger cortex openings (M4). Each stage of engulfment of yeast and fluid is compartmentalised. Phagocytosis (P), macropinocytosis (M), with each panel numbered for each stage as indicated. F-actin filaments are red, yeast are blue, and fluid is olive.

The possibility of restricted cortex openings in *Dd5p4*$^{-}$ could potentially have explained why phagocytosis almost always failed, as phagosomes may not have been able to distort and squeeze through the potentially restricted cortex openings in *Dd5p4*$^{-}$ mutant cells (Fig. 3.1.A-C., Fig. 3.5-D-H. and Fig. 3.17.A-B.). To clarify this theory however, stable expression of *D. discoideum* cofilin in *Dd5p4*$^{-}$ could be performed to cut actin filaments, which may normally not be cut at cup closure in these mutants (Aizawa et al. 1995, Ichetovkin et al. 2000). *Dd5p4*$^{-}$ mutants stably expressing cofilin could then be administered fluorescently labelled yeast to establish if the failure to remove F-actin at cup closure and the possible reduction in cortex openings were indeed the cause of the phagocytic defects that were observed in these *Dd5p4*$^{-}$ mutants. This could also address the question of whether the stable expression of *D. discoideum* cofilin could also prevent the formation of F-actin 'comets' after closure during macropinocytosis in *Dd5p4*$^{-}$ mutants.

Interestingly, Phafin2 has been shown in mammals to be important for the disassembly of actin on nascent macropinosomes (Schink et al. 2021). Phafin2 transiently interacts with macropinosomes prior to the recruitment of the OCRL F&H interactor, APPL1, as well as Rab5 and Rab31, Rabankyrin-5, and Sorting Nexin-5 (SNX5) (Schink et al. 2021). The transient localisation of Phafin2 depended strongly on the PH and FYVE domains of this protein, with the FYVE domain being shown to be important for the transient localisation of Phafin2 to nascent and early macropinosomes, whereas the PH domain was crucial for Phafin2 localisation only to nascent macropinosomes (Schink et al. 2021). Phafin2 is itself recruited to nascent macropinosomes via a Vps34-independent pathway of PI(3)P generation and was also shown to be recruited to early macropinosomes via a Vps34-dependent pathway of PI(3)P generation (Schink et al. 2021). It was also shown in this study that the low levels of PI(3)P greatly enhanced the recruitment of Phafin2 to macropinosomes that were also labelled with PI(4)P, with both the PH and FYVE domains being required for this recruitment (Schink et al. 2021). This stated that for efficient recruitment of Phafin2 to macropinosomes this protein needed to bind both PI(3)P and PI(4)P, when PI(3)P levels were negligible (Schink et al. 2021). This protein has also been shown to be important for efficient macropinocytosis to take place and for the successful formation of normal-sized macropinosomes after cup closure (Schink et al. 2021). The first burst of Phafin2 on nascent macropinosomes was indicated to occur at the same time as the alterations in actin dynamics around the nascent macropinosomes, with these observation being discovered to be due to the PH domain of Phafin2 binding directly to F-actin (Schink et al. 2021). Phafin2 was therefore able to promote macropinocytosis by governing the timely disassembly of actin from nascent macropinosomes in order to facilitate their navigation through the dense subcortical actin network (Schink et al. 2021). Phafin2 was itself also often found to be exploited in KRAS-transformed cancer cells in order to

facilitate F-actin disassembly and therefore the entry of nutrients potentially by moderately overexpressing Phafin2 (Schink et al. 2021). This moderate overexpression of Phafin2 may have enhanced the levels of macropinocytosis and potentially the scavenging of amino acids, which may have resulted in rapid cancer cell growth, and eventual metastasis (Schink et al. 2021). This study could have also provided a link to the enzymatic activities of OCRL, which has been shown to facilitate the disassembly of actin through the hydrolysis of $PI(4,5)P_2$ in mammals (Suchy and Nussbaum 2002, Bohdanowicz et al. 2012, Marion et al. 2012, Nandez et al. 2014, Daste et al. 2017, Maxson et al. 2021). The hydrolysis of $PI(4,5)P_2$ and the resulting generation of PI(4)P, which together with negligible PI(3)P levels may have collectively aided in the recruitment of Phafin2 to endosomes and may also have facilitated the disassembly of actin and thus allowed the entry of material into the cytosol (Schink et al. 2021). A homologue of Phafin2 in *D. discoideum* has thus far not been identified however, so further studies within mammals would be required to assess if the recruitment of Phafin2 was hindered in *OCRL*$^{-/-}$ mutant cells. This would aim to ascertain if the pool of PI(4)P generated by OCRL hydrolysis of $PI(4,5)P_2$ aided Phafin2 recruitment and thus actin disassembly. Further studies could also be performed within mice analysing cells in which both the activities of OCRL and INPP5B are absent in order to establish if INPP5B could compensate for the absence of OCRL activity and thus the potential recruitment of Phafin2.

Another regulator of actin dynamics, the actin polymerase, Vasodilator-Stimulated Phosphoprotein (VASP), has been shown in *D. discoideum* to be crucial for both the processes of phagocytosis and macropinocytosis. In the absence of VASP activity both macro-endocytic processes were found to be impaired, however the global levels of F-actin within endocytic cups were not noticeably altered (Koerber and Faix 2022). This protein was established to accumulate in phagocytic cups at the rim and was important for driving the protrusion of the advancing rim of phagocytic cups. The loss of VASP activity resulted in the perturbation of cup dynamics as well as delays in cup closure (Koerber and Faix 2022). These finding and the findings that I have uncovered in this project showed that *Dd5p4*$^{-}$ mutants displayed no alterations in enwrapping yeast and the closure of phagocytic cups, which may suggest that VASP activity was unlikely to be affected during phagocytic cup formation and phagocytic cup closure in *Dd5p4*$^{-}$ mutants.

In relation to PIPs at cup closure I have shown that the levels of $PI(3,4,5)P_3$ were significantly decreased and that the levels of $PI(3,4)P_2$ were significantly increased at macropinocytic cup closure in *Dd5p4*$^{-}$ cells (Fig. 3.12.C-D.). The reasoning behind this observation may have been due to the loss of Dd5p4 activity somehow enhancing the enzymatic activity of the Dd5p2 inositol 5-phosphatase, which exhibited a preference for $PI(3,4,5)P_3$ de-phosphorylation, which thereby may have resulted in an increase in the levels of $PI(3,4)P_2$ that were observed at closure of the cup in *Dd5p4*$^{-}$ (Fig.

3.12.C-D.) (Loovers et al. 2003). A surprising observation however, was that PI(4,5)P_2 levels in *Dd5p4*$^-$ macropinocytic cups were depleted to relatively similar Ax2 control cell levels upon macropinocytic cup closure (Fig. 3.11.A-C. and Fig. 3.13.D.). This indicated that a Dd5p4-independent pathway could be largely responsible for PI(4,5)P_2 degradation in *Dd5p4*$^-$ mutant cells.

The catalytic activity of Dd5p4 itself was shown by me to be crucial for the phagocytosis of yeast, as the rescue of *Dd5p4*$^-$ mutant cells with catalytically inactive Dd5p4 did not rescue the phagocytosis of yeast (Fig. 3.2.K.). This suggested that the hydrolysis of PI(4,5)P_2 that was performed by Dd5p4 facilitated F-actin disassembly at phagocytic cup closure, which may have been necessary for successful phagocytic engulfment. Myself and others have not been able to, however, show a definitive localisation of Dd5p4 within these mutant cells (Loovers et al. 2007, Luscher et al. 2019). The extra-chromosomal stable expression of GFP fusions may have resulted in excessive Dd5p4-GFP levels, which could have masked the localisation of Dd5p4 at the base of cups. Integration of a Dd5p4-GFP fusion construct therefore through restriction enzyme-mediated integration (REMI) into the genome, under the control of the host promoter, could alternatively be used. This would facilitate the generation of cell lines with endogenous expression of the fusion protein of the correct copy number, and thus allow a definitive localisation to be deduced (Fey and Cox 1997).

3.3.3. Dd5p4 activity in the formation of F-actin 'comets' on nascent macropinosomes

In this project I have shown that the dynamics of PI(4,5)P_2, and PI(3)P after macropinocytic cup closure were surprisingly largely unaltered in *Dd5p4*$^-$ mutant cells. PI(4,5)P_2, was interestingly, found to not be influenced as extensively as expected. At post-closure, PI(4,5)P_2 in *Dd5p4*$^-$ mutants were depleted to levels that were relatively similar to the Ax2 control levels, which was similar to the observations that were made at macropinocytic cup closure (Fig. 3.11.A-C., Fig. 3.13.D. and Fig. 3.14.H.). This suggested that hydrolysis of PI(4,5)P_2 was orchestrated by a Dd5p4-independent pathway. Hydrolysis of PI(4,5)P_2 may have occurred due to the presence of other inositol 5-phosphatases, such as Dd5p1, Dd5p2, or Dd5p3 (Loovers et al. 2003). Another pathway could also be via PLC, which degrades PI(4,5)P_2 to Ins(1,4,5)P_3 and DAG (Drayer et al. 1994). Interestingly, loss of PLC in *D. discoideum* resulted in phagocytic defects, but had no effect on axenic growth in liquid culture due to the *PLC*$^-$ cells degrading P(4,5)P_2 via a PLC-independent pathway (Drayer et al. 1994, Loovers et al. 2007). Another route in which PI(4,5)P_2 could have been removed could be through the phosphorylation of PI(4,5)P_2 to PI(3,4,5)P_3 by PI3K4 (Takeda et al. 2007). However, this was unlikely, as PI(3,4,5)P_3 levels were reduced after cup closure in *Dd5p4*$^-$ mutant cells at the early stages of macropinocytosis.

Interestingly, however, both PI(3,4,5)P_3 and PI(3,4)P_2 dynamics were significantly affected after closure in *Dd5p4*$^-$ (Fig. 3.10.D-I.). It was originally hypothesised that the loss of Dd5p4 could have prevented PI(3,4,5)P_3 de-phosphorylation to PI(3,4)P_2 (Loovers et al. 2003). Surprisingly, however, stable transfection of mutant cells with the PI(3,4,5)P_3 binding probe, GFP-PH-PkgE, revealed that PI(3,4,5)P_3 displayed a shorter lifetime on macropinosomes than what was observed in Ax2 control cells (Fig. 3.10.D-F.). In addition, the stable expression of the PI(3,4)P_2-binding probe, TAPP1-PH-GFP, showed PI(3,4)P_2 in abundance on *Dd5p4*$^-$ macropinosomes after cup closure (Fig. 3.10.G-I.), with PI(3,4)P_2 intriguingly remaining on macropinosomes for approximately twice as long in mutant cells compared to control cells (Fig. 3.10.I.). The data on PI(3,4,5)P_3 and PI(3,4)P_2 dynamics after macropinocytic cup closure may be due to PI(3,4,5)P_3 being de-phosphorylated more rapidly to PI(3,4)P_2 in the *Dd5p4*$^-$ mutant by another inositol 5-phosphtase, such as Dd5p1-Dd5p3 (Loovers et al. 2003). Dd5p2 could be a potential candidate for the decreased lifetime of PI(3,4,5)P_3 and the increased lifetime of PI(3,4)P_2 in *Dd5p4*$^-$ cells, as this enzyme had a greater substrate preference for PI(3,4,5)P_3 hydrolysis, resulting in more PI(3,4,5)P_3 hydrolysed to PI(3,4)P_2 (Loovers et al. 2003). It therefore may be prudent to generate *Dd5p2*$^-$ *Dd5p4*$^-$ double knockouts to confirm this theory and establish if there was a reduction in the hydrolysis of PI(3,4,5)P_3 and therefore a reduction in the generation of PI(3,4)P_2 on macropinosomes after closure in cells that lacked active Dd5p2 and Dd5p4. The Dd5p3 inositol 5-phosphatase enzyme on the other hand, has been shown to exhibit its substrate preferences primarily towards water-soluble Ins(1,3,4,5)P_4 and water-soluble Ins(1,4,5)P_3, over PIP metabolism, meaning that this enzyme is a less likely candidate to orchestrate the increased hydrolysis of PI(3,4,5)P_3 and the increased generation of PI(3,4)P_2 (Loovers et al. 2003). The substrate activity of Dd5p1 however, remains unknown and thus cannot be ruled out of influencing both PI(3,4,5)P_3 and PI(3,4)P_2 dynamics (Loovers et al. 2003). The substrate preferences of this enzyme however, could be determined through the incorporation of a Glutathione S-Transferase (GST) tag into the full-length Dd5p1 protein. The recombinant protein could then be screened for its substrate preferences using a Malachite assay (Ramadesikan et al. 2021), which could indicate if the activities of Dd5p1 could come into play to regulate PIP dynamics in the absence of Dd5p4 activity. This could be tested further through creating *Dd5p1*$^-$ *Dd5p4*$^-$ double knockouts, with these double mutants stably expressing probes for PI(3,4,5)P_3 and PI(3,4)P_2. If Dd5p1 does influence the dynamics of both PIPs after closure then both the activities of Dd5p1 and Dd5p2 could somehow be upregulated to collectively hydrolyse more PI(3,4,5)P_3 to form more PI(3,4)P_2 on macropinosomes in *Dd5p4*$^-$ cells. This could be tested through creating *Dd5p1*$^-$ *Dd5p2*$^-$ *Dd5p4*$^-$ triple mutants, which in theory may prevent or severely reduce PI(3,4,5)P_3 hydrolysis and thus PI(3,4)P_2 generation on macropinosomes via this pathway. This could be confirmed through the stable transfection of the

corresponding PIP-binding probes, with the lifetime of PI(3,4,5)P_3 on macropinosomes expected to be increased and the lifetime of PI(3,4)P_2 to be considerably decreased, with negligible levels of the PI(3,4)P_2-binding probe being expressed in the *Dd5p1*$^-$ *Dd5p2*$^-$ *Dd5p4*$^-$ triple mutants. In parallel, this may also be useful to address whether the severe reduction of PI(3,4,5)P_3 hydrolysis and therefore PI(3,4)P_2 generation could have prevented the formation of F-actin 'comets', which may provide an understanding as to how these comets could have formed when observed in *Dd5p4*$^-$. Intriguingly, PI(3,4)P_2 was present after the comets had ended and F-actin was completely removed, which may be due to comet motility reducing the de-phosphorylation efficiency of an unknown inositol 4-phosphatase (Fig. 3.15.A. and C-E.). In summary, PI(3,4,5)P_3 levels at the comet heads were initially low, and were further diminished during comet motility. PI(3,4)P_2 was abundantly present at the heads of comets for the full duration, which may suggest that this PIP could somehow drive comet formation in these mutants, although further studies would be required to unearth how this occurs mechanistically.

In relation to F-actin dynamics, I have shown using LLSM that in Ax2 cells F-actin disassembly took place 20 seconds after macropinocytic cup closure (Fig. 3.14.A.). This finding was similar to previous data gathered on this observation in *D. discoideum*, in which actin disappeared 30-50 seconds after cup closure (Lee and Knecht 2002). Interestingly, I have also shown using LLSM that in Ax2 cells that as PI(3,4)P_2 increased F-actin appeared to decrease and be dismantled on macropinosomes, however it was not clear as to how this occurred or if this was just simply a coincidental decrease and increase of F-actin and PI(3,4)P_2 respectively (Fig. 3.12.A. and Fig. 3.14.A.). In contrast, in *Dd5p4*$^-$ cells as PI(3,4)P_2 levels increased the F-actin levels remained elevated and did not appear to be dismantled on macropinosomes just after macropinocytic cup closure (Fig. 3.14.B.). It was not clear as to why there were differences between the control and mutant cell lines in relation to PI(3,4)P_2 and F-actin dynamics during the early stages of macropinocytosis, so further work would be required to unravel these uncertainties. In Ax2 cells I have identified however, that scission from the PM occurred following PI(3,4)P_2 arrival, F-actin disassembly, and macropinosome fragmentation (Fig. 3.12.A. and Fig. 3.14.A.). In *Dd5p4*$^-$ cells however, PI(3,4)P_2 arrival did not accompany F-actin disassembly, which suggested that scission may be defective in these mutants (Fig. 3.14.B.). In *Dd5p4*$^-$, comets may have formed due to a combination of F-actin disassembly not taking place after macropinocytic cup closure, and the macropinosome and the associated F-actin being forced away from the PM due to potential defects in scission, which may have formed the comets. In Ax2 however, F-actin disassembly occurred after cup closure, which allowed the macropinosome to move away from the PM without forming a comet (Fig. 3.14.A-B.). The F-actin 'comets' were only observed in *Dd5p4*$^-$ after successful macropinosome internalisation in these

mutants, meaning that they were therefore not observed during phagocytosis, in which successful phagocytic engulfment was very rare.

Interestingly, studies on the roles of the actin polymerase, VASP, after phagocytic cup closure have shown that VASP localisation was condensed at the distal side of internalised phagosomes. This localisation initiated localised *de novo* actin assembly, which propelled phagosomes via actin comets into the cytosol (Koerber and Faix 2022). These findings and the data that I have uncovered on comets formed during macropinocytosis may suggest that the loss of Dd5p4 activity could somehow have enhanced the actin polymerase activity of VASP. The enhanced actin polymerase activity of VASP may increase the levels of actin assembly, which could have potentially facilitated comet formation during macropinocytosis. This could be tested through the stable expression of VASP and F-actin probes in *Dd5p4*$^{-}$ mutant and Ax2 control cells, with LLSM live-cell imaging and the quantification of the fold enrichment of VASP in relation to the F-actin during the early stages of macropinocytosis. This could address if increased VASP activity contributed to the elevated levels of F-actin after cup closure and if VASP was also on the comets in *Dd5p4*$^{-}$. In addition, studies could also be performed in which *Dd5p4*$^{-}$ *VASP*$^{-}$ double mutants could be generated and the F-actin fold enrichment profiles compared to those of Ax2 and *Dd5p4*$^{-}$. If VASP does heavily govern actin assembly in *Dd5p4*$^{-}$ mutants after cup closure then comets would not be expected to form following macropinocytic cup closure in the *Dd5p4*$^{-}$ *VASP*$^{-}$ double mutants.

I have also demonstrated in this project that the ArpC4 (Arp2/3 complex) and its regulator, WasA (WASP), were predominantly localised at the tails and heads of comets respectively in *Dd5p4*$^{-}$ (Fig. 3.16.A-D.). WasA and the Arp2/3 complex have been extensively documented to play major roles in the regulation of actin and actin polymerisation (Miki et al. 1996, Welch et al. 1997, Mullins et al. 1998, Insall et al. 2001, Myers et al. 2005, Stradal and Scita 2006). Like the potential experimental setups that were previously mentioned in relation to VASP the same experimental setup could also be applied to WasA in order to address how heavily WasA activity contributed to comet formation. If both VASP and WasA contributed to F-actin assembly (Castellano et al. 2001) and comet formation this could be confirmed through LLSM live-cell imaging and the quantification of the F-actin fold enrichment profile of the *Dd5p4*$^{-}$ *Vasp*$^{-}$ *WasA*$^{-}$ triple mutants.

Surprisingly, PI(4,5)P_2, a well-known regulator of F-actin dynamics was not found on the comets despite it being a known activator of WASP (Fig. 3.15.C.). Previous work has demonstrated in LS patient fibroblasts, which lacked functional OCRL were unable to hydrolyse PI(4,5)P_2 during late-stage CCPs, with the prevention of PI(4,5)P_2 hydrolysis being shown to be crucial for the formation of comets during CME (Nandez et al. 2014). Comet formation occurred as a result of LS patient cells being unable to shed their clathrin coat on vesicles that were generated by CME, with

this coat consisting of various endocytic factors such as AP-2, SNX9, and clathrin (Nandez et al. 2014). This collectively stated that OCRL functions as an un-coating factor, which hydrolyses $PI(4,5)P_2$ to PI(4)P, with this hydrolysis itself facilitating the shedding of the coat of endocytic factors on vesicles during CME (Nandez et al. 2014). The work undertaken in this project however, showed that no $PI(4,5)P_2$ was present on the comets that formed during macropinocytosis. This indicated that the regulatory framework may differ between CME and macropinocytosis. To clarify this it could be more prudent to compare CME in *D. discoideum Dd5p4*$^{-}$ to the *OCRL*$^{-/-}$ LS patient fibroblasts in order to understand if and how $PI(4,5)P_2$ regulated the homologues of the clathrin-mediated endocytic factors in this social amoeba in comparison to LS patient cells.

A complete summary of the proposed model of PIP and F-actin dynamics is shown in Ax2 and *Dd5p4*$^{-}$ cells (Fig. 3.18.).

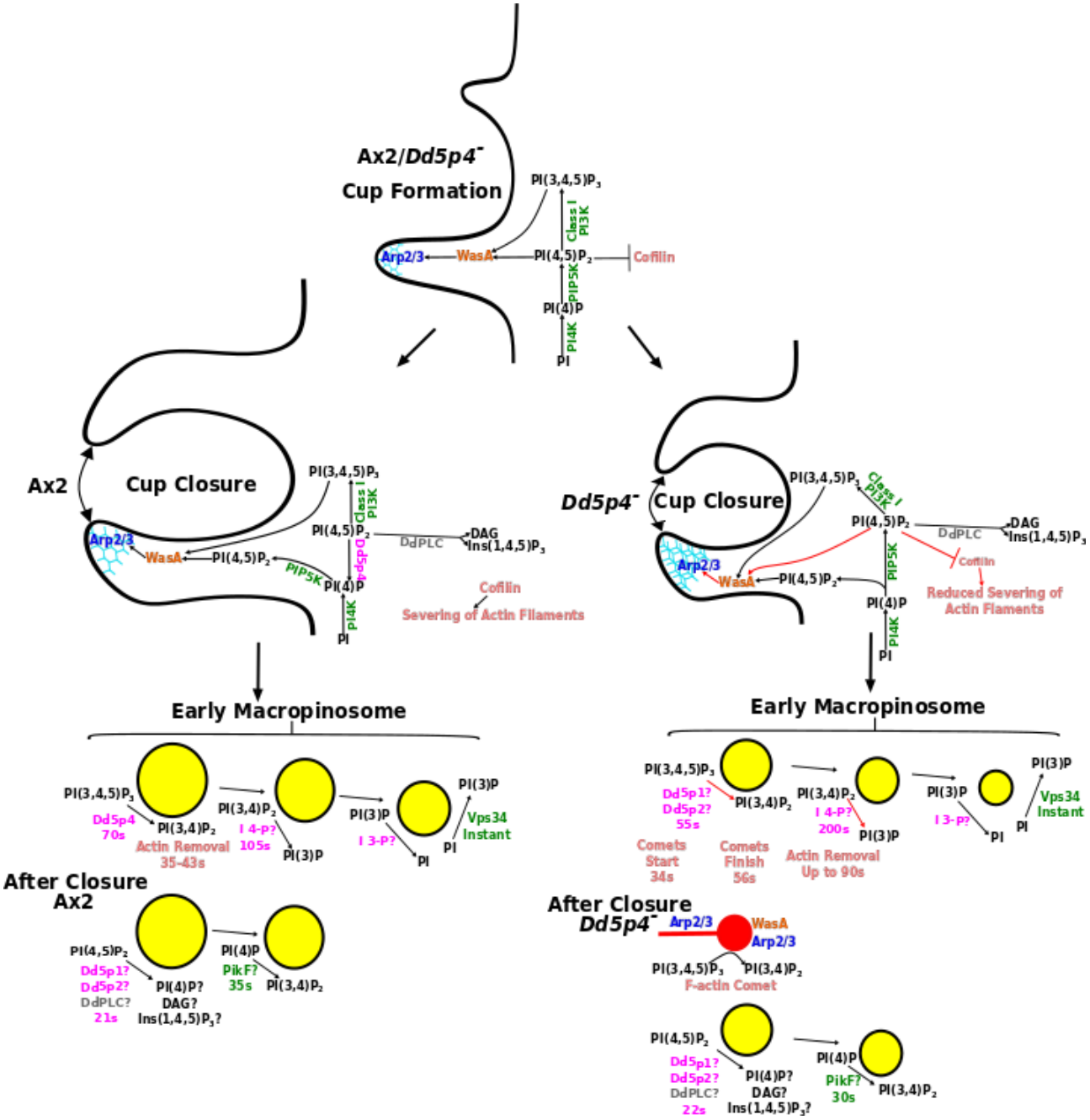

Figure 3.18. An overview of the possible macropinocytic mechanism in Ax2 and *Dd5p4*⁻ cells. During cup formation in both cell lines, PI(4,5)P_2 is synthesised, which together with PI(3,4,5)P_3, activates WasA resulting in Arp2/3 (dark blue)-dependent polymerisation at the cup tips. At cup closure in Ax2, PI(4,5)P_2 is depleted at the base of cups by Dd5p4, thus resulting in the severing of actin filaments, whereas in *Dd5p4*⁻ PI(4,5)P_2 depletion is reduced, reducing the severing of actin filaments at closure. After closure in Ax2 cells, F-actin removal takes places 35-43 seconds after closure of the cup when PI(3,4)P_2 emerges, but in *Dd5p4*⁻ F-actin removal is delayed, with comets forming 34-56 seconds after cup closure carrying PI(3,4,5)P_3, PI(3,4)P_2, WasA, and the Arp2/3 complex. PI(3,4,5)P_3 is hydrolysed and depleted more rapidly in *Dd5p4*⁻ with PI(3,4)P_2 also displaying a lifetime 2-fold greater than in Ax2 control cells. Actin regulators are orange, PIPs are black and PIP conversions are shown by black arrows, kinases are green, phosphatases magenta, PLC is grey, affected paths in *Dd5p4*⁻ are indicated by red arrows. Inositol 3-phosphatase (I 3-P), inositol 4-phosphatase (I 4-P).

The timings of the various PIPs and the corresponding F-actin at the early stages of macropinocytosis in Ax2 and *Dd5p4*⁻ mutant cells is also shown (Fig. 3.19.).

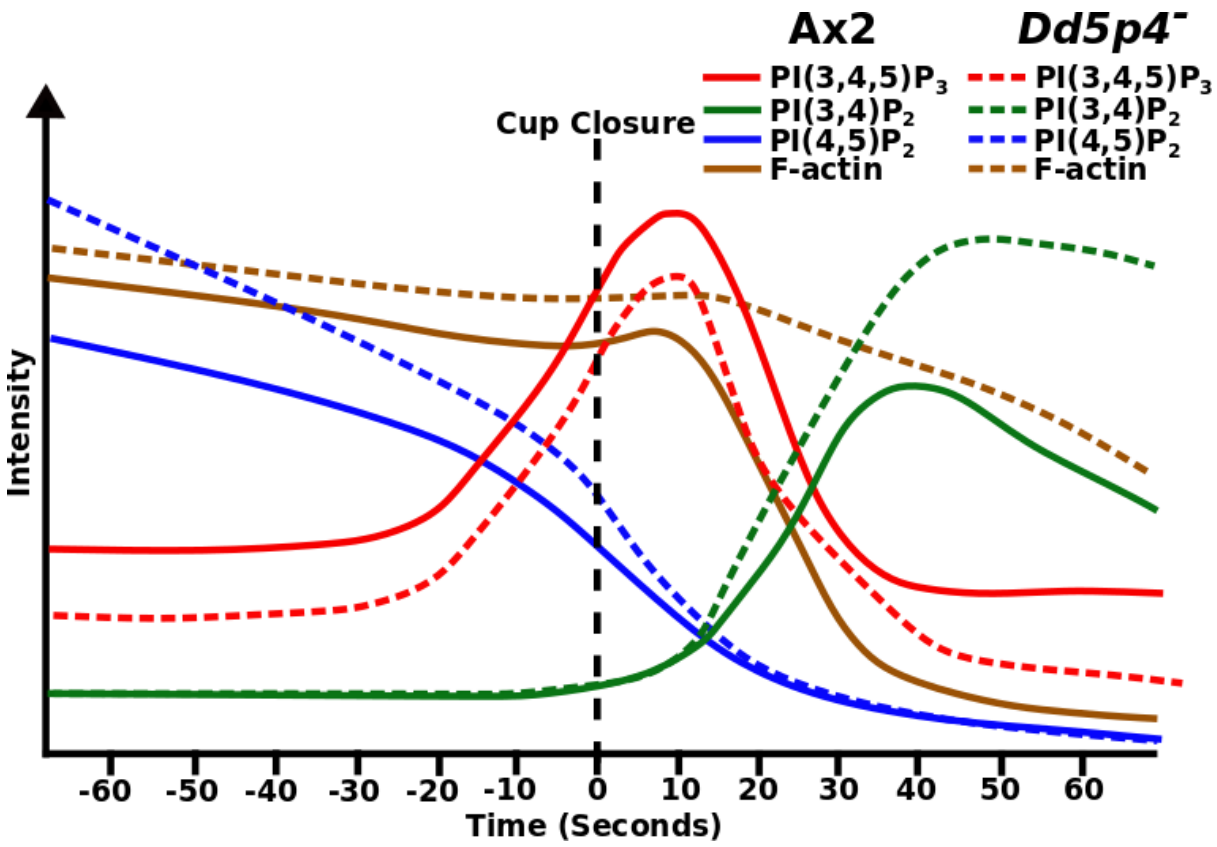

Figure 3.19. An overview of the temporal dynamics of PIPs and F-actin at the early stages of macropinocytosis in Ax2 and *Dd5p4*⁻ cells. During cup formation, the depletion of PI(4,5)P_2 was reduced in *Dd5p4*⁻ cells compared to Ax2 cells, with PI(4,5)P_2 depletion after closure being relatively unaffected across both cell lines. F-actin levels were relatively unchanged before closure, however F-actin removal after closure was considerably reduced in mutant cells compared to Ax2 cells. The decreased levels of F-actin in Ax2 cells appeared to correspond to the increase of PI(3,4)P_2 after cup closure. PI(3,4)P_2 levels were very low during cup formation as F-actin levels were elevated, but after cup closure PI(3,4)P_2 levels increased to higher levels in the mutant cells with F-actin depletion being severely reduced. Before and after cup closure the metabolism of PI(3,4,5)P_3 was largely unaffected between Ax2 and *Dd5p4*⁻ cells. Data adapted from analysis of LLSM images carried out by Kirsty Tinsley.

3.3.4. Discrepancy between the ability to stably express TAPP1-PH-GFP in *Dd5p4*⁻ mutants in this project compared to a previous study

In this project I was able to stably express the TAPP1-PH-GFP fusion protein in both Ax2 control cells and *Dd5p4*⁻ mutant cells, however in a previous study this was only successfully achieved in the Ax3 control cells and not in the Ax3 *Dd5p4*⁻ mutants (Loovers et al. 2007). In this project the more stable Ax2 genetic background was utilised in both control and mutant cell lines, however in the previous study the less stable Ax3 genetic background was used in both control and mutant cell lines (Loovers et al. 2007). The *Dd5p4*⁻ mutants used in the previous study in the Ax3 background and the *Dd5p4*⁻ mutants used in this project in the Ax2 background were both obtained from Arjan Kortholt from the van Haastert Lab, with both mutant cell lines exhibiting resistance to Blasticidin (Loovers et al. 2007). The TAPP1-PH that was used in this project was cloned into a

pDM323 vector backbone, which stably expressed a TAPP1-PH-GFP fusion protein that was under the control of the actin 15 promoter. The TAPP1-PH that was used in a previous study was cloned into a pB15 vector backbone, which stably expressed a TAPP1-PH-GFP fusion protein that was also under the control of the actin 15 promoter (Dowler et al. 2000, Dormann et al. 2004, Loovers et al. 2007). It was suggested that the reason for the lack of expression of the TAPP1-PH-GFP fusion protein in the Ax3 *Dd5p4*$^{-}$ mutants was due to the expression of this fusion protein being somehow lethal to these mutant cells (Loovers et al. 2007). It remains unclear however, as to why there were differences in being able to stably express the TAPP1-PH-GFP fusion protein in the Ax2 *Dd5p4*$^{-}$ mutants in this project in comparison to those from a previous study (Loovers et al. 2007). It could be that the less stable Ax3 *Dd5p4*$^{-}$ mutants for reasons unknown were not able to compensate for the stable expression of the TAPP1-PH-GFP fusion protein, which thus may have rendered these cells non-viable (Loovers et al. 2007). This may differ in comparison to the more stable Ax2 *Dd5p4*$^{-}$ mutants, which could somehow have compensated for the stable expression of the TAPP1-PH-GFP fusion protein, which may have thus rendered these cells viable. It should also be noted however, that different cell culture conditions were used in these studies, which could have influenced the survival capabilities of the stably transfected *Dd5p4*$^{-}$ mutant cell lines. This project used the more nutrient-rich HL-5 media, whilst the previous study used the less nutrient-rich HG5 media (Loovers et al. 2007). The presence of the less nutrient-rich HG5 media could have greatly exaggerated the macropinocytic defects of the less stable Ax3 *Dd5p4*$^{-}$ mutants, which may have thus rendered these cells non-viable (Loovers et al. 2007).

3.3.5. Comparison of *Dd5p4*$^{-}$ growth defects in the axenic Ax2 and Ax3 genetic backgrounds

I have shown in this project that the loss of Dd5p4 activity in the Ax2 genetic background resulted in a mild increase in the generation time in axenic culture to 12.5 hours, compared to 10.8 hours that were observed in Ax2 control cells (Fig. 3.3.A.). Previous work however, in Ax3 cells, which lacked Dd5p4 activity demonstrated a much more severe growth defect in axenic culture of 48.1 hours in comparison to 15.7 hours that were observed in Ax3 control cells (Loovers et al. 2007). The differences in generation times between what I have shown in this project compared to a previous study (Loovers et al. 2007), could be due to the differences in the cell culture media that was used. A previous study utilised HG5 culture media, which lacked the yeast extract, which was present in the more nutrient-rich HL-5 culture media, which I used almost exclusively in this project (see chapter two, section 2.1.). Ax3 control cells, which contained a control plasmid that were grown in HG5, had a doubling time of 15.7 hours (Loovers et al. 2007), which was longer than the doubling time of 10.8 hours of Ax2 cells grown in HL-5 nutrient-rich media in this project. This might therefore

suggest that the provision of more nutrients in HL-5 could counteract the growth defects of *Dd5p4*$^{-}$ in these experiments.

3.3.6. Insights into the roles of Dd5p4 and Dd5p4 F&H interactors during phagocytosis

Previous work has shown that Dd5p4 was able to interact with orthologues of mammalian endocytic adaptors, APPL1 and Ses1/2, and a Cdc42 Rho-GEF, Frabin, in *D. discoideum* via the F&H motif, located in the Dd5p4 Rho-GAP domain (Swan et al. 2010, Pirruccello et al. 2011, Luscher et al. 2019). These interactions could regulate the activity of Dd5p4/OCRL and influence how they could regulate endocytosis (Luscher et al. 2019). In this project, I have shown that rescue of *Dd5p4*$^{-}$ mutant cells with the Dd5p4 F&H mutant, which were incapable of forming the F&H interactions with these orthologues, was still able to rescue the phagocytosis of yeast (Fig. 3.2.K.). This suggested that the F&H motif of Dd5p4 does not appear to be essential in coordinating phagocytic engulfment, however the roles of these interactors in the regulation of endocytosis has not been studied in detail. This will therefore be explored in the next chapter.

Chapter 4

The role of the Dd5p4 interactors; APPL1-like, Ses1/2-like, and GxcU, in regulating phagocytosis and macropinocytosis in *D. discoideum*

4.1. Introduction

The mammalian inositol 5-phosphatase, OCRL, has been shown to interact with endocytic adaptors, APPL1 and Ses1/2, and a Cdc42 Rho-GEF, Frabin. These protein-protein interactions occur between the C-terminal F&H motif of the Rho-GAP domain of OCRL, and the F&H motifs of APPL1, Ses1/2, and Frabin (Erdmann et al. 2007, Swan et al. 2010, Noakes et al. 2011, Pirruccello et al. 2011, Luscher et al. 2019). APPL1 is a very early endocytic adaptor protein, which is present on the non-canonical PI(3)P-negative Rab5-positive early endosomes (Erdmann et al. 2007, Zoncu et al. 2009). Two additional endocytic adaptors, Ses1 and Ses2, were found at later stage PI(3)P-positive canonical endosomes (Swan et al. 2010, Noakes et al. 2011). The binding of APPL1 and Ses1/2 to OCRL have been shown to be mutually exclusive, and occur sequentially (Swan et al. 2010). Frabin (FGD4), the third F&H interactor, is part of the Dbl Homology (DH) family of GEFs, which can bind to PIPs including PI(3)P and PI(4,5)P_2, and also has an actin peptide binding region (Banerjee et al. 2009, Catimel et al. 2013).

In *D. discoideum*, co-immunoprecipitation followed by mass spectrometry was used to identify three F&H motif-containing proteins (Fig. 4.1.A-B.). Two of these proteins were similar in domain structure to *H. sapiens* APPL1 and Ses1/2 (Fig. 4.1.A-B.), despite the divergent amino acid sequences (Fig. 4.2.A-B.) (Luscher et al. 2019). The *D. discoideum* APPL1-like early endocytic BAR domain-containing protein, was found to be related based on domain homology to *H. sapiens* APPL1. The *D. discoideum* Ses1/2-like PH domain-containing protein, was also established to be related based on domain homology to the *H. sapiens* Ses1/2 endocytic adaptors (Fig. 4.1.A-B.). The third F&H interactor was a Rho family GEF, known as GxcU, which was also related based on domain homology to *H. sapiens* Frabin (FGD4) (Fig. 4.1.A-B.), despite the divergent amino acid sequence (Fig. 4.2.C.) (Luscher et al. 2019). Interactions between Dd5p4 and the three identified interactors all involved the F&H motif of Dd5p4 interacting with the F&H motifs of either APPL1-like, Ses1/2-like, or GxcU (Luscher et al. 2019).

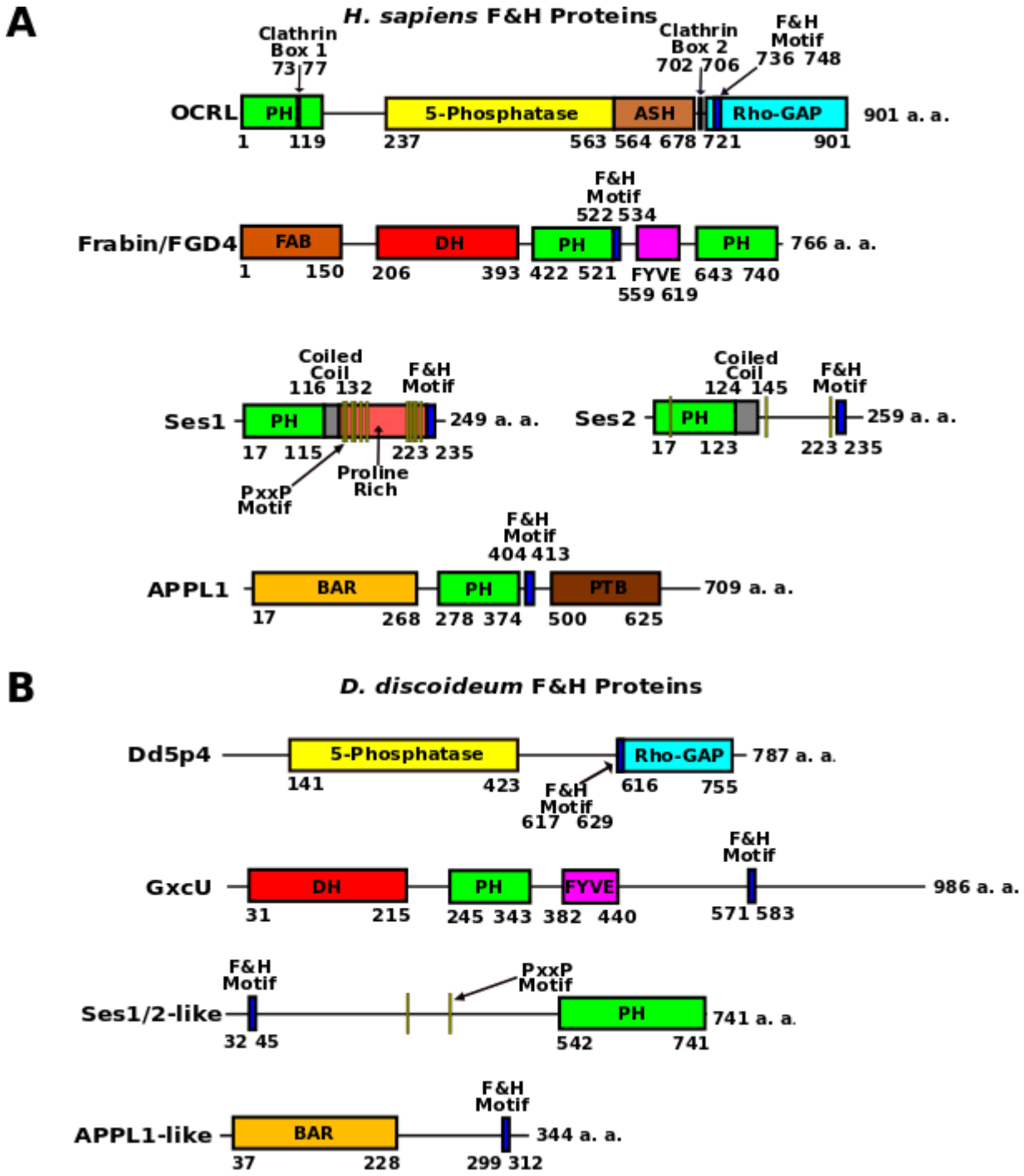

Figure 4.1. The domain structures of the OCRL/Dd5p4 F&H interactors in *H. sapiens* and *D. discoideum*. (A) Domain organisation of OCRL and its F&H interactors in *H. sapiens*. (B) Domain organisation of Dd5p4 and its F&H interactors in *D. discoideum*. Each individual domain/motif are indicated by coloured rectangles as well as the positions of each located within each protein. PxxP motifs are indicated in olive. Bin/Amphiphysin/Rvs (BAR), amino acid residues (a. a.). Adapted from (Noakes et al. 2011, Pirruccello and De Camilli 2012, Luscher et al. 2019).

It has been shown that the portion of APPL1-like between residues 37-228 exhibited very high levels of structural homology (98.8% confidence score) with the BAR domain region of the *H. sapiens* paralogue of APPL1, APPL2 (Luscher et al. 2019). The BAR domains of APPL have been documented to either form homodimers or heterodimers (Miaczynska et al. 2004, Nechamen et al. 2007, Chial et al. 2008, 2010), a feature that is very common amongst members of the BAR

superfamily (Peter et al. 2004), which is necessary for the induction, sensing, and maintenance of curved membrane structures (Peter et al. 2004). The APPL BAR and PH domains function together as a single unit (Miaczynska et al. 2004, Nechamen et al. 2007, Zhu et al. 2007, King et al. 2012), which is the structural basis for targeting to the endosomes and establishing interactions with active Rab5 (Miaczynska et al. 2004, Schenck et al. 2008). The *D. discoideum* APPL1-like protein however, only possesses the BAR domain and lacks the PH domain in comparison to APPL1 in *H. sapiens* (Fig. 4.1.A-B.) (Luscher et al. 2019), which may suggest that the absence of the BAR-PH functional unit in *D. discoideum* APPL1-like could prevent targeting to endosomes and may prevent interactions with active Rab5.

The N-terminal PH domains of the *H. sapiens* Ses1 and Ses2 proteins have been shown to be responsible for the low levels of recruitment of these endocytic adaptors to endosomes and the TGN (Noakes et al. 2011). It was established that the C-terminal regions of Ses1 and Ses2 were crucial for establishing interactions with OCRL, specifically via the F&H motif (Swan et al. 2010, Noakes et al. 2011). It should be noted however, that this was not the case in the *D. discoideum* Ses1/2-like protein as the PH domain was shown to be located in the C-terminal region and the F&H Dd5p4-binding motif was located in the N-terminal region of the Ses1/2-like protein (Fig. 4.1.B.) (Luscher et al. 2019). Both *H. sapiens* Ses1 and Ses2 proteins also possess a coiled-coil domain (Fig. 4.1.A.), which facilitates Ses homodimer and heterodimer formation (Noakes et al. 2011). In *D. discoideum* however, this coiled coil domain was absent, which stated that the Ses1/2-like protein was likely not able to form dimers to facilitate its function (Fig. 4.1.B.). In *H. sapiens*, 11 PxxP motifs have been identified within the Ses1 protein, with only three of these motifs found in the Ses2 protein (Fig. 4.1.A.) (Swan et al. 2010, Noakes et al. 2011). These PxxP motifs could establish interactions with SH3 domain-containing proteins, and thus allow Ses1 and Ses2 to establish interactions with proteins containing these domains (Swan et al. 2010). Interestingly, two PxxP motifs have been found in the central region of the Ses1/2-like protein in *D. discoideum* (Fig. 4.1.B.) (Luscher et al. 2019). Although fewer PxxP motifs are found in this protein compared to the *H. sapiens* Ses1/2 proteins, a single C-terminal PxxP motif in the *H. sapiens* slit-robo GTPase-Activating Protein 3 (srGAP3) has been shown to still be able to establish interactions with SH3 domain-containing proteins (Wuertenberger and Groemping 2015). This may suggest that the *D. discoideum* Ses1/2-like protein may still be able to form interactions with proteins containing SH3 domains.

The *D. discoideum* GxcU protein possessed a similar domain structure to the *H. sapiens* Frabin protein (Fig. 4.1.A-B.). Both GxcU and Frabin have an N-terminal Dbl Homology (DH) domain, which encodes the catalytic GEF activity, which facilitates the removal of GDP from the Rho family of small G proteins (Obaishi et al. 1998, Takai et al. 2001, Hall 2005, Luscher et al. 2019). GxcU also

possesses a PH domain adjacent to its DH domain, much like what is observed in *H. sapiens* Frabin (Fig. 4.1.A-B.). The presence of the PH domain adjacent to the DH domain has been shown in Dbl's big sister (Dbs) to be required for the specific binding to nucleotide-free small G proteins and also to aid in facilitating guanine nucleotide exchange reactions (Rossman et al. 2002). The amino acid sequence of the N-terminal portion of Frabin, which encompassed the DH domain and the first PH domain were able to stimulate guanine nucleotide exchange on the *H. sapiens* Cdc42 small G protein, but did not facilitate this exchange on the RhoA and Rac1 small G proteins (Umikawa et al. 1999). The first PH domain of Frabin has also been shown to bind most preferably to PI(3)P and PI(4,5)P_2, with the Frabin FYVE domain shown to bind specifically to PI(3)P (Catimel et al. 2013). The PH and FYVE domains of the *D. discoideum* GxcU protein are likely to possess the same or similar functions in facilitating protein localisation, GEF activity, and PIP binding in comparison to *H. sapiens* Frabin (Luscher et al. 2019). GxcU does however, lack the N-terminal FAB domain of Frabin, which facilitates binding to the side of F-actin, and also lacks the second C-terminal PH domain (Fig. 4.1.A-B.) (Obaishi et al. 1998, Luscher et al. 2019).

A comparison of the amino acid sequences between the *H. sapiens* OCRL F&H interactors and the *D. discoideum* Dd5p4 F&H interactors, excluding both OCRL and Dd5p4 is displayed (Fig. 4.2.A-C.).

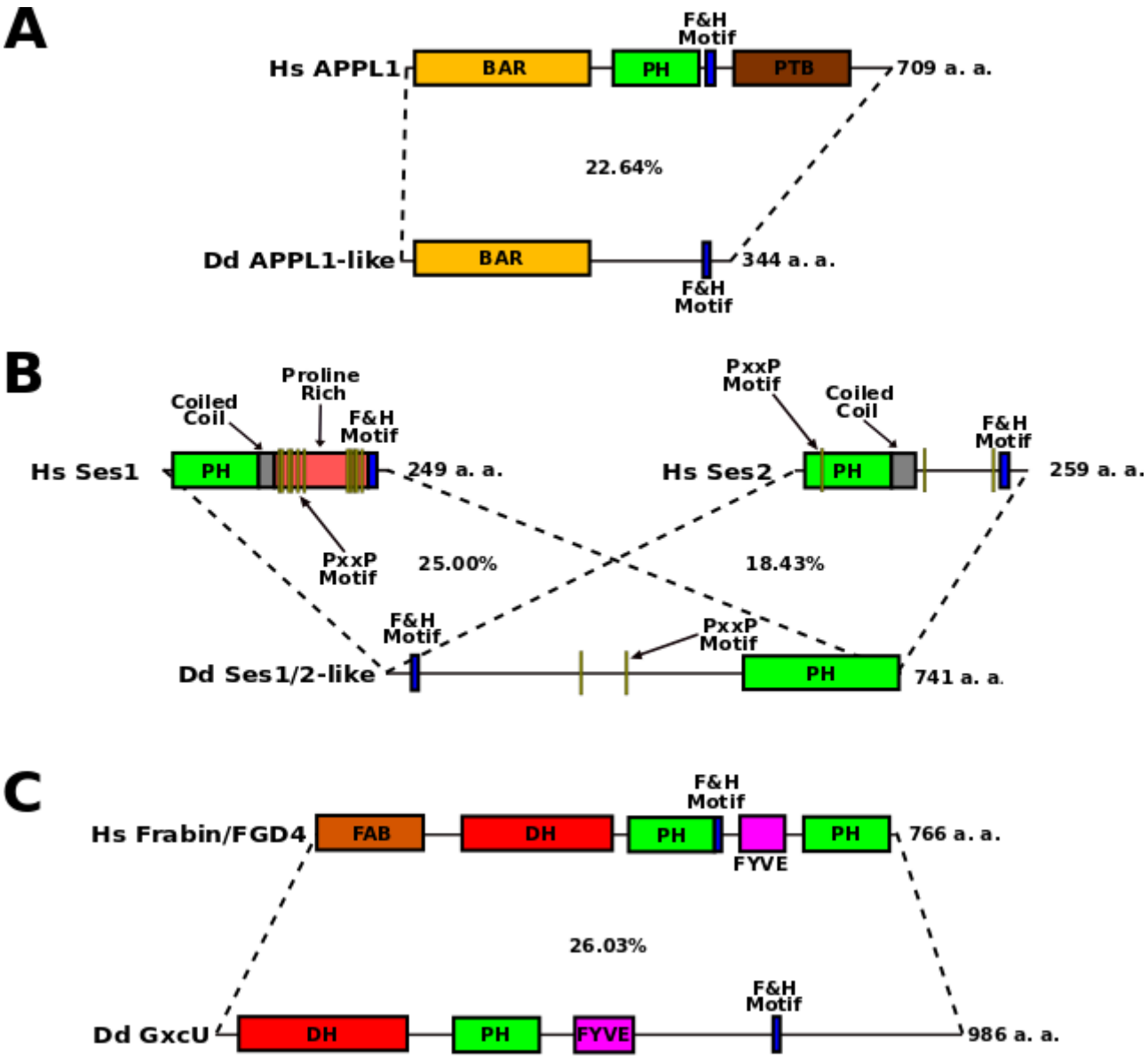

Figure 4.2. The amino acid sequence comparison between the F&H interactors of *H. sapiens* and *D. discoideum*. (A) The amino acid sequence comparison between *H. sapiens* APPL1 and *D. discoideum* APPL1-like. (B) The amino acid sequence comparison between *H. sapiens* Ses1 and Ses2 and *D. discoideum* Ses1/2-like. (C) The amino acid sequence comparison between *H. sapiens* Frabin and *D. discoideum* GxcU. The sequence similarity was determined through inputting the amino acid sequences into Clustal Omega (https://www.ebi.ac.uk/Tools/msa/clustalo/), with the percent identity matrix or the protein sequence identity displayed as a %. Each individual domain/motif are indicated by coloured rectangles within each protein. *Dictyostelium discoideum* (Dd), *Homo sapiens* (HS). Adapted from (Noakes et al. 2011, Pirruccello and De Camilli 2012, Luscher et al. 2019).

The functional roles of the Dd5p4 F&H motif interactors in *D. discoideum* is relatively unknown thus far (Luscher et al. 2019). The Ses1/2-like protein has been shown to localise at the late-acidic and post-lysosomal stage (Luscher et al. 2019). This observation stated that like the *H. sapiens* counterparts; Ses1 and Ses2, Ses1/2-like in *D. discoideum* functions as a later stage endocytic adaptor protein (Luscher et al. 2019). It has been shown that GxcU overexpression caused a significant reduction in fluid uptake, with an even greater reduction observed in *Dd5p4*$^{-}$ mutant

cells overexpressing GxcU. This indicated a functional interaction between GxcU and Dd5p4, in which Dd5p4 repressed GxcU activity (Luscher et al. 2019). GxcU has been established to be recruited to two distinct locations, the first being at the base of macropinocytic cups and the second being at newly reforming contractile vacuoles (CVs) (Luscher et al. 2019).

Numerous fresh water protists such as amoeba, many Ciliates, and Heliozoans govern water's penetration via the acts of a complex organelle, which is responsible for their osmoregulation, this organelle is known as the CV (De Chastellier et al. 1978, Patterson 1980). The CV organelle within *D. discoideum* consists of extensive networks of bladders and tubules that are joined to the PM. This organisation is crucial when cells encounter hypotonic environments where maintaining osmoregulation is essential for survival (Gerisch et al. 2002). Excess water within cells accumulates within the tubules, which fill the vacuoles, with these vacuoles subsequently fusing with the PM in order to release and expel the excess water into the extracellular environment (Heuser et al. 1993). The process by which the CV and PM transiently interconnect is known as the kiss-and-run exocytic water discharge (Mckanna 1973, 1976, Essid et al. 2012). Following on from the expulsion of excess water through the vacuoles, the tubules again elongate and subsequently collect more water to resume the CV cycle. It has been suggested that PI(4,5)P_2 regulates CV trafficking to the site of fusion at the PM, with cells that display defects in Dd5P4 enzymatic activity and thus the inability to hydrolyse PI(4,5)P_2 exhibiting inefficient CV fusion with the PM (Luscher et al. 2019). In addition to this, a combinatorial role of Dd5p4 in association with the APPL1-like protein has also been shown to occur at the CVs and PMs of *D. discoideum* during the kiss-and-run exocytic water discharge (Luscher et al. 2019). The localisation of Dd5p4, APPL1-like, and GxcU during part of the CV cycle is summarised (Fig. 4.3.).

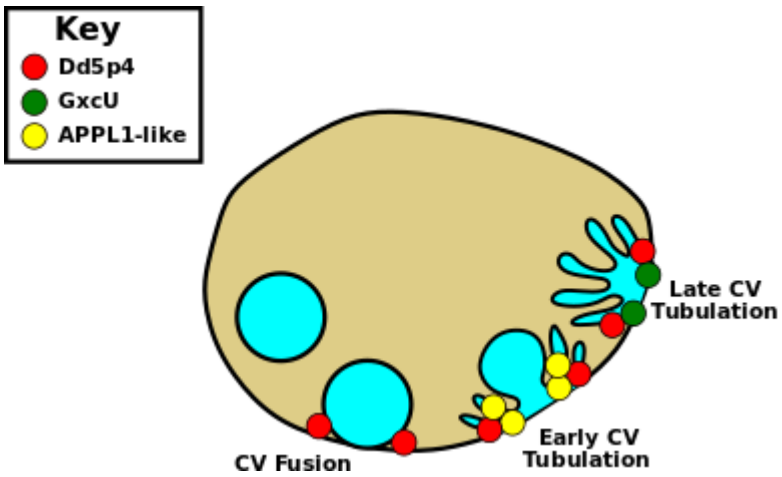

Figure 4.3. The localisation of Dd5p4, APPL1-like, and GxcU during part of the CV cycle in *D. discoideum* Ax3 cells. During the CV cycle, Dd5p4 facilitates fusion of the CV with the PM. Dd5p4 and the APPL1-like F&H interactor then together govern the stage of early tubulation, which is subsequently followed by Dd5p4 and the GxcU F&H interactor governing the later tubulation stage. Dd5p4 and its F&H interactors are colour-coded as shown in the key. Adapted from (Luscher et al. 2019).

Despite all of these observations however, the understanding of how the Dd5p4 F&H interactors regulated the dynamics of macropinocytosis and, in particular phagocytosis, remains poorly understood. Understanding how these Dd5p4 F&H interactors regulated macro-endocytosis is therefore the subject of this chapter.

4.2. Results

4.2.1. The generation of mutants of the F&H Dd5p4 interactors

D. discoideum have a single orthologue of the APPL1 protein (APPL1-like), the Ses1/2 proteins (Ses1/2-like), and the Frabin protein (GxcU), which made this organism ideal to study these Dd5p4 F&H interactors (Luscher et al. 2019). To study the roles that these interactors played in macropinocytosis and phagocytosis, the genes encoding APPL1-like, Ses1/2-like, and GxcU were disrupted. The *GxcU* locus was disrupted using CRISPR, through the administration of a short deletion by the enzymatic activity of Cas9, creating frameshift mutations from the deletion site. As Dd5p4 and GxcU were previously shown to functionally interact (Luscher et al. 2019), mutations in both genes were also investigated. The *GxcU* locus was disrupted in both the Ax2 and *Dd5p4*$^{-}$ parental backgrounds to generate *GxcU*$^{-}$ single mutants and *Dd5p4*$^{-}$ *GxcU*$^{-}$ double mutants respectively (Fig. 4.4.A-B.).

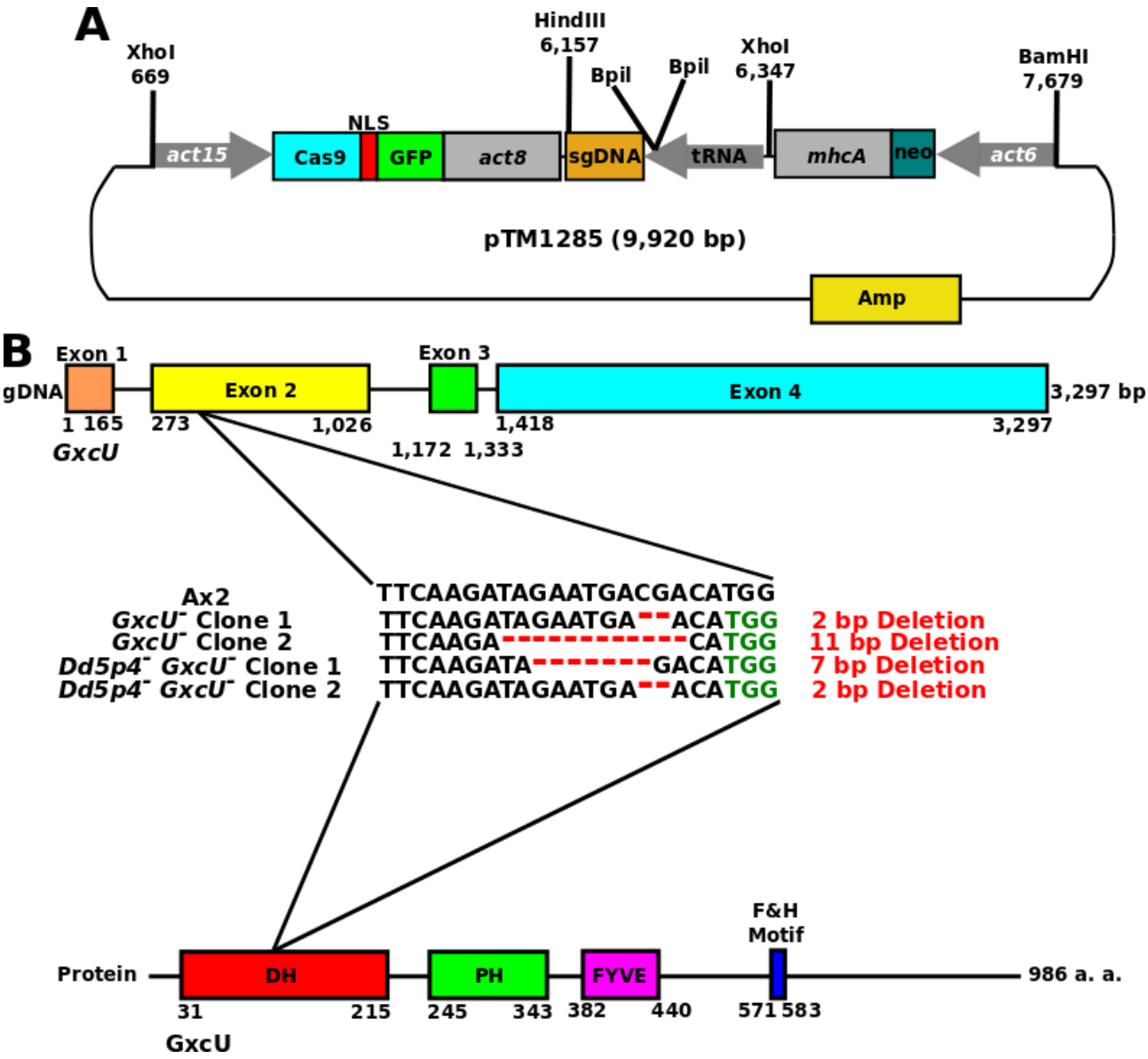

Figure 4.4. The generation of *GxcU*$^{-}$ and *Dd5p4*$^{-}$ *GxcU*$^{-}$ mutants using CRISPR. (A) Schematic overview of the all-in-one pTM1285 CRISPR/Cas9 vector. Two oligonucleotides were inserted into the vector via the Golden gate assembly method (Sekine et al. 2018). Ampicillin resistance gene (Amp), *act15* promoter (*act15*), *act8* terminator (*act8*), isoleucine tRNA (tRNA), *mhcA* terminator (*mhcA*), neomycin resistance gene (neo), *act6* promoter (*act6*). (B) gDNA schematic of the *GxcU* locus and the domain structure of the resulting protein. The target sequence is indicated, with the location of the deletions shown in red in the *GxcU*$^{-}$ and *Dd5p4*$^{-}$ *GxcU*$^{-}$ clones with the PAM site indicated in green. Base pairs (bp), amino acid residues (a. a.).

I then disrupted the *APPL1-like* and *Ses1/2-like* genes through the insertion of a Blasticidin resistance cassette into the coding region of both genes (Fig. 4.5.A-G.). *APPL1-like*$^{-}$ and *Ses1/2-like*$^{-}$ mutant cell lines were generated by homologous recombination. Whilst I was unable to obtain the complete PCR screen, due to the size and AT-rich content of the templates, successful gene disruption was confirmed by screening for the presence of the Blasticidin resistance cassette using PCR (Fig. 4.5.D. and G.).

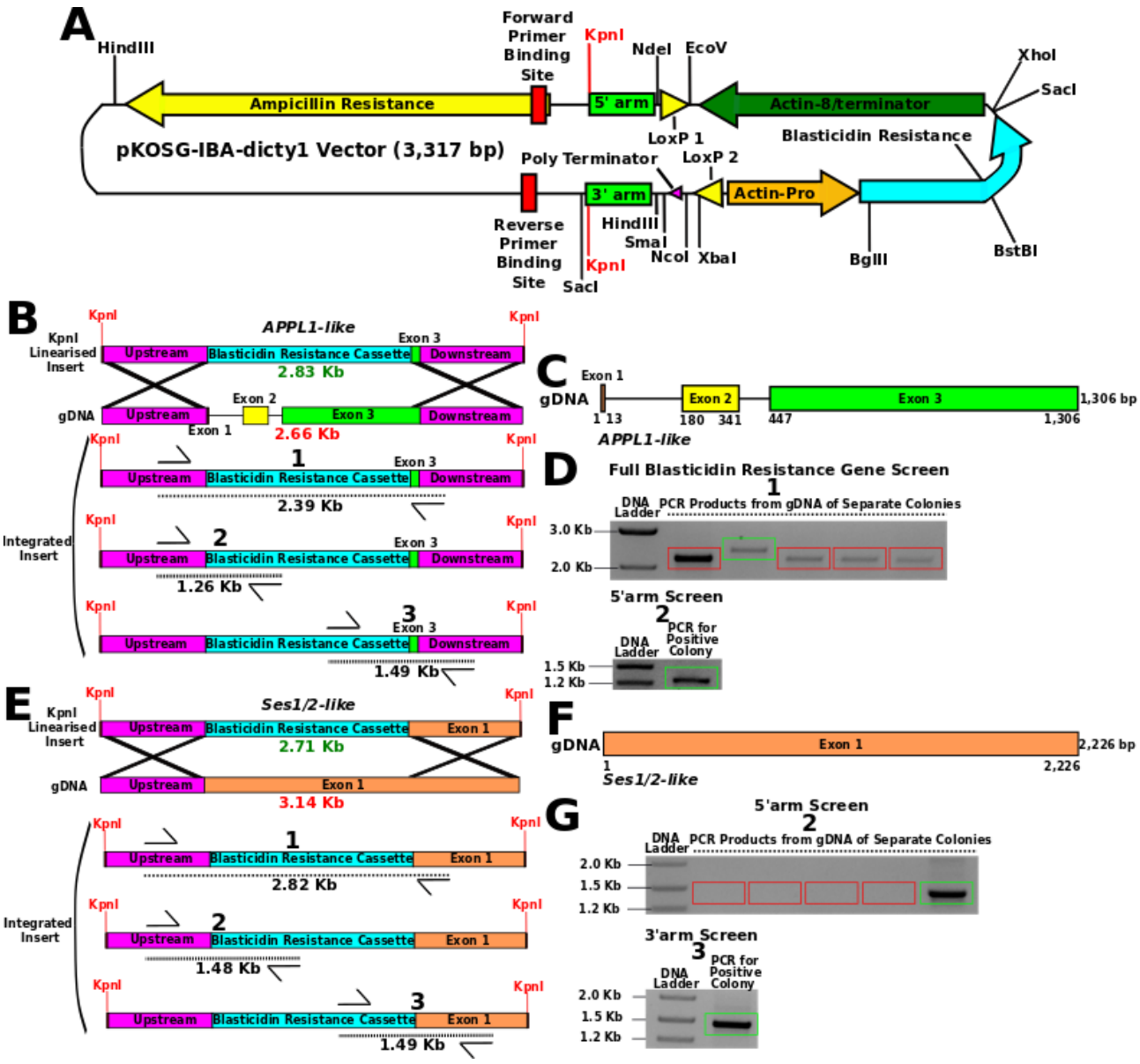

Figure 4.5. The generation of *APPL1-like*⁻ and *Ses1/2-like*⁻ mutants. (A) Schematic overview of the pKOSG-IBA-dicty1 vector with KpnI restriction enzyme sites (red) incorporated to aid the insertion of the Blasticidin resistance cassette. (B) Linearised Blasticidin cassette with *APPL1-like* homology arms (size incorporated indicated in green) and the target *APPL1-like* locus (size removed indicated in red). Each of the PCRs used to screen for the insertion of the resistance cassette and the primer pair used are numbered (expected band sizes are indicated in black). (C) gDNA schematic overview. (D) Products of PCR screening reactions from colony gDNA samples, one to screen the full Blasticidin resistance gene, the other across the 5' homology arm and the resistance cassette, and the other to screen across the 3' homology arm and the resistance cassette. The 3' homology arm screen failed to yield a product. Each gel that is displayed is numbered, which corresponds to the primer pair previously indicated (B). A positive *APPL1-like*⁻ clone is highlighted by a green box, negative colonies are highlighted by red boxes. (E) Linearised Blasticidin cassette with *Ses1/2-like* homology arms (size incorporated indicated in green) and the target *Ses1/2-like* locus (size removed indicated in red). Each of the PCRs used to screen for the insertion of the resistance cassette and the primer pair used are numbered (expected band sizes are indicated in black). (F) gDNA schematic overview. (G) Products of screening reactions from colony gDNA samples. The full Blasticidin resistance cassette screen failed to yield a product. Each gel that is displayed is numbered, which corresponds to the primer pair previously indicated (E). A positive *Ses1/2-like*⁻ clone is highlighted by a green box, negative colonies are highlighted by red boxes. Sizes of DNA schematics are not to scale.

4.2.2. Loss of GxcU, APPL1-like, and Ses1/2-like Dd5p4 F&H interactors reduced the levels of phagocytosis

Studies of the Dd5p4 F&H interactors and how they regulated phagocytosis has been limited thus far. This gave the incentive to test if any of the Dd5p4 F&H interactors affected the phagocytosis of yeast. Dd5p4 and GxcU have been shown to functionally interact (Luscher et al. 2019), so investigations of the phagocytosis of yeast in cells in which both proteins were absent was also undertaken. All cell lines were shaken for 30 minutes with fluorescently labelled red yeast prior to live-cell imaging to quantify phagocytic engulfment. The addition of trypan blue was used to quench the fluorescence of yeast that were not engulfed (Fig. 4.6.A-L.). Due to Dd5p4 and GxcU both being shown to interact I therefore also incorporated the data on the single *Dd5p4*$^{-}$ mutants and the associated Ax2 control cells from chapter three and combined the *Dd5p4*$^{-}$ Ax2 controls with the control cells associated with *GxcU*$^{-}$ single mutants, and the control cells associated with the *Dd5p4*$^{-}$ *GxcU*$^{-}$ double mutants in order to ensure valid comparisons between all cell lines (Fig. 4.6.A-L.).

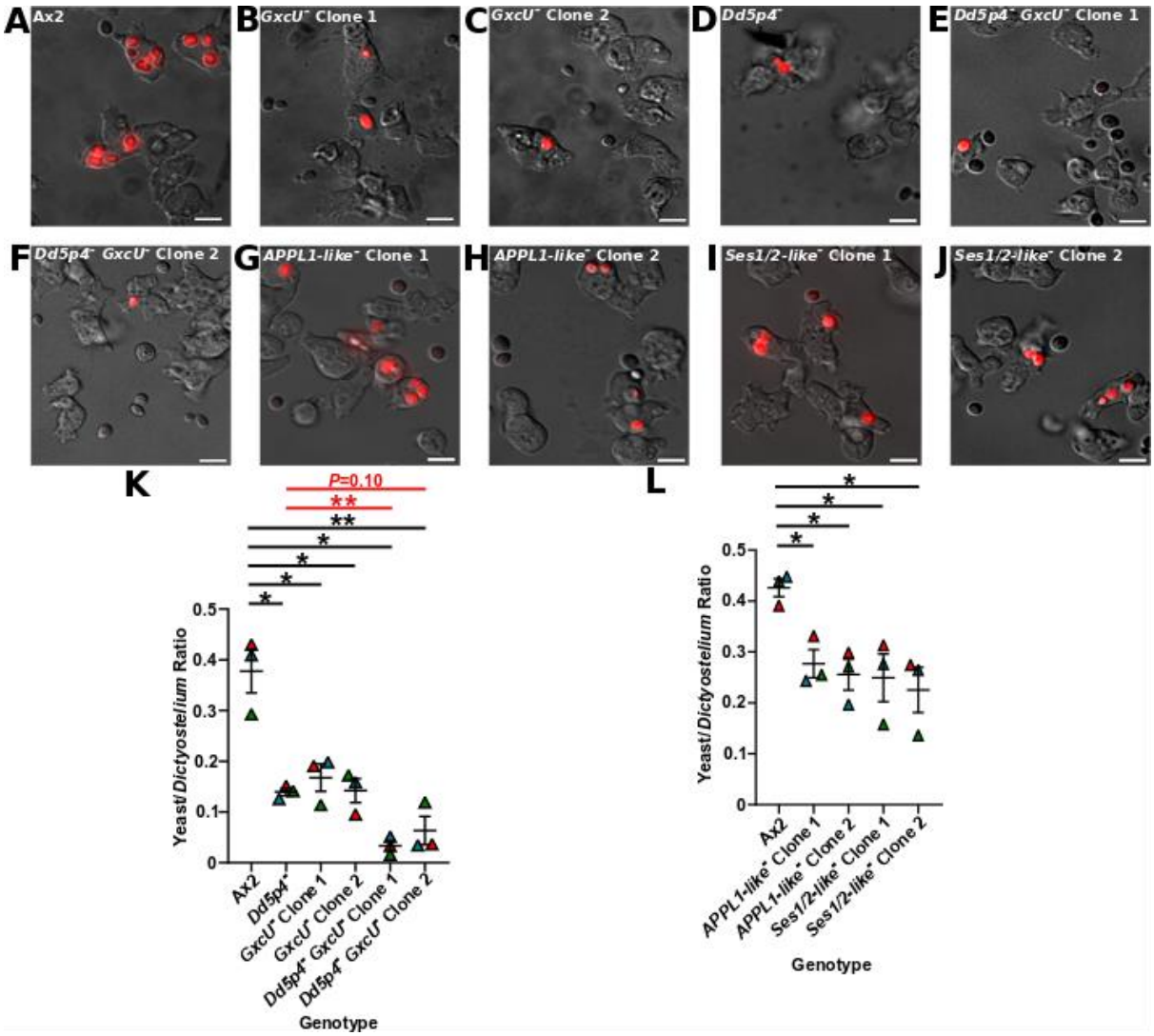

Figure 4.6. Phagocytosis of yeast was reduced in all Dd5p4 F&H interactor mutants. Representative confocal images showing Ax2 (A), *GxcU*$^{-}$ clones 1 (B), and 2 (C), *Dd5p4*$^{-}$ (D), *Dd5p4*$^{-}$ *GxcU*$^{-}$ clones 1 (E), and 2 (F), *APPL1-like*$^{-}$ clones 1 (G), and 2 (H), and *Ses1/2-like*$^{-}$ clones 1 (I), and 2 (J), engulfing fluorescently labelled red yeast following 30 minutes of shaking. (K) Quantification of yeast phagocytosis using the yeast to *D. discoideum* ratio of *Dd5p4*$^{-}$, *GxcU*$^{-}$, and *Dd5p4*$^{-}$ *GxcU*$^{-}$ clones compared to Ax2 control cells. The *Dd5p4*$^{-}$ Ax2 control cells from chapter three were combined with the Ax2 control cells associated with *GxcU*$^{-}$ mutants, and the control cells associated with the *Dd5p4*$^{-}$ *GxcU*$^{-}$ double mutants to ensure valid statistical comparisons between all cell lines. (L) Quantification of yeast phagocytosis using the yeast to *D. discoideum* ratio of *APPL1-like*$^{-}$ *and Ses1/2-like*$^{-}$ mutants compared to Ax2 control cells. A single Ax2 control cell population was used in this experiment in comparison to *APPL1-like*$^{-}$ and *Ses1/2-like*$^{-}$ mutant clones. (K-L) Statistical comparisons with Ax2 control cells are indicated in black, with *Dd5p4*$^{-}$ mutant comparisons with *Dd5p4*$^{-}$ *GxcU*$^{-}$ double mutants shown in red. The data shown are the average ratios calculated from three independent, colour-coded biological repeats, ± SEM. Scale bars are 10 microns. Significance and non-significance was determined using Welch's *t* tests. * $P < 0.05$, ** $P < 0.01$.

Quantification of the yeast to *Dictyostelium* ratio revealed that the loss of Dd5p4 activity appeared to cause a significant reduction in the levels of phagocytosis compared to Ax2 control cells, with a similar reduction appearing in both *GxcU*$^{-}$ mutant clones (Fig. 4.6.K.). The absence of both GxcU and Dd5p4 activities also appeared to cause a reduction in phagocytosis compared to

Ax2 control cells (Fig. 4.6.K.). Interestingly, the first clone of the double mutants appeared to display a more severe reduction in phagocytosis in comparison to the *Dd5p4*$^{-}$ single mutants (Fig. 4.6.K.). It should be noted however, that the second *Dd5p4*$^{-}$ *GxcU*$^{-}$ clone appeared to display no significant reduction in the levels of phagocytosis in comparison to the *Dd5p4*$^{-}$ single mutants, which appeared to be due to the unexpected, slightly raised levels of phagocytosis in the second independent biological repeat (Fig. 4.6.K.).

The absence of the early APPL1-like endocytic adaptor protein, and the later Ses1/2-like adaptor protein both reduced the levels of phagocytosis in comparison to Ax2 control cells (Fig. 4.6.L.).

This would suggest in summary that the GxcU, APPL1-like, and Ses1/2-like Dd5p4 F&H interactors played a role in phagocytosis, and that Dd5p4 and GxcU may possibly possess functionally distinct roles to coordinate successful phagocytic engulfment.

4.2.3. *Dd5p4*$^{-}$ took less time to enwrap yeast compared to Ax2 and *Dd5p4*$^{-}$ *GxcU*$^{-}$ double mutants, whilst *Ses1/2-like*$^{-}$ mutants took longer to enwrap yeast

To establish why the absence of each of the three Dd5p4 F&H interactors, and cells lacking both Dd5p4 and GxcU, resulted in less phagocytosis taking place, I first explored the stage in which yeast were enwrapped. I have compared the data on enwrapping yeast and the phagocytic failure rate of *Dd5p4*$^{-}$ cells along with the associated Ax2 control cells from chapter three with the data from this chapter on *GxcU*$^{-}$, and the *Dd5p4*$^{-}$ *GxcU*$^{-}$ double mutants and the associated Ax2 controls. This was done in order to perform statistical analyses between the *Dd5p4*$^{-}$ single and *Dd5p4*$^{-}$ *GxcU*$^{-}$ double mutants in order to outline the possible distinct roles that Dd5p4 and GxcU may play. PI(3,4,5)P_3, which is a marker of phagocytic cups, was visualised using the previously described PkgE probe used in chapter three (Ruchira et al. 2004, Goldberg et al. 2006, and van Haastert lab, unpublished data). This probe was used to test if mutants of the Dd5p4 F&H interactors were able to respond to initial contacts with yeast. The time taken for the PI(3,4,5)P_3-labelled PM to fully encircle the yeast during phagocytic engulfment events was also quantified. To determine if loss of Dd5p4 and/or GxcU altered the rates of enwrapping yeast, *Dd5p4*$^{-}$, *GxcU*$^{-}$, and *Dd5p4*$^{-}$ *GxcU*$^{-}$ clones were thereby compared to Ax2 control cells, and *Dd5p4*$^{-}$ single mutants were compared with the *Dd5p4*$^{-}$ *GxcU*$^{-}$ double mutants (Fig. 4.7.A-G.).

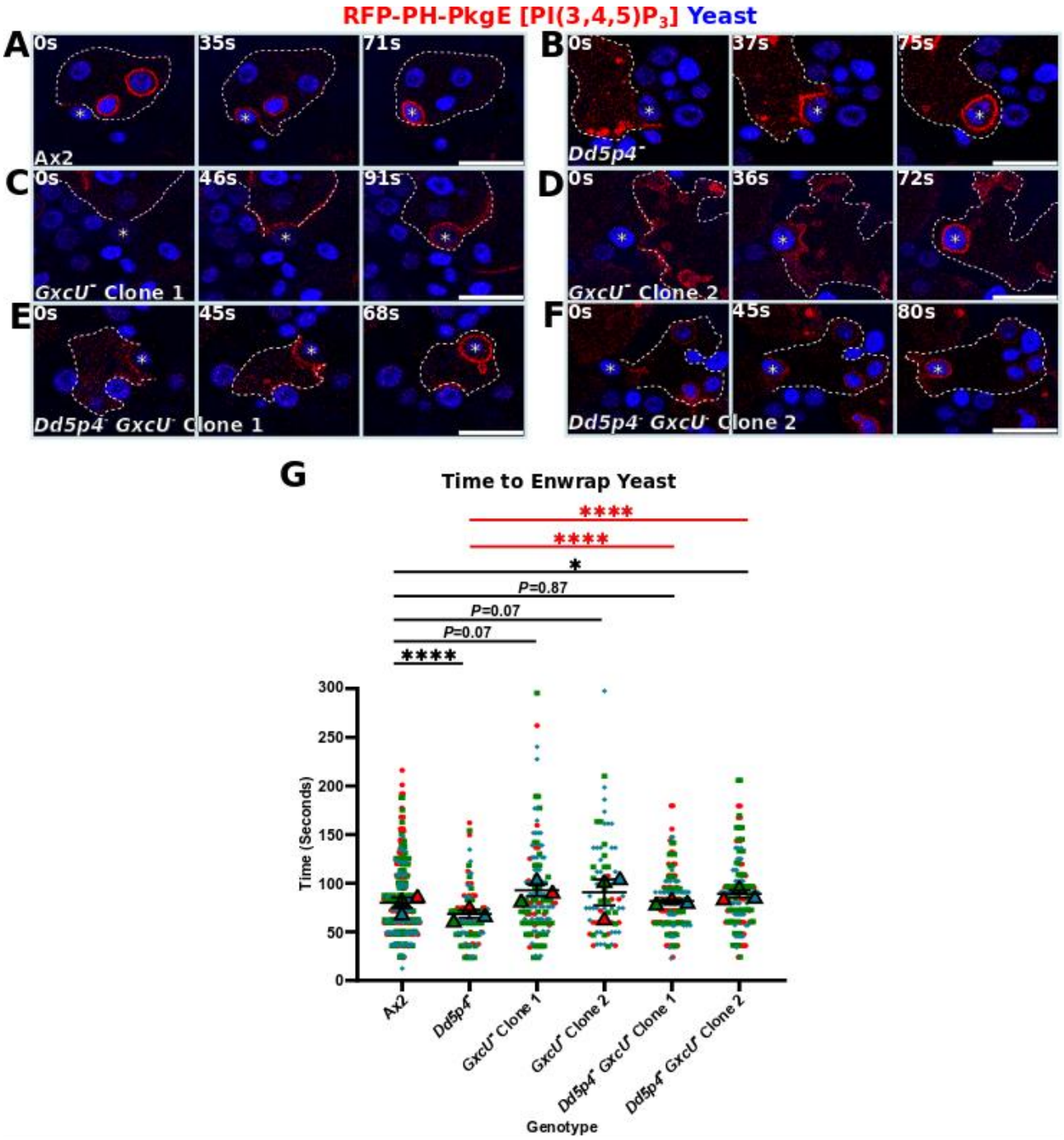

Figure 4.7. *Dd5p4*$^-$ appeared to take less time to enwrap yeast compared to Ax2 and *Dd5p4*$^-$ *GxcU*$^-$ double mutants. Confocal images of Ax2 (A), *Dd5p4*$^-$ (B), *GxcU*$^-$ clones (C-D), and *Dd5p4*$^-$ *GxcU*$^-$ clones (E-F) stably expressing RFP-PH-PkgE, which labels PI(3,4,5)P_3, engulfing fluorescent blue yeast over time. The cell peripheries are indicated by white dashed lines, with the time intervals indicated in white. Yeast of interest are indicated by white stars. (G) Quantification of the time taken during phagocytic engulfment events for the PI(3,4,5)P_3-labelled PM (red with no white dashed lines) to fully enwrap yeast from the first point of contact. *Dd5p4*$^-$ and the associated Ax2 control cells from chapter three were compared to the data on *GxcU*$^-$ and *Dd5p4*$^-$ *GxcU*$^-$, with the *Dd5p4*$^-$ Ax2 control cells combined with the control cells associated with *GxcU*$^-$ and the control cells associated with *Dd5p4*$^-$ *GxcU*$^-$ in order to ensure valid statistical comparisons. Statistical comparisons with Ax2 control cells are indicated in black, with *Dd5p4*$^-$ single mutant comparisons with *Dd5p4*$^-$ *GxcU*$^-$ double mutants shown in red. The data shown are the individual points and averages from each of the three independent, biological colour-coded repeats, ± SEM. Scale bars are 10 microns. Significance and non-significance was determined using Mann Whitney U tests. * $P < 0.05$, **** $P < 0.0001$.

In the *Dd5p4*$^{-}$ single mutants, the time taken to enwrap yeast appeared to be significantly reduced in comparison to Ax2 control cells (Fig. 4.7.G.). This however, differed from the results that compared the time taken to enwrap yeast between Ax2 and *Dd5p4*$^{-}$ mutant cells from chapter three in which no change in the time taken to enwrap yeast was observed (Fig. 3.5.A-C.). The differences were due to the presence of multiple Ax2 control cell populations from separate experiments being compared (Fig. 4.7.A-G.) in comparison to just a single Ax2 control cell population in chapter three (Fig. 3.5.A-C.). This assay typically exhibits day to day variation between biological repeats and also variation between the Ax2 control cells that were used in different experiments. Analysis of the time taken for both *GxcU*$^{-}$ mutant clones to enwrap yeast appeared to be unaltered in comparison to Ax2 cells (Fig. 4.7.A. C-D. and G.). The loss of both Dd5p4 and GxcU did however, appear to display some variation between clones 1 and 2, with clone 1 appearing to display no alterations in the time taken to enwrap yeast, whilst clone 2 in contrast appeared to display a significant increase in the time taken to enwrap yeast compared to Ax2 control cells (Fig. 4.7.A. and E-G.). Both the *Dd5p4*$^{-}$ *GxcU*$^{-}$ double mutant clones however, appeared to take a significantly longer time of 80-85 seconds to enwrap yeast when compared to just 70 seconds in the *Dd5p4*$^{-}$ single mutants (Fig. 4.7.G.).

Using the same experimental setup previously described, mutant cell lines were used to determine if the absence of endogenous APPL1-like or Ses1/2-like altered the time taken to enwrap yeast in comparison to Ax2 control cells (Fig. 4.8.A-F.).

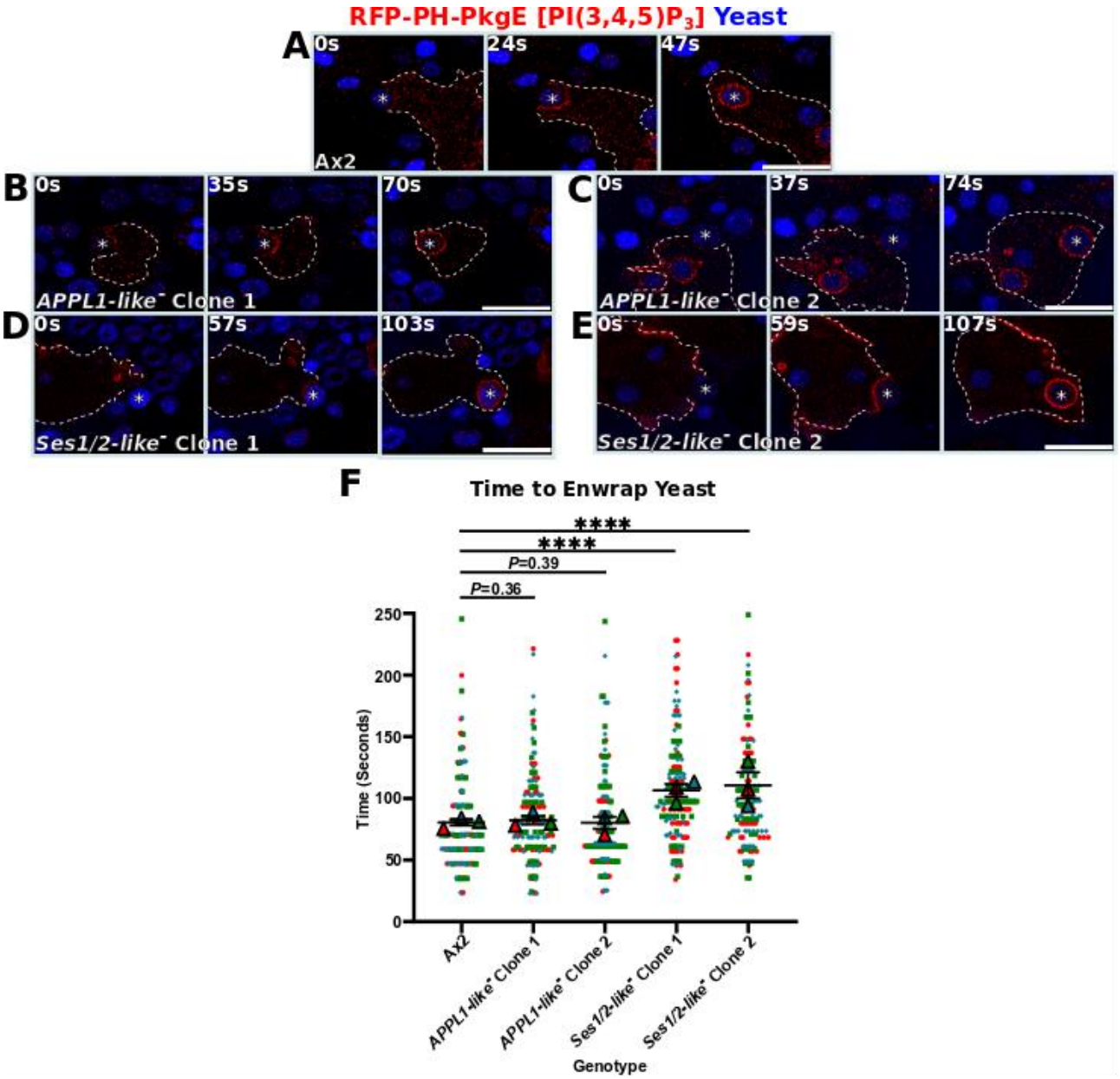

Figure 4.8. *Ses1/2-like*⁻ mutants took longer to enwrap yeast. Confocal images of Ax2 (A), *APPL1-like*⁻ clones (B-C), and *Ses1/2-like*⁻ clones (D-E) stably expressing RFP-PH-PkgE, which labels PI(3,4,5)P_3, engulfing fluorescent blue yeast over time. The cell peripheries are indicated by white dashed lines, with the time intervals indicated in white. Yeast of interest are indicated by white stars. (F) Quantification of the time taken during phagocytic engulfment events for the PI(3,4,5)P_3-labelled PM (red with no white dashed lines) to fully enwrap yeast from the first point of contact. A single Ax2 control cell population was used in this experiment in comparison to *APPL1-like*⁻ and *Ses1/2-like*⁻ mutant clones. Statistical comparisons with Ax2 control cells are indicated in black. The data shown are the individual points and averages from each of the three independent biological, colour-coded repeats, ± SEM. Scale bars are 10 microns. Significance and non-significance was determined using Mann Whitney U tests. **** $P < 0.0001$.

The loss of APPL1-like activity did not alter the rates of enwrapping yeast, compared to Ax2 control cells (Fig. 4.8.A-C. and F.). Ax2 and *APPL1-like*⁻ mutant cells took approximately 80 seconds to enwrap yeast (Fig. 4.8.F.). The absence of Ses1/2-like activity however, significantly increased the time taken to enwrap yeast compared to Ax2 control cells (Fig. 4.8.A. and D-F.). Collectively, the

Ses1/2-like^{-} mutant clones took approximately 100-110 seconds to enwrap yeast in comparison to the 80 seconds that were observed for Ax2 cells (Fig. 4.8.A. and D-F.).

4.2.4. *GxcU*$^{-}$, *Ses1/2-like*$^{-}$ and more severely *Dd5p4*$^{-}$, each displayed phagocytic defects, with altered phagocytic engulfment kinetics observed in *Dd5p4*$^{-}$ *GxcU*$^{-}$, *APPL1-like*$^{-}$ and *Ses1/2-like*$^{-}$

In addition to PI(3,4,5)P_3, PI(3)P was also visualised as this acted as a hallmark of the early phagosome after closure. In Ax2, phagosomes only acquired PI(3)P after phagocytic cup closure. I therefore used 2xFYVE as a PI(3)P reporter (Gillooly et al. 2000, Calvo-Garrido et al. 2014) to unequivocally identify phagocytic engulfment completion, as well as to identify any possible alterations in the time taken for phagocytic engulfment completion following the enwrapping of yeast (Ellson et al. 2001, Vieira et al. 2001, Desale and Chinnathambi 2021).

I have previously shown that all Dd5p4 F&H interactors and *Dd5p4*$^{-}$ *GxcU*$^{-}$ double mutants performed less phagocytosis (Fig. 4.6.A-L.), however it remained unclear as to why phagocytosis was impaired in these mutants and whether the internalisation kinetics were affected. This gave the incentive to visualise failed events using the PI(3,4,5)P_3 and PI(3)P probes to quantify the phagocytic failure rate at a much higher resolution, in order to establish and pinpoint why phagocytic engulfment was reduced. I also used this same probe to quantify if there were alterations in the time taken during successful events to internalise the phagosomes following the complete enwrapping of yeast (Fig. 4.9.A-H.). The internalisation times of *Dd5p4*$^{-}$, as outlined in chapter three, were not quantified as the number of successful phagocytic events were too rare for adequate statistical comparisons to be made.

All cells were stably transfected with the RFP-PH-PkgE GFP-2xFYVE dual expression probe and were administered fluorescent blue yeast for 10 minutes in an imaging dish, prior to the application of an agarose disc to improve visualisation (Fig. 4.9.A-H.).

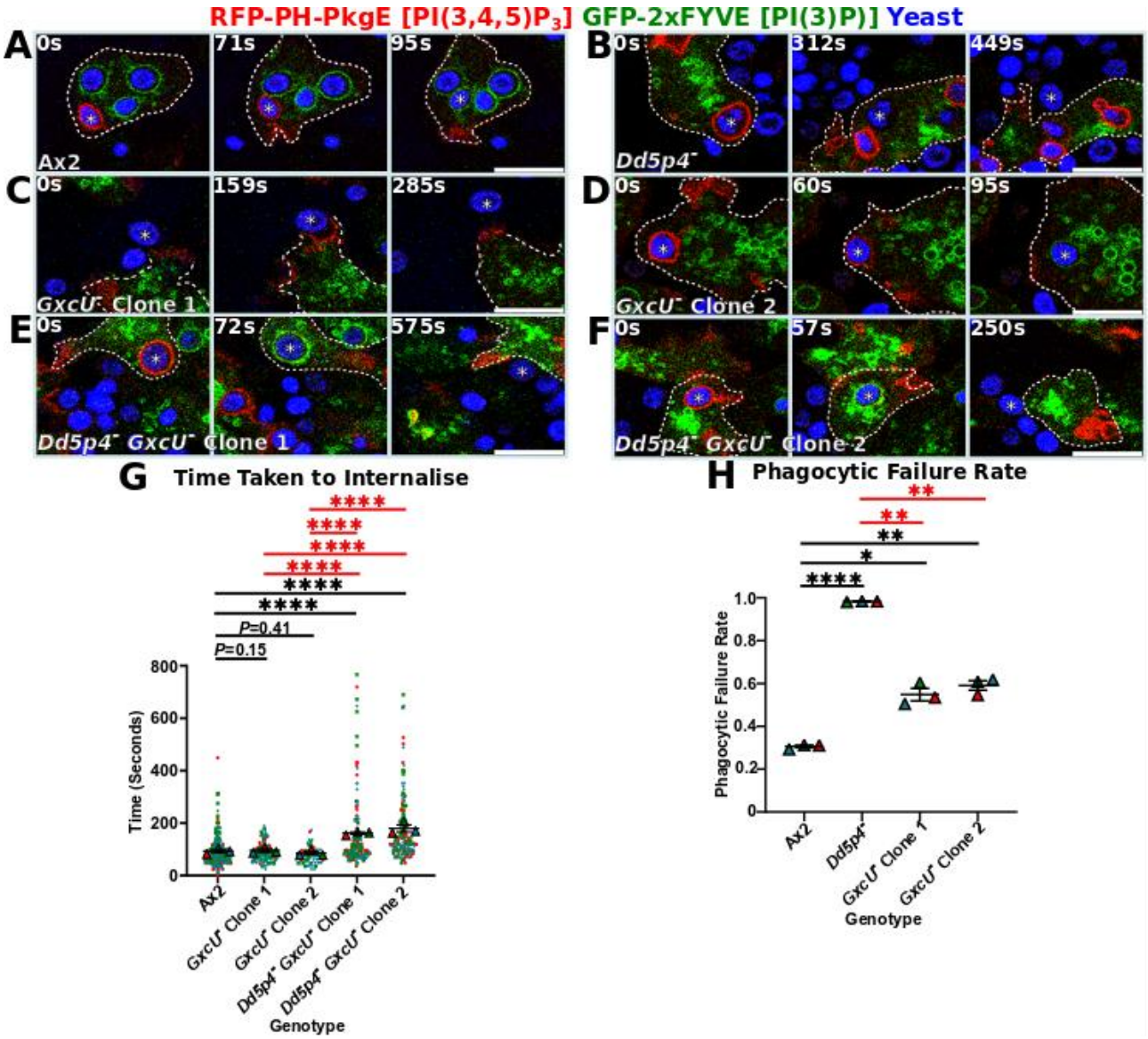

Figure 4.9. Loss of both Dd5p4 and GxcU increased the internalisation times, with *Dd5p4*$^-$ appearing to display more severe phagocytic defects. Confocal images of Ax2 (A), *Dd5p4*$^-$ (B), *GxcU*$^-$ clones (C-D), and *Dd5p4*$^-$ *GxcU*$^-$ clones (E-F) stably expressing RFP-PH-PkgE GFP-2xFYVE, labelling PI(3,4,5)P_3 and PI(3)P respectively, engulfing fluorescent yeast. The cell peripheries are indicated by white dashed lines, with the time intervals indicated in white. Yeast of interest are indicated by white stars. (G) Quantification of the time taken from the point of complete enwrapping by the PI(3,4,5)P_3-labelled PM to the point of PI(3)P formation on the membrane of the early phagosome. *GxcU*$^-$ clones were compared to *Dd5p4*$^-$ *GxcU*$^-$, with the *GxcU*$^-$ Ax2 control cells combined with the control cells associated with the *Dd5p4*$^-$ *GxcU*$^-$ double mutants in order to ensure valid statistical comparisons. Statistical comparisons with Ax2 control cells are indicated in black, with *GxcU*$^-$ single mutant comparisons with *Dd5p4*$^-$ *GxcU*$^-$ double mutants shown in red. Significance and non-significance was determined using Mann Whitney U tests. (H) Quantification of the proportion of failed events, in which PI(3)P was not formed after the first point of contact of yeast with the PI(3,4,5)P_3-labelled PM. *Dd5p4*$^-$ cells from chapter three were compared to *GxcU*$^-$ single mutant clones, with the *Dd5p4*$^-$ Ax2 control cells combined with the control cells of *GxcU*$^-$ in order to ensure valid statistical comparisons. Statistical comparisons with Ax2 control cells are indicated in black, with *Dd5p4*$^-$ single mutant comparisons with *GxcU*$^-$ single mutant clones shown in red. Significance was determined using Welch's *t* tests. The data shown are the individual points and averages from each of the three independent biological, colour-coded repeats, ± SEM. Scale bars are 10 microns. * $P < 0.05$, ** $P < 0.01$, **** $P < 0.0001$.

The absence of GxcU did not appear to alter the time taken to internalise the phagosomes in comparison to Ax2 control cells (Fig. 4.9.A. D. and G.). Both Ax2 and *GxcU*$^{-}$ mutants took approximately 80-90 seconds to internalise the phagosomes during phagocytic engulfment events (Fig. 4.9.G.). Interestingly, both *Dd5p4*$^{-}$ *GxcU*$^{-}$ double mutant clones displayed an increase in the time taken to internalise the phagosomes during engulfment events compared to Ax2 control cells (Fig. 4.9. A. and E-G.). These double mutants had an approximate internalisation time of 160-170 seconds, which was around 2-fold greater than what was observed in Ax2 cells (Fig. 4.9.G.). Another fascinating observation was that both clones of the *Dd5p4*$^{-}$ *GxcU*$^{-}$ double mutants also appeared to take significantly longer to internalise phagosomes in comparison to both *GxcU*$^{-}$ mutant clones (Fig. 4.9.D-G.). This suggested that the activity of Dd5p4 was crucial to ensure rapid internalisation kinetics following the successful enwrapping of yeast.

Interestingly, both *GxcU*$^{-}$ mutant clones appeared to display phagocytic defects in comparison to Ax2 control cells (Fig. 4.9.H.). These phagocytic defects may have been due to the reduced ability of these mutants to successfully enwrap yeast following the first point of contact as shown in *GxcU*$^{-}$ clone 1 in comparison to Ax2 cells (Fig. 4.9.A. and C.). This may explain why these mutants had an increased phagocytic failure rate of 50% compared to the Ax2 control cells (Fig. 4.9.A. C. and H.). Interestingly, the absence of both Dd5p4 and GxcU activities produced some rather surprising observations in which PI(3)P was formed, marking the aftermath of closure and progression to the early phagosome. After a short period of time however, PI(3)P was removed and the yeast were subsequently released via exocytosis (Fig. 4.9.E-F.). I therefore did not quantify the phagocytic failure rate of the *Dd5p4*$^{-}$ *GxcU*$^{-}$ double mutant clones, as it was unclear as to which phagocytic events involving PI(3)P formation remained successful during the limited acquisition time. The phenotype of the *Dd5p4*$^{-}$ *GxcU*$^{-}$ double mutants however, differed from those of the *Dd5p4*$^{-}$ and *GxcU*$^{-}$ single mutants (Fig. 4.9.B-F.). The severity of the phagocytic defects between *Dd5p4*$^{-}$ single mutants and the *GxcU*$^{-}$ single mutant clones were also compared, which revealed that *Dd5p4*$^{-}$ appeared to exhibit a more severe phagocytic defect, which was almost 2-fold greater in comparison to both *GxcU*$^{-}$ single mutant clones (Fig. 4.9.H.). This suggested that Dd5p4 played a more crucial role in the regulation of phagocytic engulfment than GxcU.

Using the same experimental setup previously described, mutant cell lines were used to investigate if the absence of endogenous APPL1-like or Ses1/2-like activities altered the time taken to internalise the phagosomes, to ascertain if phagocytic defects were observed, and to pinpoint the possible causes of phagocytic engulfment failure in these mutants (Fig. 4.10.A-G.).

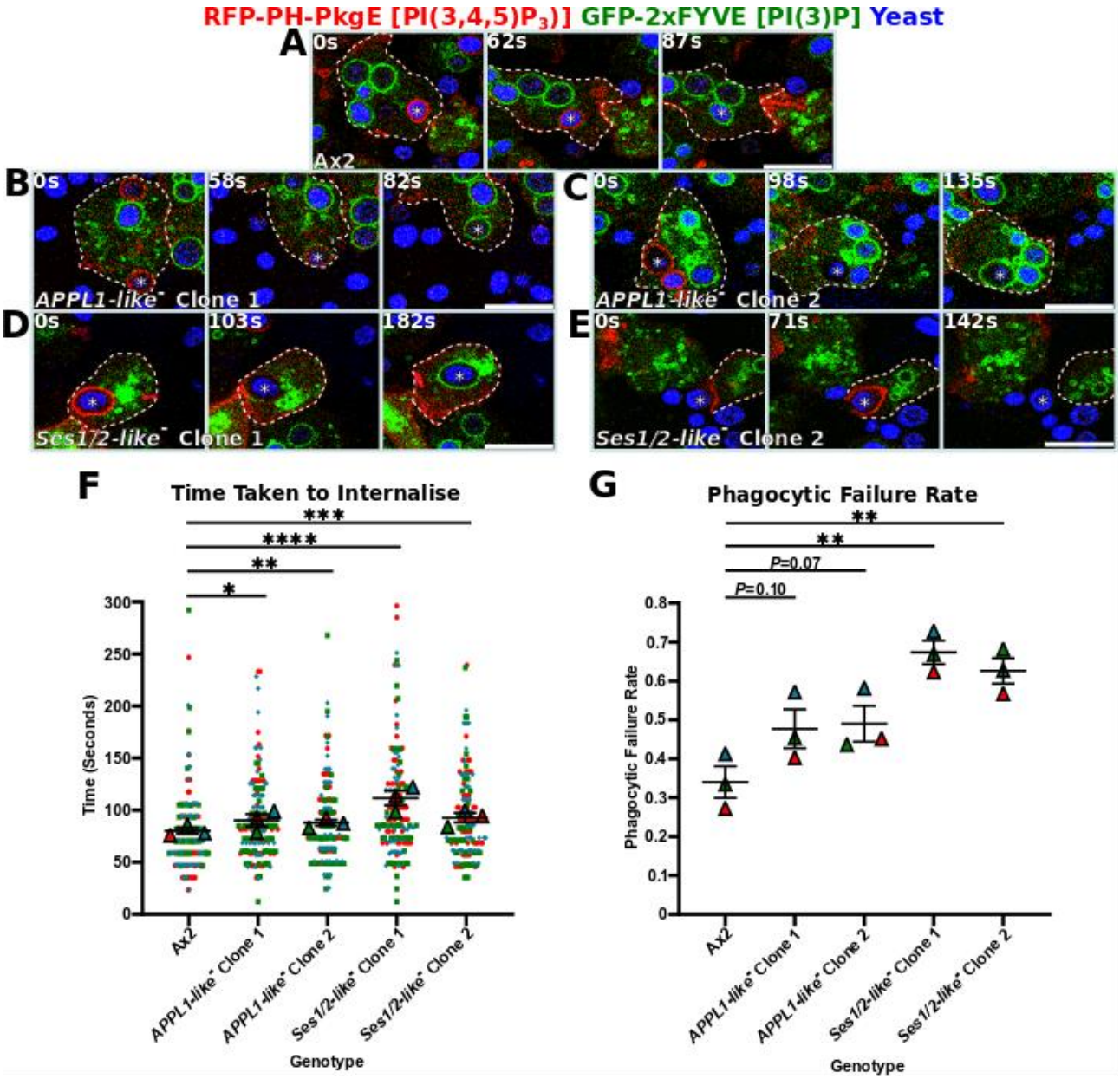

Figure 4.10. *APPL1-like*⁻ and *Ses1/2-like*⁻ mutants took longer to internalise phagosomes, and *Ses1/2-like*⁻ mutants displayed phagocytic defects. Confocal images of Ax2 (A), *APPL1-like*⁻ clones (B-C), and *Ses1/2-like*⁻ clones (D-E) stably expressing RFP-PH-PkgE GFP-2xFYVE, labelling PI(3,4,5)P_3 and PI(3)P respectively, engulfing fluorescent blue yeast over time. The cell peripheries are indicated by white dashed lines, with the time intervals indicated in white. Yeast of interest are indicated by white stars. (F) Quantification of the time taken from the point of complete enwrapping by the PI(3,4,5)P_3-labelled PM to the point of PI(3)P formation on the membrane of the early phagosome, with statistical comparisons being made with Ax2 control cells as indicated. A single Ax2 control cell population was used in this experiment in comparison to *APPL1-like*⁻ and *Ses1/2-like*⁻ mutant clones. Significance was determined using Mann Whitney U tests. (G) Quantification of the proportion of failed events, in which PI(3)P was not formed after the first point of contact with the PI(3,4,5)P_3-labelled PM. A single Ax2 control cell population was used in this experiment in comparison to *APPL1-like*⁻ and *Ses1/2-like*⁻ mutant clones. Statistical comparisons with Ax2 control cells are indicated in black. Significance and non-significance was determined using Welch's *t* tests. The data shown are the individual points and averages from each of the three independent biological, colour-coded repeats, ± SEM. Scale bars are 10 microns. * $P < 0.05$, ** $P < 0.01$, *** $P < 0.001$, **** $P < 0.0001$.

APPL1-like^{-} mutant clones both displayed significant increases in the time taken to internalise phagosomes in comparison to Ax2 control cells (Fig. 4.10.A-C. and F.). The *APPL1-like*$^{-}$ mutant clones took approximately 90 seconds overall to internalise phagosomes in comparison to 80 seconds in Ax2 cells (Fig. 4.10.F.). *Ses1/2-like*$^{-}$ mutant clones both however, appeared to display more significant increases in the time taken to internalise phagosomes (Fig. 4.10.A. and D-F.). The *Ses1/2-like*$^{-}$ mutant clones took approximately 95-100 seconds overall to internalise phagosomes in comparison to 80 seconds in Ax2 control cells (Fig. 4.10.F.).

APPL1-like^{-} mutant clones both displayed no defects in the phagocytosis of yeast compared to Ax2 control cells (Fig. 4.10.G.). *Ses1/2-like*$^{-}$ mutant clones both, on the other hand, displayed phagocytic defects with phagocytic failure seemingly occurring just after closure, as shown in *Ses1/2-like*$^{-}$ clone 2 (Fig. 4.10.E. and G.).

In summary, I have shown that the Ses1/2-like and GxcU Dd5p4 F&H interactors played a direct role in coordinating successful phagocytic engulfment. Ses1/2 activity appeared to somehow regulate the kinetics of phagocytic engulfment, and GxcU somehow appeared to play a role in coordinating the enwrapping of yeast following the establishment of initial contacts. I have also shown that despite the APPL1-like Dd5p4 F&H interactor not being particularly important in coordinating successful phagocytic engulfment it does appear to somehow regulate the kinetics of phagosome internalisation. I have also demonstrated that Dd5p4 and GxcU appeared to exhibit functionally distinct roles during the regulation of phagocytic engulfment as the double mutants lacking both endogenous proteins displayed a different phagocytic phenotype compared to the respective single mutants. Finally, I have also shown that in particular the phagosome internalisation kinetics appeared to be increased in the *Dd5p4*$^{-}$ *GxcU*$^{-}$ double mutants, and that the *Dd5p4*$^{-}$ phagocytic failure rate appeared to be more severe than that of the *GxcU*$^{-}$ mutant clones.

4.2.5. Loss of the Dd5p4 F&H interactors altered the dynamics of macropinosomes

The three Dd5p4 F&H interactors, GxcU, APPL1-like, and Ses1/2-like, have been previously shown to be associated with the process of macropinocytosis (Luscher et al. 2019). However, it was not clear as to how macropinosome dynamics were regulated by these F&H interactors. This gave the incentive to test how the absence of the individual endocytic adaptors, APPL1-like and Ses1/2-like, as well as GxcU, and GxcU and Dd5p4, affected the dynamics of macropinosomes. Macropinosomes were visualised by confocal imaging following the application of pH-sensitive FITC dextran to cells in order to visualise early, non-acidified macropinosomes. The macropinocytic volume and numbers per cell were then quantified (Fig. 4.11.A-N.).

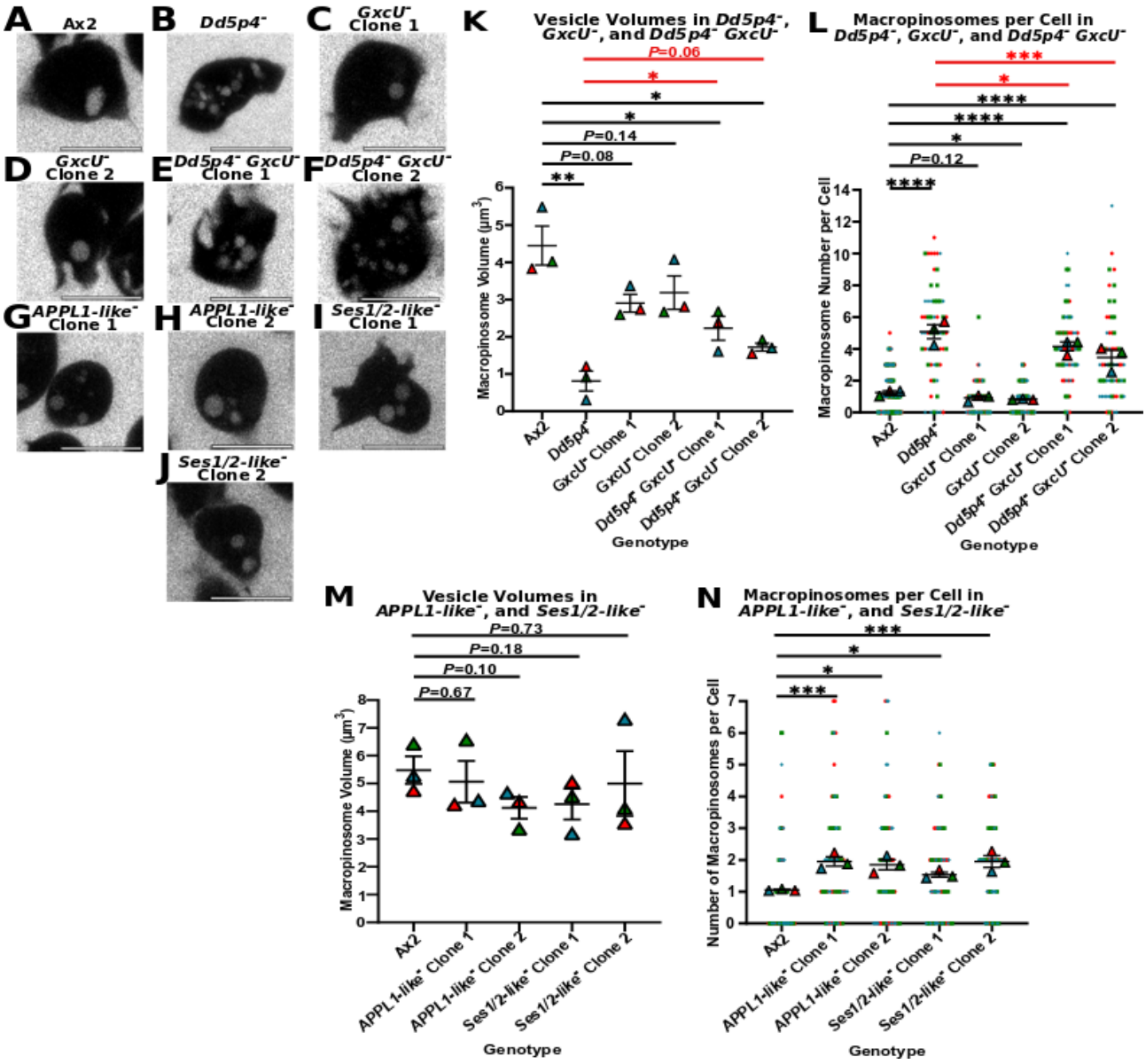

Figure 4.11. Loss of the Dd5p4 F&H interactors altered macropinosome dynamics. Media was removed from live-cells and FITC dextran was applied. Cells were imaged after 5 minutes and macropinosome dynamics were quantified at their largest volume through *z*. Stills of Ax2 (A), *Dd5p4*$^-$ (B), *GxcU*$^-$ clones (C-D), *Dd5p4*$^-$ *GxcU*$^-$ clones (E-F), *APPL1-like*$^-$ clones (G-H), *Ses1/2-like*$^-$ clones (I-J), and their associated FITC dextran-containing macropinosomes (grey spheres). (K) Quantification of the vesicle volumes of Ax2, *Dd5p4*$^-$, *GxcU*$^-$, and *Dd5p4*$^-$ *GxcU*$^-$. Significance and non-significance was determined using Welch's *t* tests. (L) Quantification of vesicle numbers per cell in Ax2, *Dd5p4*$^-$, *GxcU*$^-$, and *Dd5p4*$^-$ *GxcU*$^-$. Significance and non-significance was determined using Mann Whitney U tests. Statistical comparisons with Ax2s are indicated in black, with *Dd5p4*$^-$ comparisons with *Dd5p4*$^-$ *GxcU*$^-$ shown in red. *Dd5p4*$^-$ from chapter three were compared to *GxcU*$^-$ and *Dd5p4*$^-$ *GxcU*$^-$, with *Dd5p4*$^-$ Ax2s combined with the Ax2s of *GxcU*$^-$ and the Ax2s of *Dd5p4*$^-$ *GxcU*$^-$ to ensure valid statistical comparisons. (M) Quantification of the vesicle volumes of Ax2, *APPL1-like*$^-$, and *Ses1/2-like*$^-$. Non-significance was determined using Welch's *t* tests. (N) Quantification of vesicle numbers per cell in Ax2, *APPL1-like*$^-$, and *Ses1/2-like*$^-$. Significance was determined using Mann Whitney U tests. A single Ax2 control population was used in this experiment to compare to *APPL1-like*$^-$ and *Ses1/2-like*$^-$. Statistical comparisons with Ax2s are indicated in black. Individual data points were omitted in K and M to make the replicate averages more clearly visible. A total of 20 cells were randomly selected per cell line, per biological repeat. All data are from three independent biological, colour-coded repeats, ± SEM. Scale bars are 10 microns. * $P < 0.05$, ** $P < 0.01$, *** $P < 0.001$, **** $P < 0.0001$.

I previously demonstrated that the loss of Dd5p4 enzymatic activity reduced macropinocytic volume compared to Ax2 control cells (Fig. 3.3.D.), whilst I have demonstrated in this chapter that *GxcU*$^{-}$ cells appeared to display no change in macropinosome volume (Fig. 4.11.K.). Interestingly, the absence of both Dd5p4 and GxcU activities appeared to significantly reduce the average macropinosome volumes by more than 2-fold compared to Ax2 control cells (Fig. 4.11.K.). In comparison to *Dd5p4*$^{-}$ *GxcU*$^{-}$ clone 1, *Dd5p4*$^{-}$ cells appeared to have significantly smaller macropinosomes, whilst *Dd5p4*$^{-}$ *GxcU*$^{-}$ clone 2 appeared to display no significant differences in volume in comparison to *Dd5p4*$^{-}$ single mutants (Fig. 4.11.K.). In comparison to Ax2 cells, the absence of Dd5p4 appeared to significantly increase the number of macropinosomes by approximately 5-fold (Fig. 4.11.L.). Interestingly, no significant differences appeared to be observed when Ax2 cells were compared to *GxcU*$^{-}$ clone 1 cells, however vesicle numbers appeared to be significantly reduced by approximately 50% when *GxcU*$^{-}$ clone 2 cells were compared to Ax2 control cells (Fig. 4.11.L.). The loss of both Dd5p4 and GxcU activities appeared to significantly increase the number of vesicles between 3- and 4-fold in comparison to Ax2 cells (Fig. 4.11.L.). Interestingly, in comparison to cells lacking both Dd5p4 and GxcU activities, *Dd5p4*$^{-}$ cells appeared to display a significant increase in the number of vesicles per cell (Fig. 4.11.L.). The differences in macropinosome dynamics between *Dd5p4*$^{-}$ *GxcU*$^{-}$ double mutants and the *Dd5p4*$^{-}$ single mutants suggested that Dd5p4 and GxcU played distinct roles in the regulation of macropinosome dynamics during macropinocytosis.

The loss of both APPL1-like and Ses1/2-like endocytic adaptors displayed no significant changes in the volume of macropinosomes (Fig. 4.11.M.). Both endocytic adaptor mutants did however, display a significant increase in the number of macropinosomes in comparison to Ax2 control cells (Fig. 4.11.N.). This suggested that the presence of these endocytic adaptors may function to somehow decrease the bulk uptake of fluid over time.

4.2.6. Macropinocytic cup lengths were unaffected in *GxcU*$^{-}$ mutant cells

I have shown that the loss of GxcU activity did not appear to affect the dynamics of macropinosomes within these mutants (Fig. 4.11.K-L.). I next tested if there were any alterations in macropinocytic cup dynamics as Frabin in mammals has been shown to coordinate changes in cell shape (Nakanishi and Takai 2008). To test whether GxcU also coordinated changes in cell shape during macropinocytic cup formation I therefore stably transfected *GxcU*$^{-}$ single mutant clones and Ax2 control cells with GFP-PH-Crac, a macropinocytic cup marker (Insall et al. 1994, Parente et al. 1998, Dormann et al. 2004). Confocal images were taken of live-cells and the length of macropinocytic cups were quantified (Fig. 4.12.A-D.).

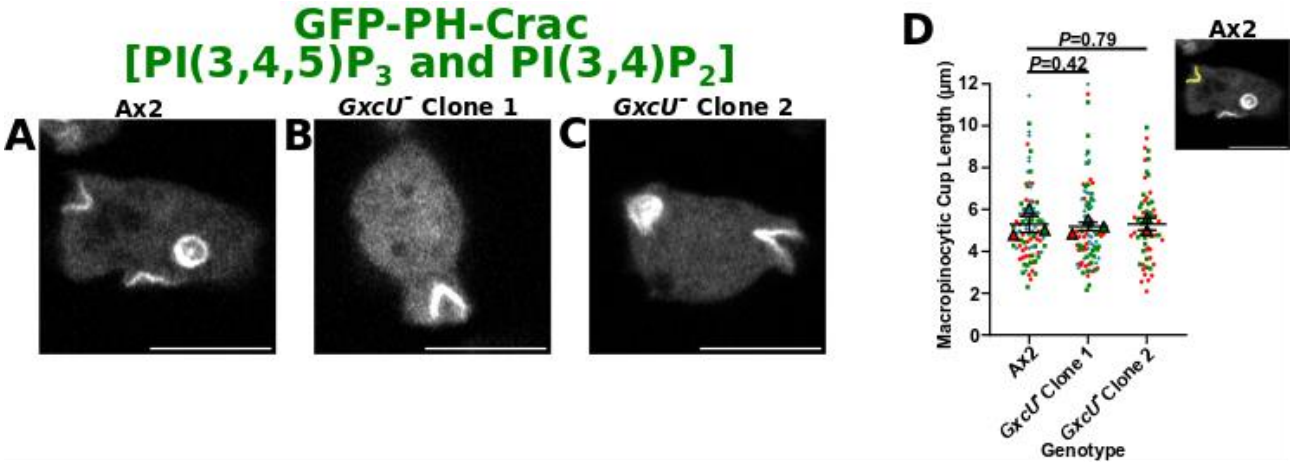

Figure 4.12. Macropinocytic cup lengths were unchanged in *GxcU*⁻ mutants. Confocal images of Ax2 (A), *GxcU*⁻ clones 1 (B), and 2 (C) stably expressing GFP-PH-Crac, which labels $PI(3,4,5)P_3$ and $PI(3,4)P_2$. (D) Quantification of the macropinocytic cup lengths, where 30 macropinocytic cups per cell line, per biological repeat were selected at random and measured at their largest size through *z* (an example measurement is shown by a yellow line across a macropinocytic cup within an Ax2 control inset image). A single Ax2 control cell population was used in this experiment to compare to *GxcU*⁻ mutant clones. Statistical comparisons with Ax2 control cells are indicated in black. All the quantified data shown are from three independent biological, colour-coded repeats, ± SEM. Data of the biological repeat three of *GxcU*⁻ clone 2 was not obtained. Scale bars are 10 microns. Non-significance was determined using Mann Whitney U tests.

The loss of GxcU activity did not alter the macropinocytic cup lengths in both *GxcU*⁻ mutant clones in comparison to Ax2 control cells (Fig. 4.12.A-D.). The macropinocytic cups in these mutants were approximately 5.0-5.5 µm in length and were very similar in comparison to the approximate 5.5 µm macropinocytic cups seen in Ax2 cells (Fig. 4.12.D.). This suggested that GxcU may not coordinate changes in cell shape that are required during macropinocytic cup formation.

4.2.7. *Dictyostelium intermedium* GxcU-GFP (DiGxcU-GFP) localisation was altered in the absence of endogenous Dd5p4 and endogenous GxcU

Dictyostelium intermedium GxcU-GFP (DiGxcU-GFP) fusion protein localisation in the less stable Ax3 genetic background has been shown to appear at sites of macropinocytic cup formation. Localisation however, of the DiGxcU-GFP fusion protein within *Dd5p4*⁻ single mutant cells was shown to be more punctate, which indicated that the fusion protein clustered more in the mutant than in Ax3 control cells (Luscher et al. 2019). Localisation studies, however, of the *D. discoideum* GxcU (DdGxcU) protein in *Dd5p4*⁻, *GxcU*⁻, and *Dd5p4*⁻ *GxcU*⁻ mutants have not been performed thus far in the more stable Ax2 genetic background. To test if DdGxcU localisation was altered in Ax2 cells, attempts were made to create a DdGxcU-GFP fusion construct. This proved highly problematic however, due to the long, low complexity, and high AT rich region of the *GxcU* locus, thus attempts to clone this gene were unsuccessful. As an alternative, a codon optimised, GxcU orthologue, which

was synthesised from the closely related *D. intermedium* to generate a C-terminal GFP fusion protein, termed DiGxcU-GFP, was used as an alternative (Schaap et al. 2006, Veltman et al. 2009, Luscher et al. 2019). This fusion construct has already been used previously to study DiGxcU-GFP protein localisation in the Ax3 genetic background (Luscher et al. 2019). DiGxcU has a very similar domain organisation to DdGxcU, and like DdGxcU, possesses an F&H motif (Fig. 4.13.A.). This construct was used to study DiGxcU localisation, in *GxcU*$^{-}$, *Dd5p4*$^{-}$, *Dd5p4*$^{-}$ *GxcU*$^{-}$, and Ax2 control cells, which were all stably transfected with DiGxcU-GFP and imaged as shown (Fig. 4.13.A-F.).

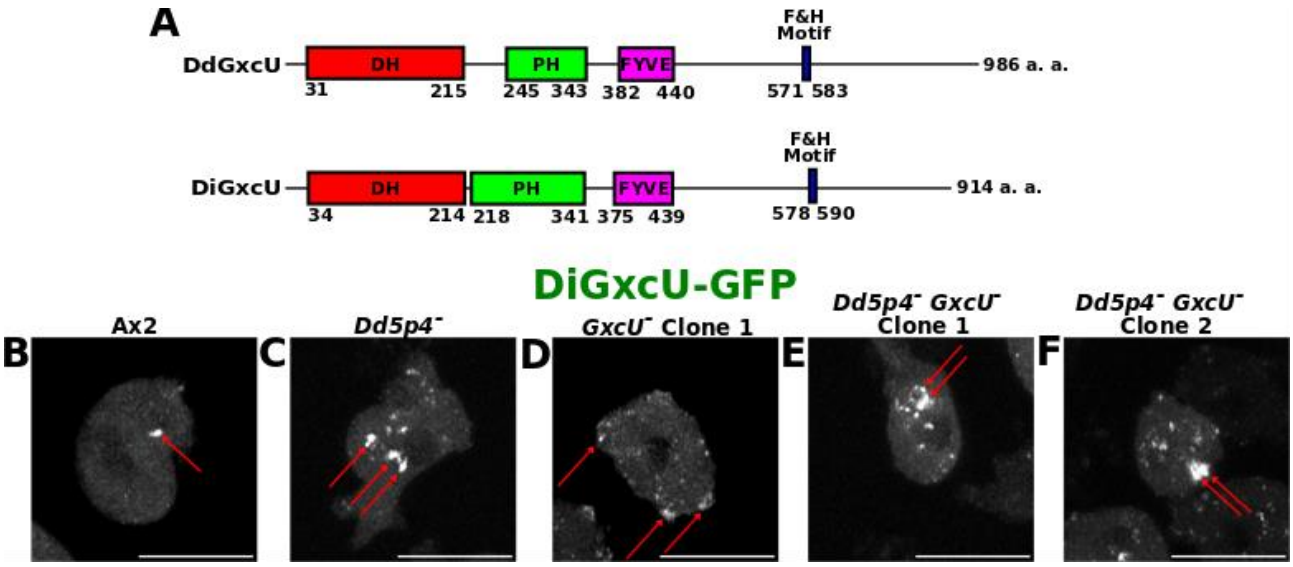

Figure 4.13. DiGxcU-GFP localisation was altered in the absence of endogenous Dd5p4 and endogenous GxcU. (A) Schematic of the domain composition of DdGxcU and DiGxcU. Each domain is colour-coded and the positions within the proteins are indicated. Cells stably expressing DiGxcU-GFP in Ax2 (B), *Dd5p4*$^{-}$ (C), *GxcU*$^{-}$ clone 1 (D), and *Dd5p4*$^{-}$ *GxcU*$^{-}$ clones 1 (E), and 2 (F). The main clusters of DiGxcU-GFP puncta are indicated by red arrows. Scale bars are 10 microns.

The stable expression of DiGxcU-GFP in Ax2 revealed that the fusion protein formed very few DiGxcU-GFP puncta (Fig. 4.13.B.), however, *Dd5p4*$^{-}$ single mutants were more punctate (Fig. 4.13.C.), which matched previous observations that were made in the Ax3 *Dd5p4*$^{-}$ mutant (Luscher et al. 2019). Interestingly, the loss of GxcU activity resulted in clusters of DiGxcU-GFP puncta localising to sites at the cell surface, possibly to sites of macropinocytic cups in the very early stages of their formation (Fig. 4.13.D.). This observation may suggest that the absence of endogenous DdGxcU removes the competition with DiGxcU-GFP, which may allow DiGxcU-GFP to potentially adopt the localisation pattern of the absent endogenous DdGxcU protein (Fig. 4.13.D.). The loss of both Dd5p4 and GxcU proteins caused larger DiGxcU-GFP puncta to form in both of the double mutant clones (Fig. 4.13.E-F.). The DiGxcU-GFP puncta formed in these double mutants were larger (Fig. 4.13.E-F.) in comparison to those observed in the *Dd5p4*$^{-}$ (Fig. 4.13.C.) and *GxcU*$^{-}$ (Fig. 4.13.D.)

single mutants. These findings may suggest that Dd5p4 and GxcU could perform distinct functional roles during macropinocytosis.

In summary, I have shown that the loss of endogenous GxcU had little effect on the dynamics of macropinosomes and that unlike mammalian Frabin, GxcU did not appear to coordinate changes in cell shape, which occurred during macropinocytic cup formation. I have also further clarified that Dd5p4 and GxcU possessed distinct functional roles during macropinocytosis, with DiGxcU-GFP being punctate in the single mutants, and more punctate in the double mutants. I have also indicated that the endocytic adaptors, APPL1-like and Ses1/2-like may regulate the bulk uptake of fluid during macropinocytosis.

4.3. Discussion

Mass spectrometry of *D. discoideum* proteins identified three Dd5p4 F&H motif-containing proteins, which were related to the *H. sapiens* OCRL F&H interactors: APPL1-like, Ses1/2-like, and GxcU (Luscher et al. 2019). Despite previous observations however, an understanding of how these three Dd5p4 F&H interactors regulated the dynamics of macropinocytosis, and in particular phagocytosis, remains poorly understood.

4.3.1. Insights into how APPL1-like regulated endocytosis in *D. discoideum*

In this project I have shown how three Dd5p4 F&H interactors regulated phagocytosis and macropinosome dynamics. APPL1-like-GFP fusions have been shown to localise to the CV, and have been established to be important in the kiss-and-run exocytic water discharge (Luscher et al. 2019). I have however, shown in this project that APPL1-like may also play a role in the regulation of the bulk uptake of fluid as more numerous, normal-sized macropinosomes were observed in *APPL1-like*$^{-}$ mutant clones (Fig. 4.11.M-N.). This could be tested through the use of macropinocytosis assays, in which *APPL1-like*$^{-}$ mutants could be administered TRITC dextran, when the uptake of dye remains in the linear phase in comparison to Ax2 control cells (Williams and Kay 2018). A higher fluorescence output in these mutants compared to control cells could suggest a role in the regulation of bulk fluid uptake. If the loss of APPL1-like activity however, did not change the fluorescence output this could be simply put down to the fact that APPL1-like does not regulate the bulk fluid uptake and may instead just function to regulate kiss-and-run exocytic water discharge (Luscher et al. 2019). An alternative explanation however, to the unchanged fluorescence output in the absence of APPL1-like activity could be due to delays in acidification. The pH-sensitive FITC dextran used in the analysis of early, non-acidic macropinosome dynamics in the *APPL1-like*$^{-}$ mutants could show not only newly formed macropinosomes, but also macropinosomes in which acidification was delayed. To test this

theory, confocal time-lapses of the *APPL1-like*$^{-}$ mutants taking up pHrodo Red Dextran, which is essentially dark in the extracellular environment, however upon macropinosome internalisation this dextran conjugate emits a bright-red fluorescent signal upon progression to endosomal acidification (Meena and Kimmel 2018). This experimental setup would allow the tracking of nascent macropinosomes and the quantification of the time taken from macropinosome formation to acidification in an attempt to uncover if the onset of acidification was delayed in the *APPL1-like*$^{-}$ mutant clones. Expression of APPL1-like-GFP fusions displayed a mostly cytosolic localisation in Ax3 cells however, with the exception of short, intense flashes of APPL1-like-GFP as the CV opens and releases excess water into the extracellular environment (Luscher et al. 2019). It is unclear if these flashes during the opening of the CV is the only distinctive localisation of APPL1-like-GFP, as it may also affect endocytosis at other stages, such as acidification. It may not be possible to visualise the GFP fusion at this later stage of endocytosis due to the excessive levels of the APPL1-like-GFP fusion protein, which could mask the localisation at the stage of acidification. Integration of an APPL1-GFP fusion construct through the use of REMI into the genome, under the control of the host promoter, could generate the optimal copy number and provide a definitive localisation of this protein beyond just the CV (Fey and Cox 1997).

In this project, I have shown that cells lacking APPL1-like activity displayed decreased levels of phagocytosis (Fig. 4.6.L.). It was not clear however, as to why this was the case, and whether or not APPL1-like played a direct functional role in the regulation of this macro-endocytic process. I have demonstrated however, that the loss of APPL1-like activity did significantly increase the time taken to internalise the phagosomes (Fig. 4.10.F.). It may be possible that the delay in acidification, which was speculated to be the cause of the increased number of macropinosomes during macropinocytosis in these mutants (Fig. 4.11.N.), may also have potentially occurred causing delays in phagosome internalisation during phagocytosis (Fig. 4.10.F.). This could be tested through *APPL1-like*$^{-}$ mutant clones and Ax2 control cells engulfing pH-sensitive pHrodo-labelled yeast, which could indicate through changes in fluorescence if there was a delay in phagosome internalisation due to delays in acidification. APPL1-like may alternatively perform indirect roles in the regulation of phagocytosis, such as through the regulation of the osmotic exocytic water discharge via the CV.

4.3.2. Mammalian APPL1 and the link to OCRL in comparison to *D. discoideum* APPL1-like and Dd5p4

A recent model outlining mammalian APPL1 in association with OCRL and Rab5 has been proposed (Maxson et al. 2021). In this model, Rab5 binds to APPL1, with APPL1 subsequently recruiting OCRL and its paralog, INPP5B, to macropinocytic cups, which was collectively required for cup closure and scission from the PM (Maxson et al. 2021). This model suggested that without

APPL1, OCRL could not be recruited to macropinocytic cups, which thereby prevented closure of macropinocytic cups. I have shown, however, that the loss of APPL1-like activity in *D. discoideum* did not result in macropinocytic or phagocytic defects like those observed in the *Dd5p4*$^{-}$ mutants (Fig. 4.9.A-B. and H., Fig. 4.10.A-C. and G. and Fig. 4.11.K. and M.). *APPL1-like*$^{-}$ mutants, like *Dd5p4*$^{-}$, mutants were able to enwrap yeast normally (Fig. 4.7.A-B. and G. and Fig. 4.8.A-C. and F.); unlike *Dd5p4*$^{-}$ mutants, *APPL1-like*$^{-}$ mutants did not fail to internalise phagosomes, nor did they display an increase in the phagocytic failure rate (Fig. 4.9.A-B. and H. and Fig. 4.10.A-C. and G.). This suggested in summary that APPL1-like F&H interactions with Dd5p4 were not crucial for cup closure, and that APPL1-like was not functionally orthologous to mammalian APPL1.

4.3.3. Insights into how Ses1/2-like regulated endocytosis in *D. discoideum* and comparison to mammalian Ses1/2

The Ses1/2-like protein has been shown to localise to the late-acidic and post-lysosomal stage of endocytosis (Luscher et al. 2019). Very little however, was known about how this PH-domain containing protein regulated phagocytosis. In this project, I have shown that this protein played a role in the regulation of phagocytosis, with what appeared to be defects just after closure were observed in cells lacking this protein (Fig. 4.6.L. and Fig. 4.10.A. and D-E. and G.). This observation appeared to show a slight overlap with the *Dd5p4*$^{-}$ phagocytic phenotype, however, the phagocytic defects of *Ses1/2-like*$^{-}$ were much less severe (Fig. 4.9.H. and Fig. 4.10.G.). To test if these observations displayed some similarity to the potential *Dd5p4*$^{-}$ phagocytic defects then beads of differing sizes could be tested on the *Ses1/2-like*$^{-}$ single mutants and *Dd5p4*$^{-}$ single mutants. This experimental setup would assess if the differences in the severity of phagocytic defects was due to differences in the size of the cortex openings to allow entry of the phagosome into the cytosol. If the cortex openings were reduced to a lesser degree in *Ses1/2-like*$^{-}$ single mutants compared to *Dd5p4*$^{-}$ single mutants then larger beads would be expected to be able to enter the cytosol in *Ses1/2-like*$^{-}$ mutants than in *Dd5p4*$^{-}$. If both the *Ses1/2-like*$^{-}$ and *Dd5p4*$^{-}$ single mutants displayed varying phagocytic defects due to differences in the size of the cortex openings then *Dd5p4*$^{-}$ *Ses1/2-like*$^{-}$ double mutants could be generated and tested. If the *Dd5p4*$^{-}$ *Ses1/2-like*$^{-}$ double mutants only allowed beads to enter the cytosol that were smaller in comparison to either the *Dd5p4*$^{-}$ or *Ses1/2-like*$^{-}$ single mutants then this could confirm a functional link between Dd5p4 and Ses1/2-like proteins in coordinating successful phagocytic engulfment.

In this project I have demonstrated that both *Ses1/2-like*$^{-}$ mutant clones displayed significant increases in the time taken to enwrap, and internalise phagosomes (Fig. 4.8.F. and Fig. 4.10.F.). This suggested that Ses1/2-like may itself have played a direct or indirect role in the regulation of these

stages of phagocytic engulfment, however this would require further study. Further investigations could however, be carried out in order to understand how Ses1/2-like could have governed the enwrapping of yeast. A possible explanation as to why *Ses1/2-like*$^{-}$ mutants displayed a significant increase in the time taken to enwrap yeast (Fig. 4.8.F.) may have been due to the absence of the Ses1/2-like protein somehow causing a reduction in the expression of various phagocytic cell-surface receptors. The reduced levels of these phagocytic cell-surface receptors may have slowed down the process in which yeast were recognised and enwrapped. Ses1/2-like could therefore be studied together with various cell-surface phagocytic receptors, such as the Similar to integrin beta A (SibA), which shares a domain organisation with mammalian integrin-β and can also bind to Talin (Cornillon et al. 2006). *D. discoideum* also possesses homologues of the mammalian scavenger receptors, a notable example of which includes LmpB, which has been proposed to be a phagocytic receptor (Dunn et al. 2018), which could be studied in conjunction with the Ses1/2-like protein. Interestingly, GPCRs within *D. discoideum* have also been implicated in coordinating both phagocytosis and chemotaxis, a fairly recent example includes the seven-transmembrane fAR1 (Pan et al. 2016), which could also be studied in conjunction with Ses1/2-like. The expression levels of each of these cell-surface receptors could be compared between Ax2 control cells and the *Ses1/2-like*$^{-}$ mutant clones in order to ascertain if Ses1/2-like could have influenced the levels of expression of these receptors, which thus may have interfered with the kinetics of enwrapping yeast. A possible mechanism as to why *Ses1/2-like*$^{-}$ mutants displayed a significant increase in the time taken to internalise phagosomes (Fig. 4.10.F.) may also have been due to the reasons that were previously stated in relation to the APPL1-like protein. *Ses1/2-like*$^{-}$ mutants could have also displayed delays in acidification, which may have caused the delays observed in phagosome internalisation during phagocytosis (Fig. 4.10.F.). This could be confirmed through *Ses1/2-like*$^{-}$ mutant clones engulfing pH-sensitive pHrodo-labelled yeast and monitoring any changes in fluorescence in order to pinpoint if the delays in acidification were possibly responsible for the delays observed in phagosome internalisation in these mutants.

I have demonstrated that cells lacking Ses1/2-like activity did display more numerous, normal-sized macropinosomes compared to Ax2 control cells (Fig. 4.11.M-N.). This could suggest that Ses1/2-like could, like APPL1-like, regulate the bulk uptake of fluid, which could be quantified through use of macropinocytosis assays. If the absence of Ses1/2-like activity caused the fluorescence output to be unchanged it could suggest that Ses1/2-like may not govern bulk fluid uptake. Alternatively however, it could have regulated the onset of acidification during macropinocytosis, which could be investigated using the same experimental setup discussed in reference to the APPL1-like protein, again through using pHrodo Red Dextran (Meena and Kimmel

2018). If Ses1/2-like does regulate acidification then this would be in agreement with previous localisation studies of Ses1/2-like-GFP in Ax3 cells, which localised to the late lysosomal stage during macropinocytosis (Luscher et al. 2019). Interestingly, it has been shown that within mutants lacking Dd5p4 activity that the localisation of Ses1/2-like-GFP in *D. discoideum* was unaffected in comparison to Ax3 control cells during macropinocytosis (Luscher et al. 2019). This may suggest that the Ses1/2-like F&H interactions with Dd5p4 were not crucial for the correct localisation of Ses1/2-like in *D. discoideum*, and that Ses1/2-like may not be functionally orthologous to the mammalian Ses1/2 endocytic adaptors during macropinocytosis.

In mammals, it has been shown that these endocytic adaptors were crucial during the later stages of endocytosis through the sorting of hydrolases. These hydrolases included Cathepsin-D and Hexosaminidase, which explained the presence of enlarged endosomes as a result of lysosomal hydrolase missorting in mammals (Noakes et al. 2011). This observation differed however, from the macropinocytic phenotype that was observed in *D. discoideum Ses1/2-like*$^{-}$ mutant clones, in that macropinosome sizes were completely unaltered (Fig. 4.11.M.). This may further suggest that the Ses1/2-like protein is not functionally orthologous to the mammalian Ses1/2 proteins during macropinocytosis.

4.3.4. Insights into how GxcU, together with Dd5p4, regulated endocytosis in *D. discoideum*

GxcU is the only one of the four *D. discoideum* Frabin-like proteins which contained an F&H motif (Luscher et al. 2019). GxcU is mostly unstudied, however knockout strains of this gene have established that GxcU is not essential for life (Wang et al. 2013). Previous work has shown that Dd5p4 and GxcU functionally interact during macropinocytosis in the Ax3 genetic background. This was shown through DiGxcU-GFP overexpression in Ax3 control cells, which phenocopied the dye uptake and processing defects that were observed in the *Dd5p4*$^{-}$ mutant cells (Luscher et al. 2019). In addition, the overexpression of DiGxcU-GFP within *Dd5p4*$^{-}$ cells further exaggerated the *Dd5p4*$^{-}$ mutant phenotype, which suggested that Dd5p4 acted to repress the function of GxcU in *D. discoideum* (Luscher et al. 2019). An alternative explanation to this finding however, could be that the overexpression of DiGxcU-GFP resulted in DiGxcU-GFP binding to endogenous GxcU within Ax3 control cells and *Dd5p4*$^{-}$ mutants, which may have caused the endocytic defects that were observed. No investigations have been performed thus far on the activities of cells lacking endogenous GxcU, nor on cells to establish if a functional interaction between Dd5p4 and GxcU occurred during phagocytosis. I have shown that the loss of GxcU activity caused defects in phagocytosis in the more stable Ax2 genetic background, however the phagocytic defects were less severe than those in the *Dd5p4*$^{-}$ single mutants (Fig. 4.9.H.). *GxcU*$^{-}$ mutants displayed phagocytic defects potentially due to a

reduced capability to successfully enwrap yeast in some cases following the establishment of initial contacts, which differed from *Dd5p4*$^{-}$ as these mutants displayed defects after closure (Fig. 4.9.A-D. and H.). This could suggest that GxcU may have a functional role upstream of Dd5p4. These findings outlined that GxcU and Dd5p4 appeared to perform distinct roles during phagocytic engulfment. Interestingly, I have also demonstrated that cells lacking both endogenous Dd5p4 and GxcU proteins possessed a unique phagocytic phenotype in comparison to the single mutants, which provided further evidence for Dd5p4 and GxcU performing distinct functional roles in the regulation of phagocytic engulfment (Fig. 4.7.A-G. and Fig. 4.9.A-H.). Live-cell imaging studies of cells lacking both Dd5p4 and GxcU revealed that *Dd5p4*$^{-}$ *GxcU*$^{-}$ clone 1 cells did not display any changes in the time taken to enwrap yeast, however *Dd5p4*$^{-}$ *GxcU*$^{-}$ clone 2 cells did display a significant increase in the time taken to enwrap yeast (Fig. 4.7.G.). This meant that it was inconclusive as to whether or not *Dd5p4*$^{-}$ *GxcU*$^{-}$ double mutants displayed altered kinetics in the enwrapping of yeast, which meant that additional biological repeats would be required to clarify this. It was much clearer in the clones of these double mutants however, that the time taken to internalise phagosomes was significantly increased, taking twice as long in comparison to Ax2 control cells (Fig. 4.9.A-G.). After progression to the early phagosomes in the *Dd5p4*$^{-}$ *GxcU*$^{-}$ mutants the PI(3)P signal faded and yeast were released via exocytosis. This phenotype differed from what I have shown in the previous chapter in *Dd5p4*$^{-}$, in which entry to the early phagosome stage was very low in frequency due to possible restricted openings in the F-actin cortex. It was unclear however, as to the mechanism behind phagocytic engulfment failure within the *Dd5p4*$^{-}$ *GxcU*$^{-}$ double mutants, although, failure could lie at the progression to the later phagosome stage. This may explain why the PI(3)P faded and the yeast were subsequently expelled from the double mutant cells via exocytosis. To establish the mechanism of phagocytic engulfment failure in these double mutants, time-lapses with much greater time coverage could be performed together with a dual expression probe employing the PkgE and novel SnxA probes (Jason King, unpublished data), which binds PI(3,4,5)P_3 (Ruchira et al. 2004, Goldberg et al. 2006, and van Haastert lab, unpublished data), and PI(3,5)P_2 (Jason King, unpublished data) respectively. This could visualise the progression of events from phagocytic cup formation to the later phagosome stage, thus providing far more certainty when quantifying the phagocytic failure rate of these double mutants and pinpointing when failure occurred. These time-lapses could also be compared to the respective single mutants along with an Ax2 control, with each stably expressing the same dual fluorescent probe.

In this investigation I have shown that the dynamics of macropinosomes were unaltered in mutants lacking endogenous GxcU, however cells lacking both endogenous Dd5p4 and GxcU displayed altered macropinosome dynamics (Fig. 4.11.K-L.). I also compared the dynamics of these

mutants to those of the *Dd5p4*$^{-}$ single mutants along with the associated Ax2 control cells from chapter three (Fig. 4.11.K-L.). The absence of GxcU did not alter the macropinocytic volume compared to Ax2 control cells (Fig. 4.11.M.). In contrast, it was unclear as to whether these *GxcU*$^{-}$ mutants displayed any effect on the number of macropinosomes per cell in comparison to Ax2 control cells, as *GxcU*$^{-}$ clone 1 cells displayed no changes in the number of macropinosomes, whereas *GxcU*$^{-}$ clone 2 cells displayed a significant decrease in the number of macropinosomes (Fig. 4.11.L.). To test if there was a biological effect on the number of macropinosomes in the *GxcU*$^{-}$ mutant clones, more independent biological repeats would need to be carried out to clarify this. Interestingly however, I have established that the length of macropinocytic cups were unchanged in both *GxcU*$^{-}$ mutant clones (Fig. 4.12.A-D.), which suggested that GxcU was not important for the formation of macropinocytic cups. This is could mean that GxcU may not be functionally orthologous to mammalian Frabin during macropinocytosis, as GxcU did not appear to be important in coordinating the changes in cell shape that were required for macropinocytic cup formation (Obaishi et al. 1998, Umikawa et al. 1999, Ono et al. 2000).

In this project however, I have shown that the stable expression of DiGxcU-GFP in *GxcU*$^{-}$ mutants caused puncta to form near to the cell surface PM, which could be possible sites of macropinocytic cups in the very early stages of their formation, although this was not clear (Fig. 4.13.B. and D.). This observation may have suggested that the removal of endogenous DdGxcU thus removed the competition with the DiGxcU-GFP fusion protein, which could have allowed the DiGxcU-GFP fusion protein to potentially adopt the localisation pattern of the absent endogenous DdGxcU protein in *GxcU*$^{-}$ (Fig. 4.13.D.). Previous localisation studies in Ax3 have suggested that DiGxcU-GFP localised to the base of possible macropinocytic cups during cup formation (Luscher et al. 2019), which provided some agreement with my findings, although this still remains rather ambiguous. It could suggest that GxcU functions as a scaffold protein and localises to the base of macropinocytic cups for the recruitment of Dd5p4. *GxcU*$^{-}$ mutants however, did not display the same macropinocytic phenotype as *Dd5p4*$^{-}$ mutant cells, which suggested that Dd5p4 may be recruited by another mechanism independent of GxcU activity (Fig. 4.13.B-D.). I have finally further demonstrated that GxcU and Dd5p4 performed distinct functional roles in the regulation of macropinocytosis in the Ax2 background, with larger DiGxcU-GFP puncta observed in *Dd5p4*$^{-}$ *GxcU*$^{-}$ mutants compared to those found in the *Dd5p4*$^{-}$ and the *GxcU*$^{-}$ single mutants (Fig. 4.13.C-F.). How GxcU functioned in accordance with Dd5p4 to coordinate macropinocytosis still however, remains unclear. This could be unearthed via future studies visualising the endogenous DdGxcU protein in Ax2 control cells through the creation of GFP knock-ins. These GFP knock-ins could be created using a near-'PAMless' recently engineered *Streptococcus pyogenes* Cas9 variant (SpRY) that has been

shown to work in *D. discoideum* (Asano et al. 2021). A similar system could also be developed and optimised in *D. discoideum* to generate Dd5p4 RFP knocks-ins to thus allow the visualisation of both endogenous proteins within the cell, and to pinpoint how they both functioned to coordinate macro-endocytosis.

4.3.5. Summary

4.3.5.1. Localisation of Dd5p4 and the Dd5p4 F&H interactors during macropinocytosis

Localisation studies have been limited in this PhD project. This was due to difficulties in pinpointing Dd5p4 localisation, the localisation of GxcU in live-cells being ambiguous, and studies not being performed due to time constraints to investigate APPL1-like-GFP and Ses1/2-like-GFP localisation within Ax2 cells during macropinocytosis. Previous work has been done however, which shows the localisation of Dd5p4, GxcU, and APPL1-like, and Ses1/2-like in the Ax3 genetic background. It should be noted however, that the definitive localisation of N- or C-terminal GFP Dd5p4 fusions were not detected at the base of macropinocytic cups (Luscher et al. 2019) (Fig. 4.14.).

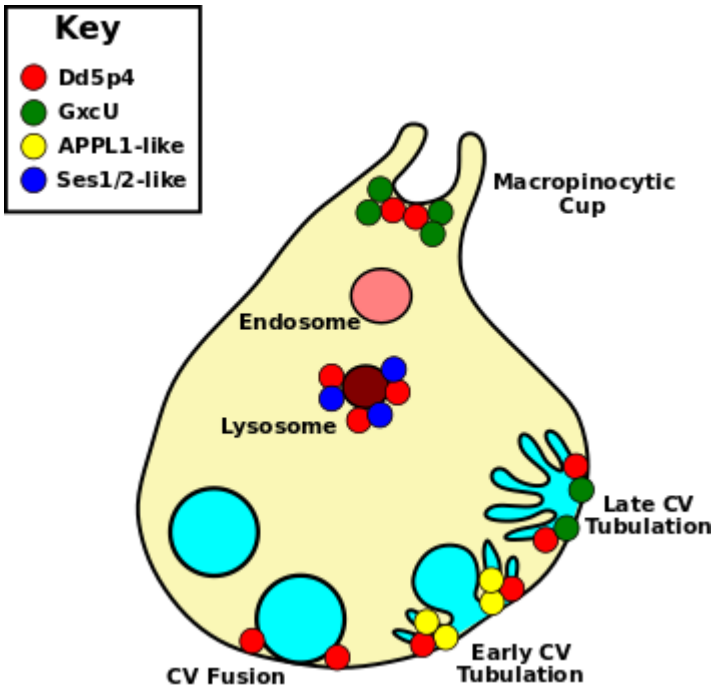

Figure 4.14. The localisation of Dd5p4 and its F&H interactors during macropinocytosis in *D. discoideum* Ax3 cells. GxcU and in theory Dd5p4, localise to macropinocytic cups, with Dd5p4 localising to the centre of cups to hydrolyse PI(4,5)P_2 and promote the entry of fluid through the F-actin cortex. Dd5p4 and Ses1/2-like associate with the later, acidic lysosomes (dark brown). During the CV cycle, Dd5p4 participates in the early stages of fusion of the CV with the PM, with Dd5p4 and the F&H interactors participating in early tubulation (APPL1-like) and later tubulation (GxcU) stages. Dd5p4 and its F&H interactors are colour-coded as shown in the key. Adapted from (Luscher et al. 2019).

The localisation of Dd5p4 was hypothesised in Ax3 control cells to localise to the base of macropinocytic cups (Luscher et al. 2019), which matches the speculations that I have made in this project in the Ax2 genetic background. I have also shown that DiGxcU-GFP localised very close to the cell surface in *GxcU*$^{-}$ mutants in the Ax2 background, however it was not clear as to whether this localised at macropinocytic cups. The roles of APPL1-like and Ses1/2-like have been shown to display potential roles in regulating bulk fluid uptake or acidification.

4.3.5.2.The roles of Dd5p4 and the Dd5p4 F&H interactors during phagocytosis

Dd5p4 has been shown to be crucial for the successful completion of phagocytosis (Loovers et al. 2007), however an understanding as to how Dd5p4 and the Dd5p4 F&H interactors coordinated phagocytic engulfment was poorly understood. The phenotypes that I have identified for mutants of Dd5p4 and the Dd5p4 F&H interactors in comparison to Ax2 control cells during phagocytosis are summarised (Table. 4.1.).

Table 4.1. A summary of the phagocytic phenotypes of *Dd5p4*$^-$, *GxcU*$^-$, *Dd5p4*$^-$ *GxcU*$^-$, *APPL1-like*$^-$, and *Ses1/2-like*$^-$ mutants in comparison to Ax2 control cells.

Genotype	Enwrapping Duration	Internalisation Duration	Phagocytic Defects?	Possible Cause of Phagocytic Defect
***APPL1-like*$^-$ Clone 1**	No Change	Increased	No	Possible indirect role, osmoregulation?
***APPL1-like*$^-$ Clone 2**	No Change	Increased	No	Possible indirect role, osmoregulation?
***Ses1/2-like*$^-$ Clone 1**	Increased	Increased	Yes	Failure at cup closure?
***Ses1/2-like*$^-$ Clone 2**	Increased	Increased	Yes	Failure at cup closure?
***GxcU*$^-$ Clone 1**	No Change	No Change	Yes	Reduced ability to enwrap following initial contacts?
***GxcU*$^-$ Clone 2**	No Change	No Change	Yes	Reduced ability to enwrap following initial contacts?
***Dd5p4*$^-$**	Decreased	N/A	Severe defects	Failure due to reduced cortex openings?
***Dd5p4*$^-$ *GxcU*$^-$ Clone 1**	No Change	Increased	N/A	Possible failure at the later phagosome stage?
***Dd5p4*$^-$ *GxcU*$^-$ Clone 2**	Increased	Increased	N/A	Possible failure at the later phagosome stage?

4.3.6. Future additional studies on how GxcU could regulate endocytosis in *D. discoideum*

GxcU possesses various domains, one of which includes the DH (Rho-GEF) domain, which, like Frabin, could very well provide a link between GxcU and the regulation of the actin cytoskeleton. Live-cell imaging of GxcU localisation in relation to the Arp2/3 complex and Arp2/3 regulators, such as WasA and SCAR, could provide a deeper understanding as to how GxcU could regulate closure of cups during macropinocytosis through altering the actin cytoskeleton. Pull-downs and yeast two-hybrid assays could also be performed to discover crucial protein-protein interactions that could regulate this process.

The links between GxcU and the actin cytoskeleton gave the incentive to investigate another regulator of F-actin dynamics in *D. discoideum*, WasA (Myers et al. 2005), which I found to localise predominantly to the heads of comets in *Dd5p4*$^{-}$ mutant cells in chapter three. This provided a functional link between WasA and Dd5p4, and so the roles of WASP in the regulation of macropinocytosis and phagocytosis in *D. discoideum* will be investigated in the final results chapter.

Chapter 5

The roles of WasA during macropinocytosis and phagocytosis in *D. discoideum*; does functional redundancy exist with WasB?

5.1. Introduction

Whilst investigating how comets formed in *Dd5p4*$^{-}$ mutant cells, an interesting observation was unearthed whilst screening for actin regulators on these comets. This finding centred around *D. discoideum* Arp2/3 (ArpC4) and its activator, *D. discoideum* WASP (WasA) (Miki et al. 1996, Myers et al. 2005) both being found on F-actin 'comets' in *Dd5p4*$^{-}$.

WASP itself is a member of the WASP family of NPFs in mammals (Veltman and Insall 2010). A member of the mammalian WASP family, N-WASP has been shown to play a role in CME, and is itself recruited to CCPs together with Dynamin through binding to SNX9, which results in Arp2/3-mediated actin polymerisation (Lundmark and Carlsson 2004, Soulet et al. 2005, Badour et al. 2007, Shin et al. 2007, Yarar et al. 2007). The recruitment of N-WASP ensures the scission of vesicles from the PM, and is particularly important when cells are under high turgor pressure (Merrifield et al. 2004). More recently, a mechanism involving membrane curvature and Arp2/3-mediated actin polymerisation has been proposed in which, PI(4,5)P_2 and PI(3)P triggered SNX9 recruitment to vesicles, which together with PI(4,5)P_2-activated Cdc42, activated N-WASP and thus the Arp2/3 complex (Daste et al. 2017).

D. discoideum WASP, which later became known as WasA, was first identified by a yeast two-hybrid screen using constitutively active human Cdc42 as the bait (Chung et al. 1998). Currently, little was known about how WasA regulated phagocytosis and macropinocytosis in *D. discoideum*.

The discovery that WasA predominantly localised to the heads of F-actin 'comets' that formed on macropinosomes in *Dd5p4*$^{-}$ mutants provided a functional link between Dd5p4 and WasA in the regulation of F-actin dynamics. In this chapter, I will therefore investigate in detail the roles of WASP in macropinocytosis and phagocytosis in *D. discoideum*.

5.2. Results

5.2.1. WasA flashes occurred at cup closure in Ax2 control cells

In chapter three, I had shown that in *Dd5p4*$^{-}$ mutant cells, WasA was localised predominantly to the heads of F-actin 'comets'. I suggested that this was due to delayed F-actin disassembly after cup closure, which caused macropinosomes to be forced apart from the F-actin associated with the PM, forming the comets. This observation provided a functional link between Dd5p4 and WasA in the regulation of F-actin dynamics at cup closure in *D. discoideum*. This accidental, yet intriguing observation gave the incentive to investigate further how WasA regulated macropinocytosis at closure in Ax2 wild-type cells. This was achieved through the stable transfection of Ax2 cells with GFP-WasA, and when using confocal imaging I noticed an apparent 'flash' of WasA at

macropinosome closure (Fig. 5.1.A.). To study this in more detail I employed LLSM for its higher spatial and temporal resolution.

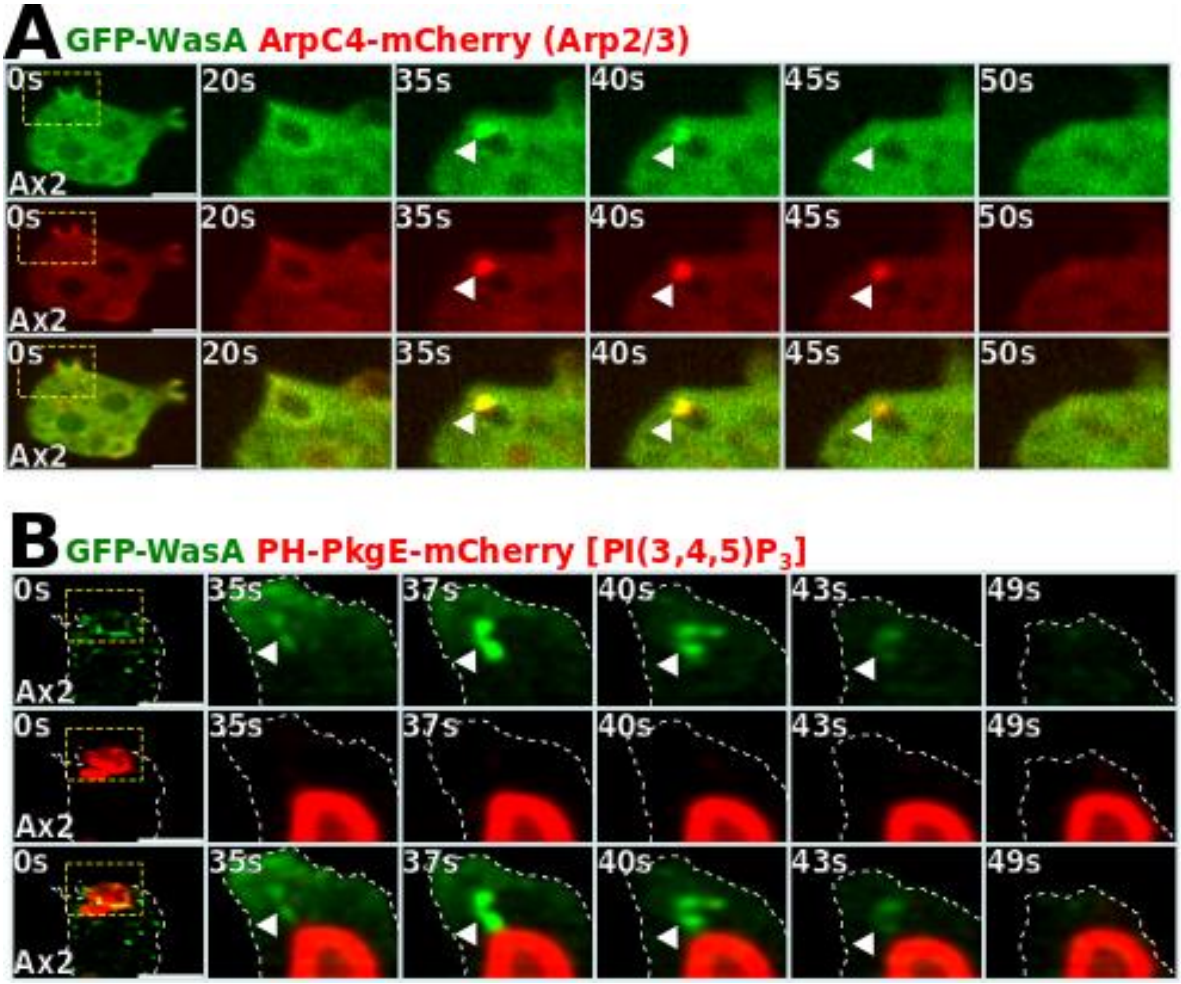

Figure. 5.1. 'Flashes' of WasA were seen at and just after macropinocytic cup closure in Ax2 control cells. (A) Spinning disc confocal time-lapse of Ax2 cells stably expressing GFP-WasA and ArpC4-mCherry. (B) LLSM time-lapse of Ax2 cells stably expressing GFP-WasA and PH-PkgE-mCherry [PI(3,4,5)P_3]. A LLSM time-lapse is available for *Dd5p4*$^-$ expressing these probes (S11). Yellow dashed boxes show the zoomed in areas of interest. Time intervals are shown in white and WasA and ArpC4 puncta are indicated by white arrow heads. All data shown are from a single biological repeat. Scale bars are 10 microns.

The 'flashes' of WasA and ArpC4 appeared to mark a region between where the cup had closed and what would become the macropinosome, which lasted for approximately 5-10 seconds, after which the WasA and ArpC4 signals both disappeared (Fig. 5.1.A.). Using LLSM, a much clearer and more definitive thin line of GFP-WasA appeared to connect the macropinocytic cup at closure to the cell-surface PM. This appeared to form the last link between what would become the macropinosome lumen and the extracellular space (Fig. 5.1.B.). The relevance of these 'flashes' of WasA at and just after macropinocytic cup closure was not clear, which gave the incentive to use LLSM to try and unearth the purpose of these 'flashes' of WasA.

5.2.2. The generation of *WasA*⁻ single mutants

In order to gain a greater understanding of the roles that WasA played during macro-endocytosis in *D. discoideum*, the *WasA* locus was disrupted through the incorporation of a Blasticidin resistance cassette into the coding region of the gene (Fig. 5.2.A-D.). *WasA*⁻ single mutants were generated through homologous recombination, and were subsequently screened via Western blotting (Fig. 5.2.E.).

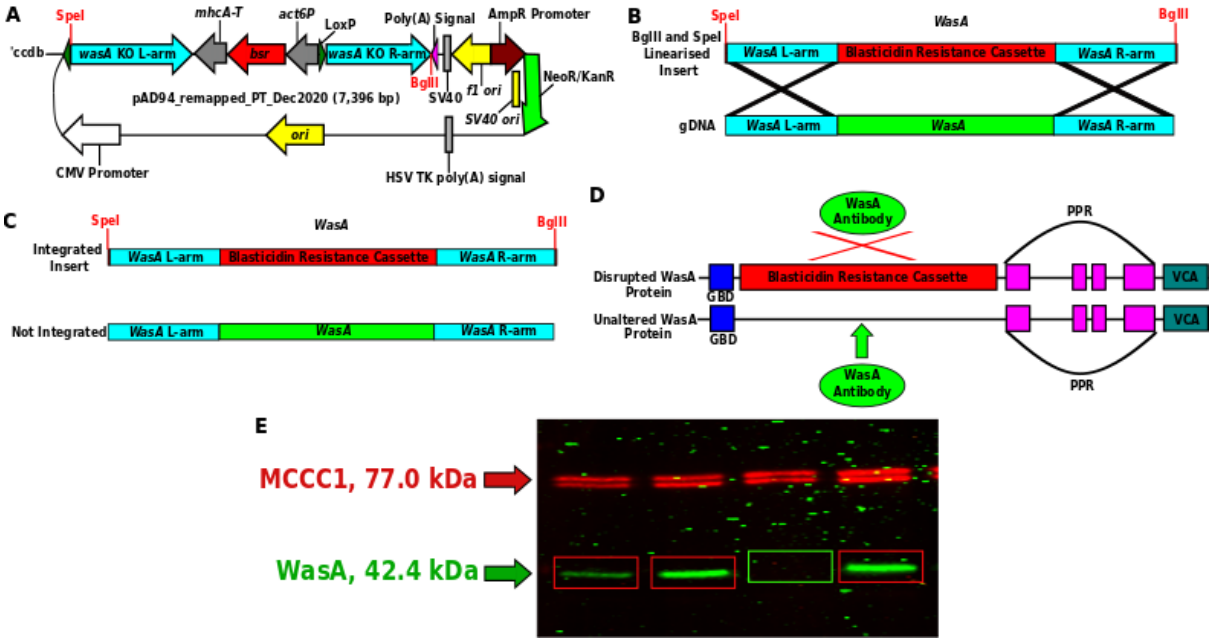

Figure 5.2. The generation of *WasA*⁻ single mutants. (A) Schematic overview of the pAD94 vector used to create *WasA*⁻ single mutants. The SpeI and BglII digested insert was incorporated into the *WasA* locus via homologous recombination. *mhcA* Terminator (*mhcA-T*), Blasticidin resistance cassette (*bsr*), *act6* Promoter (*act6P*), Simian Vacuolating virus 40 (SV40), f1 phage-derived origin of replication (*f1 ori*), Ampicillin Resistance Promoter (AmpR Promoter), Neomycin Resistance (NeoR), Kanamycin Resistance (KanR), Herpes Simplex Virus Thymidine Kinase poly(A) signal [HSV TK poly(A)], origin of replication, (*ori*), Cytomegalovirus promoter (CMV promoter). (B) Schematic displaying the incorporation of the Blasticidin cassette into the *WasA* locus via the left and right homology arms. BglII and SpeI sites are indicated in red. (C) Schematic depicting the incorporation of the resistance cassette into the genome both when successful (upper) and unsuccessful (lower). (D) Schematic of WasA proteins, with and without successful incorporation, which when undisrupted could bind the WasA-GFP antibody. This binding site was absent when the resistance cassette was translated as part of the non-functional protein. (E) Western blot screening for *WasA*⁻ clones. Binding to the WasA-GFP antibody was unperturbed in clones that were negative for the incorporation of the Blasticidin cassette into the *WasA* locus, and thus yielded a 42.4 kDa band. Clones that were positive for the incorporation of the Blasticidin cassette into the *WasA* locus did not possess the WasA-GFP antibody binding site and thus expressed the non-functional WasA protein, which therefore yielded no protein band. Negative clones are indicated by red boxes. A *WasA*⁻ positive clone is indicated by a green box. Methylcrotonyl-CoA Carboxylase Subunit 1 (MCCC1) was used as a loading control.

Whilst imaging the process of macropinocytosis by LLSM using the GFP-PH-PkgE probe, I observed the formation of what appeared to be the final link or 'tether' between the macropinocytic

cup and the PM at closure, which arose just prior to scission and consequently macropinosome formation (Fig. 5.3.A-D.). In Ax2 control cells, these tethers were short and short-lived whereas in cells lacking WasA activity these tethers appeared to be extended and more stable (Fig. 5.3.A-D.). Quantification of the maximal tether length and the tether lifetime from MIPs demonstrated that both were significantly longer in *WasA*$^{-}$ single mutants (Fig. 5.3.E-F.). These data suggested that WasA played a role in the scission of the macropinosome from the PM.

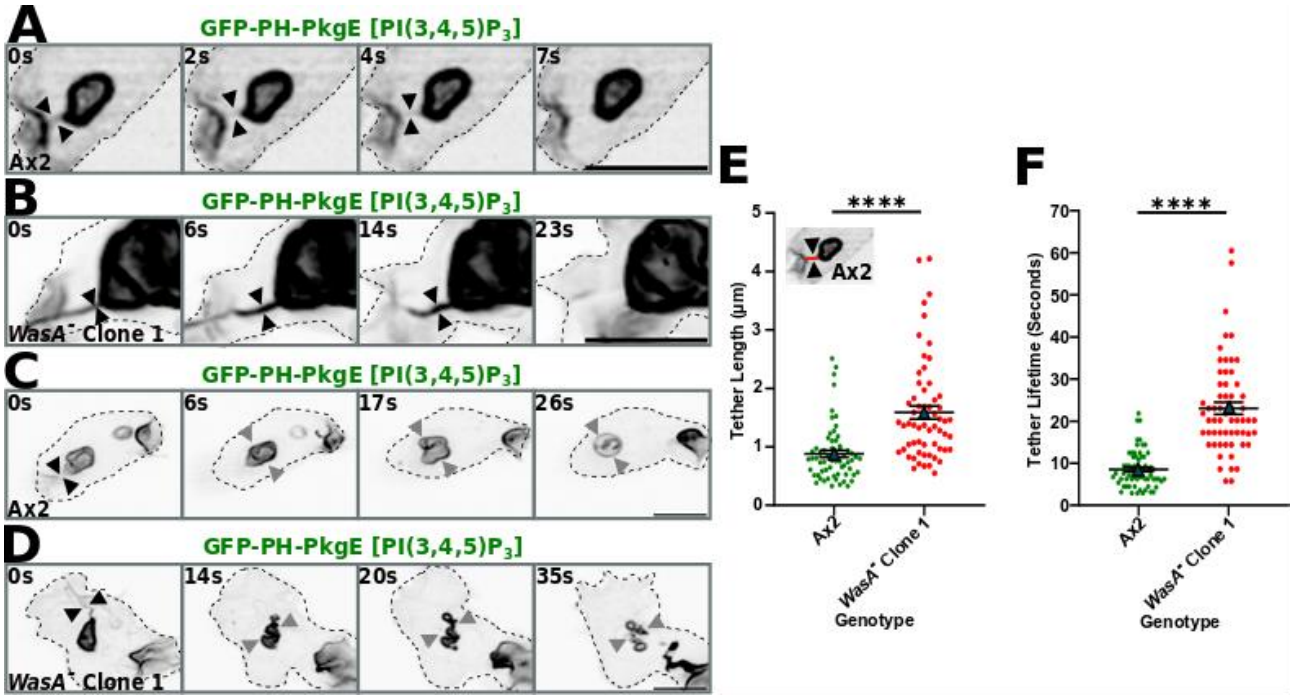

Figure. 5.3. Loss of WasA activity altered tether dynamics at and just after macropinocytic cup closure. LLSM film strips are shown for tether formation in Ax2 cells (A), and *WasA*$^{-}$ clone 1 cells (B). LLSM film strips revealed macropinosome formation after tether disappearance in Ax2 cells (C) and *WasA*$^{-}$ clone 1 cells (D). All cells were stably expressing GFP-PH-PkgE to report PI(3,4,5)P_3 localisation. A full time-lapse covering these tethers are available for Ax2 cells (S12) and *WasA*$^{-}$ clone 1 cells (S13). Tethers are shown by black arrow heads, and macropinosomes are shown by grey arrow heads, time intervals and cell peripheries are displayed by black and black dashed lines respectively. (E) Quantification of the maximal tether lengths. An example tether that was measured in Ax2 cells is overlaid with a red line. (F) Quantification of the tether lifetime from when it first appeared just at macropinocytic cup closure to when the tether disappeared and thus formed the macropinosome. The quantification of tether dynamics displayed in (E), and (F) were carried out using MIPs of LLSM time-lapses. All data shown are from a single biological repeat, with Ax2 individual data points shown as green circles, with *WasA*$^{-}$ clone 1 individual data points shown as red circles. The averages of both cell lines are indicated as dark blue triangles, ± SEM. Scale bars are 5 microns. Significance was determined comparing all individual data points using Mann Whitney U tests. **** $P < 0.0001$.

5.2.3. Bulk uptake was reduced in *WasA*$^{-}$ single mutant cells

In order to test if WasA was functionally important for regulating macropinocytosis, the bulk uptake of TRITC dextran over time was quantified in *WasA*$^{-}$ single mutant clones and was compared

to Ax2 control cells using flow cytometry (Fig. 5.4.A.). WasA had a significantly reduced bulk fluid uptake after two hours by approximately 25% in comparison to Ax2 control cells (Fig. 5.4.A.).

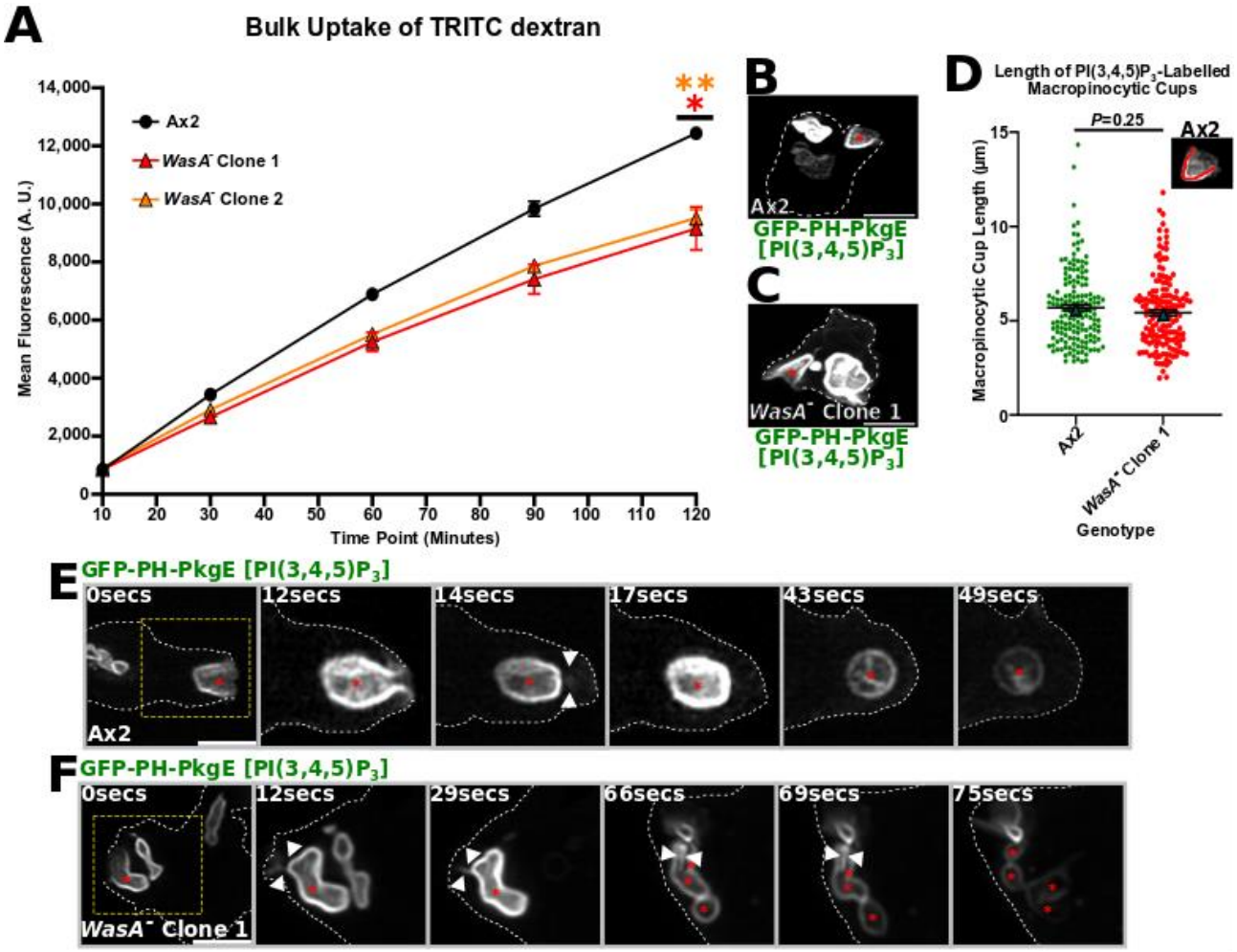

Figure 5.4. Bulk fluid uptake was reduced, with unchanged cup sizes forming numerous macropinosomes after closure in *WasA*⁻. (A) Quantification of the fluorescent dye uptake between Ax2 (black circles) *WasA*⁻ clone 1 (red triangles), and *WasA*⁻ clone 2 (orange triangles) following incubation with TRITC dextran at different time points. The data shown are from three separate day biological repeats, ± SEM. Statistical comparisons between Ax2 and each *WasA*⁻ clone at the two hour time point are indicated with the corresponding colour-coded statistical stars. Significance was determined using Welch's *t* tests. LLSM confocal images of Ax2 cells (B), and *WasA*⁻ clone 1 cells (C), stably expressing GFP-PH-PkgE, which binds to PI(3,4,5)P_3. (D) Quantification of the macropinocytic cup lengths from LLSM MIPs of Ax2 and *WasA*⁻ clone 1 cells stably expressing the equivalent probe. 160 cups per cell line were quantified at approximately 50% towards closure. An example cup measurement in Ax2 cells is outlined by a red line. The data shown are from a single biological repeat, with Ax2 shown in green, *WasA*⁻ clone 1 in red, and the averages indicated as dark-blue triangles, ± SEM. Non-significance was determined comparing all individual data points using a Mann Whitney U test. LLSM film strips are displayed for Ax2 (E) and *WasA*⁻ clone 1 (F), both stably expressing GFP-PH-PkgE. The cups between both cell lines are of similar size, which indicated that the initial macropinosomes that were generated were of similar sizes. The tethers were much shorter in Ax2 cells than in *WasA*⁻ clone 1 cells, which suggested that due to prolonged connectivity to the extracellular environment, fluid may have leaked back out of the longer, more stable tethers in the mutant cells. It would appear that as the main macropinosome remained associated via the longer-lasting tether with the PM this may have caused smaller macropinosomes to consequently bud off, yielding multiple macropinosomes in the *WasA*⁻ mutant cells. Complete time-lapses are available for Ax2 cells (S14) and *WasA*⁻ clone 1 cells (S15) both stably expressing the GFP-PH-PkgE probe. Zoomed in regions are indicated by yellow, dashed boxes. The cell peripheries of all panels are outlined by white dashed lines. Macropinocytic cups and the resulting macropinosomes are indicated by red stars. Tethers are indicated by white arrow heads. Scale bars are 5 microns. * $P < 0.05$, ** $P < 0.01$.

The reduction in bulk fluid uptake in the *WasA*$^{-}$ single mutants (Fig. 5.4.A.) was not due to changes in the lengths of macropinocytic cups as these were unaltered between control and mutant cells (Fig. 5.4.B-D.). This thereby gave the incentive to visualise macropinosome formation using LLSM in order to see what changes were observed downstream of macropinocytic cup formation in these mutants. In Ax2 cells after cup closure, the tether connecting the macropinosome to the PM lasted for a very brief duration (Fig. 5.4.E.), which suggested that this short-lived connection to the extracellular environment was also very brief in proportion. This very brief link to the extracellular environment could suggest that fluid had very little to no time to leak back out into the extracellular environment, which thus meant that the size of the macropinosomes and thereby bulk uptake was unaffected in the Ax2 control cells (Fig. 5.4.E.). As the macropinosome had long been separated from the PM in Ax2 control cells, this may have suggested that the macropinosome does not need to bud off in order to move away from the PM (Fig. 5.4.E.). In contrast, in *WasA*$^{-}$ cells a tether started to form at 12 seconds and lasted until 69 seconds, which was considerably longer in duration than what was observed in Ax2 control cells (Fig. 5.4.E-F.). This may suggest that the longer and more stable tethers formed in these mutants may have caused fluid to leak back out into the extracellular environment (Fig. 5.4.F.). This could therefore have reduced the bulk uptake and thus may be a potential explanation for the decreases that were observed in each mutant clone in comparison to the Ax2 control cells (Fig. 5.4.A.). In the mutant, it may also be due to the presence of the longer-lasting tethers that the main macropinosome remained associated with the PM for extended periods of time. These more stable tethers may have caused smaller macropinosomes to bud off from the main macropinosome that remained associated with the PM (Fig. 5.4.F.). These data suggested that alterations in the rates of scission from the PM after macropinocytic cup closure could have altered the dynamics of macropinosomes in mutants, which lacked WasA activity.

5.2.4. The generation of *WasA*$^{-}$ *WasB*$^{-}$ double mutants by CRISPR

The *D. discoideum* genome contains three putative WASP orthologues; WasB and WasC, in addition to WasA (Chung et al. 2013, Jeon and Jeon 2020). All three *D. discoideum* WASP proteins have been shown to localise to CCPs, which suggested functional redundancy (Veltman and Insall 2010). To understand if this functional redundancy also existed during macropinocytosis, I thereby also disrupted the *WasB* locus. This was performed in the *WasA*$^{-}$ clone 1 parental strain using CRISPR to generate *WasA*$^{-}$ *WasB*$^{-}$ double mutants (Fig. 5.5.A-B.). The resulting *WasA*$^{-}$ *WasB*$^{-}$ double mutants were then compared to Ax2 control cells using the same experimental set up (Fig. 5.4.A.), in order to quantify the bulk fluid uptake (Fig. 5.5.C.).

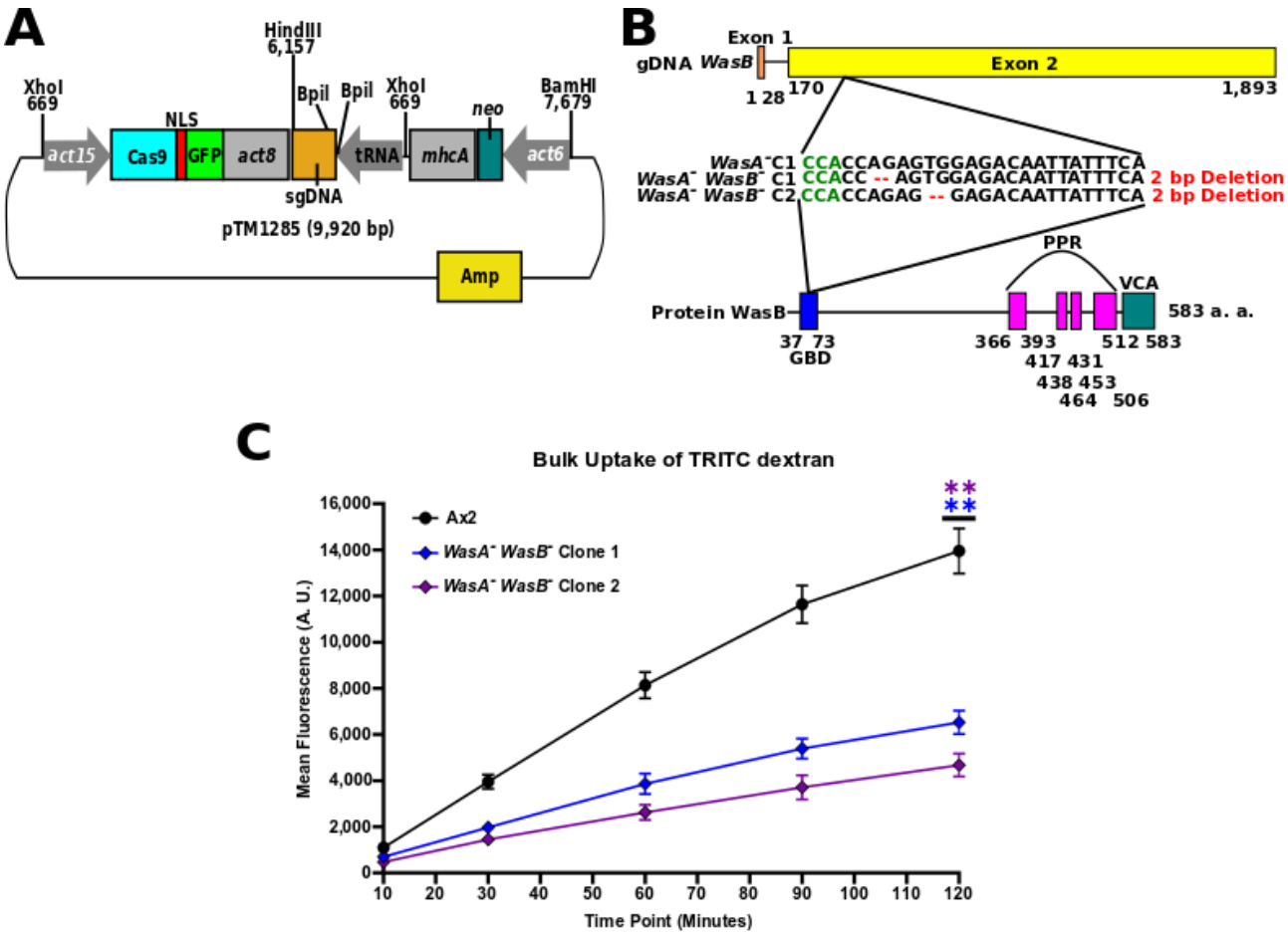

Figure 5.5. The generation of *WasA*⁻ *WasB*⁻ double mutants, which displayed a reduction in bulk fluid uptake. (A) Schematic overview of the all-in-one pTM1285 CRISPR/Cas9 vector that was used to generate deletions within the *WasB* locus. Two oligonucleotides were inserted into the vector via the Golden gate assembly method. (B) gDNA schematic of the *WasB* locus and the domain structure of the resulting protein. The target sequence is shown, with the location of the deletions indicated in red in *WasA*⁻ clone 1 (C1), and *WasA*⁻ *WasB*⁻ clones, with the PAM site on the complementary strand (CCA), indicated in green. *WasA*⁻ *WasB*⁻ clone 1 (C1), *WasA*⁻ *WasB*⁻ clone 2 (C2). (C) Quantification of the fluorescent dye uptake between Ax2 (black), *WasA*⁻ *WasB*⁻ clone 1 (dark blue diamonds), and *WasA*⁻ *WasB*⁻ clone 2 (purple diamonds) following incubation with TRITC dextran at different time points. Statistical comparisons with Ax2 at the two hour time point are indicated by a black line, with colour-coded statistical stars corresponding to each *WasA*⁻ *WasB*⁻ clone. All data shown are from three independent biological repeats, with each cell line colour-coded as shown, ± SEM. Significance was determined using Welch's *t* tests. ** $P < 0.01$.

Analysis of the bulk uptake of TRITC dextran over time in the *WasA*⁻ *WasB*⁻ double mutants indicated that cells lacking both WasA and WasB appeared to have a more severe significant reduction in fluid uptake, with a reduction of 55% in *WasA*⁻ *WasB*⁻ clone 1 cells and 70% in *WasA*⁻ *WasB*⁻ clone 2 cells in comparison to Ax2 control cells (Fig. 5.5.C.). This appeared to be more severe than the defects that were observed in the *WasA*⁻ single mutant clones (Fig 5.4.A. and Fig. 5.5.C.), which may suggest that WasA and WasB were functionally redundant.

5.2.5. *WasA*$^{-}$ and *WasA*$^{-}$ *WasB*$^{-}$ mutants displayed numerous, smaller macropinosomes

In an attempt to better understand why these WASP mutants took up less fluid, I visualised the size and number of macropinosomes in both the single and the double mutants by confocal imaging, followed by pH-sensitive FITC dextran application to visualise early, non-acidified macropinosomes. The average macropinocytic volume and macropinosome numbers per cell were then quantified in these WASP mutants (Fig. 5.6.A-I.).

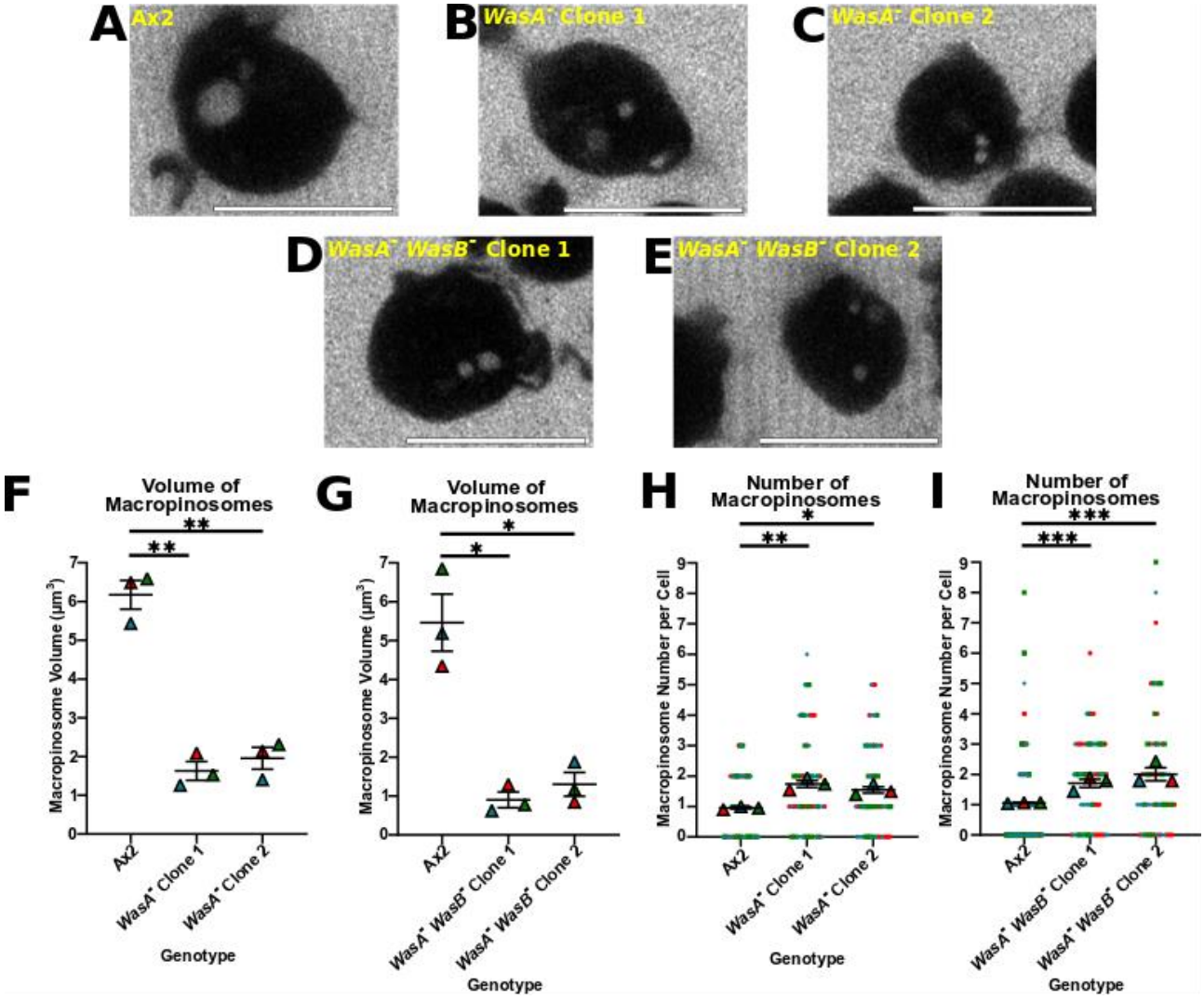

Figure. 5.6. Macropinosome dynamics were altered in *WasA*⁻ single and *WasA*⁻ *WasB*⁻ double mutants. Confocal images of Ax2 (A), *WasA*⁻ clones (B-C), and *WasA*⁻ *WasB*⁻ clones (D-E) incubated with FITC dextran, and their associated macropinosomes (grey spheres) with the genotypes indicated in yellow. (F) Quantification of the average volume of macropinosomes in *WasA*⁻ single mutants per cell at a single time point with statistical analyses being compared to their associated Ax2 control cells. (G) Equivalent analyses comparing *WasA*⁻ *WasB*⁻ double mutants to their associated Ax2 control cells. Significance was determined using Welch's *t* tests. (H) Quantification of the number of macropinosomes per cell at a single time point in *WasA*⁻ mutants with statistical analyses being compared to their associated Ax2 cells. (I) Equivalent analyses comparing *WasA*⁻ *WasB*⁻ double mutants to their associated Ax2 cells. Significance was determined using Mann Whitney U tests. Individual data points were omitted in F-G to make the averages more clearly visible. 20 cells were selected for each cell line, per biological repeat, and macropinosome numbers and volume were quantified. All data shown are from three independent, colour-coded biological repeats, ± SEM. Scale bars are 10 microns. * $P < 0.05$, ** $P < 0.01$, *** $P < 0.001$.

Consistent with the LLSM time-lapses, loss of WasA significantly reduced the volume of macropinosomes in comparison to Ax2 control cells (Fig. 5.6.F.). This reduction in volume appeared to be even more severe in *WasA*⁻ *WasB*⁻ double mutants, with an average macropinosome volume of 1 µm^3 across both clones; approximately 50% less than the average volume of macropinosomes that were observed in the *WasA*⁻ single mutants (Fig. 5.6.F-G.). In contrast, both single and double

WASP mutants contained significantly more macropinosomes per cell relative to Ax2 control cells (Fig. 5.6.H-I.). It should be noted however, that the number of macropinosomes in the double mutants in association with their corresponding Ax2 control cells appeared to display a stronger statistical increase in comparison to the single mutants in association with their Ax2 control cells (Fig. 5.6.H-I.). This could suggest that in these double mutant clones the tethers could potentially have been longer and even more stable than in the single mutants, which may have caused even more macropinosomes to bud off from the main macropinosome associated with the PM via the possibly longer and more stable tether. This could provide a possible explanation to the data displayed on macropinosome dynamics in these WASP mutants (Fig. 5.6.A-I.). In addition, the possibility of longer and more stable tethers in the double WASP mutants may provide an explanation as to the apparent more severe reduction in bulk uptake in the *WasA*$^{-}$ *WasB*$^{-}$ double mutants as fluid may have had more time to leak back out into the extracellular space than what could have occurred within the *WasA*$^{-}$ single mutants (Fig. 5.4.A. and Fig. 5.5.C.).

In summary, I have shown that WasA was recruited to tethers that connected nascent macropinosomes to the cell-surface PM at cup closure. In a single *WasA*$^{-}$ mutant clone, the length and duration of the tethers were significantly increased. These alterations in tether dynamics may have caused fluid to leak back into the extracellular environment, as well as to cause macropinosomes to bud off from the main macropinosome linked to the PM via the more stable tether. I have also shown that the *WasA*$^{-}$ *WasB*$^{-}$ double mutants appeared to display a more severe phenotype, which may suggest that more fluid may have leaked back out into the extracellular space via what could have been even longer and more stable tethers prior to scission. These potentially longer and more stable tethers in the double mutants may have given rise to a more severe reduction in fluid uptake compared to the *WasA*$^{-}$ single mutants.

5.2.6. Phagocytosis was reduced in *WasA*$^{-}$, and appeared to be more severely reduced in *WasA*$^{-}$ *WasB*$^{-}$ mutants

To test if the levels of phagocytosis were also reduced in *WasA*$^{-}$ and *WasA*$^{-}$ *WasB*$^{-}$, these WASP mutants were compared to Ax2 control cells for their ability to engulf yeast. Cells were shaken for 30 minutes with fluorescently labelled red yeast, prior to live-cell imaging, in order to quantify the levels of phagocytic engulfment. The fluorescence of yeast that were not engulfed were quenched by the addition of trypan blue (Fig. 5.7.A-G.).

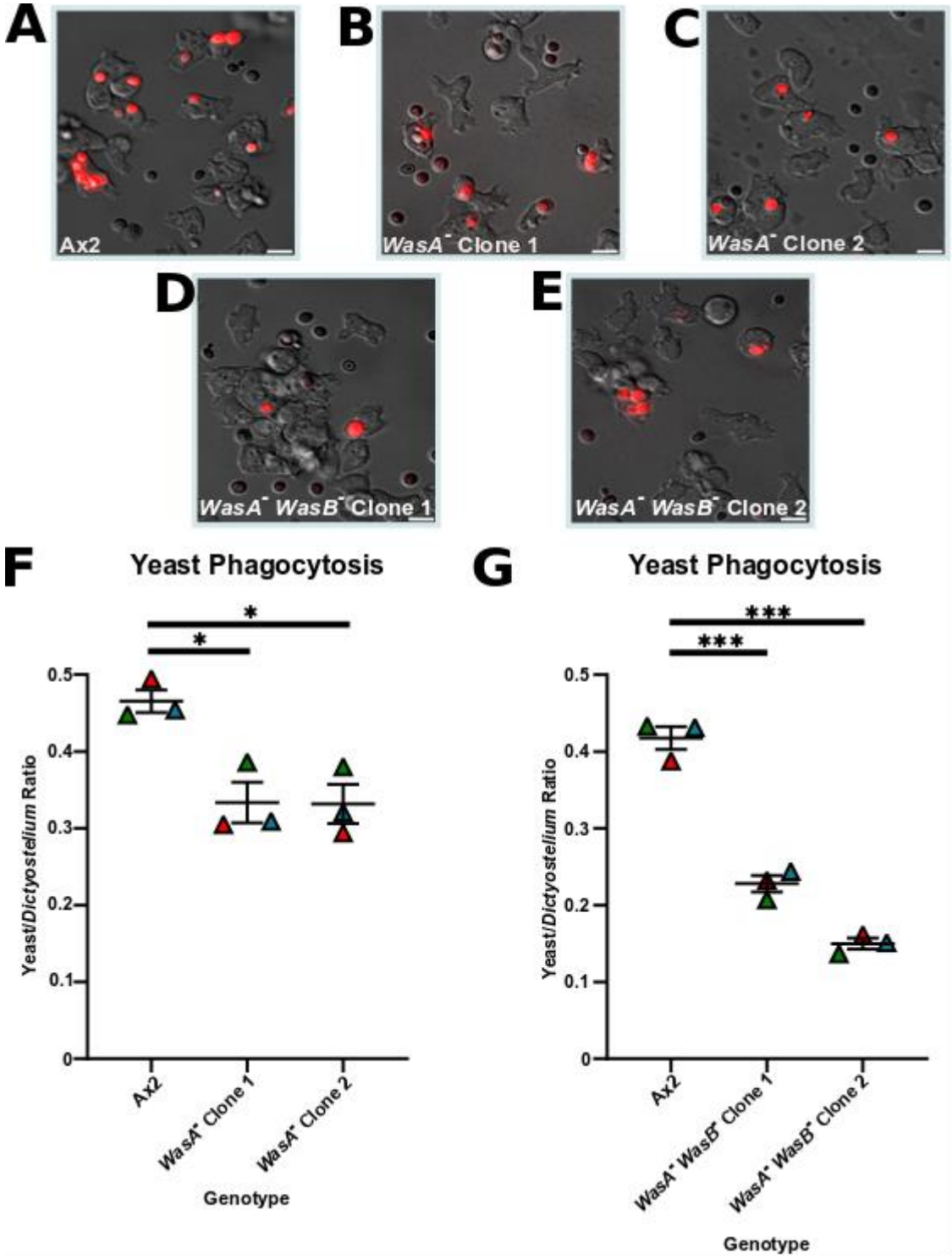

Figure 5.7. Phagocytosis was reduced in *WasA*⁻ single mutants, and appeared to be more severely reduced in *WasA*⁻ *WasB*⁻ double mutants. Confocal images of Ax2 (A), *WasA*⁻ clones 1-2 (B-C), and *WasA*⁻ *WasB*⁻ clones 1-2 (D-E), taking up fluorescently labelled red yeast following 30 minutes of shaking. (F) Quantification of the Yeast to *D. discoideum* ratio of the *WasA*⁻ clones in comparison to their associated Ax2 control cells. The equivalent data analyses is shown in (G), comparing *WasA*⁻ *WasB*⁻ double mutants to their associated Ax2 control cells. The data shown is the average ratio calculated from three independent, colour-coded biological repeats, ± SEM. Scale bars are 10 microns. Significance was determined using Welch's *t* tests. * $P < 0.05$, *** $P < 0.001$.

Quantification of the Yeast to *Dictyostelium* ratio showed that loss of WasA significantly reduced the levels of phagocytosis in comparison to Ax2 control cells by approximately 30% (Fig.

5.7.F.). This appeared to be further exaggerated in the *WasA*$^{-}$ *WasB*$^{-}$ double mutants, with an approximate reduction of 50-60% compared with their associated Ax2 control cells (Fig. 5.7.G.), which potentially may indicate functional redundancy.

5.2.7. *WasA*$^{-}$, and *WasA*$^{-}$ *WasB*$^{-}$ mutants took longer to enwrap yeast

The phagocytosis of yeast provided a more easily observable system in which to test whether WasA and WasB both contributed to either the protrusions that formed the phagocytic cup, or the final scission event. I first therefore investigated the rate at which *WasA*$^{-}$ single mutants and *WasA*$^{-}$ *WasB*$^{-}$ double mutants enwrapped yeast, using the PI(3,4,5)P_3 probe, RFP-PH-PkgE, to mark the phagocytic cup (Ruchira et al. 2004, Goldberg et al. 2006, and van Haastert lab, unpublished data) (Fig. 5.8.A-G.).

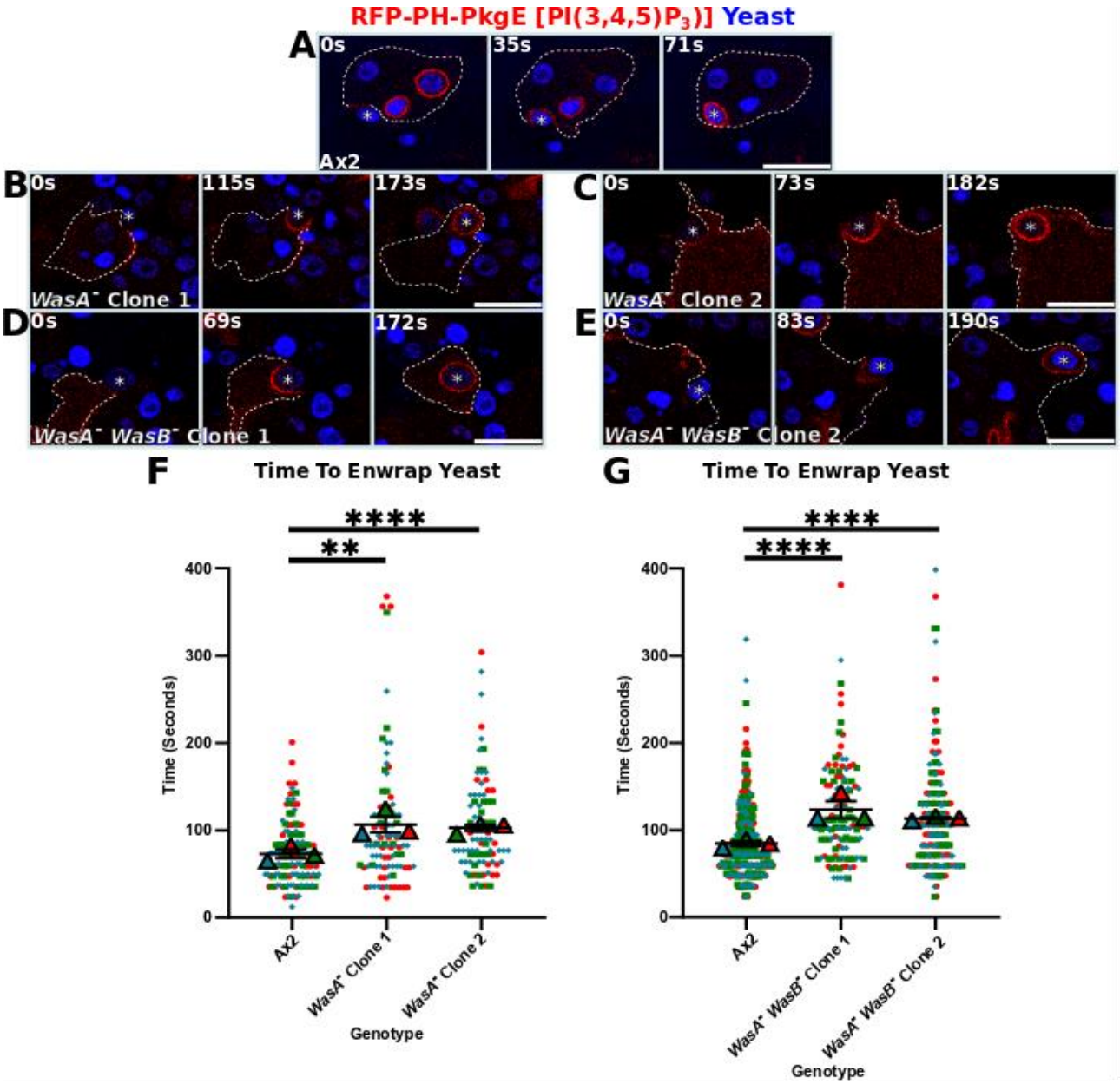

Figure 5.8. *WasA*⁻, and *WasA*⁻ *WasB*⁻ mutants took longer to enwrap yeast. Confocal images of Ax2 (A), *WasA*⁻ clones (B-C), and *WasA*⁻ *WasB*⁻ clones (D-E), stably expressing the RFP-PH-PkgE reporter for PI(3,4,5)P_3, engulfing fluorescent blue yeast over time. (F) Quantification of the time taken for the PI(3,4,5)P_3-labelled PM of *WasA*⁻ mutants and Ax2 cells (red with no white dashed lines) to fully enwrap yeast during successful and failed phagocytic engulfment events from the first point of contact, with statistical analyses being compared to Ax2 control cells. (G) Equivalent analyses comparing *WasA*⁻ *WasB*⁻ clones with their associated Ax2 control cells. The cell peripheries are indicated by white dashed lines, with the time intervals indicated in white. Yeast of interest are indicated by white stars. The data shown are the individual points and averages from each of the three independent, colour-coded biological repeats, ± SEM. Scale bars are 10 microns. Significance was determined using Mann Whitney U tests. ** $P < 0.01$, **** $P < 0.0001$.

In both *WasA*⁻ clones, the time taken to enwrap yeast was significantly increased compared to Ax2 control cells, increasing from 70 seconds in Ax2 cells to approximately 100 seconds in the *WasA*⁻ clones (Fig. 5.8.F.). In *WasA*⁻ *WasB*⁻ clone 1 cells, the time taken to enwrap yeast was significantly increased compared to Ax2 control cells, increasing from 85 seconds in Ax2 cells to

approximately 125 seconds in the *WasA*$^{-}$ *WasB*$^{-}$ clone 1 cells (Fig. 5.8.G.). In *WasA*$^{-}$ *WasB*$^{-}$ clone 2 cells, the time taken to enwrap yeast was significantly increased compared to Ax2 control cells, increasing from 85 seconds in Ax2 control cells to approximately 115 seconds in the *WasA*$^{-}$ *WasB*$^{-}$ clone 2 cells (Fig. 5.8.G.). The increases in the time taken to enwrap yeast did not appear to be worsened in the *WasA*$^{-}$ *WasB*$^{-}$ double mutants in comparison to the *WasA*$^{-}$ single mutants (Fig. 5.8.F-G.).

5.2.8. *WasA*$^{-}$, and *WasA*$^{-}$ *WasB*$^{-}$ took longer to internalise phagosomes

Why phagocytosis was reduced in both the single and the double WASP mutants was not clear (Fig. 5.7.A-G.). I therefore imaged phagocytic events by time-lapse microscopy and quantified the phagocytic failure rate, whilst also pinpointing why phagocytic engulfment failure occurred. This was previously undertaken in chapters three and four, using the stable co-expression of PI(3)P and PI(3,4,5)P_3 reporters to unequivocally identify successful phagocytic internalisation events. This, together with the quantification of the phagosome internalisation kinetics, were investigated using the *WasA*$^{-}$ single mutant clones and the *WasA*$^{-}$ *WasB*$^{-}$ double mutant clones, each in comparison to their corresponding Ax2 control cells (Fig. 5.9.A-I.).

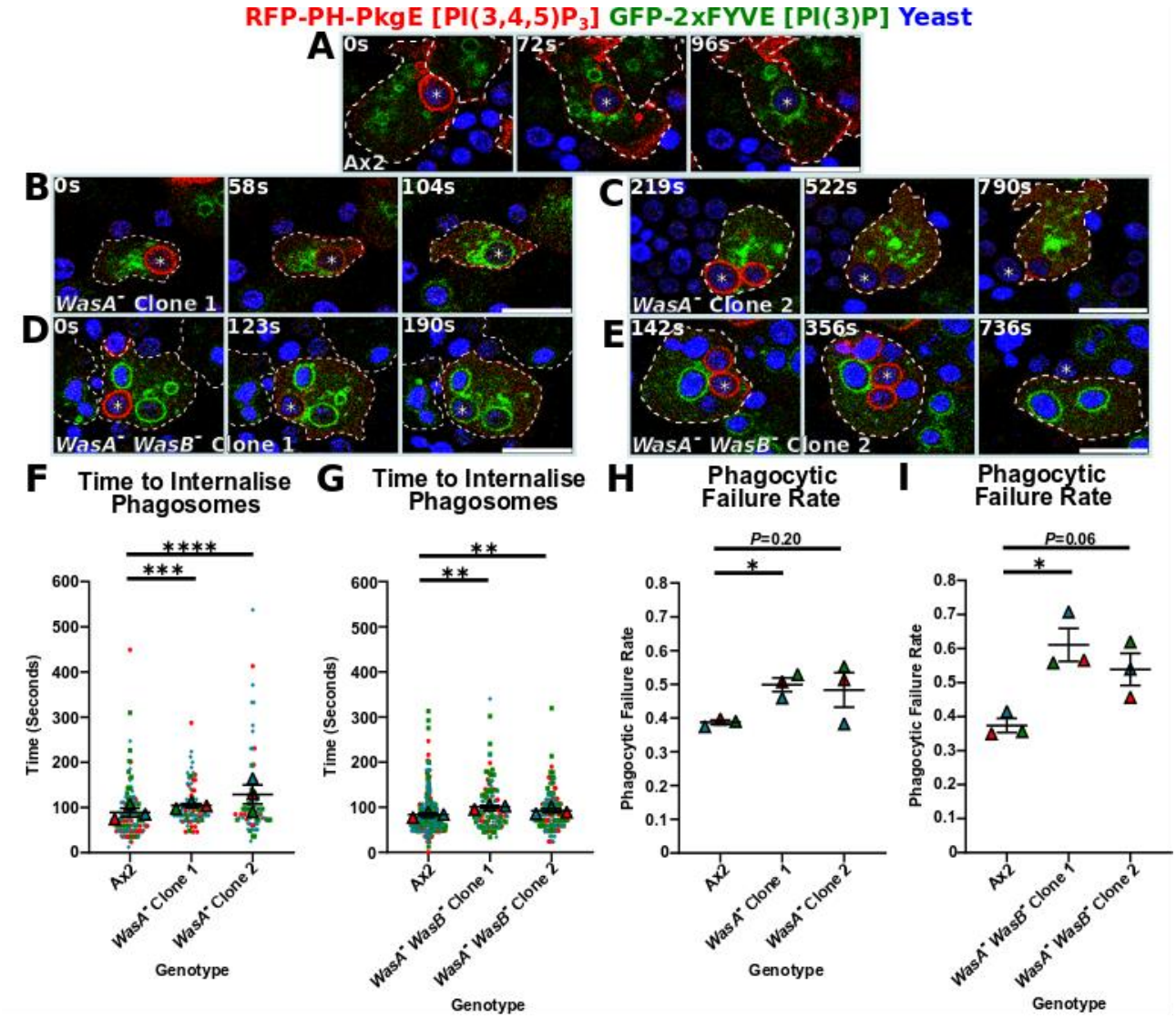

Figure 5.9. *WasA*⁻, and *WasA*⁻ *WasB*⁻ mutants displayed increases in the time taken to internalise phagosomes. Confocal images of Ax2 cells (A), *WasA*⁻ clones (B-C), and *WasA*⁻ *WasB*⁻ clones (D-E) stably expressing the RFP-PH-PkgE GFP-2xFYVE dual expression probe to report PI(3,4,5)P_3 and PI(3)P respectively, whilst engulfing fluorescent blue yeast over time. (F) Quantification of the time taken from the point of complete enwrapping by the PI(3,4,5)P_3-labelled PM to the point of PI(3)P formation on the membranes of the early phagosomes, with statistical tests being compared to the Ax2 control cells as indicated. (G) Equivalent analyses comparing *WasA*⁻ *WasB*⁻ double mutants to their corresponding Ax2 control cells. Significance was determined using Mann Whitney U tests. (H) Quantification of the proportion of failed events in *WasA*⁻ clones compared to Ax2 control cells, in which PI(3)P was not formed after the first point of contact of yeast with the PI(3,4,5)P_3-labelled PM. (I) Equivalent analyses comparing *WasA*⁻ *WasB*⁻ double mutants to Ax2 control cells. Significance and non-significance was determined using Welch's *t* tests. The cell peripheries are indicated by white dashed lines, with the time intervals indicated in white. Yeast of interest are indicated by white stars. The data shown are the individual points, and averages from each of the three independent biological, colour-coded repeats, ± SEM. Scale bars are 10 microns. * $P < 0.05$, ** $P < 0.01$, *** $P < 0.001$, **** $P < 0.0001$.

The loss of WasA significantly increased the time taken to internalise phagosomes in either clone in comparison to Ax2 control cells, increasing from 90 seconds in Ax2 cells to approximately 110 seconds in *WasA*⁻ clone 1 cells and 130 seconds in *WasA*⁻ clone 2 cells (Fig. 5.9.F.). Comparison

of the double mutant phagosome internalisation times to Ax2 control cells indicated that there was also a significant increase in the time taken to internalise phagosomes. In Ax2 cells it took 90 seconds to internalise phagosomes, whilst *WasA*$^{-}$ *WasB*$^{-}$ clone 1 cells took approximately 105 seconds and *WasA*$^{-}$ *WasB*$^{-}$ clone 2 cells took approximately 100 seconds (Fig. 5.9.G.). The time taken to internalise phagosomes in the *WasA*$^{-}$ single mutants appeared to be worsened rather interestingly in comparison to the *WasA*$^{-}$ *WasB*$^{-}$ double mutants (Fig. 5.9.F-G.). When comparing the *WasA*$^{-}$ phagocytic failure rates to Ax2 cells, it was not clear from these three biological repeats if the loss of WasA resulted in defects in phagocytosis. *WasA*$^{-}$ clone 1 cells displayed phagocytic defects compared to Ax2 cells, whilst *WasA*$^{-}$ clone 2 cells did not display phagocytic defects in comparison to Ax2 cells (Fig. 5.9.H.), meaning that additional biological repeats would therefore be needed to clarify these results. An additional finding in these single mutants was that there were some phagocytic engulfment events in which there were multiple 'flashes' of PI(3,4,5)P_3, each 'flash' presumably represented a different phagocytic engulfment attempt (data not shown). Due to the time constraints of these time-lapses, it was not clear as to whether these phagocytic engulfment events were eventually successful or not. It was also not clear if the double mutants displayed phagocytic defects as *WasA*$^{-}$ *WasB*$^{-}$ clone 1 cells displayed phagocytic defects compared to Ax2 cells, however *WasA*$^{-}$ *WasB*$^{-}$ clone 2 cells did not display any phagocytic defects compared to Ax2 cells (Fig. 5.9.I.), again indicating that additional repeats would be required to clarify these results. It was also ambiguous if the phagocytic defects appeared to be worsened if at all between the single and the double WASP mutants (Fig 5.9.H-I.).

In summary, *WasA*$^{-}$ single and *WasA*$^{-}$ *WasB*$^{-}$ double mutants both displayed increases in the time taken to enwrap yeast and to internalise phagosomes in comparison to their respective Ax2 control cells. It was not clear however, if either the single or the double WASP mutants displayed phagocytic defects in comparison to their respective Ax2 control cells. It was also ambiguous if the dynamics of phagocytosis that were quantified appeared to be worsened if at all in the *WasA*$^{-}$ *WasB*$^{-}$ double mutants compared to the *WasA*$^{-}$ single mutants. This may suggest that WasA and WasB are not functionally redundant in the regulation of phagocytic engulfment.

5.3. Discussion

5.3.1. Comparison of *D. discoideum* and mammalian WASP proteins in the regulation of endocytosis

I have demonstrated during this project that 'flashes' of WasA were observed at cup closure in *D. discoideum*. These investigations unearthed the presence of tethers in Ax2 and *WasA*$^{-}$ mutant cells. I found that these tethers were longer and more stable in the *WasA*$^{-}$ single mutants, which indicated that WasA appeared to be functionally important for regulating scission. These tethers

marked the final link between what would become the macropinosome and the PM, as once severed, the formation of the macropinosome was completed (Fig. 5.1.A-B.). As macropinocytic cup sizes were unaffected in these *WasA*$^{-}$ single mutants (Fig. 5.4.B-D.), the dynamics of macropinosomes were next investigated and the macropinosomes themselves were established to be smaller, and more numerous, in comparison to Ax2 control cells (Fig. 5.6.A-I.). The elongated and more stable tethers in the *WasA*$^{-}$ single mutants potentially may have caused fluid to leak back out through the tether tubules into the extracellular environment (Fig. 5.4.E-F.). Furthermore, due to the presence of longer and more stable tethers, numerous, smaller macropinosomes appeared to bud off from the main macropinosome that remained associated with the PM through the tether (Fig. 5.3.A-F. and Fig. 5.4.E-F.). This suggested that WasA somehow facilitated rapid-onset scission, by which the tether was severed and the macropinosome internalised. The possible mechanism in Ax2 cells and *WasA*$^{-}$ single mutant cells is summarised (Fig. 5.10.).

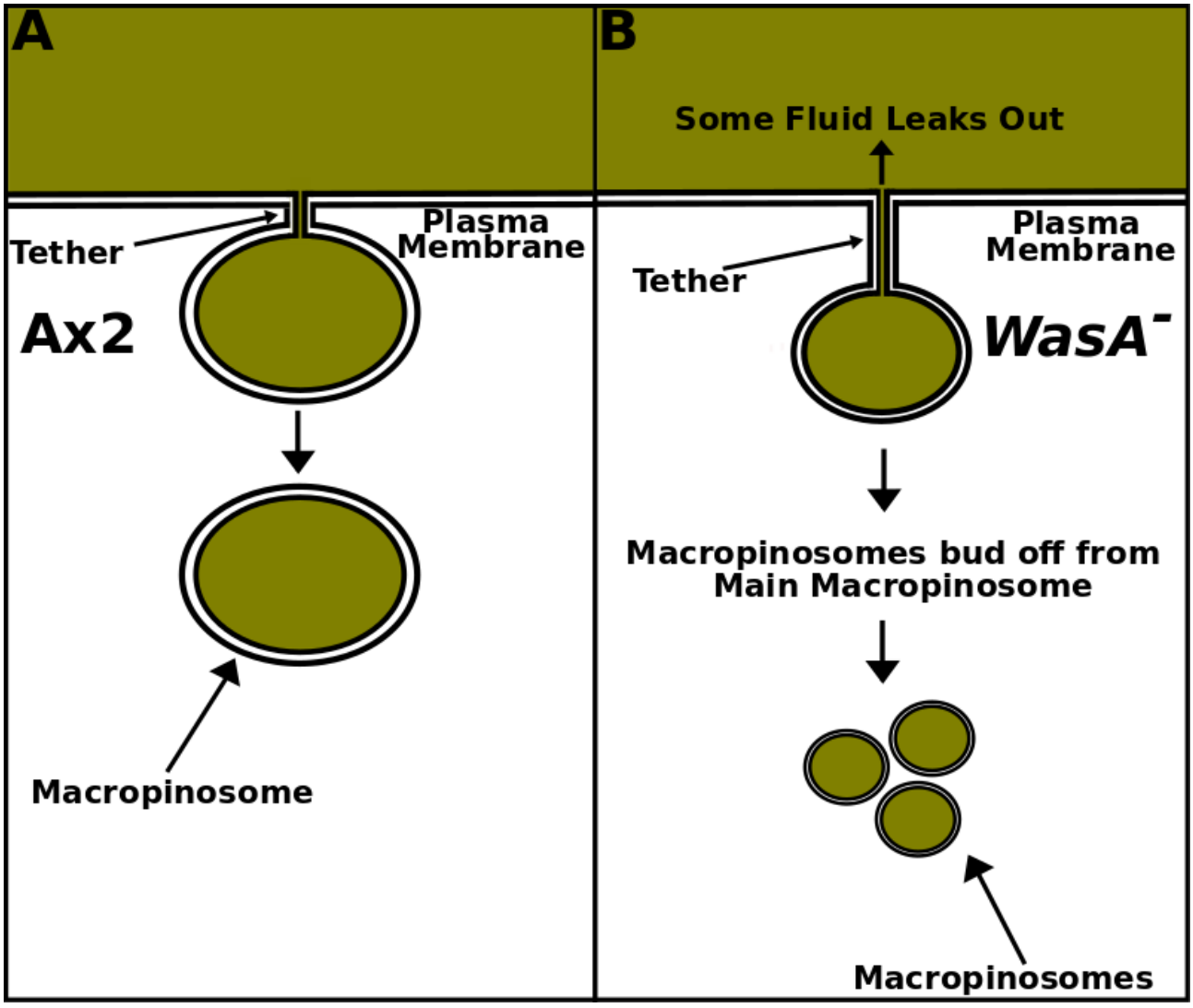

Figure 5.10. The loss of WasA altered the tether and macropinosome dynamics after cup closure. In both cell lines, the size of macropinocytic cups was completely unaffected. In Ax2 cells after macropinocytic cup closure the presence of WasA activity resulted in shorter, less stable tethers forming, which possibly prevented fluid from leaking back into the extracellular space. Due to the brief link with the PM via the tether no macropinosome budding occurred, which resulted in fewer, normal-sized macropinosomes within Ax2 cells. In *WasA*$^{-}$ cells, the lack of WasA activity formed longer, and more stable tethers, which may have caused fluid to leak back into the extracellular space. Due to the extended link with the PM via the tether in these mutants, macropinosomes consequently appeared to bud off from the main macropinosome, which resulted in more numerous, and smaller macropinosomes forming in these *WasA*$^{-}$ mutants. Fluid is olive.

In mammals, N-WASP, a member of the NPF WASP family, has been shown to be involved in the regulation of endocytosis, and in particular CME (Daste et al. 2017). During CME, as CCPs mature they adopt a Ω-shape and acquire N-WASP, which drives Arp2/3-mediated actin polymerisation. In mammals, membrane curvature has been shown to occur through the activities of proteins, which possess either BAR or Extended Fes-CIP4 homology (EFC) domains, which are also capable of forming homodimers. Interactions with Dynamin and N-WASP are established through the SH3 domain binding of proteins, which also contain BAR or EFC domains. These interactions are crucial

to mediate mechanical fission of membrane tubules leading to the generation of vesicles (Otsuki et al. 2003, Kamioka et al. 2004, Itoh et al. 2005, Tsujita et al. 2006). Collectively, this suggests that N-WASP-driven actin polymerisation, Dynamin, and BAR- or EFC-domain-containing proteins are involved in fission. This mechanism to drive vesicle fission is required as membranes are not able to fuse in isolation and give rise to endosomes alone. A summary of the roles of BAR- or EFC-domain-containing proteins, and the possible mechanisms of vesicle fission during endocytosis is shown (Fig. 5.11.).

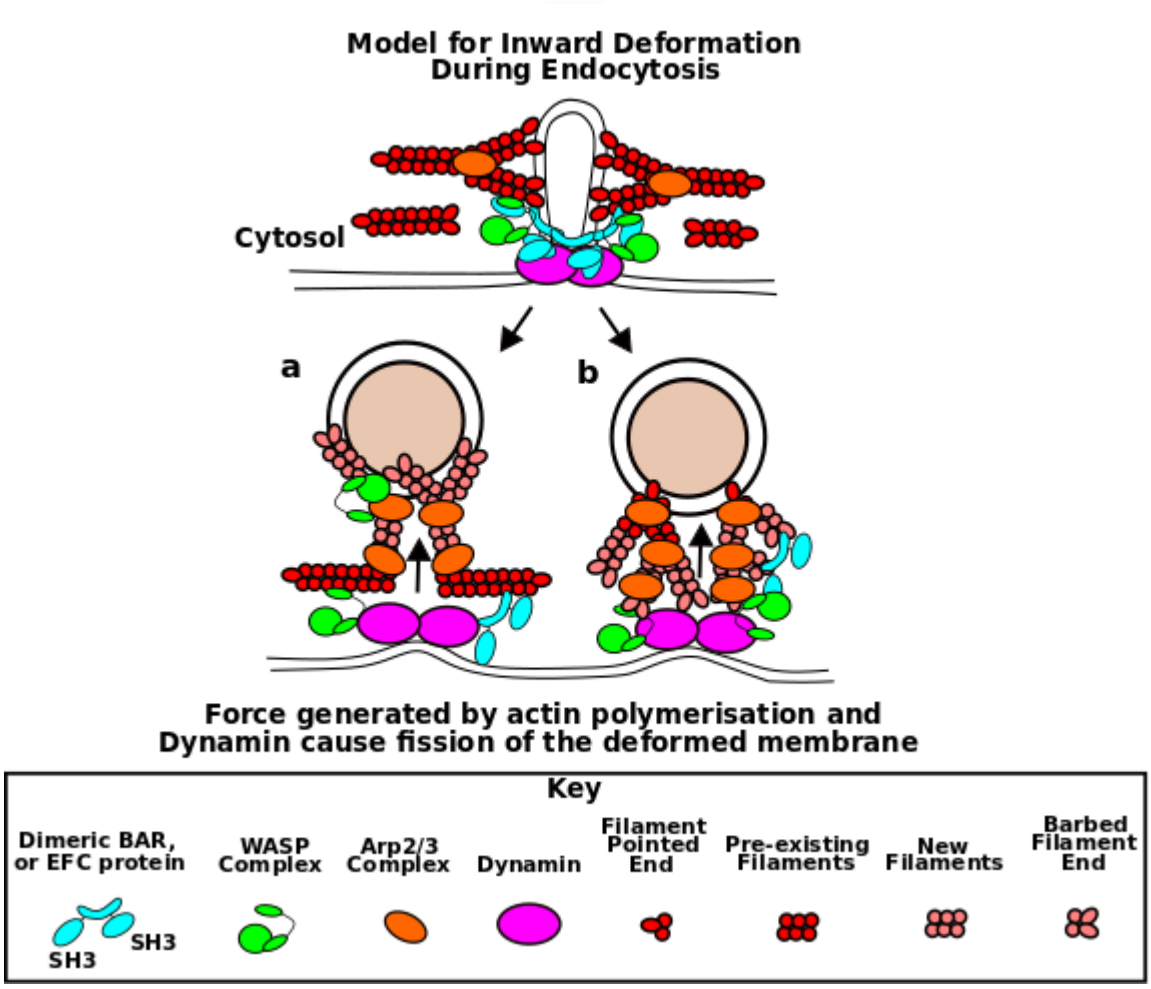

Figure 5.11. The roles of WASP, BAR- or EFC-domain-containing proteins that coordinates the curvature of the PM and the cytoskeleton during fission. During endocytosis, the direction in which actin polymerisation occurs, that is the direction of the barbed end of actin filaments (pointed ends), which either faces towards the endocytic vesicle as shown in (a), or towards the PM as shown in (b). In both paths the BAR- or EFC-domain-containing proteins (aqua blue) act to recruit both N-WASP (green) and Dynamin (magenta), resulting in membrane fission. In path (a) the extending barbed filament ends (pink) pushes endocytic vesicles away from the PM for vesicle movement and subsequent vesicle internalisation. In path (b) the extending pointed end of filaments (red) pushes or alternatively the extending filament barbed ends pushes towards the PM, which generates a force that is required for vesicle fission. A key showing each of the individual components, which regulates vesicle fission are indicated. Adapted from (Takenawa and Suetsugu 2007).

These studies in mammals suggest that in *D. discoideum* a similar process may indeed happen during macropinocytosis. In *WasA*$^{-}$ cells, tether dynamics were affected and scission appeared to be delayed. This suggested that WasA may be involved and forms part of the unit of proteins required to facilitate efficient scission of the macropinosome from the PM, much like what N-WASP does in collaboration with SNX9 and Dynamin in mammals during CME. In *D. discoideum* there are no known homologues of SNX9, however homologues of Dynamin have been identified (Noethe and Manstein 1998, Wienke et al. 1999), which thus allows potential future studies between WasA and the homologues of Dynamin to be performed. It could be that WasA was important for the rapid recruitment of the homologues of Dynamin to the tethers, which thus facilitated rapid scission. To ascertain this, GFP knock-ins of Dynamin could be generated in Ax2 control cells and the *WasA*$^{-}$ single mutants and the time taken for the recruitment of GFP-Dynamin to the tethers between Ax2 and *WasA*$^{-}$ mutants could be quantified using LLSM.

Further studies could also be done to visualise and to quantify tether dynamics in *WasA*$^{-}$ *WasB*$^{-}$ cells stably expressing GFP-PH-PkgE using LLSM in order to establish if WasA and WasB were functionally redundant in the regulation of macropinosome fission.

I have identified that the bulk uptake of fluid in the single *WasA*$^{-}$ mutant clones were reduced by approximately 25% compared to Ax2 control cells (Fig. 5.4.A.), suggesting that the fluid uptake defects could be due to the inability to efficiently resolve the tethers. This appeared to be more pronounced in the *WasA*$^{-}$ *WasB*$^{-}$ double mutants (Fig. 5.5.C.), which stated that WasA and WasB may be functionally redundant in being able to efficiently resolve the tethers during macropinocytosis. In *D. discoideum*, a third WASP protein exists, WasC (Jeon and Jeon 2020), which may also play a functionally redundant role in efficiently resolving the tethers. This could be tested through the creation of *WasA*$^{-}$ *WasB*$^{-}$ *WasC*$^{-}$ triple mutants using CRISPR, which does not require the incorporation of an additional selective antibiotic resistance gene. Cell culture of these triple mutants would allow one to firstly establish if these cells were viable. If this was the case, quantification of bulk fluid uptake overtime in these triple mutants, and subsequent visualisation and quantification of tether dynamics using LLSM could be subsequently performed.

5.3.2. Insights into how WasA and WasB affected phagocytosis in *D. discoideum*

In this project I have shown that the time taken to enwrap yeast and the time taken to internalise phagosomes during phagocytosis were both significantly increased following the loss of WasA activity (Fig. 5.8.F. and Fig. 5.9.F.). It was however, unclear if these mutants possessed any phagocytic defects due to the discrepancies between *WasA*$^{-}$ clone 1 cells and *WasA*$^{-}$ clone 2 cells (Fig. 5.9.H.). This differed from previous studies that have been made in *WasA*$^{-}$ cells, in which defects

in the uptake of bacteria, which were smaller and possessed a different geometry to yeast were observed (Veltman and Insall 2010, Davidson et al. 2018). This may suggest that the defects in these mutants may be exaggerated if the object to be engulfed was smaller and possessed a certain geometry, although more studies would be needed to clarify this theory. Based on the data acquired from macropinocytosis in which WasA was shown to efficiently resolve the tethers, this could potentially also be applied to phagocytosis, which in theory could allow more rapid internalisation of the phagosome. WasB interestingly, may not have been involved in regulating this process as the phenotype of the *WasA*$^{-}$ *WasB*$^{-}$ double mutants did not appear to be worsened if at all in comparison to the *WasA*$^{-}$ single mutants. This could suggest that WasB may not be important for coordinating the more rapid enwrapping of yeast or the more rapid internalisation of the phagosome (Fig. 5.8.G. and Fig. 5.9.G.). Like the observations that were made in reference to the *WasA*$^{-}$ single mutants, it was also not clear if the *WasA*$^{-}$ *WasB*$^{-}$ mutants possessed any phagocytic defects due to the discrepancies between *WasA*$^{-}$ *WasB*$^{-}$ clone 1 cells and *WasA*$^{-}$ *WasB*$^{-}$ clone 2 cells (Fig. 5.9.I.). Overall this suggested that WasB could be less important for the regulation of successful phagocytic engulfment. Recruitment of the WasA and WasB proteins in contrast however, were found to be essential during CME when the cells were under increased tension (Merrifield et al. 2004). A fairly recent study has also shown that WasA regulated the expression of receptors, such as the cAMP Receptor 1 (cAR1), which was not expressed in the *WasA*$^{-}$ single mutants (Davidson et al. 2018). This implied that the *D. discoideum* WasA protein may have regulated the expression of phagocytic receptors, such as SibA, which could have caused alterations in the kinetics and thus the efficiency of phagocytosis. This could also provide a plausible explanation as to why alterations in the phagocytic kinetics were observed in the *WasA*$^{-}$ single mutants, but did not appear to be worsened in the *WasA*$^{-}$ *WasB*$^{-}$ double mutants. This suggested that WasA and not WasB could have regulated the expression of various phagocytic receptors and thus the time taken to enwrap yeast and to coordinate efficient phagocytosis.

Interestingly, macropinocytosis was more perturbed in comparison to phagocytosis when analysing the *WasA*$^{-}$ and *WasA*$^{-}$ *WasB*$^{-}$ mutants in comparison to the Ax2 control cells. I have speculated that during macropinocytosis, the presence of more stable tethers in the *WasA*$^{-}$ mutants could have resulted in some fluid leaking back out into the extracellular space due to the malleable nature of the liquid media. The delays in the macropinocytic kinetics and thus the severing of the tethers in these *WasA*$^{-}$ mutants could have caused numerous, smaller macropinosomes to bud off from the main macropinosome that was linked to the PM by the more stable tether. Collectively this could have caused the reduction in bulk fluid uptake and the changes in macropinosome dynamics due to these slowed macropinocytic kinetics in the *WasA*$^{-}$ mutant cells. In contrast,

phagocytosis may have been less perturbed as the solid object, which by nature was unlike the more malleable liquid media, did not appear to move away from the initial point of contact in response to the slower phagocytic kinetics in *WasA*$^{-}$ cells. The yeast were instead enwrapped more slowly, with the slower kinetics in this setting not appearing to influence the phagocytic failure rate.

5.3.3. Summary

A summary of the phagocytic phenotypes of the *WasA*$^{-}$ single and *WasA*$^{-}$ *WasB*$^{-}$ double mutants is shown (Table 5.1.).

Table 5.1. A summary of the phagocytic phenotypes of *WasA*$^{-}$ single and *WasA*$^{-}$ *WasB*$^{-}$ double mutants compared to Ax2 control cells.

Genotype	Enwrapping Duration	Internalisation Duration	Phagocytic Defects?	Possible Causes of Phagocytic Defect
***WasA*$^{-}$ Clone 1**	Increased	Increased	Yes	Less efficient at resolving tethers? Ensuring optimal phagocytic receptor expression?
***WasA*$^{-}$ Clone 2**	Increased	Increased	No	Unclear, more repeats required.
***WasA*$^{-}$ *WasB*$^{-}$ Clone 1**	Increased	Increased	Yes	Less efficient at resolving tethers? Ensuring optimal phagocytic receptor expression?
***WasA*$^{-}$ *WasB*$^{-}$ Clone 2**	Increased	Increased	No	Unclear, more repeats required.

In summary, I have shown that during the process of macropinocytosis the loss of WasA activity altered the tether dynamics at macropinocytic cup closure and increased their stability, which possibly caused fluid to leak back out into the extracellular space. This observation, combined with the numerous, smaller macropinosomes budding off from the main macropinosome linked to the PM via the more stable tether, could have decreased the bulk fluid uptake and altered the macropinosome dynamics in these single mutants. Bulk fluid uptake interestingly, appeared to be

more severely reduced in the *WasA*$^{-}$ *WasB*$^{-}$ double mutants than what was observed in the *WasA*$^{-}$ single mutants, which suggested that WasA and WasB may play a functionally redundant role in efficiently resolving the tethers during macropinocytosis. In contrast, during phagocytosis I have shown that WasA appeared to play an important role in coordinating more rapid and efficient phagocytosis, with WasB seemingly being less important in regulating this process. It was not clear if either *WasA*$^{-}$ or *WasA*$^{-}$ *WasB*$^{-}$ mutants possessed any noticeable phagocytic defects. Phagocytosis also appeared in general to be less perturbed by the slower kinetics in these mutants of WASP in comparison to what was observed in macropinocytosis.

Chapter 6

Discussion of the main findings, and future questions to address how Dd5p4, Dd5p4 F&H interactors, and the WASP proteins regulate endocytosis in *D. discoideum*

6.1. Introduction

My PhD has been split into three main sections, the first was understanding how Dd5p4 regulated PIP and F-actin dynamics during macropinocytosis and phagocytosis and to understand how macropinocytic F-actin 'comets' formed in *D. discoideum Dd5p4*$^{-}$ mutants. The second part was understanding how the Dd5p4 F&H interactors regulated phagocytosis and macropinocytosis. The third and final section aimed to address how WasA, which was found on the heads of F-actin 'comets' in *Dd5p4*$^{-}$ mutants regulated macropinocytosis and phagocytosis, whilst also establishing if WasA and WasB displayed functional redundancy during these processes. A summary of the key findings I have discovered during my PhD project and how this links in with current knowledge in mammalian models, as well as the limitations encountered during this project, and the potential future studies to address unanswered questions will all be covered.

6.2. Insights into how Dd5p4/OCRL regulates endocytic F-actin dynamics during closure

In this project I have shown that the loss of Dd5p4 activity, caused a reduction in PI(4,5)P_2 hydrolysis at the centre of phagocytic cups and resulted in delayed F-actin disassembly at cup closure. This is similar to what has been shown in mammalian OCRL-deficient macrophages. In mammals, OCRL and its paralog, INPP5B, function collectively to deplete PI(4,5)P_2 levels resulting in the remodelling of actin and thereby phagosome formation. Rab5 is recruited to phagosomes during phagosome sealing, and Rab5 subsequently recruits the early adaptor, APPL1, followed by the OCRL and INPP5B inositol 5-phosphatase enzymes (Fig. 6.1.B.) (Bohdanowicz et al. 2012). Depletion of PI(4,5)P_2 and PI(3,4,5)P_3 prevents further activation of the kinase activity of Akt (Fig. 6.1.B.). The loss of Rab5 or APPL1 activity prevented OCRL and INPP5B localisation to the phagosome, which consequently increased the lifetime of PI(4,5)P_2 and F-actin on the membranes of phagosomes (Bohdanowicz et al. 2012). A summary of this mechanism is illustrated (Fig. 6.1.A-C.).

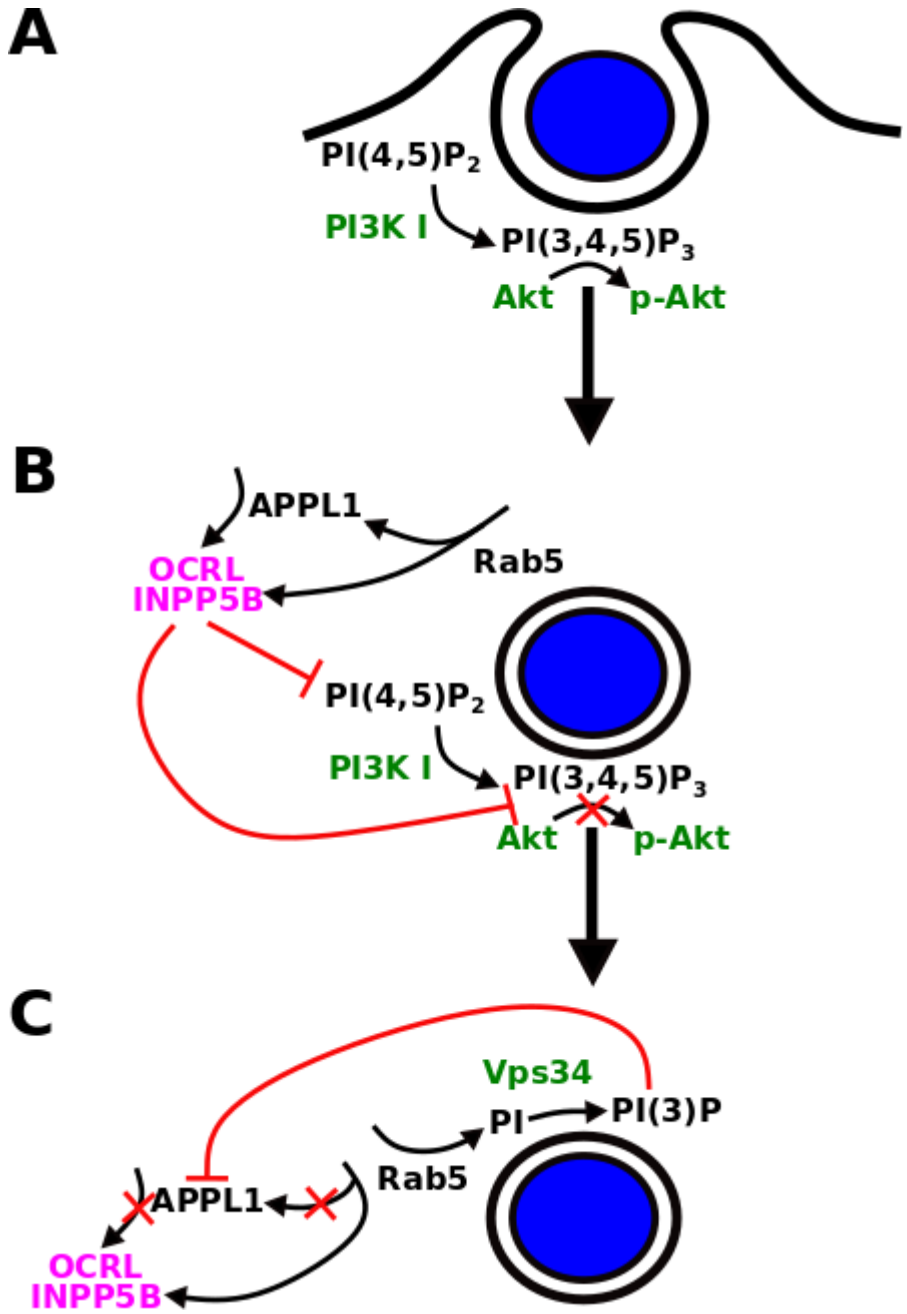

Figure 6.1. The roles of OCRL, Rab5, and APPL1 during the early stages of phagocytosis in macrophages. (A) During phagocytic cup formation PI(3,4,5)P_3 is synthesised from PI(4,5)P_2 phosphorylation by the PI3K class I kinase enzymes, which leads to the phosphorylation and activation of the kinase activity of Akt. (B) The phagosome is sealed, Rab5 is recruited, Rab5 then recruits APPL1, and subsequently the inositol 5-phosphatases, OCRL and INPP5B, which depletes any remaining PI(4,5)P_2 and PI(3,4,5)P_3, and thus prevents Akt activation. (C) Rab5 recruits the class III kinase activity of Vps34, which phosphorylates PI to PI(3)P. The accumulation of PI(3)P results in the dissociation of APPL1 from the maturing phagosome. Kinases are shown in green, phosphatases in magenta, activation reactions are shown by black arrows, and inhibitory pathways are shown in red. Yeast are shown in blue and the membrane of the phagosome is shown in white. Adapted from (Bohdanowicz et al. 2012).

There are some differences to highlight however, between this model and what I have shown in this PhD project. I have outlined that in *D. discoideum* Ax2 cells that PI(4,5)P_2 is depleted progressively by Dd5p4 enzymatic activity towards phagocytic cup closure, however PI(4,5)P_2 levels

were not completely depleted at closure. This was unlike what has been observed within macrophages, as the complete depletion of $PI(4,5)P_2$ was required to facilitate successful phagocytic engulfment (Bohdanowicz et al. 2012). I have also demonstrated that abolishment of the F&H interaction motif within Dd5p4 did not hinder phagocytic engulfment, which suggested that APPL1-like was not important for the recruitment of Dd5p4 and thus the hydrolysis of $PI(4,5)P_2$ in *D. discoideum*. It could be possible that Dd5p4 was alternatively recruited via its Rho-GAP domain by either active Ras or active Rac at the forming phagocytic cup.

In macrophages, another model has also been proposed, which involved the activities of the protein B-cell lymphoma/leukemia-10 (Bcl-10). This protein has been linked to a signalling complex assembly, which resulted in FcR, and antigen receptor-induced NF-κB activation, which regulated actin dynamics. Bcl-10 exerted its influence on actin dynamics through the regulation of vesicles, which possessed both AP1 and OCRL (Marion et al. 2012). The absence of Bcl-10 activity resulted in the impaired activation of both PI3K and Rac1. This resulted in the formation of phagocytic cups that were rich in $PI(4,5)P_2$, as well as Cdc42, and F-actin, which was rescued through the administration of low doses of the F-actin depolymerising drug, Lat-A (Marion et al. 2012). Bcl-10 was established to form a complex with the Clathrin adaptors; AP1, and Epsin-Related (EpsinR) proteins. The binding of Bcl-10 to AP1 resulted in the recruitment of OCRL to nascent phagocytic cups, which resulted in the subsequent hydrolysis of $PI(4,5)P_2$ at the base of phagocytic cups and F-actin depolymerisation and the consequent completion of phagosome closure (Marion et al. 2012). A summary of this mechanism is illustrated (Fig. 6.2.).

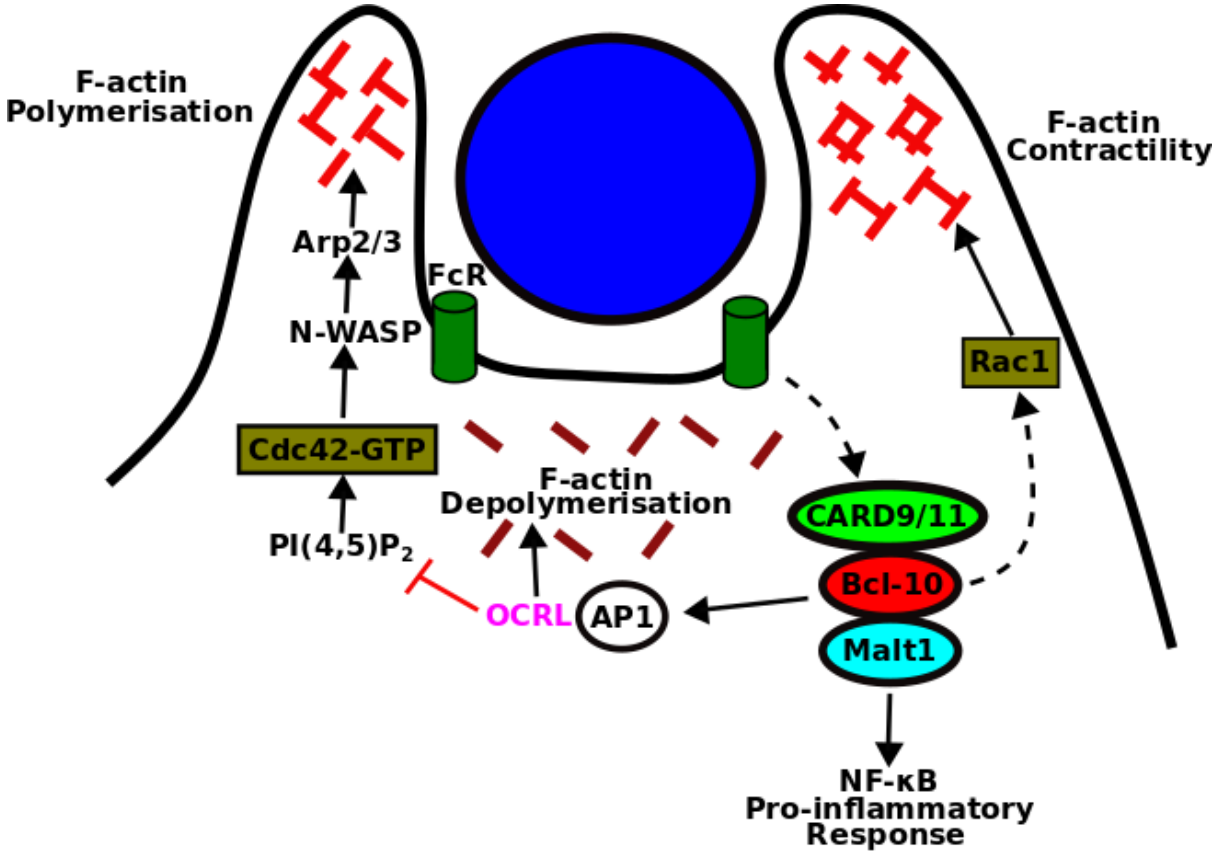

Figure 6.2. The mechanism at the base of phagocytic cups in macrophages involving OCRL and Bcl-10. Bcl-10 exists as a complex with the Caspase Recruitment Domain 9/11 (CARD9/11), and Mucosa-Associated Lymphoid Tissue Lymphoma Translocation Protein 1 (Malt1) proteins, which forms the Carma1-Bcl-10-Malt1 (CBM) signalling complex. Bcl-10 interacts with the AP1 adaptor, which recruits OCRL to nascent phagocytic cups within macrophages. Depletion of $PI(4,5)P_2$ by OCRL prevents Cdc42 activation, and the subsequent activation of N-WASP and the Arp2/3 complex, which thereby prevents F-actin polymerisation, and facilitates F-actin depolymerisation. Bcl-10 itself leads to the activation of PI3K and Rac1, which results in F-actin contractility. The combined activities of the FcR and the CBM complex results in the activation of NF-κB and the initiation of pro-inflammatory responses within macrophages. Adapted from (Marion et al. 2012).

These studies outlined that the roles that OCRL played at the base of phagocytic cups within macrophages did display a relatively similar picture to the data that I have shown on Dd5p4 enzymatic activity depleting $PI(4,5)P_2$ at the base of phagocytic cups at cup closure, which resulted in the disassembly of F-actin, and phagosome internalisation through the F-actin cortex and into the cytosol.

6.3. Comparison of the mechanism behind comet formation in *D. discoideum* and mammals

6.3.1. Insights into how *Dd5p4*$^-$ mutant cells formed F-actin 'comets'

I have shown that *D. discoideum* cells lacking Dd5p4 activity formed F-actin 'comets' after macropinocytic cup closure. These comets may have formed due to delayed F-actin disassembly at cup closure, which forced the macropinosomes and the associated F-actin away from the PM upon

internalisation. I also showed that WasA was recruited predominantly to the heads of F-actin 'comets' in these mutants (Fig. 6.3.A.). Surprisingly, however, hydrolysis of PI(4,5)P_2 at cup closure appeared to be relatively normal in *Dd5p4*$^-$ mutants, and PI(4,5)P_2 was also surprisingly not found at the heads of comets in these mutants. Interestingly however, PI(3,4,5)P_3 was found on the heads of these comets, which may have been sufficient to ensure the activation of WasA found predominantly at the comet heads in *Dd5p4*$^-$ (Fig. 6.3.A.) (Myers et al. 2005). The traces of WasA found on the comet tails may have also been sufficient to ensure the activation of the Arp2/3 complex, which was predominantly found at the tails of these comets (Fig. 6.3.A.). Collectively, these findings could have potentially explained how Arp2/3-mediated polymerisation took place. The depolymerisation of F-actin in the Ax2 control cells just after cup closure could suggest that WasA and other regulators of actin were somehow inactivated, although the precise mechanism for how this occurred still remains elusive. In control cells however, I did find that F-actin disassembly occurred upon the emergence of PI(3,4)P_2, however F-actin disassembly did not occur following the emergence of PI(3,4)P_2 in the *Dd5p4*$^-$ mutant. I suggested that this may somehow be due to the more rapid hydrolysis of PI(3,4,5)P_3 to PI(3,4)P_2 in *Dd5p4*$^-$, which may have potentially been orchestrated by the somehow upregulated activities of the inositol 5-phosphatases, Dd5p2 and/or Dd5p1, which may have a preference for the hydrolysis of PI(3,4,5)P_3 to PI(3,4)P_2 (Fig. 6.3.A.) (Loovers et al. 2003). This theory could explain why PI(3,4,5)P_3 were present on macropinosomes for a reduced duration after cup closure compared to control cells and why PI(3,4)P_2 were present on *Dd5p4*$^-$ macropinosome comets, and also remained on macropinosomes long after the comets had disappeared (Fig. 6.3.A.). The alteration of the dynamics of PI(3,4,5)P_3 and PI(3,4)P_2 on macropinosomes after cup closure may somehow have influenced the dynamics of F-actin, which may have given rise to the formation of comets in *Dd5p4*$^-$, the mechanism behind how these comets arose however, still remains unclear. Despite this I have outlined that PI(3,4,5)P_3 was present at the start of comet formation, but was hydrolysed during comet motility, most likely by Dd5p2 and/or Dd5p1 (Fig. 6.3.A.) (Loovers et al. 2003). PI(3,4)P_2 in contrast, was found to be localised to the heads of comets at the start of comet formation and did not appear to be depleted during comet motility, which suggested that comet motility could have reduced the enzymatic efficiency of an unidentified inositol 4-phosphatase to convert PI(3,4)P_2 to PI(3)P within *Dd5p4*$^-$ mutants (Fig. 6.3.A.). An alternative possibility for the increased lifetime of PI(3,4)P_2 following cup closure could be due to the kinase activity of PikF, which facilitates the phosphorylation of PI(4)P to PI(3,4)P_2 (Takeda et al. 2007, Hoeller et al. 2013) being somehow upregulated in the absence of Dd5p4 activity (Fig. 6.3.A.). I have however, demonstrated that the lifetime of PI(4)P on macropinosomes was indeed reduced in *Dd5p4*$^-$, which suggested that upregulation of PikF may have caused the reduced PI(4)P lifetime

on macropinosomes in *Dd5p4*$^{-}$ by orchestrating the increased phosphorylation rate of PI(4)P to PI(3,4)P_2 (Takeda et al. 2007, Hoeller et al. 2013). The combined activities of Dd5p2 and/or Dd5p1 inositol 5-phosphatases, and the kinase activity of PikF could somehow be upregulated together in the absence of Dd5p4 activity and may have contributed to the alterations in the dynamics of PI(3,4)P_2 after macropinocytic cup closure (Fig. 6.3.A.), although this would require further clarification.

6.3.2. Comparison of the mechanisms of comet formation in *Dd5p4*$^{-}$ with *OCRL*$^{-/-}$ mutant cells

In mammalian cells, OCRL regulates the dynamics of PIPs and F-actin during endocytosis, and like *Dd5p4*$^{-}$ cells, cells lacking OCRL enzymatic activity formed comets (Fig. 6.3.A-B.). LS disease pathology resulted from the ectopic PI(4,5)P_2 accumulation as a result of mutations within the *OCRL* locus, which thereby prevented hydrolysis of PI(4,5)P_2 to PI(4)P. Elevated levels of PI(4,5)P_2 resulted in increased N-WASP and consequently Arp2/3 complex activities, and thus resulted in F-actin polymerisation on the membranes of EEs (Fig. 6.3.B.) (Miki et al. 1996, Merrifield et al. 2004, Vicinanza et al. 2011).

Unlike what was observed in mammalian cells, I did find that the lifetime of PI(4)P on macropinosomes were reduced in *D. discoideum Dd5p4*$^{-}$ cells (Fig. 6.3.A-B.). I have however, not been able to clarify due to time constraints if PI(4)P were present on *Dd5p4*$^{-}$ comets, which made the role of PI(4)P in comet formation ambiguous (Fig. 6.3.A.).

PI(4,5)P_2 in mammals activates Cdc42, which is absent within *D. discoideum*, with Cdc42 subsequently activating various mammalian actin regulators, such as N-WASP (Fig. 6.3.B.). This highlighted differential WASP regulation in mammals compared to what has been shown in *D. discoideum* in which the presence of PI(4,5)P_2 and PI(3,4,5)P_3 were sufficient for WasA activation (Myers et al. 2005). I was not able to test the importance however, of high membrane curvature and the roles that the BAR-domain-containing proteins could have played within *D. discoideum* in the formation of comets due to time constraints. Despite this, it could be plausible to speculate that macropinosomes were larger in size and thus displayed much less curvature than the clathrin-mediated endosomes. In addition, comets also appeared to form on macropinosomes of all sizes in *D. discoideum*. In mammals, whilst PI(3)P was required for comet formation and was present on the rocketing endosomal membrane, PI(3)P was not found on the macropinosome comets in *D. discoideum Dd5p4*$^{-}$ cells (Fig. 6.3.A-B.). It was not clear what signal gave rise to macropinosome comet formation, but it appeared to be different from that found on mammalian clathrin-mediated endosomes.

It is also worth highlighting that all studies performed in mammals looked at comet formation during CME, whilst I on the other hand have studied comet formation during macropinocytosis in *D. discoideum* (Fig. 6.3.A-B.). There are some other differences between these two processes. Mammalian clathrin-derived endosomes possess numerous other proteins with notable examples including the AP-2 adaptor, a clathrin coat made up of the clathrin-light chain a (CLCa), the clathrin light chain b (CLCb), the CHC, N-WASP, and SNX9 (Motley et al. 2003, Huang et al. 2004, Mitsunari et al. 2005, Poupon et al. 2008, Ferreira et al. 2012, Biancospino et al. 2019). These proteins are all absent on macropinosomes. A direct comparison between *Dd5p4*$^{-}$ and *OCRL*$^{-/-}$ mutants is illustrated (Fig. 6.3.A-B.).

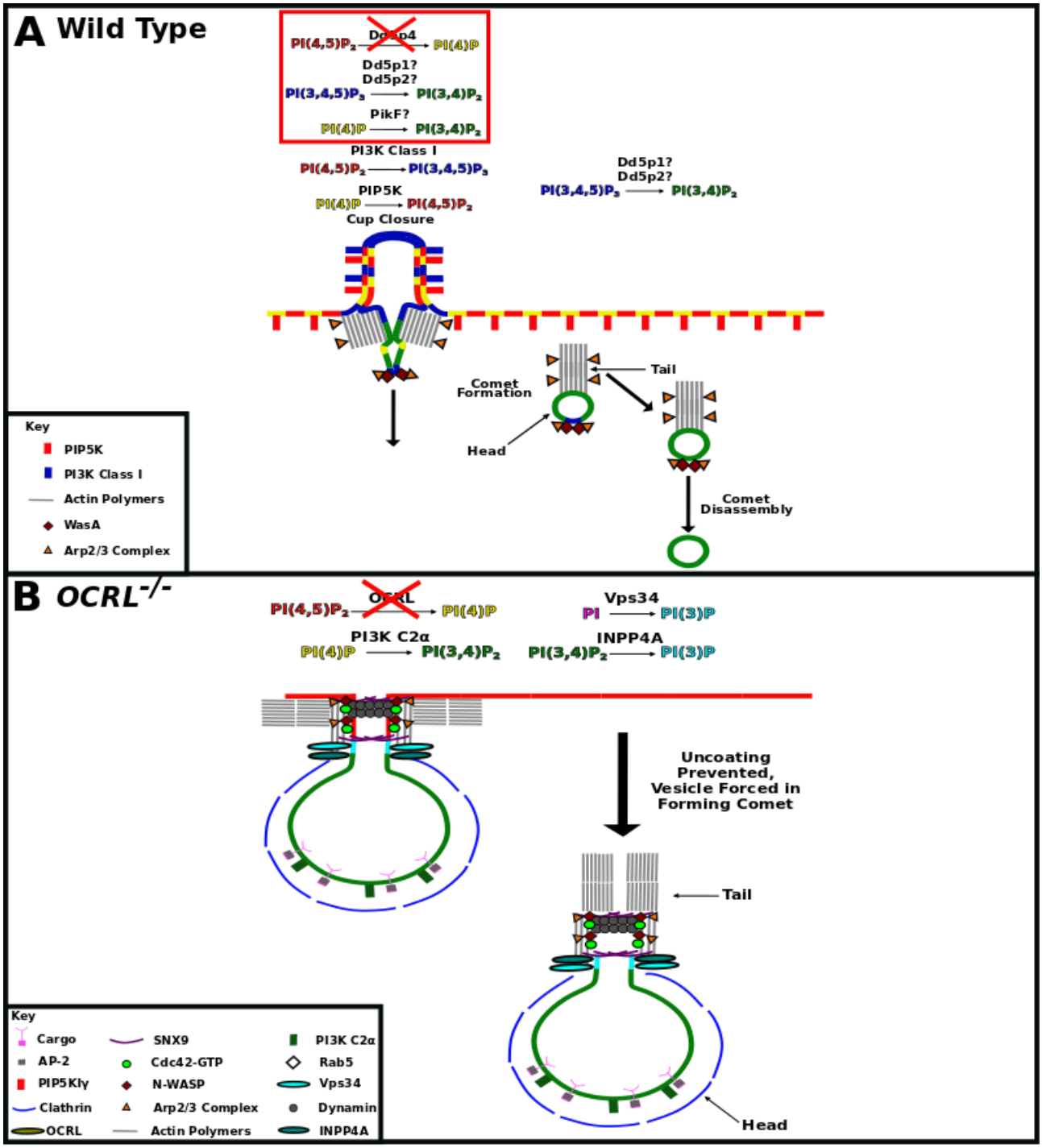

Figure 6.3. Mechanistic comparison of comet formation between *Dd5p4*$^{-}$ and *OCRL*$^{-/-}$ mutants. (A) The potential mechanism of F-actin 'comet' formation during macropinocytosis in axenic *Dd5p4*$^{-}$ mutant cells. PIP conversion reactions that are potentially affected as a result of the loss of Dd5p4 activity are indicated within a red box. (B) The mechanism of F-actin 'comet' formation during CME in RPE-1 cells lacking functional OCRL enzymatic activity. PIPs are colour-coded, and the various components of the actin machinery and the enzymes involved in comet formation are indicated.

6.4. Comparison of mammalian and *D. discoideum* PIP dynamics during macropinocytosis

This project has provided some insight into how Dd5p4 phosphatase activity regulated PIP dynamics during macropinocytosis and phagocytosis. Work done on this project, together with the

literature on PIP dynamics in *D. discoideum*, however showed some similarities and differences in comparison to mammals, in particular during macropinocytosis.

In mammalian cells, macropinocytic PI(4,5)P_2 accumulated at the start of cup formation and is completely degraded at closure (Welliver and Swanson 2012). In *D. discoideum*, a similar pattern of PI(4,5)P_2 levels were observed in this project, as PI(4,5)P_2 levels increased at cup formation and were depleted towards cup closure.

Earlier mammalian studies of PI(3,4,5)P_3, showed that PI(3,4,5)P_3 peaked just prior to cup closure in A431 cells and in macrophages, and was degraded earlier than what I have observed (Araki et al. 2007, Yoshida et al. 2009, Welliver and Swanson 2012). More recent studies however, using LLSM have shown that use of the Akt-PH probe, which binds to both PI(3,4,5)P_3 and PI(3,4)P_2 peaks just after cup closure in macrophages and decreases later on (Quinn et al. 2021). These more recent findings are very similar to what I have shown using LLSM for both PIPs in *D. discoideum*. The differences in the PIP dynamics that have been documented from the less recent studies within the literature could have been due to the lack of the highly sensitive and rapid image acquisition rate of LLSM technology that was available at the time to these less recent scientific investigations (Araki et al. 2007, Yoshida et al. 2009, Welliver and Swanson 2012).

I have also demonstrated that the emergence of PI(3)P in *D. discoideum* appeared to be instantaneous after macropinosome internalisation, which was very similar to the observations that have been made in mammals (Welliver and Swanson 2012).

6.5. Comparison of macropinocytosis and phagocytosis in *Dd5p4*$^-$

Macropinocytosis and phagocytosis are thought to be orchestrated by relatively similar mechanisms. The main difference however, is that in macropinocytosis cup formation occurs spontaneously in space, whilst the formation of a phagocytic cup takes place around a defined object, such as a yeast particle (Buckley and King 2017). A feature of phagocytosis, which differentiates it from macropinocytosis, is that phagocytosis is receptor-mediated, in which a specific group of receptors interacts with a multivalent, particulate ligand (Grinstein 2012). Another difference, which I have outlined in this project, was that there were differences in the PIP gradients formed during cup formation. The formation of much stronger PIP gradients around phagosomes may be due to the picket-fence model, which stated that engagement of receptors could have prevented PIP diffusion (Mylvaganam et al. 2018). At phagocytic cups, I showed that the gradient of PI(4,5)P_2 from the cup tips to the centre of cups increased progressively towards closure. The gradient increase of PI(4,5)P_2 towards closure was likely to be due to the increased need to stimulate greater levels of F-actin disassembly, thus allowing the entry of the phagosome through the F-actin

cortex. In contrast, during the early stages of macropinocytosis much smaller PIP gradients were observed, which may have been due to the smaller sized macropinocytic cups that formed. The smaller cups could have meant that less $PI(4,5)P_2$ formation was required, and therefore less $PI(4,5)P_2$ depletion would have been needed to stimulate F-actin disassembly at macropinocytic cup closure.

6.6. The roles of OCRL, and the mammalian OCRL F&H interactors in the primary cilia

In *D. discoideum*, conserved F&H interactors of the mammalian homologue of OCRL, Dd5p4, were identified (Luscher et al. 2019). Despite the conservation of these F&H interactors in *D. discoideum* I have however, shown that they appear to be less important in regulating both phagocytosis and macropinocytosis. I have outlined that the F&H motif interaction between Dd5p4 and GxcU, appeared to be important for the localisation of GxcU. GxcU itself possesses a DH domain, which provides a link with the regulation of the actin cytoskeleton (Luscher et al. 2019). In mammals, Frabin has been shown to play a role in the regulation of cell shape (Obaishi et al. 1998, Umikawa et al. 1999, Ono et al. 2000), although how or if GxcU regulated cell shape in *D. discoideum* currently remains unclear. Nevertheless, the interactions between Dd5p4 and GxcU in the regulation of GxcU localisation and the functional relevance of this would require further exploration. I have also shown that Dd5p4 recruitment to cups does not appear to rely on the F&H motif and that this recruitment takes place much earlier. This differed from mammals in which OCRL was recruited after cup closure, which also required binding with Rab5 and APPL1 (Bohdanowicz et al. 2012).

In *D. discoideum*, interactions between Dd5p4 and the Dd5p4 F&H interactors, APPL1-like and GxcU were however, important for the recruitment of Dd5p4 to the CV (Luscher et al. 2019). This suggested that this F&H motif does indeed direct the localisation of Dd5p4 during exocytic water discharge, but this F&H motif for unknown reasons, appeared to be less important during endocytosis.

Although a greater understanding of how OCRL regulated PIPs and endocytosis is required, more work also needs to be done on the OCRL F&H interactors; APPL1, Ses1/2, and Frabin. In mammals, it currently remains poorly understood as to how these F&H interactors regulated the activities of OCRL. The additional presence of the mammalian OCRL paralogue, INPP5B, which also possesses an F&H motif, adds further complication in determining how OCRL and its F&H interactors contributed to LS pathology. Unfortunately, myself and others, have not been able to pinpoint the localisation of Dd5p4 within *D. discoideum*, although I have speculated that it localises at the base of macro-endocytic cups. This would require clarification via future studies in order to ascertain and confirm where Dd5p4 exerts its catalytic activity in order to regulate macro-endocytosis.

Collectively, these future studies could also highlight additional similarities and differences in how OCRL and its homologue, Dd5p4, and their associated F&H interactors orchestrated endocytosis and trafficking in these systems.

6.7. Summary of the roles of Dd5p4 and WasA in *D. discoideum* during the early stages of macropinocytosis

A diagram focusing on the roles of Dd5p4 and WasA during the early stages of macropinocytosis in *D. discoideum* is illustrated (Fig. 6.4.).

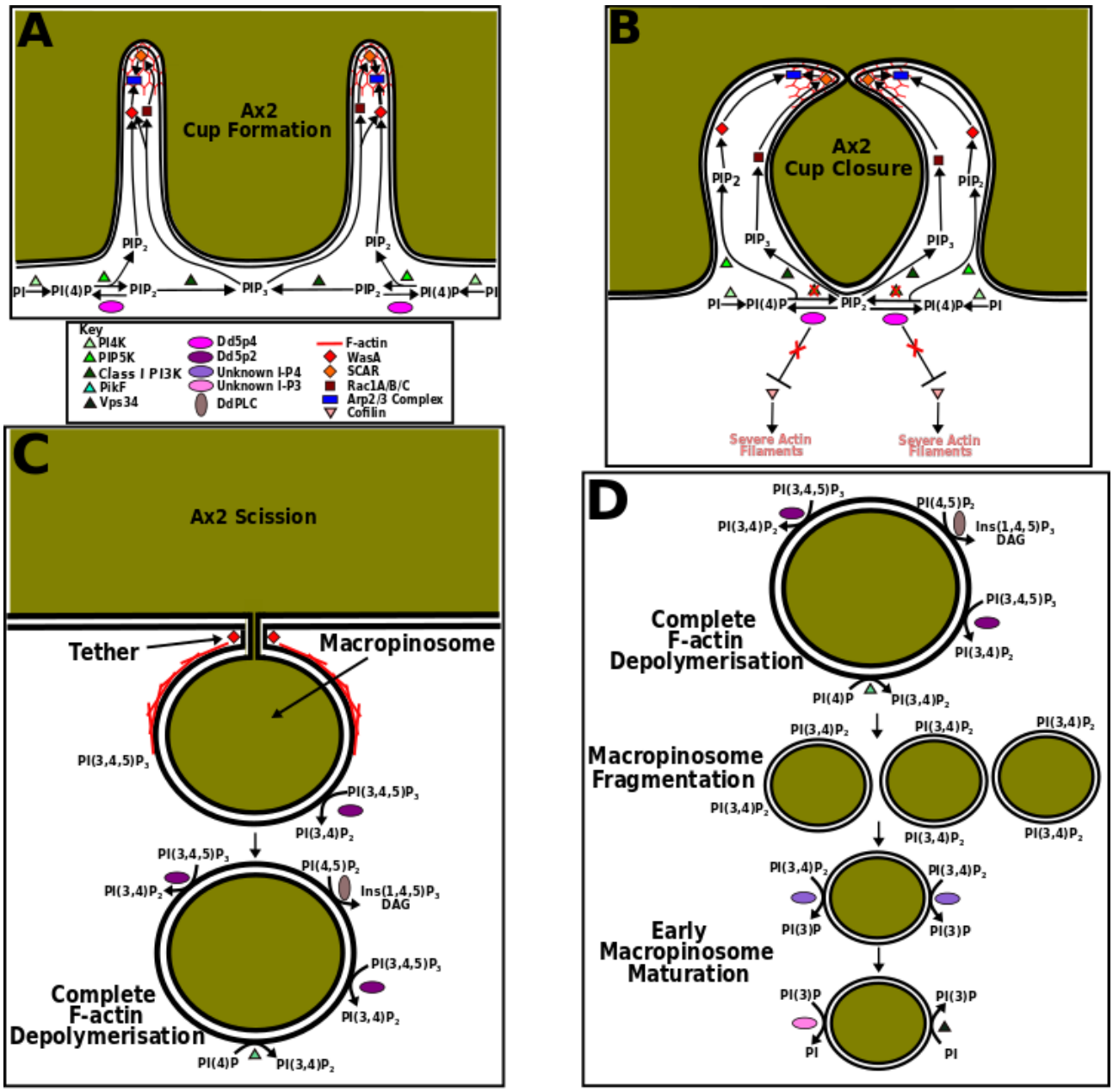

Figure 6.4. The possible roles that Dd5p4 and WasA played during the early stages of macropinocytosis in Ax2 cells. (A) Cup formation in Ax2 cells. (B) Cup closure in Ax2 cells. (C) Scission when WasA possibly recruited Dynamin A/B, which potentially cut the tethers and facilitated macropinosome internalisation. (D) The early stages of macropinosome processing and maturation. Proteins are indicated as coloured shapes shown in the key. In (A-B) $PI(3,4,5)P_3$ is (PIP_3), and $PI(4,5)P_2$ is PIP_2. Inositol 3-Phosphatase (I 3-P), Inositol 4-Phosphatase (I 4-P).

During cup formation $PI(4,5)P_2$ is synthesised by PIP5K, which activates WasA (Fig. 6.4.A.) (Myers et al. 2005). $PI(3,4,5)P_3$ synthesis occurs through class I PI3K kinase enzymatic activity, which activates WasA, with Rac1A/B/C activation subsequently activating SCAR (Dumontier et al. 2000). SCAR together with WasA results in Arp2/3-driven polymerisation at the cup tips. Dd5p4 at the cup base, starts to deplete $PI(4,5)P_2$ (Fig. 6.4.A.). At cup closure $PI(4,5)P_2$ is further depleted at the cup base by Dd5p4, which together with the inhibition of PIP5K, and the phosphorylation of $PI(4,5)P_2$, collectively frees the inhibition of the actin severing activity of cofilin (Fig. 6.4.B.) (Aizawa et al.

1995). At the final stage of scission WasA potentially recruits Dynamin A/B, which may cut the tethers and thus allow internalisation of the macropinosome (Fig. 6.4.C.). PI(3,4)P_2 is formed by PI(4)P phosphorylation by PikF, and/or de-phosphorylation of PI(3,4,5)P_3 by possibly Dd5p2 and/or Dd5p1, which potentially could facilitate the completion of F-actin removal (Loovers et al. 2003, Hoeller et al. 2013). Macropinosome fragmentation could then occur following PI(3,4)P_2 formation and F-actin depletion, with PI(3,4)P_2 being subsequently degraded by an unknown inositol 4-phosphatase to PI(3)P, which is then followed by progression to the early stages of macropinosome maturation (Fig. 6.4.D.).

6.8. Cofilin, an actin severing protein, which may be key to understanding how actin disassembly is coordinated during endocytosis in *D. discoideum*

I found that F-actin depolymerisation appeared to be delayed after macropinocytic cup closure in the absence of Dd5p4 activity, which resulted in comet formation. In order to understand how comets may have formed, future studies that could aim to understand how actin depolymerisation was regulated by proteins such as the actin severing cofilin, could well be important (Aizawa et al. 1995).

Fibroblasts from patients with LS displayed numerous defects including a reduction in the 300 kDa mannose 6-phosphate receptor (MPR300)-mediated uptake of the lysosomal enzyme, Arylsulfatase B, an increase in the surface number of MRP300, and contained enlarged retromer-positive endosomes that were highly enriched with MRP300 (van Rahden et al. 2012). OCRL-deficient cells displayed defects in the retrograde transportation of MRP300 to the TGN as a result of the lack of functional OCRL, which was established to be crucial for the regulation of the Rac1-cofilin signalling pathway (van Rahden et al. 2012). In cells lacking functional OCRL, the activities of Rac1 and RhoA decreased and increased respectively, which resulted in elevated levels of phosphorylated, inactive cofilin (van Rahden et al. 2012). RhoA functions to orchestrate the phosphorylation of cofilin via the Rho-associated Coiled-coil-containing protein Kinase/Lin11, Isl-1 and Mec-3 kinase (ROCK/LIM) pathway and thus, negatively regulate cofilin actin severing activity (Maekawa et al. 1999). Active Rac1 in contrast, orchestrated the de-phosphorylation of cofilin and thus positively regulated the actin severing activity of this protein (Pandey et al. 2009). This stated overall that an increase in PI(4,5)P_2 levels in OCRL-deficient cells negatively regulated the actin severing activity of cofilin (van Rahden et al. 2012). OCRL functions thereby to reduce the levels of PI(4,5)P_2 and in turn the levels of phosphorylation of cofilin via active Rac1, which thus allows cofilin to adopt its active conformation in order to orchestrate the severing of actin filaments (van Rahden et al. 2012).

It is not clear however, as to if and how cofilin was regulated in *D. discoideum Dd5p4*$^{-}$ mutants in comparison to Ax2 control cells, thus exploring the potential involvements of this actin severing protein may shed some light on the mechanism behind the delayed disassembly of F-actin after closure in *Dd5p4*$^{-}$ mutants.

6.9. How might work from this PhD project provide additional insights into work done on mammalian OCRL and the wider biological processes?

In this project I have demonstrated that F-actin 'comets' formed during macropinocytosis in *D. discoideum Dd5p4*$^{-}$ mutants. Previous studies within mammals have investigated the formation of comets in cells lacking functional OCRL activity in the setting of CME (Suchy and Nussbaum 2002, Allen 2003, Nandez et al. 2014, Daste et al. 2017), however no clear understanding of how these comets formed during macropinocytosis has thus far been unearthed. The data I have uncovered on how comets could have formed in *D. discoideum Dd5p4*$^{-}$ mutants during macropinocytosis may serve as a platform for studying how macropinocytosis could be affected within mammalian cells that lack functional OCRL. DCs are an example of a cell type within *H. sapiens* that performs constitutive macropinocytosis like axenic *D. discoideum* strains. DCs use constitutive macropinocytosis to constitutively capture antigens and present them on their cell surfaces (Sallusto et al. 1995, Norbury et al. 1997, West et al. 2000). Understanding how OCRL coordinates this process and if dysregulation of OCRL results in comet formation during constitutive macropinocytosis, like what I have observed within *D. discoideum Dd5p4*$^{-}$, may shed some light on the roles that OCRL may play on the presentation of antigens on the surfaces of DCs. Possible defects in macropinocytosis and the possible formation of comets in DC *OCRL*$^{-/-}$ mutants may inhibit the presentation of antigens on the cell surfaces of DCs, which could thereby prevent the coordination of immune responses in response to infection. This possibly could be a potential mechanism that pathogens may exploit in order to avoid immune detection. Thus, future studies focusing on DCs may aid to understand if comet formation could arise through macropinocytosis in mammals and if the dysregulation of this process in cells such as DCs could facilitate the avoidance of immune detection and thus pathogenic infection.

In the later stages of this project, I identified that 'flashes' of WasA were observed after macropinocytic cup closure in *D. discoideum* Ax2 control cells. The presence of WasA activity shortened the duration and the length of tethers that formed the final link between the macropinosome and the PM during macropinocytosis. This suggested that WasA played a role in the scission of these tethers, possibly through the recruitment of the Dynamin GTPase. In *H. sapiens*, however it is currently not known if flashes of either WASP or N-WASP occurred at macropinocytic

cup closure in cells such as DCs. It could therefore be of interest to observe if flashes of WASP/N-WASP occurred at macropinocytic cup closure in DCs and to pinpoint how WASP/N-WASP were recruited during closure of the macropinocytic cup if these WASP/N-WASP 'flashes' were observed. Additionally, it could also be of great interest to establish if proteins like the Dynamin GTPase and the curvature-sensing BAR domain-containing proteins also played a role in collaboration with WASP/N-WASP during the scission of macropinosomes from the PM of DCs. It could then be prudent to ascertain which if any of these proteins also associated with WASP/N-WASP during CME (Nandez et al. 2014, Daste et al. 2017) and to ascertain if there were any similarities into how scission was regulated during CME and macropinocytosis. Understanding the roles of WASP/N-WASP within cells of the immune system could provide a greater understanding of immune system functionality and also to pinpoint how dysregulation could potentially lead to the onset of diseases in *H. sapiens*.

6.10. Limitations on the work performed in this PhD project

During this PhD project there were some limitations that were encountered along the way as this work was performed. Firstly, despite the fact that most of the reporters used in this project were identified and verified within *D. discoideum* and were thus optimised for use in this organism, there were four probes that were used in this project, which were discovered and identified within different organisms, which were expressed within *D. discoideum*. For reasons that were unknown, the well-characterised Pleckstrin Homology-Phospholipase C isoform δ (PH-PLC-δ) probe, which has been shown to bind PI(4,5)P_2 and also displays strong homology with DdPLC (Drayer and Vanhaastert 1992), only exhibited cytosolic localisation when stably transfected into *D. discoideum*, which made this probe unsuitable. I therefore, as an alternative used the Nodulin-GFP probe, however this reporter was derived from *Arabidopsis* root hairs (Ghosh et al. 2015). Another probe that was also used and derived from another organism was that of the PI(4)P reporter, which was taken from the secreted effector protein, SidM, from the bacterial pathogen *Legionella pneumophila* (Hammond et al. 2014). The third probe was the TAPP1-PH PI(3,4)P_2 probe, which was derived from *H. sapiens* cDNA (Dowler et al. 2000). The fourth and final probe was the GxcU-GFP reporter, which was cloned from *D. intermedium* due to the problematic cloning difficulties encountered in trying to generate a *D. discoideum* GxcU-GFP fusion construct (Luscher et al. 2019). All four of these reporters, each from different organisms could have displayed different binding capabilities when stably expressed within *D. discoideum*, which could have led to these reporters behaving strangely within this organism. This problem could be avoided however, by cloning the residential *D. discoideum* PIP reporters and optimising them if necessary to facilitate non-lethal fusion protein expression.

All of the probes that were used in this project were stably expressed from extra-chromosomal DNA within *D. discoideum* cells, which does however, pose some disadvantages. The ligation of a fluorescent protein to the protein of interest could in some cases impair the function of the protein, and sometimes the stable expression of the construct could also adversely influence cellular functions (Jensen 2012). As an example an increase in the levels of TAPP1-PH-GFP expression following the stable transfection of this construct would bind and sequester more $PI(3,4)P_2$ than would normally be observed, which could potentially influence the endocytic processes under investigation, as well as other functions, and the overall behaviour of the cell. The adverse effects of stable extra-chromosomal fusion protein expression could be reduced through the generation of GFP knock-ins, which when under the regulation of the host promoter could ensure that the correct copy number of the protein is maintained. Use of GFP knock-ins and integration into the host genome could thus ensure that more physiological conditions are maintained within the cell (Fey and Cox 1997).

In all studies performed on the process of phagocytosis in *D. discoideum* in this PhD project I have exclusively used yeast. I have outlined during this project that there were differences in PIP dynamics during the different stages of cup closure between phagocytosis and macropinocytosis. These differences in PIP dynamics could also be due to the geometry and size of the object that is engulfed, which could consequently alter the PIP dynamics as a result. Some studies have used bacteria and some have used yeast when studying the process of phagocytosis within *D. discoideum* (Loovers et al. 2007, Davidson et al. 2018). Depending on the species of bacteria, some could be of differing shapes and sizes in comparison to the yeast that were used exclusively in this project. This suggests that the use of prey of differing sizes could therefore result in different biological outcomes when investigating the same cell line. This issue could be overcome by using the equivalent prey that were used in previous studies that investigated phagocytosis in relation to a particular protein or group of proteins, which could therefore allow more direct comparisons to be made on the biological outcomes between studies performed within different laboratories.

One of the issues with some of the data that were generated in this project was the reduced levels of reproducibility in some of the tested cell lines. An example of this was repeatedly observed in the phagocytosis of yeast in suspension assay, in which the Ax2 control cells in particular displayed in some cases considerable variation in the yeast to *D. discoideum* ratio between different day biological repeats. This biological variation could thereby have altered the statistical validity and conclusions that were drawn when mutant cell lines were compared to these Ax2 control cells. In other experiments such as the quantification of the time taken to enwrap yeast, there were differences between clones of the *Dd5p4*$^{-}$ *GxcU*$^{-}$ double mutants, which meant that conclusions

were thus ambiguous. To overcome these issues, six separate day biological repeats could be performed instead of the three that were performed for most of the experiments in this project. This would aid to make the data and conclusions drawn more reproducible and valid. Some of the experiments, which mostly centred on LLSM image analysis only consisted of a single biological repeat. To address this, like with all other experiments, six separate day biological repeats could also be performed to strengthen and make these data more reproducible and valid, whilst also ensuring that these biological effects were not just a spontaneous occurrence.

Another issue with some of the data generated in this project was that in the context of single and double mutant comparisons, cells were taken from experiments that were performed on different days. This would have thereby weakened and restricted statistical conclusions that could have been made from these data, whilst also introducing variation amongst different batches of the same cell line. To address this issue, separate day biological repeats could be performed for all control, single and double mutant cell lines at the same time, thus allowing valid statistical analyses such as the one-way Analysis Of Variance (one-way ANOVA) to be carried out between multiple cell lines. This could be performed for example between Ax2 control cells, *Dd5p4*$^{-}$ single mutants, *GxcU*$^{-}$ single mutants, and the *Dd5p4*$^{-}$ *GxcU*$^{-}$ double mutants in order to reduce the variability that may arise from different batches of the same cell line.

Another problem that was encountered during this project was the simple fact that the PIPs present in *D. discoideum* possess slightly different chemistry in comparison to the PIPs observed in *H. sapiens* (Clark et al. 2014). In *H. sapiens* the lipid ligated to the *sn*-1 part of the glycerol backbone is attached via an ester bond, whilst in *D. discoideum* this link occurs via an ether bond (Fig. 1.19.). The differences in lipid tail chemistry between PIP species could very well alter the behaviours of the PIPs observed in *H. sapiens* in comparison to the PIPs observed in *D. discoideum*, which could mean that direct comparisons between these species may not be valid. As an example PI(3)P in mammals is typically represented as C38:4 PI(3)P (1-stearoyl-2-arachidonoyl-*sn*-glycero-3-phospho-1D-*myo*-inositol 3-phosphate), whereas in *D. discoideum* PI(3)P would be represented as C34:1e PI(3)P [1-hexadecyl-2-(11Z-octadecenoyl)-*sn*-glycero-3-phospho-1D-*myo*-inositol 3-phosphate] (Clark et al. 2014, Barneda et al. 2019). A recent study has also demonstrated that acyl variants were present in the cells of the prostates of *Pten*-deficient mice in comparison to healthy control cells. In the cells of the prostates of *Pten*-deficient mice the levels of C32:0 PI(3,4,5)P_3 and C34:1 PI(3,4,5)P_3 were increased by approximately 50-fold in comparison to the healthy control cells in which the levels of C38:4 PI(3,4,5)P_3 were almost unaltered (Morioka et al. 2022). This suggests that different genetic backgrounds could very well influence the PIP lipid tail chemistry and the functionality of the PIPs in question, and thus the biological behaviours of different cell types.

6.11. Future studies

In this project clarifying the localisation of Dd5p4 proved to be problematic, however I speculated that Dd5p4 was likely to be recruited to the base of endocytic cups. To address and clarify this, integration of a Dd5p4-GFP fusion construct through the use of REMI into the genome could be performed. Dd5p4-GFP expression under the control of the host promoter may facilitate the generation of cell lines with endogenous expression of the fusion protein of the correct copy number, thus allowing a definitive localisation of Dd5p4 to be deduced (Fey and Cox 1997).

I speculated in this project that restricted cortex openings could potentially underlie the phagocytic and macropinocytic phenotypes of *Dd5p4*$^-$, however this was not verified. To validate this possible mechanism, *Dd5p4*$^-$ cells could be administered Texas red dextran, and the cells stably transfected with GFP-LifeAct to visualise the F-actin and clarify the movements of the Texas red dextran through the restricted cortex openings in *Dd5p4*$^-$. To verify the phagocytic phenotype of *Dd5p4*$^-$ mutants, cells could be administered beads of differing sizes and could be visualised using confocal imaging and separately quantified using larger cell populations via flow cytometry. These experiments could address whether cortex openings were reduced in these mutants and thus could only enable the successful phagocytic engulfment of smaller beads compared to those engulfed by Ax2 control cells.

I have shown that *Dd5p4*$^-$ comets may have been driven by enhanced PI(3,4,5)P_3 hydrolysis and PI(3,4)P_2 synthesis. In order to validate this theory studies involving the enzymatic activities of Dd5p2 and Dd5p1 could be performed. Firstly, Dd5p2 has been shown to have a preference for PI(3,4,5)P_3 hydrolysis (Loovers et al. 2003), so the stable expression of a Dd5p2-GFP fusion protein would firstly confirm if this enzyme was on the comets, and if this was the enzyme at least partly responsible for hydrolysing PI(3,4,5)P_3 to PI(3,4)P_2. A similar study could also be performed in reference to the Dd5p1 enzyme, whilst also using a Malachite assay (Ramadesikan et al. 2021) to confirm Dd5p1 substrate specificity, as this has not been specified to date (Loovers et al. 2003). If both of these enzymes were present on the comets then *Dd5p2*$^-$ *Dd5p4*$^-$ double mutants could be generated using CRISPR in the *Dd5p4*$^-$ mutant parental background, and *Dd5p1*$^-$ *Dd5p2*$^-$ *Dd5p4*$^-$ triple mutants subsequently generated using CRISPR in the *Dd5p2*$^-$ *Dd5p4*$^-$ parental background. The presence of comets could then be tested by the stable expression of mCherry-LifeAct and GFP-PH-PkgE [PI(3,4,5)P_3 binding] or TAPP1-PH-GFP [PI(3,4)P_2 binding] probes to analyse the PIP dynamics in the *Dd5p2*$^-$ *Dd5p4*$^-$ double mutants and the *Dd5p1*$^-$ *Dd5p2*$^-$ *Dd5p4*$^-$ triple mutants. These experiments could confirm the importance of these inositol 5-phosphatases in the formation of comets during macropinocytosis in *D. discoideum*. In addition, the importance of the kinase activity of PikF (Takeda et al. 2007, Hoeller et al. 2013), could also be tested by synthesising a PikF-GFP

fusion protein and stably expressing this together with mCherry-LifeAct within *Dd5p4*$^{-}$ mutants to assess if this kinase was present on the comets and thus was partly responsible for the synthesis of PI(3,4)P_2 from PI(4)P phosphorylation. If this was proven to be the case then *Dd5p1*$^{-}$ *Dd5p2*$^{-}$ *Dd5p4*$^{-}$ *PikF*$^{-}$ quadruple mutants could be generated using CRISPR in the *Dd5p1*$^{-}$ *Dd5p2*$^{-}$ *Dd5p4*$^{-}$ triple mutant parental background to address through the stable expression of mCherry-LifeAct, whether this kinase and the three inositol 5-phosphatases were collectively required for comet formation. The absence of comets in these *Dd5p1*$^{-}$ *Dd5p2*$^{-}$ *Dd5p4*$^{-}$ *PikF*$^{-}$ quadruple mutants could confirm this hypothesis.

Another aspect on which to possibly investigate how comets could have formed in *Dd5p4*$^{-}$ mutants could be through studying the activities of *D. discoideum* cofilin (Aizawa et al. 1995, Ichetovkin et al. 2000) with respect to Dd5p4. This could ascertain if Dd5p4 phosphatase activity and the reduction in PI(4,5)P_2 levels increased the actin severing activity of cofilin, and thus facilitated internalisation of the phagosome through the cortex. This could be tested through developing a cofilin-GFP fusion protein and stably expressing this in relation to the mCherry-LifeAct F-actin probe. Increased levels of cofilin-GFP in Ax2 cells after cup closure in areas of F-actin disassembly would suggest that the levels of active non-phosphorylated cofilin could be high to facilitate the severing of F-actin. In contrast, in the *Dd5p4*$^{-}$ mutant, cofilin-GFP would also be expected to increase after cup closure, however, F-actin disassembly would not occur, suggesting that cofilin may adopt its phosphorylated inactive state and thus could not severe F-actin after cup closure. This may suggest that the loss of Dd5p4 activity could have somehow increased the levels of phosphorylated inactive cofilin, much like what has already been observed in *H. sapiens* LS patient fibroblasts (van Rahden et al. 2012). This could be further clarified using GFP knock-ins of cofilin into both Ax2 and *Dd5p4*$^{-}$ backgrounds with point mutations at key phosphorylation sites to prevent cofilin phosphorylation and thereby prevent cofilin inactivation. If cofilin phosphorylation was prevented and comets were no longer observed in *Dd5p4*$^{-}$ mutants then this may clarify that the loss of Dd5p4 activity somehow increased the levels of cofilin phosphorylation and thus its consequent inactivation, preventing the severing of F-actin after macropinocytic cup closure. These investigations could therefore provide some insight into how comets could have formed in *D. discoideum Dd5p4*$^{-}$ mutants.

In this project I have outlined that the stable expression of Dd5p4^{D319G}-GFP in *Dd5p4*$^{-}$ did not rescue phagocytosis in these mutants, however the stable expression of Dd5p4^{W620A}-GFP in *Dd5p4*$^{-}$ was capable of rescuing phagocytosis in *Dd5p4*$^{-}$. To address if comets formed in *Dd5p4*$^{-}$ cells that were stably expressing these constructs, *Dd5p4*$^{-}$ could be separately stably transfected with Dd5p4^{D319G}-GFP, or Dd5p4^{W620A}-GFP, along with *Dd5p4*$^{-}$ stably expressing Dd5p4-GFP. Each Dd5p4

probe could then be visualised using confocal live-cell imaging together with the F-actin binding probe. This could determine the importance of active Dd5p4 catalytic phosphatase activity and intact Dd5p4 F&H binding in the formation of comets in *Dd5p4*$^{-}$ mutants. LLSM could also be used to quantify F-actin fold enrichment before and after cup closure to gain a greater understanding of how the catalytic activity and the F&H motif of Dd5p4 may influence F-actin dynamics during the early stages of macropinocytosis.

I have outlined that the Dd5p4 F&H motif appeared to be less important in the regulation of endocytosis in comparison to studies in mammals, which showed that this F&H motif was crucial for the recruitment of OCRL (Bohdanowicz et al. 2012). I have also demonstrated that *APPL1-like*$^{-}$ mutants did not mimic the phagocytic phenotype of *Dd5p4*$^{-}$ mutants, which collectively suggested that Dd5p4 recruitment occurred much earlier and may not appear to require APPL1-like and most likely Rab5 for recruitment to phagocytic cups. This differed to the observations in mammals, in which OCRL recruitment occurred just after closure of the cup, and required both Rab5 and APPL1 for its recruitment (Bohdanowicz et al. 2012). It was not clear as to how Dd5p4 itself was recruited to the base of endocytic cups in *D. discoideum*, however as Dd5p4 possesses a Rho-GAP domain this phosphatase may be recruited to endocytic cups via active Ras and/or active Rac (Loovers et al. 2003). To determine if Dd5p4 could bind to active Ras and/or active Rac, GST pull-down assays could be utilised to verify these interactions. Clarification of active Ras and/or active Rac binding to Dd5p4 could thereby provide a possible route for Dd5p4 recruitment to endocytic cups.

I have also demonstrated that in addition to $PI(3,4,5)P_3$ and $PI(3,4)P_2$, WasA and the Arp2/3 complex were also found on the comets in *Dd5p4*$^{-}$ mutants. In order to assess the importance of WasA in the formation of comets in *Dd5p4*$^{-}$, *Dd5p4*$^{-}$ *WasA*$^{-}$ double mutants could be generated via the use of CRISPR, and the double mutants subsequently stably transfected with the F-actin probe to visualise if comets could still form in these double mutants. GFP fusion proteins of two other *D. discoideum* WASP proteins, WasB and WasC, could also be visualised in *Dd5p4*$^{-}$ mutants to establish if these proteins were also present on the comets and could therefore perform functionally redundant roles in the activation of the Arp2/3 complex on comets in *Dd5p4*$^{-}$. The creation of *Dd5p4*$^{-}$ *WasA*$^{-}$ *WasB*$^{-}$ triple mutants and *Dd5p4*$^{-}$ *WasA*$^{-}$ *WasB*$^{-}$ *WasC*$^{-}$ quadruple mutants, each stably expressing the F-actin probe, could verify the potential functional redundancy of these three WASP proteins in coordinating Arp2/3-mediated F-actin polymerisation on the comets in the absence of Dd5p4 activity.

In this PhD project I have shown that 'flashes' of WasA formed at tethers during the scission of macropinosomes from the PM. It was not clear during macropinocytosis however, how WasA recruitment to these tethers occurred, and which other proteins were involved in the scission of

macropinosomes. Potential candidates could include the *D. discoideum* homologues of Dynamin, Dynamin A and Dynamin B, which may have been recruited to the tethers via WasA. To this end Dynamin GFP knock-ins could be created and imaged in parallel with the stable expression of RFP-WasA to confirm this potential recruitment. Stable expression of GFP-WasB in Ax2 control cells could also be investigated to address if flashes of WasB were also observed at macropinocytic cup closure, which could possibly indicate a functionally redundant role with WasA. If flashes of WasB were observed then the roles of WasB could also be investigated in tandem with WasA by LLSM imaging of the *WasA*$^{-}$ *WasB*$^{-}$ double mutants stably expressing the PI(3,4,5)P_3 GFP-PH-PkgE probe. This experiment would aim to address if the absence of both WasA and WasB increased both the length and the lifetime of the tethers, and to confirm if there was functional redundancy between WasA and WasB in coordinating the scission of tethers. The third WASP protein, WasC, could also be studied by the stable expression of a GFP-WasC fusion protein in Ax2 cells to ascertain if flashes of WasC were also observed at macropinocytic cup closure. If flashes of WasC were observed, then *WasA*$^{-}$ *WasB*$^{-}$ *WasC*$^{-}$ triple mutants could be created via CRISPR and could be subjected to LLSM imaging to clarify if there was functional redundancy with WasA, WasB, and WasC in coordinating the scission of tethers. The bulk fluid uptake of TRITC dextran across various time points could also be quantified in the *WasA*$^{-}$ *WasB*$^{-}$ *WasC*$^{-}$ triple mutants, the *WasA*$^{-}$ *WasB*$^{-}$ double mutants, and the *WasA*$^{-}$ single mutants, together with an Ax2 control. This could clarify if these three WASP proteins functioned together to coordinate the bulk uptake of extracellular fluid. To improve the visualisation of tethers and to clarify the movement of fluid in each of these WASP mutants, mutant cells stably expressing GFP-PH-PkgE could be administered Texas red dextran and imaged under LLSM to confirm the movements of fluid during the early stages of macropinocytosis in these WASP mutants.

I have outlined in this project that GxcU played a role in coordinating successful phagocytic engulfment, although the precise mechanism behind how this was achieved was not clear. GxcU itself possesses a DH domain, which may provide a link with the actin cytoskeleton (Luscher et al. 2019). This could therefore provide a link to the regulators of actin such as WASP, SCAR, and WASH, as well as all of the Rac proteins, which could be tested using pull-down assays to try and pinpoint how GxcU could influence the actin cytoskeleton during the early stages of endocytosis. Any hits from these pull-down assays could each be subsequently visualised using confocal microscopy in relation to F-actin in order to address how GxcU could regulate the actin cytoskeleton in axenic culture and in the presence of yeast. I did outline that *GxcU*$^{-}$ mutants may have had a potential defect in being able to enwrap yeast following the establishment of initial contacts, which may have been the cause of phagocytic defects in these mutants. This suggested that GxcU could somehow regulate the expression of various phagocytic receptors such as SibA, LmpB, and fAR1, during the

stage of particle recognition. This could be verified through the creation of cell lines, each containing a separate phagocytic receptor GFP knock-in, which through live-cell imaging could confirm if the expression levels of each of the phagocytic receptors were altered in *GxcU*$^{-}$ mutants in comparison to Ax2 control cells.

In this project I have showed that the stable expression of DiGxcU-GFP in *GxcU*$^{-}$ mutants caused puncta to form near to the cell surface PM, which may have been the potential sites of macropinocytic cup formation. The functional relevance however, of DiGxcU-GFP localisation to the base of these possible macropinocytic cups was thus far unclear, but could be further clarified through performing confocal time-lapses of Ax2 cells and *GxcU*$^{-}$ mutants stably expressing DiGxcU-GFP. This may pinpoint if this fusion protein localised to sites of macropinocytic cup formation in the absence of endogenous GxcU, which could also be assessed in the presence of yeast to see if similar observations were made during phagocytosis.

Interestingly, I have demonstrated that *Dd5p4*$^{-}$ *GxcU*$^{-}$ double mutants possessed a unique phagocytic phenotype in comparison to the *Dd5p4*$^{-}$ and *GxcU*$^{-}$ single mutants. It was not clear as to why there were defects in phagocytosis in these double mutants due to the limited time resolution and the lack of a more prudent PIP marker to label the later stages of phagocytosis where failure may have occurred. To potentially uncover the mechanism of phagocytic failure in these double mutants, time-lapses with much greater time coverage of up to at least 1 hour could be performed together with the stable expression of a dual expression probe employing the $PI(3,4,5)P_3$ PkgE probe and the novel SnxA probe, which binds to $PI(3,5)P_2$. This could visualise the progression of events from phagocytic cup formation to the stages of the later phagosome, potentially providing more certainty in the quantification of the phagocytic failure rate of these double mutants, as well as to pinpoint when engulfment failure occurred. These time-lapses could also be compared to the respective single mutants, along with an Ax2 control stably expressing the same dual fluorescent probe. Beads of varying sizes could also be tested and visualised using confocal microscopy and in parallel using flow cytometry to validate if cortex openings were also somehow altered in the *Dd5p4*$^{-}$ *GxcU*$^{-}$ double mutants. In both phagocytosis and macropinocytosis I demonstrated that GxcU and Dd5p4 performed distinct functional roles during both macro-endocytic processes, however, how GxcU functioned in accordance with Dd5p4 to coordinate macro-endocytosis remained unclear. This could possibly be unearthed via visualising endogenous GxcU in Ax2 control cells through the creation of GFP knock-ins. These GFP knock-ins could be created using a near-'PAMless' recently developed and engineered *Streptococcus pyogenes* Cas9 variant (SpRY) that has been shown to work within *D. discoideum* (Asano et al. 2021). A similar system could also be developed and optimised in *D. discoideum* to generate Dd5p4 RFP knocks-ins to allow the visualisation of both

endogenous GxcU and endogenous Dd5p4 within Ax2 cells, and thus pinpoint how they both may function to coordinate macro-endocytosis.

I have demonstrated that APPL1-like had a minimal part to play in the regulation of phagocytosis and could have played a more indirect role through the regulation of exocytic water discharge via the CV (Luscher et al. 2019). To this end *APPL1-like*$^{-}$ mutants could be studied in comparison to Ax2 control cells through the application of the FM4-64 dye, which labels CV membranes (Heuser et al. 1993, Nishihara et al. 2007). The rate of exocytosis could then be compared between Ax2 control cells and *APPL1-like*$^{-}$ mutant clones, which could indicate if the absence of APPL1-like impacted the exocytic water discharge rate. The rate of exocytosis could also be quantified from rescue experiments in which Ax2 cells and *APPL1-like*$^{-}$ mutant clones could be stably transfected with the APPL1-like-GFP construct and separately with an APPL1-like-GFP construct possessing a point mutation within the F&H motif, which would prevent F&H motif binding. The combinatorial roles of Dd5p4 and APPL1-like in the regulation of exocytic water discharge could be further clarified through the generation of *APPL1-like*$^{-}$ *Dd5p4*$^{-}$ double mutants via CRISPR. Quantification of the exocytosis rate of *APPL1-like*$^{-}$ *Dd5p4*$^{-}$ double mutants could be compared to that of the *APPL1-like*$^{-}$ single mutant clones and the *Dd5p4*$^{-}$ single mutants using the FM4-64 dye. A combinatorial role of APPL1-like and Dd5p4 in exocytic water discharge could be confirmed if the rate of exocytosis was significantly slower in the double mutant than in both respective single mutants.

In this project I have shown that Ses1/2-like played a more crucial role in the regulation of phagocytic engulfment. The increase in the time taken to enwrap yeast may have suggested that similar to GxcU, the Ses1/2-like protein may also somehow have influenced the expression of various phagocytic receptors. The difference in *Ses1/2-like*$^{-}$ mutants however, could be that the initial number of phagocytic receptors on the cell surface may have been sufficient to allow the establishment of initial contacts with yeast. The subsequent stage of enwrapping could have been slowed in these mutants due to slowed phagocytic receptor recycling to the PM following the initial binding of yeast. This could be tested through the creation of GFP knock-ins of receptors like SibA, LmpB, and fAR1, which would aim to track and verify the levels of each phagocytic receptor on the cell surface of *Ses1/2-like*$^{-}$ mutants during the process of enwrapping fluorescent yeast in comparison to Ax2 control cells. I have also shown that these mutants displayed a possible slight overlap with the *Dd5p4*$^{-}$ phagocytic phenotype, however the phagocytic defects of the *Ses1/2-like*$^{-}$ mutants were less severe. To test if these observations displayed a degree of similarity to the potential *Dd5p4*$^{-}$ phagocytic phenotype, then beads of differing sizes could be applied to the *Ses1/2-like*$^{-}$ and *Dd5p4*$^{-}$ single mutants. This experimental setup would assess if the differences in the

severity of the phagocytic defects were due to the differences in the sizes of the cortex openings. If the cortex openings were reduced to a lesser degree in the *Ses1/2-like*$^{-}$ single mutant in comparison to the *Dd5p4*$^{-}$ single mutant, then larger sized beads could enter the cytosol in the *Ses1/2-like*$^{-}$ mutants than in *Dd5p4*$^{-}$ mutants. If both of these single mutants displayed varying phagocytic defects as a result of differences in the sizes of cortex openings then *Dd5p4*$^{-}$ *Ses1/2-like*$^{-}$ double mutants could be created via CRISPR and subsequently tested. If the double mutants only allowed beads into the cytosol, which were smaller than those compared to either respective single mutant cell line then this could establish a functional link between Dd5p4 and the Ses1/2-like in coordinating successful phagocytic engulfment.

A shared feature of both *APPL1-like*$^{-}$ and *Ses1/2-like*$^{-}$ mutants during phagocytosis was that both sets of mutants displayed significant increases in the time taken to internalise phagosomes. The increases in the time taken to internalise phagosomes in both sets of mutants could be due to delays in the onset of acidification. This could be confirmed through live-cell imaging of *APPL1-like*$^{-}$ and *Ses1/2-like*$^{-}$ mutant clones engulfing pH-sensitive pHrodo-labelled yeast, with the changes in fluorescence monitored during phagocytosis to establish if there were delays in phagosome internalisation due to delays in acidification.

In this project I have demonstrated that both *APPL1-like*$^{-}$ and *Ses1/2-like*$^{-}$ mutants displayed very similar macropinocytic phenotypes. Both APPL1-like and Ses1/2-like could have possibly played a role in the regulation of the bulk uptake of fluid, which was speculated as more numerous, normal-sized macropinosomes were observed in both sets of mutants. This theory could be tested through performing macropinocytosis assays, in which both sets of mutants could be given TRITC dextran over various time points in comparison to Ax2 cells (Williams and Kay 2018). A higher fluorescence output in these mutants could suggest a role in the regulation of bulk fluid uptake. If the loss of either APPL1-like or Ses1/2-like displayed no changes in the fluorescence output then this could alternatively be due to delays in the onset of acidification. The pH-sensitive FITC dextran that I have used in the analyses of early, non-acidic macropinosome dynamics in both mutant sets in this project may have showed not only newly formed macropinosomes, but also macropinosomes in which the onset of acidification was delayed. To validate this theory, confocal time-lapses of the *APPL1-like*$^{-}$ mutants and *Ses1/2-like*$^{-}$ mutants taking up pHrodo red dextran could be performed. This dextran is dark when present in the extracellular environment, however following macropinosome internalisation, a bright-red fluorescent signal would be emitted, which would indicate progression to endosomal acidification (Meena and Kimmel 2018). This setup could allow the tracking of nascent macropinosomes and the quantification of the time taken from macropinosome formation to the onset of acidification, which could clarify if acidification was

delayed in both of these mutants. To provide further clarification of the possible roles of APPL1-like and Ses1/2-like in the regulation of acidification, then APPL1-like and Ses1/2-like GFP knock-ins could be created to generate the optimal copy number and provide a definitive localisation of the APPL1-like and the Ses1/2-like proteins (Luscher et al. 2019).

Chapter 7

Appendix

7.1. Python script for measuring PI(4,5)P_2/PI(4)P levels across phagocytic and macropinocytic cups.

```
#!/usr/bin/env python3
import os, pandas, string, numpy as np, scipy as sp, scipy.interpolate, matplotlib.pyplot as plt, configparser
from tkinter import Tk
from tkinter.filedialog import  askopenfilename

class Config():
    #collects configuration data and saves as 'master'.
    def __init__(self):
        self.write_config()
        self.configpoo = configparser.RawConfigParser(allow_no_value=True)
        res = self.configpoo.read("config.yml")



        #asks user for input file and defines input + output directories.
        Tk().withdraw()
        self.input_path = askopenfilename()
        self.output_dir, self.input_file = os.path.split(self.input_path)
        self.filename, self.input_ext = os.path.splitext(self.input_file)
        self.output_file = str(self.filename) + "_processed"
        self.output_ext = "csv"

        #runs configuration input
        self.input_file_setup()
        self.fix_inputs()
        self.check_inputs()

    def write_config(self):
        configfile_name = "config.yml"
        if not os.path.isfile(configfile_name):
            #Create the configuration file as it doesn't exist yet
            cfgfile = open(configfile_name, 'w')
```

```
        # Add content to the file
        Config = configparser.ConfigParser()
        Config.add_section("main")
        Config.set("main", "linescans_sheet_name", "linescans") #input name of sheet with the linescans on. suggested: 'linescans'
        Config.set("main", "linescans_first_row", "3") #input the row number of the first value in the excel spreadsheet.
        Config.set("main", "linescans_last_row", "303")  #input the row number of the last value in the excel spreadsheet - don't worry if not all columns go this deep.
        Config.set("main", "linescans_first_col", 'B') #input column letter of the first value in the excel spreadsheet.
        Config.set("main", "linescans_last_col", 'AE') #input the column letter of the last value in the excel spreadsheet.


        Config.set("main", "backgrounds_sheet_name", 'background') #input name of sheet with the linescans on. suggested: 'background'
        Config.set("main", "backgrounds_cytosolic_row", "3") #input the row number of the cytosolic_background row in the excel spreadsheet.
        Config.set("main", "backgrounds_nonprotruding_row", "4") #input the row number of the nonprotruding_background row in the excel spreadsheet.
        Config.set("main", "backgrounds_first_col", 'B') #input column letter of the first value in the excel spreadsheet.
        Config.set("main", "backgrounds_last_col", 'AE') #input the column letter of the last value in the excel spreadsheet.


        Config.write(cfgfile)
        cfgfile.close()
    def input_file_setup(self):
        #USER: input any changable variables here.
        self.vals_per_repeat = 10 #input the number of values per repeat.

        self.linescans_sheet_name = self.configpoo.get("main", "linescans_sheet_name") #input name of sheet with the linescans on. suggested: 'linescans'
```

```
        self.linescans_first_row = 3 #input the row number of the first value in the excel spreadsheet.
        self.linescans_last_row = 303  #input the row number of the last value in the excel spreadsheet - don't worry if not all columns go this deep.
        self.linescans_first_col = 'B' #input column letter of the first value in the excel spreadsheet.
        self.linescans_last_col = 'AE' #input the column letter of the last value in the excel spreadsheet.


        self.backgrounds_sheet_name = 'background' #input name of sheet with the linescans on. suggested: 'background'
        self.backgrounds_cytosolic_row = 3 #input the row number of the cytosolic_background row in the excel spreadsheet.
        self.backgrounds_nonprotruding_row = 4 #input the row number of the nonprotruding_background row in the excel spreadsheet.
        self.backgrounds_first_col = 'B' #input column letter of the first value in the excel spreadsheet.
        self.backgrounds_last_col = 'AE' #input the column letter of the last value in the excel spreadsheet.

    def fix_inputs(self):
        #fixes user inputs (from input_file_setup) so they are in pandas readable format.
        self.linescans_first_row -= 2
        self.linescans_last_row -= 2
        self.linescans_first_col = letter_to_int(self.linescans_first_col)-1
        self.linescans_last_col = letter_to_int(self.linescans_last_col)

        self.backgrounds_cytosolic_row -= 2
        self.backgrounds_nonprotruding_row -= 2
        self.backgrounds_first_col = letter_to_int(self.backgrounds_first_col)-1
        self.backgrounds_last_col = letter_to_int(self.backgrounds_last_col)

    def check_inputs(self):
        #check for possible errors in input
        if((self.linescans_last_col - self.linescans_first_col) != (self.backgrounds_last_col - self.backgrounds_first_col)):
            #check for linescan and background columns being unequal.
```

```
        print("ERROR. Your linescan and background data does not match.")
        print("Please select the same number of columns for linescan as background.")
        print("Exiting...")
        exit()

class Data_formatting():
    #extracts data from excel document into pandas DataFrames.
    def __init__(self, master):
        linescans = pandas.read_excel(master.input_path, sheet_name=master.linescans_sheet_name)
        linescans = pandas.DataFrame(linescans)
        self.linescans = linescans.iloc[master.linescans_first_row:master.linescans_last_row, master.linescans_first_col:master.linescans_last_col]

        backgrounds = pandas.read_excel(master.input_path, sheet_name=master.backgrounds_sheet_name)
        backgrounds = pandas.DataFrame(backgrounds)
        self.cytosolic_backgrounds = backgrounds.iloc[master.backgrounds_cytosolic_row, master.backgrounds_first_col:master.backgrounds_last_col]
        self.nonprotruding_backgrounds = backgrounds.iloc[master.backgrounds_nonprotruding_row, master.backgrounds_first_col:master.backgrounds_last_col]

def process_data(linescans, cytosolic_backgrounds, nonprotruding_backgrounds):
    #reads data from pandas DataFrame and processes it.

    output_df = pandas.DataFrame()
    #defines the final output variable.


    for i in range(0, len(linescans.columns)):
        #loops through each column in linescans

        col = linescans[linescans.columns[i]]
```

```
    col = col.dropna()
    col_len = len(col)
    #removes blank values from column and saves length.


    x = range(1,col_len+1)
    y = col
    spl = sp.interpolate.InterpolatedUnivariateSpline(x, y, ext=3)
    #plots a spline. uses column length as x (ie from 0 to col_len) and the column data as y.

    interval = np.linspace(1, col_len, 1000)
    #calculatse new interval.

    #plot_graph(spl, col, col_len)
    ##plots a graph of both datas:

    output_serise = []
    #definds an intermediate output variable.
    for j in range(0,len(interval)):
        #loops through the new interval to read from the spline.
        val = spl(interval[j])
        cytosolic_background = cytosolic_backgrounds[i]
        nonprotruding_background = nonprotruding_backgrounds[i]
        #retreves all information from the spline and backgrounds.

        val_ratio = (val-cytosolic_background)/(nonprotruding_background-cytosolic_background)
        #calculates val_ratio as: (spline_reading-
cytosolic_background)/(nonprotruding_background-cytosolic_background)

        output_serise.append(val_ratio)
        #append the val_ratio to the output list.

    output_serise = pandas.Series(output_serise)
    output_df[str(i)] = output_serise
```

```
        #turns the output into a DataFrame

    return output_df

def averaging(master, output_df):
    mean = output_df.mean(axis=1)
    sd = output_df.std(axis=1)
    average_df = pandas.DataFrame()
    average_df.insert(0, "mean", mean, True)
    average_df.insert(1, "sd", sd, True)
    return average_df
    #master.vals_per_repeat



def output_data(master, output_df):
    output_df.to_csv(os.path.join(master.output_dir, master.output_file + "." + master.output_ext))

def plot_graph(spl, col, col_len):
    xs = np.linspace(1, col_len, 81)
    plt.figure()
    plt.plot(xs, spl(xs)) #spline line
    col.plot() #original data
    plt.show()

def letter_to_int(col):
    num = 0
    for c in col:
        if c in string.ascii_letters:
            num = num * 26 + (ord(c.upper()) - ord('A')) + 1
    return num

def run():
    master = Config()
    data = Data_formatting(master)
```

```
    output_df = process_data(data.linescans, data.cytosolic_backgrounds,
data.nonprotruding_backgrounds)
    #output_df = averaging(master, output_df)
    output_data(master, output_df)

run()
```

7.2. Python script for measuring PI(3,4,5)P_3 levels across phagocytic and macropinocytic cups.

```
#!/usr/bin/env python3
import os, pandas, string, numpy as np, scipy as sp, scipy.interpolate, matplotlib.pyplot as plt, configparser
from tkinter import Tk
from tkinter.filedialog import  askopenfilename

class Config():
    #collects configuration data and saves as 'master'.
    def __init__(self):
        self.write_config()
        self.configpoo = configparser.RawConfigParser(allow_no_value=True)
        res = self.configpoo.read("config.yml")



        #asks user for input file and defines input + output directories.
        Tk().withdraw()
        self.input_path = askopenfilename()
        self.output_dir, self.input_file = os.path.split(self.input_path)
        self.filename, self.input_ext = os.path.splitext(self.input_file)
        self.output_file = str(self.filename) + "_processed"
        self.output_ext = "csv"

        #runs configuration input
        self.input_file_setup()
        self.fix_inputs()
        self.check_inputs()

    def write_config(self):
        configfile_name = "config.yml"
        if not os.path.isfile(configfile_name):
            #Create the configuration file as it doesn't exist yet
            cfgfile = open(configfile_name, 'w')
```

```
        # Add content to the file
        Config = configparser.ConfigParser()
        Config.add_section("main")
        Config.set("main", "linescans_sheet_name", "linescans") #input name of sheet with the linescans on. suggested: 'linescans'
        Config.set("main", "linescans_first_row", "3") #input the row number of the first value in the excel spreadsheet.
        Config.set("main", "linescans_last_row", "303")  #input the row number of the last value in the excel spreadsheet - don't worry if not all columns go this deep.
        Config.set("main", "linescans_first_col", 'B') #input column letter of the first value in the excel spreadsheet.
        Config.set("main", "linescans_last_col", 'AE') #input the column letter of the last value in the excel spreadsheet.


        Config.set("main", "backgrounds_sheet_name", 'background') #input name of sheet with the linescans on. suggested: 'background'
        Config.set("main", "backgrounds_nonprotruding_row", "3") #input the row number of the nonprotruding_background row in the excel spreadsheet.
        #Config.set("main", "backgrounds_intracellular_row", "4") #input the row number of the intracellular_background row in the excel spreadsheet.
        Config.set("main", "backgrounds_first_col", 'B') #input column letter of the first value in the excel spreadsheet.
        Config.set("main", "backgrounds_last_col", 'AE') #input the column letter of the last value in the excel spreadsheet.


        Config.write(cfgfile)
        cfgfile.close()
    def input_file_setup(self):
        #USER: input any changable variables here.
        self.vals_per_repeat = 10 #input the number of values per repeat.

        self.linescans_sheet_name = self.configpoo.get("main", "linescans_sheet_name") #input name of sheet with the linescans on. suggested: 'linescans'
```

```
        self.linescans_first_row = 3 #input the row number of the first value in the excel spreadsheet.
        self.linescans_last_row = 303  #input the row number of the last value in the excel spreadsheet - don't worry if not all columns go this deep.
        self.linescans_first_col = 'B' #input column letter of the first value in the excel spreadsheet.
        self.linescans_last_col = 'AE' #input the column letter of the last value in the excel spreadsheet.


        self.backgrounds_sheet_name = 'background' #input name of sheet with the linescans on. suggested: 'background'
        self.backgrounds_nonprotruding_row = 3 #input the row number of the nonprotruding_background row in the excel spreadsheet.
        #self.backgrounds_intracellular_row = 4 #input the row number of the intracellular_background row in the excel spreadsheet.
        self.backgrounds_first_col = 'B' #input column letter of the first value in the excel spreadsheet.
        self.backgrounds_last_col = 'AE' #input the column letter of the last value in the excel spreadsheet.

    def fix_inputs(self):
        #fixes user inputs (from input_file_setup) so they are in pandas readable format.
        self.linescans_first_row -= 2
        self.linescans_last_row -= 2
        self.linescans_first_col = letter_to_int(self.linescans_first_col)-1
        self.linescans_last_col = letter_to_int(self.linescans_last_col)

        self.backgrounds_nonprotruding_row -= 2
        #self.backgrounds_intracellular_row -= 2
        self.backgrounds_first_col = letter_to_int(self.backgrounds_first_col)-1
        self.backgrounds_last_col = letter_to_int(self.backgrounds_last_col)

    def check_inputs(self):
        #check for possible errors in input
        if((self.linescans_last_col - self.linescans_first_col) != (self.backgrounds_last_col - self.backgrounds_first_col)):
            #check for linescan and background columns being unequal.
```

```
        print("ERROR. Your linescan and background data does not match.")
        print("Please select the same number of columns for linescan as background.")
        print("Exiting...")
        exit()

class Data_formatting():
    #extracts data from excel document into pandas DataFrames.
    def __init__(self, master):
        linescans = pandas.read_excel(master.input_path, sheet_name=master.linescans_sheet_name)
        linescans = pandas.DataFrame(linescans)
        self.linescans = linescans.iloc[master.linescans_first_row:master.linescans_last_row, master.linescans_first_col:master.linescans_last_col]

        backgrounds = pandas.read_excel(master.input_path, sheet_name=master.backgrounds_sheet_name)
        backgrounds = pandas.DataFrame(backgrounds)
        self.nonprotruding_backgrounds = backgrounds.iloc[master.backgrounds_nonprotruding_row, master.backgrounds_first_col:master.backgrounds_last_col]
        #self.intracellular_backgrounds = backgrounds.iloc[master.backgrounds_intracellular_row, master.backgrounds_first_col:master.backgrounds_last_col]

def process_data(linescans, nonprotruding_backgrounds):
    #reads data from pandas DataFrame and processes it.

    output_df = pandas.DataFrame()
    #defines the final output variable.


    for i in range(0, len(linescans.columns)):
        #loops through each column in linescans

        col = linescans[linescans.columns[i]]
```

```
col = col.dropna()
col_len = len(col)
#removes blank values from column and saves length.


x = range(1,col_len+1)
y = col
spl = sp.interpolate.InterpolatedUnivariateSpline(x, y, ext=3)
#plots a spline. uses column length as x (ie from 0 to col_len) and the column data as y.

interval = np.linspace(1, col_len, 1000)
#calculatse new interval.

#plot_graph(spl, col, col_len)
##plots a graph of both datas:

output_serise = []
#definds an intermediate output variable.
for j in range(0,len(interval)):
    #loops through the new interval to read from the spline.
    val = spl(interval[j])
    nonprotruding_background = nonprotruding_backgrounds[i]
    #intracellular_background = intracellular_backgrounds[i]
    #retreves all information from the spline and backgrounds.

    val_ratio = (val)/(nonprotruding_background)
    #calculates val_ratio as: (spline reading)/(nonprotruding_background)

    output_serise.append(val_ratio)
    #append the val_ratio to the output list.

output_serise = pandas.Series(output_serise)
output_df[str(i)] = output_serise
#turns the output into a DataFrame
```

```
    return output_df

def averaging(master, output_df):
    mean = output_df.mean(axis=1)
    sd = output_df.std(axis=1)
    average_df = pandas.DataFrame()
    average_df.insert(0, "mean", mean, True)
    average_df.insert(1, "sd", sd, True)
    return average_df
    #master.vals_per_repeat



def output_data(master, output_df):
    output_df.to_csv(os.path.join(master.output_dir, master.output_file + "." + master.output_ext))

def plot_graph(spl, col, col_len):
    xs = np.linspace(1, col_len, 81)
    plt.figure()
    plt.plot(xs, spl(xs)) #spline line
    col.plot() #original data
    plt.show()

def letter_to_int(col):
    num = 0
    for c in col:
        if c in string.ascii_letters:
            num = num * 26 + (ord(c.upper()) - ord('A')) + 1
    return num

def run():
    master = Config()
    data = Data_formatting(master)
    output_df = process_data(data.linescans, data.nonprotruding_backgrounds)
    #output_df = averaging(master, output_df)
```

```
    output_data(master, output_df)


run()
```

Chapter 8

References

1. Ai J, Maturu A, Johnson W, Wang YJ, Marsh CB, Tridandapani S. 2006. The Inositol Phosphatase SHIP2 Downregulates Fc Gamma R-mediated Phagocytosis in Murine Macrophages Independently of SHIP1. Blood 107: 813–820.

2. Aizawa H, Sutoh K, Tsubuki S, Kawashima S, Ishii A, Yahara I. 1995. Identification, Characterisation, and Intracellular Distribution of Cofilin in *Dictyostelium discoideum*. Journal of Biological Chemistry 270: 10923–10932.

3. Alekhina O, Burstein E, Billadeau DD. 2017. Cellular Functions of WASP Family Proteins at a Glance. Journal of Cell Science 130: 2235–2241.

4. Allen PG. 2003. Actin Filament Un-capping Localises to Ruffling Lamellae and Rocketing Vesicles. Nature Cell Biology 5: 972–979.

5. Almeida-Souza L, Frank RAW, García-Nafría J, Colussi A, Gunawardana N, Johnson CM, Yu M, Howard G, Andrews B, Vallis Y, McMahon HT. 2018. A Flat BAR Protein Promotes Actin Polymerisation at the Base of Clathrin-Coated Pits. Cell 174: 325-337.e14.

6. Annesley SJ, Fisher PR. 2009. *Dictyostelium discoideum* — A Model for Many Reasons. Molecular and Cellular Biochemistry 329: 73–91.

7. Anton IM, Lu WG, Mayer BJ, Ramesh N, Geha RS. 1998. The Wiskott-Aldrich Syndrome Protein-Interacting Protein (WIP) Binds to the Adaptor Protein Nck. Journal of Biological Chemistry 273: 20992–20995.

8. Araki N, Egami Y, Watanabe Y, Hatae T. 2007. Phosphoinositide Metabolism during Membrane Ruffling and Macropinosome Formation in EGF-Stimulated A431 Cells. Experimental Cell Research 313: 1496–1507.

9. Araki N, Johnson MT, Swanson JA. 1996. A Role for Phosphoinositide 3-Kinase in the Completion of Macropinocytosis and Phagocytosis by Macrophages. Journal of Cell Biology 135: 1249–1260.

10. Asano T, Mochizuki Y, Matsumoto K, Takenawa T, Endo T. 1999. Pharbin, a Novel Inositol Polyphosphate 5-phosphatase, Induces Dendritic Appearances in Fibroblasts. Biochemical and Biophysical Research Communications 261: 188–195.

11. Asano Y, Yamashita K, Hasegawa A, Ogasawara T, Iriki H, Muramoto T. 2021. Knock-In and Precise Nucleotide Substitution using near-PAMless Engineered Cas9 Variants in *Dictyostelium discoideum*. Scientific Reports 11: 11163.

12. Astle MV, Horan KA, Ooms LM, Mitchell CA. 2007. The Inositol Polyphosphate 5-phosphatases: Traffic Controllers, Waistline Watchers and Tumour Suppressors? Pages 161–181 in Wakelam MJO, ed. Cell Biology of Inositol Lipids and Phosphates, vol. 74. Portland Press Ltd.

13. Ates KM, Wang T, Moreland T, Veeranan-Karmegam R, Ma M, Jeter C, Anand P, Wenzel W, Kim H-G, Wolfe LA, Stephen J, Adams DR, Markello T, Tifft CJ, Settlage R, Gahl WA, Gonsalvez GB, Malicdan MC, Flanagan-Steet H, Pan YA. 2020. Deficiency in the Endocytic Adaptor Proteins PHETA1/2 Impairs Renal and Craniofacial Development. Disease Models & Mechanisms 13: dmm041913.

14. Attree O, Olivos IM, Okabe I, Bailey LC, Nelson DL, Lewis RA, McInnes RR, Nussbaum RL. 1992. The Lowe's Oculocerebrorenal Syndrome Gene Encodes a Protein Highly Homologous to Inositol Polyphosphate 5-phosphatase. Nature 358: 239–242.

15. Aung KT, Yoshioka K, Aki S, Ishimaru K, Takuwa N, Takuwa Y. 2019. The Class II Phosphoinositide 3-Kinases PI3K-C2 Alpha and PI3K-C2 Beta Differentially Regulate Clathrin-Dependent Pinocytosis in Human Vascular Endothelial Cells. Journal of Physiological Sciences 69: 263–280.

16. Baba Y, Nonoyama S, Matsushita M, Yamadori T, Hashimoto S, Imai K, Arai S, Kunikata T, Kurimoto M, Kurosaki T, Ochs HD, Yata J, Kishimoto T, Tsukada S. 1999. Involvement of Wiskott-Aldrich Syndrome Protein in B-cell Cytoplasmic Tyrosine Kinase Pathway. Blood 93: 2003–2012.

17. Badour K, McGavin MKH, Zhang J, Freeman S, Vieira C, Filipp D, Julius M, Mills GB, Siminovitch KA. 2007. Interaction of the Wiskott–Aldrich Syndrome Protein with Sorting Nexin 9 is required for CD28 Endocytosis and Co-signalling in T-cells. Proceedings of the National Academy of Sciences of the United States of America 104: 1593–1598.

18. Bago R, Malik N, Munson MJ, Prescott AR, Davies P, Sommer E, Shpiro N, Ward R, Cross D, Ganley IG, Alessi DR. 2014. Characterisation of IIPS34-IN1, a Selective Inhibitor of Vps34, Reveals that the Phosphatidylinositol 3-Phosphate-Binding SGK3 Protein Kinase is a Downstream Target of Class lll Phosphoinositide 3-Kinase. Biochemical Journal 463: 413–427.

19. Balla T. 2013. Phosphoinositides: Tiny Lipids with Giant Impact on Cell Regulation. Physiological Reviews 93: 1019–1137.

20. Banach-Orlowska M, Pilecka I, Torun A, Pyrzynska B, Miaczynska M. 2009. Functional Characterisation of the Interactions between Endosomal Adaptor Protein, APPL1, and the NuRD Co-repressor Complex. Biochemical Journal 423: 389–400.

21. Banerjee J, Fischer CC, Wedegaertner PB. 2009. The Amino Acid Motif L/IIxxFE Defines a Novel Actin-Binding Sequence in PDZ-Rho-GEF. Biochemistry 48: 8032–8043.

22. Bao W, Xia H, Liang Y, Ye Y, Lu Y, Xu X, Duan A, He J, Chen Z, Wu Y, Wang X, Zheng C, Liu Z, Shi S. 2016. Toll-like Receptor 9 can be activated by Endogenous Mitochondrial DNA to Induce Podocyte Apoptosis. Scientific Reports 6: 22579.

23. Barneda D, Cosulich S, Stephens L, Hawkins P. 2019. How is the Acyl Chain Composition of Phosphoinositides Created and Does it Matter? Biochemical Society Transactions 47: 1291–1305.

24. Berger SB, Romero X, Ma C, Wang G, Faubion WA, Liao G, Compeer E, Keszei M, Rameh L, Wang N, Boes M, Regueiro JR, Reinecker H-C, Terhorst C. 2010. SLAM is a Microbial Sensor that Regulates Bacterial Phagosome Functions in Macrophages. Nature Immunology 11: 920-U70.

25. Biancospino M, Buel GR, Nino CA, Maspero E, Di Perrotolo RS, Raimondi A, Redlingshofer L, Weber J, Brodsky FM, Walters KJ, Polo S. 2019. Clathrin Light Chain A Drives Selective Myosin VI Recruitment to Clathrin-Coated Pits under Membrane Tension. Nature Communications 10: 4974.

26. Biggs WH, Meisenhelder J, Hunter T, Cavenee WK, Arden KC. 1999. Protein Kinase B/Akt-mediated Phosphorylation Promotes Nuclear Exclusion of the Winged Helix Transcription Factor FKHR1. Proceedings of the National Academy of Sciences of the United States of America 96: 7421–7426.

27. Bilanges B, Posor Y, Vanhaesebroeck B. 2019. PI3K Isoforms in Cell Signalling and Vesicle Trafficking. Nature Reviews Molecular Cell Biology 20: 515–534.

28. Blanchoin L, Amann KJ, Higgs HN, Marchand JB, Kaiser DA, Pollard TD. 2000. Direct Observation of Dendritic Actin Filament Networks Nucleated by Arp2/3 Complex and WASP/SCAR Proteins. Nature 404: 1007–1011.

29. Blanchoin L, Boujemaa-Paterski R, Sykes C, Plastino J. 2014. Actin Dynamics, Architecture, and Mechanics in Cell Motility. Physiological Reviews 94: 235–263.

30. Bloomfield G, Tanaka Y, Skelton J, Ivens A, Kay RR. 2008. Widespread Duplications in the Genomes of Laboratory Stocks of *Dictyostelium discoideum*. Genome Biology 9: R75.

31. Bloomfield G, Traynor D, Sander SP, Veltman DM, Pachebat JA, Kay RR. 2015. Neurofibromin Controls Macropinocytosis and Phagocytosis in *Dictyostelium*. Elife 4: e04940.

32. Blundell MP, Bouma G, Metelo J, Worth A, Calle Y, Cowell LA, Westerberg LS, Moulding DA, Mirando S, Kinnon C, Cory GO, Jones GE, Snapper SB, Burns SO, Thrasher AJ. 2009. Phosphorylation of WASP is a Key Regulator of Activity and Stability *in vivo*.

Proceedings of the National Academy of Sciences of the United States of America 106: 15738–15743.

33. Bockenhauer D, Bokenkamp A, van't Hoff W, Levtchenko E, Holthe JEK, Tasic V, Ludwig M. 2008. Renal Phenotype in Lowe Syndrome: A Selective Proximal Tubular Dysfunction. Clinical Journal of the American Society of Nephrology 3: 1430–1436.

34. Bodour K, Zhang JY, Shi F, Leng S, Collins M, Siminovitch KA. 2004. Fyn and PTP-PEST-mediated Regulation of Wiskott-Aldrich Syndrome Protein (WASP) Tyrosine Phosphorylation is required for Coupling T-cell Antigen Receptor Engagement to WASP Effector Function and T-cell Activation. Journal of Experimental Medicine 199: 99–111.

35. Bohdanowicz M, Balkin DM, De Camilli P, Grinstein S. 2012. Recruitment of OCRL and INPP5B to Phagosomes by Rab5 and APPL1 Depletes Phosphoinositides and Attenuates Akt Signalling. Faseb Journal 26.

36. Bokenkamp A, Bockenhauer D, Cheong HI, Hoppe B, Tasic V, Unwin R, Ludwig M. 2009. Dent-2 Disease: A Mild Variant of Lowe Syndrome. Journal of Pediatrics 155: 94–99.

37. Bothwell SP, Chan E, Bernardini IM, Kuo Y-M, Gahl WA, Nussbaum RL. 2011. Mouse Model for Lowe Syndrome/Dent Disease 2 Renal Tubulopathy. Journal of the American Society of Nephrology 22: 443–448.

38. Bothwell SP, Farber LW, Hoagland A, Nussbaum RL. 2010. Species Specific Difference in Expression and Splice Site Choice in INPP5B, an Inositol Polyphosphate 5-phosphatase Paralogous to the Enzyme Deficient in Lowe Syndrome. Mammalian Genome 21: 458–466.

39. Boucrot E, Ferreira APA, Almeida-Souza L, Debard S, Vallis Y, Howard G, Bertot L, Sauvonnet N, McMahon HT. 2015. Endophilin Marks and Controls a Clathrin-Independent Endocytic Pathway. Nature 517: 460-465.

40. Brunet A, Bonni A, Zigmond MJ, Lin MZ, Juo P, Hu LS, Anderson MJ, Arden KC, Blenis J, Greenberg ME. 1999. Akt Promotes Cell Survival by Phosphorylating and Inhibiting a Forkhead Transcription Factor. Cell 96: 857–868.

41. Buckley CM, King JS. 2017. Drinking Problems: Mechanisms of Macropinosome Formation and Maturation. The FEBS Journal 284: 3778–3790.

42. Buckley CM, Pots H, Gueho A, Vines JH, Munn CJ, Phillips BA, Gilsbach B, Traynor D, Nikolaev A, Soldati T, Parnell AJ, Kortholt A, King JS. 2020. Coordinated Ras and Rac Activity Shapes Macropinocytic Cups and Enables Phagocytosis of Geometrically Diverse Bacteria. Current Biology 30: 2912-2926.

43. Burgering B, Coffer P. 1995. Protein Kinase B (c-Akt) in Phosphatidylinositol-3-OH Kinase Signal Transduction. Nature 376: 599–602.

44. De Chastellier C, Quiviger B, Ryter A. 1978. Observations on the Functioning of the Contractile Vacuole of *Dictyostelium discoideum* with the Electron Microscope. Journal of Ultrastructure Research 62: 220–227.

45. Calvo-Garrido J, King JS, Munoz-Braceras S, Escalante R. 2014. Vmp1 Regulates PtdIns3P Signalling During Autophagosome Formation in *Dictyostelium discoideum*. Traffic 15: 1235–1246.

46. Campellone KG, Webb NJ, Znameroski EA, Welch MD. 2008. WHAMM is an Arp2/3 Complex Activator that Binds Microtubules and Functions in ER to Golgi Transport. Cell 134: 148–161.

47. Cantley LC. 2002. The Phosphoinositide 3-Kinase Pathway. Science 296: 1655–1657.

48. Cao M, Peng B, Chen H, Yang M, Chen P, Ye L, Wang H, Ren L, Xie J, Zhu J, Xu X, Xu W, Geng L, Gong S. 2022. miR-34a Induces Neutrophil Apoptosis by Regulating Cdc42-WASP-Arp2/3 Pathway-Mediated F-actin Remodelling and ROS Production. Redox Report 27: 167–175.

49. Cardelli J. 2001. Phagocytosis and Macropinocytosis in *Dictyostelium*: Phosphoinositide-Based Processes, Biochemically Distinct. Traffic 2: 311–320.

50. Carim SC, Ben El Kadhi K, Yen G, Sweeney ST, Hickson GR, Carreno S, Lowe M. 2019. IPIP27 Coordinates PtdIns(4,5)P_2 Homeostasis for Successful Cytokinesis. Current Biology 29: 775-789.

51. Castellano F, Le Clainche C, Patin D, Carlier M-F, Chavrier P. 2001. A WASP–VASP Complex Regulates Actin Polymerisation at the Plasma Membrane. The EMBO Journal 20: 5603–5614.

52. Catimel B, Kapp E, Yin M-X, Gregory M, Wong LS-M, Condron M, Church N, Kershaw N, Holmes AB, Burgess AW. 2013. The PI(3)P Interactome from a Colon Cancer Cell. Journal of Proteomics 82: 35–51.

53. Chang-Ileto B, Frere SG, Chan RB, Voronov SV, Roux A, Di Paolo G. 2011. Synaptojanin 1-mediated PI(4,5)P_2 Hydrolysis is modulated by Membrane Curvature and Facilitates Membrane Fission. Developmental Cell 20: 206–218.

54. Chial HJ, Lenart P, Chen YQ. 2010. APPL Proteins FRET at the BAR: Direct Observation of APPL1 and APPL2 BAR Domain-Mediated Interactions on Cell Membranes using FRET Microscopy. Plos One 5: e12471.

55. Chial HJ, Wu R, Ustach CV, McPhail LC, Mobley WC, Chen YQ. 2008. Membrane Targeting by APPL1 and APPL2: Dynamic Scaffolds that Oligomerise and Bind Phosphoinositides. Traffic 9: 215–229.

56. Choi S, Thapa N, Tan X, Hedman AC, Anderson RA. 2015. PIP Kinases Define PI(4,5)P_2 Signalling Specificity by Association with Effectors. Biochimica Et Biophysica Acta-Molecular and Cell Biology of Lipids 1851: 711–723.

57. Choudhury R, Diao AP, Zhang F, Eisenberg E, Saint-Pol A, Williams C, Konstantakopoulos A, Lucocq J, Johannes L, Rabouille C, Greene LE, Lowe M. 2005. Lowe Syndrome Protein OCRL1 Interacts with Clathrin and Regulates Protein Trafficking Between Endosomes and the Trans-Golgi Network. Molecular Biology of the Cell 16: 3467–3479.

58. Choudhury R, Noakes CJ, McKenzie E, Kox C, Lowe M. 2009. Differential Clathrin Binding and Subcellular Localisation of OCRL1 Splice Isoforms. Journal of Biological Chemistry 284: 9965–9973.

59. Christoforidis S, Miaczynska M, Ashman K, Wilm M, Zhao L, Yip S-C, Waterfield MD, Backer JM, Zerial M. 1999. Phosphatidylinositol-3-OH Kinases are Rab5 Effectors. Nature Cell Biology 1: 249–252.

60. Chung CY, Feoktistov A, Hollingsworth RJ, Rivero F, Mandel NS. 2013. An Attenuating Role of a WASP-Related Protein, WASP-B, in the Regulation of F-actin Polymerisation and Pseudopod Formation via the Regulation of RacC during *Dictyostelium* Chemotaxis. Biochemical and Biophysical Research Communications 436: 719–724.

61. Chung CY, Reddy TBK, Zhou KM, Firtel RA. 1998. A Novel, Putative MEK Kinase Controls Developmental Timing and Spatial Patterning in *Dictyostelium* and is Regulated by Ubiquitin-Mediated Protein Degradation. Genes & Development 12: 3564–3578.

62. Cioni J-M, Wong HH-W, Bressan D, Kodama L, Harris WA, Holt CE. 2018. Axon-Axon Interactions Regulate Topographic Optic Tract Sorting via CYFIP2-dependent WAVE Complex Function. Neuron 97: 1078-1093.

63. Clark J, Kay RR, Kielkowska A, Niewczas I, Fets L, Oxley D, Stephens LR, Hawkins PT. 2014. *Dictyostelium* uses Ether-Linked Inositol Phospholipids for Intracellular Signalling. Embo Journal 33: 2188–2200.

64. Clarke JH, Emson PC, Irvine RF. 2009. Distribution and Neuronal Expression of Phosphatidylinositol Phosphate Kinase II Gamma in the Mouse Brain. Journal of Comparative Neurology 517: 296–312.

65. Coon BG, Hernandez V, Madhivanan K, Mukherjee D, Hanna CB, Ramirez IB-R, Lowe M, Beales PL, Aguilar RC. 2012. The Lowe Syndrome Protein OCRL1 is Involved in Primary Cilia Assembly. Human Molecular Genetics 21: 1835–1847.

66. Coon BG, Mukherjee D, Hanna CB, Riese DJ, Lowe M, Aguilar RC. 2009. Lowe Syndrome Patient Fibroblasts Display OCRL1-Specific Cell Migration Defects that cannot be

rescued by the Homologous INPP5B Phosphatase. Human Molecular Genetics 18: 4478–4491.

67. Cornillon S, Gebbie L, Benghezal M, Nair P, Keller S, Wehrle-Haller B, Charette SJ, Bruckert F, Letourneur F, Cosson P. 2006. An Adhesion Molecule in Free-Living *Dictyostelium* Amoebae with Integrin Beta Features. Embo Reports 7: 617–621.

68. Cory GOC, Garg R, Cramer R, Ridley AJ. 2002. Phosphorylation of Tyrosine Enhances the Ability of WASP to Stimulate Actin Polymerisation and Filopodium Formation. Journal of Biological Chemistry 277: 45115–45121.

69. Cui S, Guerriero CJ, Szalinski CM, Kinlough CL, Hughey RP, Weisz OA. 2010. OCRL1 Function in Renal Epithelial Membrane Traffic. American Journal of Physiology Renal Physiology 298: F335–F345.

70. Dambournet D, Machicoane M, Chesneau L, Sachse M, Rocancourt M, El Marjou A, Formstecher E, Salomon R, Goud B, Echard A. 2011. Rab35 GTPase and OCRL Phosphatase Remodel Lipids and F-actin for Successful Cytokinesis. Nature Cell Biology 13: 981-988.

71. Damen JE, Liu L, Rosten P, Humphries RK, Jefferson AB, Majerus PW, Krystal G. 1996. The 145 kDa Protein Induced to Associate with Shc by Multiple Cytokines is an Inositol Tetraphosphate and Phosphatidylinositol 3,4,5-Triphosphate 5-phosphatase. Proceedings of the National Academy of Sciences of the United States of America 93: 1689–1693.

72. Daste F, Walrant A, Holst MR, Gadsby JR, Mason J, Lee J-E, Brook D, Mettlen M, Larsson E, Lee SF, Lundmark R, Gallop JL. 2017. Control of Actin Polymerisation via the Coincidence of Phosphoinositides and High Membrane Curvature. Journal of Cell Biology 216: 3745–3765.

73. Davidson AJ, Amato C, Thomason PA, Insall RH. 2018. WASP Family Proteins and Formins Compete in Pseudopod- and Bleb-Based Migration. Journal of Cell Biology 217: 701–714.

74. Davidson AJ, King JS, Insall RH. 2013. The use of Streptavidin Conjugates as Immunoblot Loading Controls and Mitochondrial Markers for use with *Dictyostelium discoideum*. BioTechniques 55: 39–41.

75. De Leo MG, Staiano L, Vicinanza M, Luciani A, Carissimo A, Mutarelli M, Di Campli A, Polishchuk E, Di Tullio G, Mona V, Levtchenko E, Oltrabella F, Starborg T, Santoro M, di Bernardo D, Devuyst O, Lowe M, Medina DL, Ballabio A, De Matteis MA. 2016. Autophagosome-Lysosome Fusion Triggers a Lysosomal Response Mediated by TLR9 and Controlled by OCRL. Nature Cell Biology 18: 839-850.

76. De Matteis MA, Staiano L, Emma F, Devuyst O. 2017. The 5-phosphatase OCRL in Lowe Syndrome and Dent Disease 2. Nature Reviews Nephrology 13: 455–470.

77. De Matteis MA, Wilson C, D'Angelo G. 2013. Phosphatidylinositol-4-Phosphate: The Golgi and Beyond. Bioessays 35: 612–622.

78. Delague V, Jacquier A, Hamadouche T, Poitelon Y, Baudot C, Boccaccio I, Chouery E, Chaouch M, Kassouri N, Jabbour R, Grid D, Megarbane A, Haase G, Levy N. 2007. Mutations in FGD4 Encoding the Rho GDP/GTP Exchange Factor Frabin Cause Autosomal Recessive Charcot-Marie-Tooth Type 4H. American Journal of Human Genetics 81: 1–16.

79. Derivery E, Sousa C, Gautier JJ, Lombard B, Loew D, Gautreau A. 2009. The Arp2/3 Activator WASH Controls the Fission of Endosomes through a large Multi-protein Complex. Developmental Cell 17: 712–723.

80. Derry J, Ochs H, Francke U. 1994. Isolation of a Novel Gene Mutated in Wiskott-Aldrich Syndrome. Cell 78: 635–644.

81. Desale SE, Chinnathambi S. 2021. Phosphoinositides Signalling Modulates Microglial Actin Remodelling and Phagocytosis in Alzheimer's disease. Cell Communication and Signalling 19: 1–12.

82. Desmedt F, Verjans B, Mailleux P, Erneux C. 1994. Cloning and Expression of Human Brain Type I Inositol 1,4,5-Trisphosphate 5-phosphatase - High-levels of mRNA in Cerebellar Purkinje Cells. Febs Letters 347: 69–72.

83. Devreotes P, Zigmond S. 1988. Chemotaxis in Eukaryotic Cells - A Focus on Leukocytes and *Dictyostelium*. Annual Review of Cell Biology 4: 649–686.

84. Di Paolo G, De Camilli P. 2006. Phosphoinositides in Cell Regulation and Membrane Dynamics. Nature 443: 651–657.

85. Dickson EJ. 2019. Recent Advances in Understanding Phosphoinositide Signalling in the Nervous System. F1000Research 8: F1000 Faculty Rev-278.

86. Diggins NL, Webb DJ. 2017. APPL1 is a Multifunctional Endosomal Signalling Adaptor Protein. Biochemical Society Transactions 45: 771–779.

87. Dominguez R. 2007. The Beta-Thymosin/WH2 Fold - Multifunctionality and Structure. Pages 86–94 in Goldstein AL and Garaci E, eds. Thymosins in Health and Disease: First International Symposium, vol. 1112. Blackwell Publishing.

88. Dong R, Saheki Y, Swarup S, Lucast L, Harper JW, De Camilli P. 2016. Endosome-ER Contacts Control Actin Nucleation and Retromer Function through VAP-dependent Regulation of PI(4)P. Cell 166: 408–423.

89. Dong X, Shen D, Wang X, Dawson T, Li X, Zhang Q, Cheng X, Zhang Y, Weisman LS, Delling M, Xu H. 2010. PI(3,5)P_2 Controls Membrane Trafficking by Direct Activation of Mucolipin Ca^{2+} Release Channels in the Endolysosome. Nature Communications 1: 38.

90. Dormann D, Weijer G, Dowler S, Weijer CJ. 2004. *In vivo* Analysis of 3-Phosphoinositide Dynamics during *Dictyostelium* in Phagocytosis and Chemotaxis. Journal of Cell Science 117: 6497–6509.

91. Dowler S, Currie RA, Campbell DG, Deak M, Kular G, Downes CP, Alessi DR. 2000. Identification of Pleckstrin Homology Domain-Containing Proteins with Novel Phosphoinositide-Binding Specificities. Biochemical Journal 351: 19–31.

92. Drayer A, Vanhaastert P. 1992. Molecular Cloning and Expression of a Phosphoinositide-Specific Phospholipase C of *Dictyostelium discoideum*. Journal of Biological Chemistry 267: 18387–18392.

93. Drayer AL, Van der Kaay J, Mayr GW, Van Haastert PJ. 1994. Role of Phospholipase C in *Dictyostelium*: Formation of Inositol 1,4,5-Trisphosphate and Normal Development in Cells Lacking Phospholipase C Activity. The EMBO journal 13: 1601–1609.

94. Dressman MA, Olivos-Glander IM, Nussbaum RL, Suchy SF. 2000. OCRL1, a Ptdlns(4,5)P_2 5-phosphatase, is localised to the Trans-Golgi Network of Fibroblasts and Epithelial Cells. Journal of Histochemistry & Cytochemistry 48: 179–189.

95. Dumontier M, Hocht P, Mintert U, Faix J. 2000. Rac1 GTPases Control Filopodia Formation, Cell Motility, Endocytosis, Cytokinesis and Development in *Dictyostelium*. Journal of Cell Science 113: 2253–2265.

96. Dunn JD, Bosmani C, Barisch C, Raykov L, Lefrançois LH, Cardenal-Muñoz E, López-Jiménez AT, Soldati T. 2018. Eat Prey, Live: *Dictyostelium discoideum* as a Model for Cell Autonomous Defenses. Frontiers in Immunology 8.

97. Egami Y, Taguchi T, Maekawa M, Arai H, Araki N. 2014. Small GTPases and Phosphoinositides in the Regulatory Mechanisms of Macropinosome Formation and Maturation. Frontiers in Physiology 5: 374.

98. Eichinger L, Pachebat JA, Glockner G, Rajandream MA, Sucgang R, Berriman M, Song J, Olsen R, Szafranski K, Xu Q, Tunggal B, Kummerfeld S, Madera M, Konfortov BA, Rivero F, Bankier AT, Lehmann R, Hamlin N, Davies R, Gaudet P, Fey P, Pilcher K, Chen G, Saunders D, Sodergren E, Davis P, Kerhornou A, Nie X, Hall N, Anjard C, Hemphill L, Bason N, Farbrother P, Desany B, Just E, Morio T, Rost R, Churcher C, Cooper J, Haydock S, van Driessche N, Cronin A, Goodhead I, Muzny D, Mourier T, Pain A, Lu M, Harper D, Lindsay R, Hauser H, James K, Quiles M, Babu MM, Saito T, Buchrieser C, Wardroper A, Felder M, Thangavelu M, Johnson

D, Knights A, Loulseged H, Mungall K, Oliver K, Price C, Quail MA, Urushihara H, Hernandez J, Rabbinowitsch E, Steffen D, Sanders M, Ma J, Kohara Y, Sharp S, Simmonds M, Spiegler S, Tivey A, Sugano S, White B, Walker D, Woodward J, Winckler T, Tanaka Y, Shaulsky G, Schleicher M, Weinstock G, Rosenthal A, Cox EC, Chisholm RL, Gibbs R, Loomis WF, Platzer M, Kay RR, Williams J, Dear PH, Noegel AA, Barrell B, Kuspa A. 2005. The Genome of the Social Amoeba *Dictyostelium discoideum*. Nature 435: 43–57.

99. El Kadhi KB, Roubinet C, Solinet S, Emery G, Carreno S. 2011. The Inositol 5-phosphatase dOCRL Controls PI(4,5)P_2 Homeostasis and is necessary for Cytokinesis. Current Biology 21: 1074–1079.

100. El-Bazzal L, Ghata A, Esteve C, Gadacha J, Quintana P, Castro C, Roeckel-Trevisiol N, Lembo F, Lenfant N, Megarbane A, Borg J-P, Levy N, Bartoli M, Poitelon Y, Roubertoux PL, Delague V, Bernard-Marissal N. 2022. Imbalance of NRG1-ERBB2/3 Signalling Underlies Altered Myelination in Charcot-Marie-Tooth Disease 4H. Brain : a Journal of Neurology.

101. Ellson CD, Anderson KE, Morgan G, Chilvers ER, Lipp P, Stephens LR, Hawkins PT. 2001. Phosphatidylinositol 3-Phosphate is generated in Phagosomal Membranes. Current Biology 11: 1631–1635.

102. Engelman JA, Luo J, Cantley LC. 2006. The Evolution of Phosphatidylinositol 3-Kinases as Regulators of Growth and Metabolism. Nature Reviews Genetics 7: 606–619.

103. Erdmann KS, Mao Y, McCrea HJ, Zoncu R, Lee S, Paradise S, Modregger J, Biemesderfer D, Toomre D, De Camillil P. 2007. A Role of the Lowe Syndrome Protein OCRL in Early Steps of the Endocytic Pathway. Developmental Cell 13: 377–390.

104. Essid M, Gopaldass N, Yoshida K, Merrifield C, Soldati T. 2012. Rab8a Regulates the Exocyst-Mediated Kiss-and-Run Discharge of the *Dictyostelium* Contractile Vacuole. Molecular Biology of the Cell 23: 1267–1282.

105. Faucherre A, Desbois P, Nagano F, Satre V, Lunardi J, Gacon G, Dorseuil O. 2005. Lowe Syndrome Protein OCRL1 is translocated to Membrane Ruffles upon Rac GTPase Activation: A New Perspective on Lowe Syndrome Pathophysiology. Human Molecular Genetics 14: 1441–1448.

106. Faucherre A, Desbois P, Satre V, Lunardi J, Dorseuil O, Gacon G. 2003. Lowe Syndrome Protein OCRL1 Interacts with Rac GTPase in the Trans-Golgi Network. Human Molecular Genetics 12: 2449–2456.

107. Ferreira F, Foley M, Cooke A, Cunningham M, Smith G, Woolley R, Henderson G, Kelly E, Mundell S, Smythe E. 2012. Endocytosis of G Protein-Coupled Receptors is regulated by Clathrin Light Chain Phosphorylation. Current Biology 22: 1361–1370.

108. Fey P, Cox EC. 1997. Gene Trapping with GFP: The Isolation of Developmental Mutants in the Slime Mold *Polysphondylium*. Current Biology 7: 909–912.

109. Filippakis H, Belaid A, Siroky B, Wu C, Alesi N, Hougard T, Nijmeh J, Lam HC, Henske EP. 2018. Vps34-Mediated Macropinocytosis in Tuberous Sclerosis Complex 2-Deficient Cells Supports Tumourigenesis. Scientific Reports 8: 14161.

110. Fisher S, Black G, Lloyd S, Hatchwell E, Wrong O, Thakker R, Craig I. 1994. Isolation and Partial Characterisation of a Chloride Channel Gene which is expressed in Kidney and is a Candidate for Dents Disease (an X-Linked Hereditary Nephrolithiasis). Human Molecular Genetics 3: 2053–2059.

111. Flannagan RS, Jaumouille V, Grinstein S. 2012. The Cell Biology of Phagocytosis. Pages 61–98 in Abbas AK, Galli SJ, and Howley PM, eds. Annual Review of Pathology: Mechanisms of Disease, Vol 7, vol. 7. Annual Reviews.

112. Fotin A, Cheng YF, Grigorieff N, Walz T, Harrison SC, Kirchhausen T. 2004. Structure of an Auxilin-Bound Clathrin Coat and its Implications for the Mechanism of Un-coating. Nature 432: 649–653.

113. Foukas LC, Claret M, Pearce W, Okkenhaug K, Meek S, Peskett E, Sancho S, Smith AJH, Withers DJ, Vanhaesebroeck B. 2006. Critical Role for the p110 Alpha Phosphoinositide-3-OH Kinase in Growth and Metabolic Regulation. Nature 441: 366–370.

114. Fox M, Mott HR, Owen D. 2020. Class IA PI3K Regulatory Subunits: p110-Independent Roles and Structures. Biochemical Society Transactions 48: 1397–1417.

115. Franke T, Yang S, Chan T, Datta K, Kazlauskas A, Morrison D, Kaplan D, Tsichlis P. 1995. The Protein Kinase Encoded by the Akt Proto-Oncogene is a Target of the PDGF-Activated Phosphatidylinositol 3-Kinase. Cell 81: 727–736.

116. Freeman SA, Grinstein S. 2014. Phagocytosis: Receptors, Signal Integration, and the Cytoskeleton. Immunological Reviews 262: 193–215.

117. Fruman DA, Snapper SB, Yballe CM, Davidson L, Yu JY, Alt FW, Cantley LC. 1999. Impaired B-cell Development and Proliferation in the Absence of Phosphoinositide 3-Kinase p85 Alpha. Science 283: 393–397.

118. Gaidarov I, Smith MEK, Domin J, Keen JH. 2001. The Class II Phosphoinositide 3-Kinase C2 Alpha is Activated by Clathrin and Regulates Clathrin-Mediated Membrane Trafficking. Molecular Cell 7: 443–449.

119. Gallop JL, Walrant A, Cantley LC, Kirschner MW. 2013. Phosphoinositides and Membrane Curvature Switch the Mode of Actin Polymerisation via Selective Recruitment of

TOCA-1 and SNX9. Proceedings of the National Academy of Sciences of the United States of America 110: 7193–7198.

120. Gerisch G, Heuser J, Clarke M. 2002. Tubular-Vesicular Transformation in the Contractile Vacuole System of *Dictyostelium*. Cell Biology International 26: 845–852.

121. Ghosh R, de Campos MKF, Huang J, Huh SK, Orlowski A, Yang Y, Tripathi A, Nile A, Lee H-C, Dynowski M, Schaefer H, Rog T, Lete MG, Ahyayauch H, Alonso A, Vattulainen I, Igumenova TI, Schaaf G, Bankaitis VA. 2015. Sec14-Nodulin Proteins and the Patterning of Phosphoinositide Landmarks for Developmental Control of Membrane Morphogenesis. Molecular Biology of the Cell 26: 1764–1781.

122. Gillooly DJ, Morrow IC, Lindsay M, Gould R, Bryant NJ, Gaullier JM, Parton RG, Stenmark H. 2000. Localisation of Phosphatidylinositol 3-Phosphate in Yeast and Mammalian Cells. Embo Journal 19: 4577–4588.

123. Glynn P, Clarke K. 1984. An Investigation of Adhesion and Detachment in Slime Mold Amoebas Using Columns of Hydrophobic Beads. Experimental Cell Research 152: 117–126.

124. Goetz SC, Anderson KV. 2010. The Primary Cilium: A Signalling Centre during Vertebrate Development. Nature Reviews Genetics 11: 331–344.

125. Goldberg JM, Manning G, Liu A, Fey P, Pilcher KE, Xu Y, Smith JL. 2006. The *Dictyostelium* Kinome - Analysis of the Protein Kinases from a Simple Model Organism. Plos Genetics 2: 291–303.

126. Goley ED, Welch MD. 2006. The Arp2/3 Complex: An Actin Nucleator Comes of Age. Nature Reviews Molecular Cell Biology 7: 713–726.

127. Gomez TS, Gorman JA, de Narvajas AA-M, Koenig AO, Billadeau DD. 2012. Trafficking Defects in WASH-Knockout Fibroblasts Originate from Collapsed Endosomal and Lysosomal Networks. Molecular Biology of the Cell 23: 3215–3228.

128. Gorbatyuk VY, Nosworthy NJ, Robson SA, Bains NPS, Maciejewski MW, dos Remedios CG, King GF. 2006. Mapping the Phosphoinositide-Binding Site on Chick Cofilin explains how PIP_2 Regulates the Cofilin-Actin Interaction. Molecular Cell 24: 511–522.

129. Gordon S. 2016. Phagocytosis: An Immunobiologic Process. Immunity 44: 463–475.

130. Grassart A, Dujeancourt A, Lazarow PB, Dautry-Varsat A, Sauvonnet N. 2008. Clathrin-Independent Endocytosis used by the IL-2 Receptor is regulated by Rac1, Pak1 and Pak2. Embo Reports 9: 356–362.

131. Grinstein S. 2012. Phagocytosis Here and Now. Traffic 13: 1041–1041.

132. Gu Y, Filippi MD, Cancelas JA, Siefring JE, Williams EP, Jasti AC, Harris CE, Lee AW, Prabhakar R, Atkinson SJ, Kwiatkowski DJ, Williams DA. 2003. Haematopoietic Cell Regulation by Rac1 and Rac2 Guanosine Triphosphatases. Science 302: 445–449.

133. Guinamard R, Aspenstrom P, Fougereau M, Chavrier P, Guillemot JC. 1998. Tyrosine Phosphorylation of the Wiskott-Aldrich Syndrome Protein by Lyn and Btk is regulated by Cdc42. Febs Letters 434: 431–436.

134. Gustincich S, Schneider C. 1993. Serum Deprivation Response Gene is induced by Serum Starvation but not by Contact Inhibition. Cell Growth & Differentiation 4: 753–760.

135. Habermann B. 2004. The BAR-Domain Family of Proteins: A Case of Bending and Binding? The Membrane Bending and GTPase-Binding Functions of Proteins from the BAR-Domain Family. Embo Reports 5: 250–255.

136. Hacker U, Albrecht R, Maniak M. 1997. Fluid-Phase Uptake by Macropinocytosis in *Dictyostelium*. Journal of Cell Science 110: 105–112.

137. Hall A. 2005. Rho GTPases and the Control of Cell Behaviour. Biochemical Society Transactions 33: 891–895.

138. Hammond GRV, Balla T. 2015. Polyphosphoinositide Binding Domains: Key to Inositol Lipid Biology. Biochimica Et Biophysica Acta-Molecular and Cell Biology of Lipids 1851: 746–758.

139. Hammond GRV, Machner MP, Balla T. 2014. A Novel Probe for Phosphatidylinositol 4-Phosphate Reveals Multiple Pools beyond the Golgi. Journal of Cell Biology 205: 113–126.

140. Herman PK, Emr SD. 1990. Characterisation of Vps34, a Gene Required for Vacuolar Protein Sorting and Vacuole Segregation in *Saccharomyces cerevisiae*. Molecular and Cellular Biology 10: 6742–6754.

141. Heuser J, Zhu Q, Clarke M. 1993. Proton Pumps Populate the Contractile Vacuoles of *Dictyostelium* Amoebas. Journal of Cell Biology 121: 1311–1327.

142. Hichri H, Rendu J, Monnier N, Coutton C, Dorseuil O, Poussou RV, Baujat G, Blanchard A, Nobili F, Ranchin B, Remesy M, Salomon R, Satre V, Lunardi J. 2011. From Lowe Syndrome to Dent Disease: Correlations between Mutations of the OCRL1 Gene and Clinical and Biochemical Phenotypes. Human Mutation 32: 379–388.

143. Higgs HN, Blanchoin L, Pollard TD. 1999. Influence of the C-terminus of Wiskott-Aldrich Syndrome Protein (WASP) and the Arp2/3 Complex on Actin Polymerisation. Biochemistry 38: 15212–15222.

144. Higgs HN, Pollard TD. 2001. Regulation of Actin Filament Network Formation through the Arp2/3 Complex: Activation by a Diverse Array of Proteins. Annual Review of Biochemistry 70: 649–676.

145. Hill MM, Bastiani M, Luetterforst R, Kirkham M, Kirkham A, Nixon SJ, Walser P, Abankwa D, Oorschot VMJ, Martin S, Hancock JF, Parton RG. 2008. PTRF-Cavin, a Conserved Cytoplasmic Protein Required for Caveola Formation and Function. Cell 132: 113–124.

146. Hoeller O, Bolourani P, Clark J, Stephens LR, Hawkins PT, Weiner OD, Weeks G, Kay RR. 2013. Two Distinct Functions for PI3-Kinases in Macropinocytosis. Journal of Cell Science 126: 4296–4307.

147. Hokin MR, Hokin LE. 1953. Enzyme Secretion and the Incorporation of P^{32} into Phospholipids of Pancreas Slices. The Journal of Biological Chemistry 203: 967–977.

148. Homma K, Terui S, Minemura M, Qadota H, Anraku Y, Kanaho Y, Ohya Y. 1998. Phosphatidylinositol-4-Phosphate 5-Kinase Localised on the Plasma Membrane is Essential for Yeast Cell Morphogenesis. Journal of Biological Chemistry 273: 15779–15786.

149. Hoopes RR, Shrimpton AE, Knohl SJ, Hueber P, Hoppe B, Matyus J, Simckes A, Tasic V, Toenshoff B, Suchy SF, Nussbaum RL, Scheinman SJ. 2005. Dent Disease with Mutations in OCRL1. American Journal of Human Genetics 76: 260–267.

150. Horan KA, Watanabe K, Kong AM, Bailey CG, Rasko JEJ, Sasaki T, Mitchell CA. 2007. Regulation of Fc Gamma R-Stimulated Phagocytosis by the 72-kDa Inositol Polyphosphate 5-phosphatase: SHIP1, but not the 72 kDa 5-phosphatase, Regulates Complement Receptor 3-mediated Phagocytosis by Differential Recruitment of these 5-phosphatases to the Phagocytic Cup. Blood 110: 4480–4491.

151. Horn M, Baumann R, Pereira JA, Sidiropoulos PNM, Somandin C, Welzl H, Stendel C, Luehmann T, Wessig C, Toyka KV, Relvas JB, Senderek J, Suter U. 2012. Myelin is Dependent on the Charcot-Marie-Tooth Type 4H Disease Culprit Protein Frabin/FGD4 in Schwann Cells. Brain 135: 3567–3583.

152. Hou X, Hagemann N, Schoebel S, Blankenfeldt W, Goody RS, Erdmann KS, Itzen A. 2011. A Structural Basis for Lowe Syndrome Caused by Mutations in the Rab-Binding Domain of OCRL1. The EMBO Journal 30: 1659–1670.

153. Huang FT, Khvorova A, Marshall W, Sorkin A. 2004. Analysis of Clathrin-Mediated Endocytosis of Epidermal Growth Factor Receptor by RNA Interference. Journal of Biological Chemistry 279: 16657–16661.

154. Huang L, Zhang H, Cheng C-Y, Wen F, Tam POS, Zhao P, Chen H, Li Z, Chen L, Tai Z, Yamashiro K, Deng S, Zhu X, Chen W, Cai L, Lu F, Li Y, Cheung C-MG, Shi Y, Miyake M, Lin Y,

Gong B, Liu X, Sim K-S, Yang J, Mori K, Zhang X, Cackett PD, Tsujikawa M, Nishida K, Hao F, Ma S, Lin H, Cheng J, Fei P, Lai TYY, Tang S, Laude A, Inoue S, Yeo IY, Sakurada Y, Zhou Y, Iijima H, Honda S, Lei C, Zhang L, Zheng H, Jiang D, Zhu X, Wong T-Y, Khor C-C, Pang C-P, Yoshimura N, Yang Z. 2016. A Missense Variant in FGD6 Confers Increased Risk of Polypoidal Choroidal Vasculopathy. Nature Genetics 48: 640-647.

155. Hubner S, Couvillon AD, Kas JA, Bankaitis VA, Vegners R, Carpenter CL, Janmey PA. 1998. Enhancement of Phosphoinositide 3-Kinase (PI 3-Kinase) Activity by Membrane Curvature and Inositol-Phospholipid-Binding Peptides. European Journal of Biochemistry 258: 846–853.

156. Husi H, Ward MA, Choudhary JS, Blackstock WP, Grant SGN. 2000. Proteomic Analysis of NMDA Receptor-Adhesion Protein Signalling Complexes. Nature Neuroscience 3: 661–669.

157. Husson C, Renault L, Didry D, Pantaloni D, Carlier M-F. 2011. Cordon-Bleu uses WH2 Domains as Multifunctional Dynamisers of Actin Filament Assembly. Molecular Cell 43: 464–477.

158. Hyvola N, Diao A, McKenzie E, Skippen A, Cockcroft S, Lowe M. 2006. Membrane Targeting and Activation of the Lowe Syndrome Protein OCRL1 by Rab GTPases. Embo Journal 25: 3750–3761.

159. Ichetovkin I, Han JH, Pang KM, Knecht DA, Condeelis JS. 2000. Actin Filaments are severed by both Native and Recombinant *Dictyostelium* Cofilin but to Different Extents. Cell Motility and the Cytoskeleton 45: 293–306.

160. Ijuin T, Mochizuki Y, Fukami K, Funaki M, Asano T, Takenawa T. 2000. Identification and Characterisation of a Novel Inositol Polyphosphate 5-phosphatase. Journal of Biological Chemistry 275: 10870–10875.

161. Inaba H, Yoda K, Adachi H. 2017. The F-actin-Binding Rap-GEF GflB is required for Efficient Macropinocytosis in *Dictyostelium*. Journal of Cell Science 130: 3158–3172.

162. Inoue K, Balkin DM, Liu L, Nandez R, Wu Y, Tian X, Wang T, Nussbaum R, De Camilli P, Ishibe S. 2017. Kidney Tubular Ablation of OCRL/INPP5B Phenocopies Lowe Syndrome Tubulopathy. Journal of the American Society of Nephrology 28: 1399–1407.

163. Insall R. 2005. The *Dictyostelium* Genome: The Private Life of a Social Model Revealed? Genome Biology 6: 222.

164. Insall R, Kuspa A, Lilly P, Shaulsky G, Levin L, Loomis W, Devreotes P. 1994. Crac, a Cytosolic Protein Containing a Pleckstrin Homology Domain, is Required for Receptor and G-

Protein-Mediated Activation of Adenylyl-Cyclase in *Dictyostelium*. Journal of Cell Biology 126: 1537–1545.

165. Insall R, Muller-Taubenberger A, Machesky L, Kohler J, Simmeth E, Atkinson SJ, Weber I, Gerisch G. 2001. Dynamics of the *Dictyostelium* Arp2/3 Complex in Endocytosis, Cytokinesis, and Chemotaxis. Cell Motility and the Cytoskeleton 50: 115–128.

166. Isik N, Brzostowski JA, Jin T. 2008. An Elmo-Like Protein Associated with Myosin II Restricts Spurious F-actin Events to Coordinate Phagocytosis and Chemotaxis. Developmental Cell 15: 590–602.

167. Itakura E, Kishi C, Inoue K, Mizushima N. 2008. Beclin 1 Forms Two Distinct Phosphatidylinositol 3-Kinase Complexes with Mammalian Atg14 and UVRAG. Molecular Biology of the Cell 19: 5360–5372.

168. Itakura E, Kishi-Itakura C, Mizushima N. 2012. The Hairpin-Type Tail-Anchored SNARE Syntaxin 17 Targets to Autophagosomes for Fusion with Endosomes/Lysosomes. Cell 151: 1256–1269.

169. Itoh T, Erdmann KS, Roux A, Habermann B, Werner H, De Camilli P. 2005. Dynamin and the Actin Cytoskeleton Cooperatively Regulate Plasma Membrane Invagination by BAR and F-BAR Proteins. Developmental Cell 9: 791–804.

170. Ivetac I, Munday AD, Kisseleva MV, Zhang XM, Luff S, Tiganis T, Whisstock JC, Rowe T, Majerus PW, Mitchell CA. 2005. The Type I Alpha Inositol Polyphosphate 4-phosphatase Generates and Terminates Phosphoinositide 3-Kinase Signals on Endosomes and the Plasma Membrane. Molecular Biology of the Cell 16: 2218–2233.

171. Izumi Y, Hirai S, Tamai Y, FujiseMatsuoka A, Nishimura Y, Ohno S. 1997. A Protein Kinase C Delta-Binding Protein SRBC Whose Expression is induced by Serum Starvation. Journal of Biological Chemistry 272: 7381–7389.

172. Jansa P, Mason SW, Hoffmann-Rohrer U, Grummt I. 1998. Cloning and Functional Characterisation of PTRF, a Novel Protein which Induces Dissociation of Paused Ternary Transcription Complexes. Embo Journal 17: 2855–2864.

173. Jefferson A, Majerus P. 1995. Properties of Type II Inositol Polyphosphate 5-phosphatase. Journal of Biological Chemistry 270: 9370–9377.

174. Jefferson AB, Majerus PW. 1996. Mutation of the Conserved Domains of Two Inositol Polyphosphate 5-phosphatases. Biochemistry 35: 7890–7894.

175. Jensen EC. 2012. Use of Fluorescent Probes: Their Effect on Cell Biology and Limitations. The Anatomical Record 295: 2031–2036.

176. Jeon P, Jeon TJ. 2020. WasC, a WASP Family Protein, is involved in Cell Adhesion and Migration through Regulation of F-actin Polymerisation in *Dictyostelium*. Journal of Microbiology (Seoul, Korea) 58: 696–702.

177. Joshi P, Greco TM, Guise AJ, Luo Y, Yu F, Nesvizhskii AI, Cristea IM. 2013. The Functional Interactome Landscape of the Human Histone Deacetylase Family. Molecular Systems Biology 9: 672.

178. Ju Y, Guo H, Edman M, Hamm-Alvarez SF. 2020. Application of Advances in Endocytosis and Membrane Trafficking to Drug Delivery. Advanced Drug Delivery Reviews 157: 118–141.

179. Kabrawala S, Zimmer MD, Campellone KG. 2020. WHIMP Links the Actin Nucleation Machinery to Src-Family Kinase Signalling During Protrusion and Motility. Plos Genetics 16: e1008694.

180. Kamioka Y, Fukuhara S, Sawa H, Nagashima J, Masuda M, Matsuda M, Mochizuki N. 2004. A Novel Dynamin-Associating Molecule, Formin-Binding Protein 17, Induces Tubular Membrane Invaginations and Participates in Endocytosis. Journal of Biological Chemistry 279: 40091–40099.

181. Kaplan OI, Doroquez DB, Cevik S, Bowie RV, Clarke L, Sanders AAWM, Kida K, Rappoport JZ, Sengupta P, Blacque OE. 2012. Endocytosis Genes Facilitate Protein and Membrane Transport in *C. elegans* Sensory Cilia. Current Biology 22: 451–460.

182. Katoh M. 2013. Functional Proteomics, Human Genetics and Cancer Biology of GIPC Family Members. Experimental and Molecular Medicine 45: e26.

183. Kaushik S, Cuervo AM. 2012. Chaperone-Mediated Autophagy: A Unique Way to Enter the Lysosome World. Trends in Cell Biology 22: 407–417.

184. Kavanaugh WM, Pot DA, Chin SM, Deuter-Reinhard M, Jefferson AB, Norris FA, Masiarz FR, Cousens LS, Majerus PW, Williams LT. 1996. Multiple Forms of an Inositol Polyphosphate 5-phosphatase Form Signalling Complexes with Shc and Grb2. Current biology: CB 6: 438–445.

185. Kelly AE, Kranitz H, Dotsch V, Mullins RD. 2006. Actin Binding to the Central Domain of WASP/SCAR Proteins Plays a Critical Role in the Activation of the Arp2/3 Complex. Journal of Biological Chemistry 281: 10589–10597.

186. Kerr MC, Teasdale RD. 2009. Defining Macropinocytosis. Traffic 10: 364–371.

187. Kihara A, Noda T, Ishihara N, Ohsumi Y. 2001. Two Distinct Vps34 Phosphatidylinositol 3–Kinase Complexes Function in Autophagy and Carboxypeptidase Y Sorting in *Saccharomyces cerevisiae*. The Journal of Cell Biology 152: 519–530.

188. Kim M, Wende H, Walcher J, Kueehnemund J, Cheret C, Kempa S, McShane E, Selbach M, Lewin GR, Birchmeier C. 2018. Maf Links Neuregulin1 Signalling to Cholesterol Synthesis in Myelinating Schwann Cells. Genes & Development 32: 645–657.

189. Kim YJ, Guzman-Hernandez ML, Balla T. 2011. A Highly Dynamic ER-Derived Phosphatidylinositol-Synthesising Organelle Supplies Phosphoinositides to Cellular Membranes. Developmental Cell 21: 813–824.

190. Kimura T, Takabatake Y, Takahashi A, Kaimori J, Matsui I, Namba T, Kitamura H, Niimura F, Matsusaka T, Soga T, Rakugi H, Isaka Y. 2011. Autophagy Protects the Proximal Tubule from Degeneration and Acute Ischemic Injury. Journal of the American Society of Nephrology 22: 902–913.

191. King GJ, Stoeckli J, Hu S-H, Winnen B, Duprez WGA, Meoli CC, Junutula JR, Jarrott RJ, James DE, Whitten AE, Martin JL. 2012. Membrane Curvature Protein Exhibits Interdomain Flexibility and Binds a Small GTPase. Journal of Biological Chemistry 287: 40996–41006.

192. King J, Insall RH. 2003. Parasexual Genetics of *Dictyostelium* Gene Disruptions: Identification of a Ras Pathway using Diploids. Bmc Genetics 4: 12.

193. King JS, Gueho A, Hagedorn M, Gopaldass N, Leuba F, Soldati T, Insall RH. 2013. WASH is required for Lysosomal Recycling and Efficient Autophagic and Phagocytic Digestione. Molecular Biology of the Cell 24: 2714–2726.

194. King JS, Insall RH. 2009. Chemotaxis: Finding the Way Forward with *Dictyostelium*. Trends in Cell Biology 19: 523–530.

195. King JS, Kay RR. 2019. The Origins and Evolution of Macropinocytosis. Philosophical Transactions of the Royal Society B Biological Sciences 374: 20180158.

196. King JS, Teo R, Ryves J, Reddy JV, Peters O, Orabi B, Hoeller O, Williams RSB, Harwood AJ. 2009. The Mood Stabiliser Lithium Suppresses PIP_3 Signalling in *Dictyostelium* and Human Cells. Disease Models & Mechanisms 2: 306–312.

197. Knecht D, Cohen S, Loomis W, Lodish H. 1986. Developmental Regulation of *Dictyostelium discoideum* Actin Gene Fusions Carried on Low-Copy and High-Copy Transformation Vectors. Molecular and Cellular Biology 6: 3973–3983.

198. Knoedler A, Feng S, Zhang J, Zhang X, Das A, Peranen J, Guo W. 2010. Coordination of Rab8 and Rab11 in Primary Ciliogenesis. Proceedings of the National Academy of Sciences of the United States of America 107: 6346–6351.

199. Kocks C, Gouin E, Tabouret M, Berche P, Ohayon H, Cossart P. 1992. L-Monocytogenes-Induced Actin Assembly Requires the Acta Gene-Product, a Surface Protein. Cell 68: 521–531.

200. Kocks C, Marchand J, Gouin E, Dhauteville H, Sansonetti P, Carlier M, Cossart P. 1995. The Unrelated Surface-Proteins Acta of *Listeria monocytogenes* and Icsa of *Shigella flexneri* are Sufficient to Confer Actin-Based Motility on *Listeria innocua* and *Escherichia coli* respectively. Molecular Microbiology 18: 413–423.

201. Koerber S, Faix J. 2022. VASP Boosts Protrusive Activity of Macro-Endocytic Cups and Drives Phagosome Rocketing after Internalisation. European Journal of Cell Biology 101: 151200.

202. Kollmar M, Lbik D, Enge S. 2012. Evolution of the Eukaryotic Arp2/3 Activators of the WASP Family: WASP, WAVE, WASH, and WHAMM, and the Proposed New Family Members WAWH and WAML. BMC Research Notes 5: 1–23.

203. Kops G, de Ruiter ND, De Vries-Smits AMM, Powell DR, Bos JL, Burgering BMT. 1999. Direct Control of the Forkhead Transcription Factor AFX by Protein Kinase B. Nature 398: 630–634.

204. Kortholt A, King JS, Keizer-Gunnink I, Harwood AJ, Van Haastert PJM. 2007. Phospholipase C Regulation of Phosphatidylinositol 3,4,5-Trisphosphate-Mediated Chemotaxis. Molecular Biology of the Cell 18: 4772–4779.

205. Kramer DA, Piper HK, Chen B. 2022. WASP Family Proteins: Molecular Mechanisms and Implications in Human Disease. European Journal of Cell Biology 101: 151244.

206. Kuehbacher A, Dambournet D, Echard A, Cossart P, Pizarro-Cerda J. 2012. Phosphatidylinositol 5-phosphatase Oculocerebrorenal Syndrome of Lowe Protein (OCRL) Controls Actin Dynamics during Early Steps of *Listeria monocytogenes* Infection. Journal of Biological Chemistry 287: 13128–13136.

207. Laxminarayan K, Chan B, Tetaz T, Bird P, Mitchell C. 1994. Characterisation of a cDNA-Encoding the 43 kDa Membrane-Associated Inositol Polyphosphate 5-phosphatase. Journal of Biological Chemistry 269: 17305–17310.

208. Laxminarayan K, Matzaris M, Speed C, Mitchell C. 1993. Purification and Characterisation of a 43 kDa Membrane-Associated Inositol Polyphosphate 5-phosphatase from Human Placenta. Journal of Biological Chemistry 268: 4968–4974.

209. Lee E, Knecht DA. 2002. Visualisation of Actin Dynamics During Macropinocytosis and Exocytosis. Traffic 3: 186–192.

210. Leverrier Y, Okkenhaug K, Sawyer C, Bilancio A, Vanhaesebroeck B, Ridley AJ. 2003. Class I Phosphoinositide 3-Kinase p110 Beta is required for Apoptotic Cell and Fc Gamma Receptor-Mediated Phagocytosis by Macrophages. Journal of Biological Chemistry 278: 38437–38442.

211. Levin R, Grinstein S, Schlam D. 2015. Phosphoinositides in Phagocytosis and Macropinocytosis. Biochimica Et Biophysica Acta-Molecular and Cell Biology of Lipids 1851: 805–823.

212. Lewis WH. 1937. Pinocytosis by Malignant Cells. Amer Jour Cancer 29: 666–679.

213. Li J, Mao X, Dong LQ, Liu F, Tong L. 2007. Crystal Structures of the BAR-PH and PTB Domains of Human APPL1. Structure 15: 525–533.

214. Lichter-Konecki U, Farber LW, Cronin JS, Suchy SF, Nussbaum RL. 2006. The Effect of Missense Mutations in the Rho-GAP-Homology Domain on OCRL1 Function. Molecular Genetics and Metabolism 89: 121–128.

215. Lieber MR. 2010. The Mechanism of Double-Strand DNA Break Repair by the Non-Homologous DNA End-Joining Pathway. Pages 181–211 in Kornberg RD, Raetz CRH, Rothman JE, and Thorner JW, eds. Annual Review of Biochemistry, Vol 79, vol. 79. Annual Reviews.

216. Lim JP, Gleeson PA. 2011. Macropinocytosis: An Endocytic Pathway for Internalising Large Gulps. Immunology and Cell Biology 89: 836–843.

217. Lim JP, Gosavi P, Mintern JD, Ross EM, Gleeson PA. 2015. Sorting Nexin 5 Selectively Regulates Dorsal-Ruffle-Mediated Macropinocytosis in Primary Macrophages. Journal of Cell Science 128: 4407–4419.

218. Lin DC, Quevedo C, Brewer NE, Bell A, Testa JR, Grimes ML, Miller FD, Kaplan DR. 2006. APPL1 Associates with TrkA and GIPC1 and is required for Nerve Growth Factor-Mediated Signal Transduction. Molecular and Cellular Biology 26: 8928–8941.

219. Linardopoulou EV, Parghi SS, Friedman C, Osborn GE, Parkhurst SM, Trask BJ. 2007. Human Subtelomeric WASH Genes Encode a New Subclass of the WASP Family. Plos Genetics 3: 2477–2485.

220. Liu J, Yao F, Wu RP, Morgan M, Thorburn A, Finley RL, Chen YQ. 2002. Mediation of the DCC Apoptotic Signal by DIP13 Alpha. Journal of Biological Chemistry 277: 26281–26285.

221. Loomis W. 1971. Sensitivity of *Dictyostelium discoideum* to Nucleic Acid Analogues. Experimental Cell Research 64: 484-.

222. Loovers HM, Kortholt A, Groote H de, Whitty L, Nussbaum RL, Haastert PJM van. 2007. Regulation of Phagocytosis in *Dictyostelium* by the Inositol 5-phosphatase OCRL Homolog, Dd5P4. Traffic 8: 618–628.

223. Loovers HM, Veenstra K, Snippe H, Pesesse X, Erneux C, van Haastert PJM. 2003. A Diverse Family of Inositol 5-phosphatases playing a Role in Growth and Development in *Dictyostelium discoideum*. Journal of Biological Chemistry 278: 5652–5658.

224. Lord SJ, Velle KB, Mullins RD, Fritz-Laylin LK. 2020. Super-Plots: Communicating Reproducibility and Variability in Cell Biology. Journal of Cell Biology 219: e202001064.

225. Losson R, Lacroute F. 1979. Interference of Non-sense Mutations with Eukaryotic mRNA Stability. Proceedings of the National Academy of Sciences of the United States of America 76: 5134–5137.

226. Lowe C, Terrey M, MaClachlan EA. 1952. Organic-Aciduria, Decreased Renal Ammonia Production, Hydrophthalmos, and Mental Retardation: A Clinical Entity. A.M.A. American Journal of Diseases of Children 83: 164–184.

227. Lowe M. 2005. Structure and Function of the Lowe Syndrome Protein OCRL1. Traffic (Copenhagen, Denmark) 6: 711–719.

228. Lundmark R, Carlsson SR. 2004. Regulated Membrane Recruitment of Dynamin-2 Mediated by Sorting Nexin 9. Journal of Biological Chemistry 279: 42694–42702.

229. Luo LQ. 2002. Actin Cytoskeleton Regulation in Neuronal Morphogenesis and Structural Plasticity. Annual Review of Cell and Developmental Biology 18: 601–635.

230. Luo N, Conwell MD, Chen X, Kettenhofen CI, Westlake CJ, Cantor LB, Wells CD, Weinreb RN, Corson TW, Spandau DF, Joos KM, Iomini C, Obukhov AG, Sun Y. 2014. Primary Cilia Signalling Mediates Intraocular Pressure Sensation. Proceedings of the National Academy of Sciences of the United States of America 111: 12871–12876.

231. Luo N, Kumar A, Conwell M, Weinreb RN, Anderson R, Sun Y. 2013. Compensatory Role of Inositol 5-phosphatase INPP5B to OCRL in Primary Cilia Formation in Oculocerebrorenal Syndrome of Lowe. Plos One 8: e66727.

232. Luo N, West CC, Murga-Zamalloa CA, Sun L, Anderson RM, Wells CD, Weinreb RN, Travers JB, Khanna H, Sun Y. 2012. OCRL Localises to the Primary Cilium: A New Role for Cilia in Lowe Syndrome. Human Molecular Genetics 21: 3333–3344.

233. Luscher A, Fröhlich F, Barisch C, Littlewood C, Metcalfe J, Leuba F, Palma A, Pirruccello M, Cesareni G, Stagi M, Walther TC, Soldati T, De Camilli P, Swan LE. 2019. Lowe Syndrome–Linked Endocytic Adaptors Direct Membrane Cycling Kinetics with OCRL in *Dictyostelium discoideum*. Molecular Biology of the Cell 30: 2268–2282.

234. Luzio JP, Parkinson MDJ, Gray SR, Bright NA. 2009. The Delivery of Endocytosed Cargo to Lysosomes. Biochemical Society Transactions 37: 1019–1021.

235. Lykke-Andersen J, Bennett EJ. 2014. Protecting the Proteome: Eukaryotic Co-translational Quality Control Pathways. Journal of Cell Biology 204: 467–476.

236. Machesky L, Atkinson S, Ampe C, Vandekerckhove J, Pollard T. 1994. Purification of a Cortical Complex Containing 2 Unconventional Actins from *Acanthamoeba* by Affinity Chromatography on Profilin Agarose. Journal of Cell Biology 127: 107–115.

237. Machesky LM, Insall RH. 1998. SCAR1 and the Related Wiskott-Aldrich Syndrome Protein, WASP, Regulate the Actin Cytoskeleton through the Arp2/3 Complex. Current biology: CB 8: 1347–1356.

238. Maekawa M, Ishizaki T, Boku S, Watanabe N, Fujita A, Iwamatsu A, Obinata T, Ohashi K, Mizuno K, Narumiya S. 1999. Signalling from Rho to the Actin Cytoskeleton through Protein Kinases ROCK and LIM-Kinase. Science (New York, N.Y.) 285: 895–898.

239. Majerus PW, Kisseleva MV, Norris FA. 1999. The Role of Phosphatases in Inositol Signalling Reactions. Journal of Biological Chemistry 274: 10669–10672.

240. Mao XM, Kikani CK, Riojas RA, Langlais P, Wang LX, Ramos FJ, Fang QC, Christ-Roberts CY, Hong JY, Kim RY, Liu F, Dong LQ. 2006. APPL1 Binds to Adiponectin Receptors and Mediates Adiponectin Signalling and Function. Nature Cell Biology 8: 516-523.

241. Mao Y, Balkin DM, Zoncu R, Erdmann KS, Tomasini L, Hu F, Jin MM, Hodsdon ME, De Camilli P. 2009. A PH Domain within OCRL Bridges Clathrin-Mediated Membrane Trafficking to Phosphoinositide Metabolism. Embo Journal 28: 1831–1842.

242. Maquat L, Kinniburgh A, Rachmilewitz E, Ross J. 1981. Unstable Beta-Globin mRNA in mRNA-Deficient Beta-O Thalassemia. Cell 27: 543–553.

243. Marat AL, Haucke V. 2016. Phosphatidylinositol 3-Phosphates at the Interface between Cell Signalling and Membrane Traffic. Embo Journal 35: 561–579.

244. Marchand JB, Kaiser DA, Pollard TD, Higgs HN. 2001. Interaction of WASP/SCAR Proteins with Actin and Vertebrate Arp2/3 Complex. Nature Cell Biology 3: 76–82.

245. Marion S, Mazzolini J, Herit F, Bourdoncle P, Kambou-Pene N, Hailfinger S, Sachse M, Ruland J, Benmerah A, Echard A, Thome M, Niedergang F. 2012. The NF-kappa B Signalling Protein Bcl10 Regulates Actin Dynamics by Controlling AP1 and OCRL-Bearing Vesicles. Developmental Cell 23: 954–967.

246. Marshall JG, Booth JW, Stambolic V, Mak T, Balla T, Schreiber AD, Meyer T, Grinstein S. 2001. Restricted Accumulation of Phosphatidylinositol 3-Kinase Products in a Plasmalemmal Subdomain during Fc Gamma Receptor-Mediated Phagocytosis. Journal of Cell Biology 153: 1369–1380.

247. Maselli A, Laevsky G, Knecht DA. 2002. Kinetics of Binding, Uptake and Degradation of Live Fluorescent (DsRed) Bacteria by *Dictyostelium discoideum*. Microbiology 148: 413–420.

248. Massaad MJ, Ramesh N, Geha RS. 2013. Wiskott-Aldrich Syndrome: A Comprehensive Review. Pages 26–43 in Rose NR, ed. Year in Immunology, vol. 1285. Blackwell Science Publ.

249. Massol RH, Boll W, Griffin AM, Kirchhausen T. 2006. A Burst of Auxilin Recruitment Determines the Onset of Clathrin-Coated Vesicle Uncoating. Proceedings of the National Academy of Sciences of the United States of America 103: 10265–10270.

250. Maxson ME, Sarantis H, Volchuk A, Brumell JH, Grinstein S. 2021. Rab5 Regulates Macropinocytosis by Recruiting the Inositol 5-phosphatases OCRL and INPP5B that Hydrolyse PtdIns(4,5)P_2. Journal of Cell Science 134: jcs252411.

251. Mckanna J. 1973. Fine-Structure of Contractile Vacuole Pore in *Paramecium*. Journal of Protozoology 20: 631–638.

252. Mckanna J. 1976. Fine-Structure of Fluid Segregation Organelles of *Paramecium* Contractile Vacuoles. Journal of Ultrastructure Research 54: 1–10.

253. McPherson PS, Garcia EP, Slepnev VI, David C, Zhang XM, Grabs D, Sossin WS, Bauerfeind R, Nemoto Y, DeCamilli P. 1996. A Presynaptic Inositol 5-phosphatase. Nature 379: 353–357.

254. Meena NP, Kimmel AR. 2018. Quantification of Live Bacterial Sensing for Chemotaxis and Phagocytosis and of Macropinocytosis. Frontiers in Cellular and Infection Microbiology 8.

255. Mehta ZB, Pietka G, Lowe M. 2014. The Cellular and Physiological Functions of the Lowe Syndrome Protein OCRL1. Traffic 15: 471–487.

256. Merlot S, Meili R, Pagliarini DJ, Maehama T, Dixon JE, Firtel RA. 2003. A PTEN-Related 5-Phosphatidylinositol Phosphatase Localised in the Golgi. Journal of Biological Chemistry 278: 39866–39873.

257. Merrifield CJ, Qualmann B, Kessels MM, Almers W. 2004. Neural Wiskott Aldrich Syndrome Protein (N-WASP) and the Arp2/3 Complex are Recruited to Sites of Clathrin-Mediated Endocytosis in Cultured Fibroblasts. European Journal of Cell Biology 83: 13–18.

258. Mettlen M, Chen P-H, Srinivasan S, Danuser G, Schmid SL. 2018. Regulation of Clathrin-Mediated Endocytosis. Pages 871–896 in Kornberg RD, ed. Annual Review of Biochemistry, Vol 87, vol. 87. Annual Reviews.

259. Miaczynska M, Christoforidis S, Giner A, Shevchenko A, Uttenweiler-Joseph S, Habermann B, Wilm M, Parton RG, Zerial M. 2004. APPL Proteins Link Rab5 to Nuclear Signal Transduction via an Endosomal Compartment. Cell 116: 445–456.

260. Miki H, Miura K, Takenawa T. 1996. N-WASP, a Novel Actin Depolymerising Protein, Regulates the Cortical Cytoskeletal Rearrangement in a PIP_2-Dependent Manner Downstream of Tyrosine Kinases. Embo Journal 15: 5326–5335.

261. Miki H, Sasaki T, Takai Y, Takenawa T. 1998a. Induction of Filopodium Formation by a WASP Related Actin Depolymerising Protein N-WASP. Nature 391: 93–96.

262. Miki H, Suetsugu S, Takenawa T. 1998b. WAVE, a Novel WASP-Family Protein Involved in Actin Reorganisation Induced by Rac. Embo Journal 17: 6932–6941.

263. Milne SB, Ivanova PT, Armstrong MD, Myers DS, Lubarda J, Shulga YV, Topham MK, Brown HA, Epand RM. 2008. Dramatic Differences in the Roles in Lipid Metabolism of Two Isoforms of Diacylglycerol Kinase. Biochemistry 47: 9372–9379.

264. Mitsunari T, Nakatsu F, Shioda N, Love PE, Grinberg A, Bonifacino JS, Ohno H. 2005. Clathrin Adaptor AP-2 is Essential for Early Embryonal Development. Molecular and Cellular Biology 25: 9318–9323.

265. Mizushima N, Levine B, Cuervo AM, Klionsky DJ. 2008. Autophagy Fights Disease through Cellular Self-Digestion. Nature 451: 1069–1075.

266. Mochizuki Y, Takenawa T. 1999. Novel Inositol Polyphosphate 5-phosphatase Localises at Membrane Ruffles. Journal of Biological Chemistry 274: 36790–36795.

267. Montjean R, Aoidi R, Desbois P, Rucci J, Trichet M, Salomon R, Rendu J, Faure J, Lunardi J, Gacon G, Billuart P, Dorseuil O. 2015. OCRL-Mutated Fibroblasts from Patients with Dent-2 Disease Exhibit INPP5B-Independent Phenotypic Variability Relatively to Lowe Syndrome Cells. Human Molecular Genetics 24: 994–1006.

268. Moorhead AM, Jung J-Y, Smirnov A, Kaufer S, Scidmore MA. 2010. Multiple Host Proteins that Function in Phosphatidylinositol-4-Phosphate Metabolism are recruited to the Chlamydial Inclusion. Infection and Immunity 78: 1990–2007.

269. Morel E, Chamoun Z, Lasiecka ZM, Chan RB, Williamson RL, Vetanovetz C, Dall'Armi C, Simoes S, Du Jour KSP, McCabe BD, Small SA, Di Paolo G. 2013. Phosphatidylinositol-3-Phosphate Regulates Sorting and Processing of Amyloid Precursor Protein through the Endosomal System. Nature Communications 4: 2250.

270. Morioka S, Nakanishi H, Yamamoto T, Hasegawa J, Tokuda E, Hikita T, Sakihara T, Kugii Y, Oneyama C, Yamazaki M, Suzuki A, Sasaki J, Sasaki T. 2022. A Mass Spectrometric Method for In-Depth Profiling of Phosphoinositide Regioisomers and their Disease-Associated Regulation. Nature Communications 13: 83.

271. Motley A, Bright NA, Seaman MNJ, Robinson MS. 2003. Clathrin-Mediated Endocytosis in AP-2-Depleted Cells. Journal of Cell Biology 162: 909–918.

272. Mullins RD, Heuser JA, Pollard TD. 1998. The Interaction of Arp2/3 Complex with Actin: Nucleation, High Affinity Pointed End Capping, and Formation of Branching Networks of Filaments. Proceedings of the National Academy of Sciences 95: 6181–6186.

273. Muro S, Mateescu M, Gajewski C, Robinson M, Muzykantov VR, Koval M. 2006. Control of Intracellular Trafficking of ICAM-1-Targeted Nanocarriers by Endothelial Na^+/H^+ Exchanger Proteins. American Journal of Physiology-Lung Cellular and Molecular Physiology 290: L809–L817.

274. Muro S, Wiewrodt R, Thomas A, Koniaris L, Albelda SM, Muzykantov VR, Koval M. 2003. A Novel Endocytic Pathway Induced by Clustering Endothelial ICAM-1 or PECAM-1. Journal of Cell Science 116: 1599–1609.

275. Myers SA, Han JW, Lee Y, Firtel RA, Chung CY. 2005. A *Dictyostelium* Homologue of WASP is required for Polarised F-actin Assembly during Chemotaxis. Molecular Biology of the Cell 16: 2191–2206.

276. Mylvaganam SM, Grinstein S, Freeman SA. 2018. Picket-Fences in the Plasma Membrane: Functions in Immune Cells and Phagocytosis. Seminars in Immunopathology 40: 605–615.

277. Nakada-Tsukui K, Okada H, Mitra BN, Nozaki T. 2009. Phosphatidylinositol-Phosphates Mediate Cytoskeletal Reorganisation during Phagocytosis via a Unique Modular Protein Consisting of Rho-GEF/DH and FYVE Domains in the Parasitic Protozoon *Entamoeba histolytica*. Cellular Microbiology 11: 1471–1491.

278. Nakada-Tsukui K, Watanabe N, Maehama T, Nozaki T. 2019. Phosphatidylinositol Kinases and Phosphatases in *Entamoeba histolytica*. Frontiers in Cellular and Infection Microbiology 9.

279. Nakanishi H, Takai Y. 2008. Frabin and other Related Cdc42-Specific Guanine Nucleotide Exchange Factors Couple the Actin Cytoskeleton with the Plasma Membrane. Journal of Cellular and Molecular Medicine 12: 1169–1176.

280. Nandez R, Balkin DM, Messa M, Liang L, Paradise S, Czapla H, Hein MY, Duncan JS, Mann M, De Camilli P. 2014. A Role of OCRL in Clathrin-Coated Pit Dynamics and Un-coating Revealed by Studies of Lowe Syndrome Cells. Elife 3: e02975.

281. Nechamen CA, Thomas RM, Dias JA. 2007. APPL1, APPL2, Akt2 and FOXO1a Interact with FSHR in a Potential Signalling Complex. Molecular and Cellular Endocrinology 260: 93–99.

282. Nemoto Y, Arribas M, Haffner C, DeCamilli P. 1997. Synaptojanin 2, a Novel Synaptojanin Isoform with a Distinct Targeting Domain and Expression Pattern. Journal of Biological Chemistry 272: 30817–30821.

283. Ngoenkam J, Paensuwan P, Wipa P, Schamel WWA, Pongcharoen S. 2021. Wiskott-Aldrich Syndrome Protein: Roles in Signal Transduction in T-cells. Frontiers in Cell and Developmental Biology 9.

284. Nichols JME, Veltman D, Kay RR. 2015. Chemotaxis of a Model Organism: Progress with *Dictyostelium*. Current Opinion in Cell Biology 36: 7–12.

285. Nishihara E, Shimmen T, Sonobe S. 2007. New Aspects of Membrane Dynamics of *Amoeba proteus* Contractile Vacuole Revealed by Vital Staining with FM4-64. Protoplasma 231: 25–30.

286. Noakes CJ, Lee G, Lowe M. 2011. The PH Domain Proteins IPIP27A and B Link OCRL1 to Receptor Recycling in the Endocytic Pathway. Molecular Biology of the Cell 22: 606–623.

287. Nobukuni T, Joaquin M, Roccio M, Dann SG, Kim SY, Gulati P, Byfield MP, Backer JM, Natt F, Bos JL, Zwartkruis FJT, Thomas G. 2005. Amino Acids Mediate mTOR/Raptor Signalling Through Activation of Class 3 Phosphatidylinositol 3-OH-Kinase. Proceedings of the National Academy of Sciences of the United States of America 102: 14238–14243.

288. Noethe HB, Manstein DJ. 1998. Identification and Characterisation of *Dictyostelium* Dynamin B. Molecular Biology of the Cell 9: 198A.

289. Norbury CC, Chambers BJ, Prescott AR, Ljunggren HG, Watts C. 1997. Constitutive Macropinocytosis Allows TAP-Dependent Major Histocompatibility Complex Class I Presentation of Exogenous Soluble Antigen by Bone Marrow-Derived Dendritic Cells. European Journal of Immunology 27: 280–288.

290. Norbury CC, Hewlett LJ, Prescott AR, Shastri N, Watts C. 1995. Class I MHC Presentation of Exogenous Soluble Antigen via Macropinocytosis in Bone Marrow Macrophages. Immunity 3: 783–791.

291. Nussbaum RL, Orrison BM, Janne PA, Charnas L, Chinault AC. 1997. Physical Mapping and Genomic Structure of the Lowe Syndrome Gene OCRL1. Human Genetics 99: 145–150.

292. Obaishi H, Nakanishi H, Mandai K, Satoh K, Satoh A, Takahashi K, Miyahara M, Nishioka H, Takaishi K, Takai Y. 1998. Frabin, a Novel FGD1-Related Actin Filament-Binding Protein Capable of Changing Cell Shape and Activating c-Jun N-terminal Kinase. Journal of Biological Chemistry 273: 18697–18700.

293. Oda A, Ochs HD, Druker BJ, Ozaki K, Watanabe C, Handa M, Miyakawa Y, Ikeda Y. 1998. Collagen Induces Tyrosine Phosphorylation of Wiskott-Aldrich Syndrome Protein in Human Platelets. Blood 92: 1852–1858.

294. Odai H, Sasaki K, Iwamatsu A, Nakamoto T, Ueno H, Yamagata T, Mitani K, Yazaki Y, Hirai H. 1997. Purification and Molecular Cloning of SH2- and SH3-containing Inositol Polyphosphate 5-phosphatase, which is Involved in the Signalling Pathway of Granulocyte-Macrophage Colony-Stimulating Factor, Erythropoietin, and Bcr-Abl. Blood 89: 2745–2756.

295. Ogata T, Ueyama T, Isodono K, Tagawa M, Takehara N, Kawashima T, Harada K, Takahashi T, Shioi T, Matsubara H, Oh H. 2008. MURC, a Muscle-Restricted Coiled-Coil Protein that Modulates the Rho/ROCK Pathway, Induces Cardiac Dysfunction and Conduction Disturbance. Molecular and Cellular Biology 28: 3424–3436.

296. Olivosglander I, Janne P, Nussbaum R. 1995. The Oculocerebrorenal Syndrome Gene-Product is a 105 kDa Protein Localised to the Golgi Complex. American Journal of Human Genetics 57: 817–823.

297. Oltrabella F, Pietka G, Ramirez IB-R, Mironov A, Starborg T, Drummond IA, Hinchliffe KA, Lowe M. 2015. The Lowe Syndrome Protein OCRL1 is required for Endocytosis in the Zebrafish Pronephric Tubule. Plos Genetics 11: e1005058.

298. Ono M, Bolland S, Tempst P, Ravetch JV. 1996. Role of the Inositol Phosphatase SHIP in Negative Regulation of the Immune System by the Receptor Fc Gamma RIIB. Nature 383: 263–266.

299. Ono Y, Nakanishi H, Nishimura M, Kakizaki M, Takahashi K, Miyahara M, Satoh-Horikawa K, Mandai K, Takai Y. 2000. Two Actions of Frabin: Direct Activation of Cdc42 and Indirect Activation of Rac. Oncogene 19: 3050–3058.

300. Otsuki M, Itoh T, Takenawa T. 2003. Neural Wiskott-Aldrich Syndrome Protein is recruited to Rafts and Associates with Endophilin A in Response to Epidermal Growth Factor. Journal of Biological Chemistry 278: 6461–6469.

301. Padrick SB, Cheng H-C, Ismail AM, Panchal SC, Doolittle LK, Kim S, Skehan BM, Umetani J, Brautigam CA, Leong JM, Rosen MK. 2008. Hierarchical Regulation of WASP/WAVE Proteins. Molecular Cell 32: 426–438.

302. Padrick SB, Doolittle LK, Brautigam CA, King DS, Rosen MK. 2011. Arp2/3 Complex is Bound and Activated by Two WASP Proteins. Proceedings of the National Academy of Sciences of the United States of America 108: E472–E479.

303. Paesmans J, Martin E, Deckers B, Berghmans M, Sethi R, Loeys Y, Pardon E, Steyaert J, Verstreken P, Galicia C, Versees W. 2020. A Structure of Substrate-Bound Synaptojanin1 Provides New Insights in its Mechanism and the Effect of Disease Mutations. Elife 9: e64922.

304. Pan M, Xu X, Chen Y, Jin T. 2016. Identification of a Chemoattractant G-Protein-Coupled Receptor for Folic Acid that Controls both Chemotaxis and Phagocytosis. Developmental Cell 36: 428–439.

305. Panchal SC, Kaiser DA, Torres E, Pollard TD, Rosen MK. 2003. A Conserved Amphipathic Helix in WASP/SCAR Proteins is Essential for Activation of Arp2/3 Complex. Nature Structural Biology 10: 591–598.

306. Pandey D, Goyal P, Dwivedi S, Siess W. 2009. Unraveling a Novel Rac1-mediated Signalling Pathway that Regulates Cofilin De-phosphorylation and Secretion in Thrombin-Stimulated Platelets. Blood 114: 415–424.

307. Parente CA, Blacklock BJ, Froehlich WM, Murphy DB, Devreotes PN. 1998. G-Protein Signalling Events are activated at the Leading Edge of Chemotactic Cells. Cell 95: 81–91.

308. Paschke P, Knecht DA, Silale A, Traynor D, Williams TD, Thomason PA, Insall RH, Chubb JR, Kay RR, Veltman DM. 2018. Rapid and Efficient Genetic Engineering of both Wild Type and Axenic Strains of *Dictyostelium discoideum*. PLOS ONE 13: e0196809.

309. Pasteris N, Cadle A, Logie L, Porteous M, Schwartz C, Stevenson R, Glover T, Wilroy R, Gorski J. 1994. Isolation and Characterisation of the Faciogenital Dysplasia (Aarskog-Scott Syndrome) Gene - A Putative Rho/Rac Guanine-Nucleotide Exchange Factor. Cell 79: 669–678.

310. Patterson D. 1980. Contractile Vacuoles and Associated Structures - Their Organisation and Function. Biological Reviews 55: 1-46.

311. Paunola E, Mattila PK, Lappalainen P. 2002. WH2 domain: A Small, Versatile Adapter for Actin Monomers. Febs Letters 513: 92–97.

312. Pereira-Leal JB, Seabra MC. 2001. Evolution of the Rab Family of Small GTP-Binding Proteins. Journal of Molecular Biology 313: 889–901.

313. Perera RM, Zoncu R, Lucast L, De Camilli P, Toomre D. 2006. Two Synaptojanin 1 Isoforms are recruited to Clathrin-Coated Pits at Different Stages. Proceedings of the National Academy of Sciences of the United States of America 103: 19332–19337.

314. Pernier J, Orban J, Avvaru BS, Jegou A, Romet-Lemonne G, Guichard B, Carlier M-F. 2013. Dimeric WH2 Domains in *Vibrio* VopF Promote Actin Filament Barbed-End Uncapping and Assisted Elongation. Nature Structural & Molecular Biology 20: 1069-1076.

315. Pesesse X, Deleu S, DeSmedt F, Drayer L, Erneux C. 1997. Identification of a Second SH2-Domain-Containing Protein Closely Related to the Phosphatidylinositol Polyphosphate 5-phosphatase SHIP. Biochemical and Biophysical Research Communications 239: 697–700.

316. Peter BJ, Kent HM, Mills IG, Vallis Y, Butler PJG, Evans PR, McMahon HT. 2004. BAR Domains as Sensors of Membrane Curvature: The Amphiphysin BAR Structure. Science 303: 495–499.

317. Pirruccello M, De Camilli P. 2012. Inositol 5-phosphatases: Insights from the Lowe Syndrome Protein OCRL. Trends in Biochemical Sciences 37: 134–143.

318. Pirruccello M, Swan LE, Folta-Stogniew E, De Camilli P. 2011. Recognition of the F&H Motif by the Lowe Syndrome Protein OCRL. Nature Structural & Molecular Biology 18: 789-795.

319. Pollard TD. 2007. Regulation of Actin Filament Assembly by the Arp2/3 Complex and Formins. Annual Review of Biophysics and Biomolecular Structure 36: 451–477.

320. Pollard TD. 2016. Actin and Actin-Binding Proteins. Cold Spring Harbor Perspectives in Biology 8: a018226.

321. Pollard TD, Cooper JA. 2009. Actin, a Central Player in Cell Shape and Movement. Science 326: 1208–1212.

322. Pollitt AY, Insall RH. 2009. Loss of *Dictyostelium* HSPC300 Causes a SCAR-Like Phenotype and Loss of SCAR Protein. Bmc Cell Biology 10: 13.

323. Ponting CP. 2006. A Novel Domain Suggests a Ciliary Function for ASPM, a Brain Size Determining Gene. Bioinformatics 22: 1031–1035.

324. Posor Y, Eichhorn-Gruenig M, Puchkov D, Schoeneberg J, Ullrich A, Lampe A, Mueller R, Zarbakhsh S, Gulluni F, Hirsch E, Krauss M, Schultz C, Schmoranzer J, Noe F, Haucke V. 2013. Spatiotemporal Control of Endocytosis by Phosphatidylinositol-3,4-Bisphosphate. Nature 499: 233-237.

325. Posor Y, Eichhorn-Grünig M, Haucke V. 2015. Phosphoinositides in Endocytosis. Biochimica et Biophysica Acta (BBA) - Molecular and Cell Biology of Lipids 1851: 794–804.

326. Posor Y, Jang W, Haucke V. 2022. Phosphoinositides as Membrane Organisers. Nature Reviews Molecular Cell Biology 1–20.

327. Poupon V, Girard M, Legendre-Guillemin V, Thomas S, Bourbonniere L, Philie J, Bright NA, McPherson PS. 2008. Clathrin Light Chains Function in Mannose Phosphate Receptor Trafficking via Regulation of Actin Assembly. Proceedings of the National Academy of Sciences of the United States of America 105: 168–173.

328. Prehoda KE, Scott JA, Mullins RD, Lim WA. 2000. Integration of Multiple Signals through Cooperative Regulation of the N-WASP-Arp2/3 Complex. Science 290: 801–806.

329. Pylypenko O, Lundmark R, Rasmuson E, Carlsson SR, Rak A. 2007. The PX-BAR Membrane Remodelling Unit of Sorting Nexin 9. Embo Journal 26: 4788–4800.

330. Quinlan ME, Heuser JE, Kerkhoff E, Mullins RD. 2005. *Drosophila* Spire is an Actin Nucleation Factor. Nature 433: 382–388.

331. Quinn SE, Huang L, Kerkvliet JG, Swanson JA, Smith S, Hoppe AD, Anderson RB, Thiex NW, Scott BL. 2021. The Structural Dynamics of Macropinosome Formation and PI3-Kinase-Mediated Sealing Revealed by Lattice Light Sheet Microscopy. Nature Communications 12: 4838.

332. Rabinovitch M. 1995. Professional and Non-professional Phagocytes - An Introduction. Trends in Cell Biology 5: 85–87.

333. Racoosin EL, Swanson JA. 1993. Macropinosome Maturation and Fusion with Tubular Lysosomes in Macrophages. Journal of Cell Biology 121: 1011–1020.

334. Raghavan V, Weisz OA. 2015. Flow Stimulated Endocytosis in the Proximal Tubule. Current Opinion in Nephrology and Hypertension 24: 359–365.

335. van Rahden VA, Brand K, Najm J, Heeren J, Pfeffer SR, Braulke T, Kutsche K. 2012. The 5-phosphatase OCRL Mediates Retrograde Transport of the Mannose 6-Phosphate Receptor by Regulating a Rac1-Cofilin Signalling Module. Human Molecular Genetics 21: 5019–5038.

336. Ramadesikan S, Skiba L, Lee J, Madhivanan K, Sarkar D, De La Fuente A, Hanna CB, Terashi G, Hazbun T, Kihara D, Aguilar RC. 2021. Genotype & Phenotype in Lowe Syndrome: Specific OCRL1 Patient Mutations Differentially Impact Cellular Phenotypes. Human Molecular Genetics 30: 198–212.

337. Ramirez IB-R, Pietka G, Jones DR, Divecha N, Alia A, Baraban SC, Hurlstone AFL, Lowe M. 2012. Impaired Neural Development in a Zebrafish Model for Lowe Syndrome. Human Molecular Genetics 21: 1744–1759.

338. Raper KB, Thom C. 1932. The Distribution of *Dictyostelium* and Other Slime Molds in the Soil. Jour Washington Acad Sci 22: 92–96.

339. Rbaibi Y, Cui S, Mo D, Carattino M, Rohatgi R, Satlin LM, Szalinski CM, Swanhart LM, Foelsch H, Hukriede NA, Weisz OA. 2012. OCRL1 Modulates Cilia Length in Renal Epithelial Cells. Traffic 13: 1295–1305.

340. Rodriguez-Gabin AG, Ortiz E, Demoliner K, Si Q, Almazan G, Larocca JN. 2010. Interaction of Rab31 and OCRL-1 in Oligodendrocytes: Its Role in Transport of Mannose 6-Phosphate Receptors. Journal of Neuroscience Research 88: 589–604.

341. Rohatgi R, Ma L, Miki H, Lopez M, Kirchhausen T, Takenawa T, Kirschner MW. 1999. The Interaction between N-WASP and the Arp2/3 Complex Links Cdc42-Dependent Signals to Actin Assembly. Cell 97: 221–231.

342. Rosales C, Uribe-Querol E. 2017. Phagocytosis: A Fundamental Process in Immunity. BioMed Research International 2017: 1–18.

343. Rossman KL, Worthylake DK, Snyder JT, Siderovski DP, Campbell SL, Sondek J. 2002. A Crystallographic View of Interactions between Dbs and Cdc42: PH Domain-Assisted Guanine Nucleotide Exchange. Embo Journal 21: 1315–1326.

344. Rostislavleva K, Soler N, Ohashi Y, Zhang L, Pardon E, Burke JE, Masson GR, Johnson C, Steyaert J, Ktistakis NT, Williams RL. 2015. Structure and Flexibility of the Endosomal Vps34 Complex Reveals the Basis of its Function on Membranes. Science 350: 140.

345. Rotty JD, Wu C, Bear JE. 2013. New Insights into the Regulation and Cellular Functions of the Arp2/3 Complex. Nature Reviews Molecular Cell Biology 14: 7–12.

346. Roux A, Uyhazi K, Frost A, De Camilli P. 2006. GTP-Dependent Twisting of Dynamin Implicates Constriction and Tension in Membrane Fission. Nature 441: 528–531.

347. Rozycka M, Lu YJ, Brown RA, Lau MR, Shipley JM, Fry MJ. 1998. cDNA Cloning of a Third Human C2-Domain-Containing Class II Phosphoinositide 3-Kinase, PI3K-C2 Gamma, and Chromosomal Assignment of this Gene (PIK3C2G) to 12p12. Genomics 54: 569–574.

348. Ruchira, Hink MA, Bosgraaf L, van Haastert PJM, Visser A. 2004. Pleckstrin Homology Domain Diffusion in *Dictyostelium* Cytoplasm Studied Using Fluorescence Correlation Spectroscopy. Journal of Biological Chemistry 279: 10013–10019.

349. Ryder PV, Vistein R, Gokhale A, Seaman MN, Puthenveedu MA, Faundez V. 2013. The WASH Complex, an Endosomal Arp2/3 Activator, Interacts with the Hermansky–Pudlak Syndrome Complex BLOC-1 and its Cargo Phosphatidylinositol-4-Kinase Type IIα. Molecular Biology of the Cell 24: 2269–2284.

350. Sallusto F, Cella M, Danieli C, Lanzavecchia A. 1995. Dendritic Cells Use Macropinocytosis and the Mannose Receptor to Concentrate Macromolecules in the Major Histocompatibility Complex Class II Compartment - Downregulation by Cytokines and Bacterial Products. Journal of Experimental Medicine 182: 389–400.

351. Sarantis H, Balkin DM, De Camilli P, Isberg RR, Brumell JH, Grinstein S. 2012. *Yersinia* Entry into Host Cells Requires Rab5-Dependent De-phosphorylation of PI(4,5)P_2 and Membrane Scission. Cell Host & Microbe 11: 117–128.

352. Sasahara Y, Rachid R, Byrne MJ, De La Fuente MA, Abraham RT, Ramesh N, Geha RS. 2002. Mechanism of Recruitment of WASP to the Immunological Synapse and of its Activation Following TCR Ligation. Molecular Cell 10: 1269–1281.

353. Satir P, Pedersen LB, Christensen ST. 2010. The Primary Cilium at a Glance. Journal of Cell Science 123: 499–503.

354. Schaap P, Winckler T, Nelson M, Alvarez-Curto E, Elgie B, Hagiwara H, Cavender J, Milano-Curto A, Rozen DE, Dingermann T, Mutzel R, Baldauf SL. 2006. Molecular Phylogeny and Evolution of Morphology in the Social Amoebas. Science (New York, N.Y.) 314: 661–663.

355. Schenck A, Goto-Silva L, Collinet C, Rhinn M, Giner A, Habermann B, Brand M, Zerial M. 2008. The Endosomal Protein APPL1 Mediates Akt Substrate Specificity and Cell Survival in Vertebrate Development. Cell 133: 486–497.

356. Schink KO, Tan KW, Spangenberg H, Martorana D, Sneeggen M, Stévenin V, Enninga J, Campsteijn C, Raiborg C, Stenmark H. 2021. The Phosphoinositide Coincidence Detector Phafin2 Promotes Macropinocytosis by Coordinating Actin Organisation at Forming Macropinosomes. Nature Communications 12: 6577.

357. Schink KO, Tan K-W, Stenmark H. 2016. Phosphoinositides in Control of Membrane Dynamics. Pages 143–171 in Schekman R, ed. Annual Review of Cell and Developmental Biology, Vol 32, vol. 32. Annual Reviews.

358. Schlam D, Bagshaw RD, Freeman SA, Collins RF, Pawson T, Fairn GD, Grinstein S. 2015. Phosphoinositide 3-Kinase Enables Phagocytosis of Large Particles by Terminating Actin Assembly Through Rac/Cdc42 GTPase-Activating Proteins. Nature Communications 6: 8623.

359. Schmid AC, Wise HM, Mitchell CA, Nussbaum R, Woscholski R. 2004. Type II Phosphoinositide 5-phosphatases have Unique Sensitivities towards Fatty Acid Composition and Head Group Phosphorylation. Febs Letters 576: 9–13.

360. Schoeneberg J, Lehmann M, Ullrich A, Posor Y, Lo W-T, Lichtner G, Schmoranzer J, Haucke V, Noe F. 2017. Lipid-Mediated PX-BAR Domain Recruitment Couples Local Membrane Constriction to Endocytic Vesicle Fission. Nature Communications 8: 15873.

361. Schu PV, Takegawa K, Fry MJ, Stack JH, Waterfield MD, Emr SD. 1993. Phosphatidylinositol 3-Kinase Encoded by Yeast Vps34 Gene Essential for Protein Sorting. Science (New York, N.Y.) 260: 88–91.

362. Schwarz EC, Neuhaus EM, Kistler C, Henkel AW, Soldati T. 2000. *Dictyostelium* Myosin IK is involved in the Maintenance of Cortical Tension and Affects Motility and Phagocytosis. Journal of Cell Science 113: 621–633.

363. Sekine R, Kawata T, Muramoto T. 2018. CRISPR/Cas9 Mediated Targeting of Multiple Genes in *Dictyostelium*. Scientific Reports 8: 8471.

364. Shaaban M, Chowdhury S, Nolen BJ. 2020. Cryo-EM Reveals the Transition of Arp2/3 Complex from Inactive to Nucleation-Competent State. Nature Structural & Molecular Biology 27: 1009-1016.

365. Shalaby AK, Emery-Billcliff P, Baralle D, Dabir T, Begum S, Waller S, Tabernero L, Lowe M, Self J. 2018. Identification and Functional Analysis of a Novel Oculocerebrorenal Syndrome of Lowe (OCRL) Gene Variant in Two Pedigrees with Varying Phenotypes Including Isolated Congenital Cataracts. Molecular Vision 24: 847–852.

366. Shikama N, Lee CW, France S, Delavaine L, Lyon J, Krstic-Demonacos M, La Thangue NB. 1999. A Novel Cofactor for p300 that regulates the p53 Response. Molecular Cell 4: 365–376.

367. Shin HW, Hayashi M, Christoforidis S, Lacas-Gervais S, Hoepfner S, Wenk MR, Modregger J, Uttenweiler-Joseph S, Wilm M, Nystuen A, Frankel WN, Solimena M, De Camilli P, Zerial M. 2005. An Enzymatic Cascade of Rab5 Effectors Regulates Phosphoinositide Turnover in the Endocytic Pathway. Journal of Cell Biology 170: 607–618.

368. Shin N, Lee S, Ahn N, Kim S-A, Ahn S-G, YongPark Z, Chang S. 2007. Sorting Nexin 9 Interacts with Dynamin 1 and N-WASP and Coordinates Synaptic Vesicle Endocytosis. Journal of Biological Chemistry 282: 28939–28950.

369. Shpetner H, Vallee R. 1989. Identification of Dynamin, a Novel Mechanochemical Enzyme that Mediates Interactions between Microtubules. Cell 59: 421–432.

370. Shrimpton AE, Hoopes RR, Knohl SJ, Hueber P, Reed AAC, Christie PT, Igarashi T, Lee P, Lehman A, White C, Milford DV, Sanchez MR, Unwin R, Wrong OM, Thakker RV, Scheinman SJ. 2009. OCRL1 Mutations in Dent 2 Patients Suggest a Mechanism for Phenotypic Variability. Nephron Physiology 112: 27–36.

371. Sinha B, Koester D, Ruez R, Gonnord P, Bastiani M, Abankwa D, Stan RV, Butler-Browne G, Vedie B, Johannes L, Morone N, Parton RG, Raposo G, Sens P, Lamaze C, Nassoy P. 2011. Cells Respond to Mechanical Stress by Rapid Disassembly of Caveolae. Cell 144: 402–413.

372. Somesh BP, Vlahou G, Iijima M, Insall RH, Devreotes P, Rivero F. 2006. RacG Regulates Morphology, Phagocytosis, and Chemotaxis. Eukaryotic Cell 5: 1648–1663.

373. Soulet F, Yarar D, Leonard M, Schmid SL. 2005. SNX9 Regulates Dynamin Assembly and is required for Efficient Clathrin-Mediated Endocytosis. Molecular Biology of the Cell 16: 2058–2067.

374. Speed CJ, Little PJ, Hayman JA, Mitchell CA. 1996. Underexpression of the 43 kDa Inositol Polyphosphate 5-phosphatase is Associated with Cellular Transformation. Embo Journal 15: 4852–4861.

375. Staiano L, De Leo MG, Persico M, De Matteis MA. 2015. Mendelian Disorders of PI Metabolising Enzymes. Biochimica et Biophysica Acta (BBA) - Molecular and Cell Biology of Lipids 1851: 867–881.

376. Steinert M, Leippe M, Roeder T. 2003. Surrogate Hosts: Protozoa and Invertebrates as Models for Studying Pathogen-Host Interactions. International Journal of Medical Microbiology 293: 321–332.

377. Stradal TE, Scita G. 2006. Protein Complexes Regulating Arp2/3-Mediated Actin Assembly. Current Opinion in Cell Biology 18: 4–10.

378. Suchy SF, Nussbaum RL. 2002. The Deficiency of PIP_2 5-phosphatase in Lowe Syndrome Affects Actin Polymerisation. American Journal of Human Genetics 71: 1420–1427.

379. Suetsugu S, Miki H, Takenawa T. 1999. Identification of Two Human WAVE/SCAR Homologues as General Actin Regulatory Molecules which Associate with the Arp2/3 Complex. Biochemical and Biophysical Research Communications 260: 296–302.

380. Sun Q, Fan W, Chen K, Ding X, Chen S, Zhong Q. 2008. Identification of Barkor as a Mammalian Autophagy-Specific Factor for Beclin 1 and Class III Phosphatidylinositol 3-Kinase. Proceedings of the National Academy of Sciences of the United States of America 105: 19211–19216.

381. Sun X, Wei Y, Lee PP, Ren B, Li C. 2019. The Role of WASP in T-cells and B-cells. Cellular Immunology 341: 103919.

382. Swan LE, Tomasini L, Pirruccello M, Lunardi J, De Camilli P. 2010. Two Closely Related Endocytic Proteins that Share a Common OCRL-Binding Motif with APPL1. Proceedings of the National Academy of Sciences of the United States of America 107: 3511–3516.

383. Swanson J. 1989. Phorbol Esters Stimulate Macropinocytosis and Solute Flow Through Macrophages. Journal of Cell Science 94: 135–142.

384. Swanson JA. 2008. Shaping Cups into Phagosomes and Macropinosomes. Nature Reviews Molecular Cell Biology 9: 639–649.

385. Sweitzer SM, Hinshaw JE. 1998. Dynamin Undergoes a GTP-Dependent Conformational Change Causing Vesiculation. Cell 93: 1021–1029.

386. Tagawa M, Ueyama T, Ogata T, Takehara N, Nakajima N, Isodono K, Asada S, Takahashi T, Matsubara H, Oh H. 2008. MURC, a Muscle-Restricted Coiled-Coil Protein, is

involved in the Regulation of Skeletal Myogenesis. American Journal of Physiology Cell Physiology 295: C490–C498.

387. Takai Y, Sasaki T, Matozaki T. 2001. Small GTP-Binding Proteins. Physiological Reviews 81: 153–208.

388. Takeda K, Sasaki AT, Ha H, Seung H-A, Firtel RA. 2007. Role of Phosphatidylinositol 3-Kinases in Chemotaxis in *Dictyostelium*. Journal of Biological Chemistry 282: 11874–11884.

389. Takei K, Slepnev VI, Haucke V, De Camilli P. 1999. Functional Partnership between Amphiphysin and Dynamin in Clathrin-Mediated Endocytosis. Nature Cell Biology 1: 33–39.

390. Takenawa T, Suetsugu S. 2007. The WASP-WAVE Protein Network: Connecting the Membrane to the Cytoskeleton. Nature Reviews Molecular Cell Biology 8: 37–48.

391. Tamura N, Hazeki K, Okazaki N, Kametani Y, Murakami H, Takaba Y, Ishikawa Y, Nigorikawa K, Hazeki O. 2009. Specific Role of Phosphoinositide 3-Kinase p110 Alpha in the Regulation of Phagocytosis and Pinocytosis in Macrophages. Biochemical Journal 423: 99–108.

392. Taylor MJ, Perrais D, Merrifield CJ. 2011. A High Precision Survey of the Molecular Dynamics of Mammalian Clathrin-Mediated Endocytosis. Plos Biology 9: e1000604.

393. Torres E, Rosen MK. 2003. Contingent Phosphorylation/De-phosphorylation Provides a Mechanism of Molecular Memory in WASP. Molecular Cell 11: 1215–1227.

394. Tresaugues L, Silvander C, Flodin S, Welin M, Nyman T, Graslund S, Hammarstrom M, Berglund H, Nordlund P. 2014. Structural Basis for Phosphoinositide Substrate Recognition, Catalysis, and Membrane Interactions in Human Inositol Polyphosphate 5-phosphatases. Structure 22: 744–755.

395. Tsolakos N, Durrant TN, Chessa T, Suire SM, Oxley D, Kulkarni S, Downward J, Perisic O, Williams RL, Stephens L, Hawkins PT. 2018. Quantitation of Class IA PI3Ks in Mice Reveals p110-Free-p85s and Isoform-Selective Subunit Associations and Recruitment to Receptors. Proceedings of the National Academy of Sciences of the United States of America 115: 12176–12181.

396. Tsujita K, Suetsugu S, Sasaki N, Furutani M, Oikawa T, Takenawa T. 2006. Coordination between the Actin Cytoskeleton and Membrane Deformation by a Novel Membrane Tubulation Domain of PCH Proteins is involved in Endocytosis. Journal of Cell Biology 172: 269–279.

397. Umikawa M, Obaishi H, Nakanishi H, Satoh-Horikawa K, Takahashi K, Hotta I, Matsuura Y, Takai Y. 1999. Association of Frabin with the Actin Cytoskeleton is Essential for

Microspike Formation through Activation of Cdc42 Small G-protein. Journal of Biological Chemistry 274: 25197–25200.

398. Ungewickell A, Ward ME, Ungewickell E, Majerus PW. 2004. The Inositol Polyphosphate 5-phosphatase OCRL Associates with Endosomes that are Partially Coated with Clathrin. Proceedings of the National Academy of Sciences of the United States of America 101: 13501–13506.

399. Vadas O, Dbouk HA, Shymanets A, Perisic O, Burke JE, Saab WFA, Khalil BD, Harteneck C, Bresnick AR, Nuernberg B, Backer JM, Williams RL. 2013. Molecular Determinants of PI3K Gamma-Mediated Activation Downstream of G-Protein-Coupled Receptors (GPCRs). Proceedings of the National Academy of Sciences of the United States of America 110: 18862–18867.

400. Vaduva G, Martinez-Quiles N, Anton IM, Martin NC, Geha RS, Hopper AK, Ramesh N. 1999. The Human WASP-Interacting Protein, WIP, Activates the Cell Polarity Pathway in Yeast. Journal of Biological Chemistry 274: 17103–17108.

401. Vanhaesebroeck B, Guillermet-Guibert J, Graupera M, Bilanges B. 2010. The Emerging Mechanisms of Isoform-Specific PI3K Signalling. Nature Reviews Molecular Cell Biology 11: 329–341.

402. Varnai P, Gulyas G, Toth DJ, Sohn M, Sengupta N, Balla T. 2017. Quantifying Lipid Changes in Various Membrane Compartments Using Lipid Binding Protein Domains. Cell Calcium 64: 72–82.

403. Varsano T, Taupin V, Guo L, Baterina OY, Farquhar MG. 2012. The PDZ Protein GIPC Regulates Trafficking of the LPA(1) Receptor from APPL Signalling Endosomes and Attenuates the Cell's Response to LPA. Plos One 7: e49227.

404. Veltman DM, Akar G, Bosgraaf L, Van Haastert PJM. 2009. A New Set of Small, Extra-chromosomal Expression Vectors for *Dictyostelium discoideum*. Plasmid 61: 110–118.

405. Veltman DM, Insall RH. 2010. WASP Family Proteins: Their Evolution and its Physiological Implications. Molecular Biology of the Cell 21: 2880–2893.

406. Veltman DM, Williams TD, Bloomfield G, Chen B-C, Betzig E, Insall RH, Kay RR. 2016. A Plasma Membrane Template for Macropinocytic Cups. Elife 5: e20085.

407. Vergarajauregui S, Connelly PS, Daniels MP, Puertollano R. 2008. Autophagic Dysfunction in Mucolipidosis Type IV Patients. Human Molecular Genetics 17: 2723–2737.

408. Viaud J, Boal F, Tronchere H, Gaits-Iacovoni F, Payrastre B. 2014. Phosphatidylinositol 5-Phosphate: A Nuclear Stress Lipid and a Tuner of Membranes and Cytoskeleton Dynamics. Bioessays 36: 260–272.

409. Vicinanza M, Di Campli A, Polishchuk E, Santoro M, Di Tullio G, Godi A, Levtchenko E, De Leo MG, Polishchuk R, Sandoval L, Marzolo M-P, De Matteis MA. 2011. OCRL Controls Trafficking Through Early Endosomes via PtdIns(4,5)P_2-Dependent Regulation of Endosomal Actin. Embo Journal 30: 4970–4985.

410. Vicinanza M, Korolchuk VI, Ashkenazi A, Puri C, Menzies FM, Clarke JH, Rubinsztein DC. 2015. PI(5)P Regulates Autophagosome Biogenesis. Molecular Cell 57: 219–234.

411. Vieira OV, Botelho RJ, Rameh L, Brachmann SM, Matsuo T, Davidson HW, Schreiber A, Backer JM, Cantley LC, Grinstein S. 2001. Distinct Roles of Class I and Class III Phosphatidylinositol 3-Kinases in Phagosome Formation and Maturation. Journal of Cell Biology 155: 19–25.

412. Vines JH, King JS. 2019. The Endocytic Pathways of *Dictyostelium discoideum*. International Journal of Developmental Biology 63: 461–471.

413. Wang HR, Zhang Y, Ozdamar B, Ogunjimi AA, Alexandrova E, Thomsen GH, Wrana JL. 2003. Regulation of Cell Polarity and Protrusion Formation by Targeting RhoA for Degradation. Science 302: 1775–1779.

414. Wang JTH, Teasdale RD, Liebl D. 2014. Macropinosome Quantitation Assay. MethodsX 1: 36–41.

415. Wang Y, Senoo H, Sesaki H, Iijima M. 2013. Rho GTPases Orient Directional Sensing in Chemotaxis. Proceedings of the National Academy of Sciences 110: E4723–E4732.

416. Watts DJ, Ashworth JM. 1970. Growth of Myxamoebae of the Cellular Slime Mould *Dictyostelium discoideum* in Axenic Culture. Biochemical Journal 119: 171–174.

417. Welch MD, DePace AH, Verma S, Iwamatsu A, Mitchison TJ. 1997. The Human Arp2/3 Complex is Composed of Evolutionarily Conserved Subunits and is localised to Cellular Regions of Dynamic Actin Filament Assembly. The Journal of Cell Biology 138: 375–384.

418. Welliver TP, Swanson JA. 2012. A Growth Factor Signalling Cascade Confined to Circular Ruffles in Macrophages. Biology Open 1: 754–760.

419. Wennstrom S, Hawkins P, Cooke F, Hara K, Yonezawa K, Kasuga M, Jackson T, Claessonwelsh L, Stephens L. 1994. Activation of Phosphoinositide 3-Kinase is required for PDGF-Stimulated Membrane Ruffling. Current Biology 4: 385–393.

420. West MA, Prescott AR, Eskelinen EL, Ridley AJ, Watts C. 2000. Rac is required for Constitutive Macropinocytosis by Dendritic Cells but does not Control its Downregulation. Current Biology 10: 839–848.

421. Wheeler M, Domin J. 2001. Recruitment of the Class II Phosphoinositide 3-Kinase C2 Beta to the Epidermal Growth Factor Receptor: Role of Grb2. Molecular and Cellular Biology 21: 6660–6667.

422. Whisstock JC, Romero S, Gurung R, Nandurkar H, Ooms LM, Bottomley SP, Mitchell CA. 2000. The Inositol Polyphosphate 5-phosphatases and the Apurinic/Apyrimidinic Base Excision Repair Endonucleases Share a Common Mechanism for Catalysis. Journal of Biological Chemistry 275: 37055–37061.

423. Wienke DC, Knetsch MLW, Neuhaus EM, Reedy MC, Manstein DJ. 1999. Disruption of a Dynamin Homologue Affects Endocytosis, Organelle Morphology, and Cytokinesis in *Dictyostelium discoideum*. Molecular Biology of the Cell 10: 225–243.

424. Wilkins A, Chubb JR, Insall RH. 2000. A Novel *Dictyostelium* Ras-GEF is required for Normal Endocytosis, Cell Motility and Multicellular Development. Current Biology 10: 1427–1437.

425. Wilkins A, Insall RH. 2001. Small GTPases in *Dictyostelium*: Lessons from a Social Amoeba. Trends in Genetics 17: 41–48.

426. Williams TD, Kay RR. 2018. The Physiological Regulation of Macropinocytosis during *Dictyostelium* Growth and Development. Journal of Cell Science 131: jcs213736.

427. Williams TD, Paschke PI, Kay RR. 2019. Function of Small GTPases in *Dictyostelium* Macropinocytosis. Philosophical Transactions of the Royal Society B: Biological Sciences 374: 20180150.

428. Wuertenberger S, Groemping Y. 2015. A Single PxxP Motif in the C-terminal Region of srGAP3 Mediates Binding to Multiple SH3 Domains. FEBS Letters 589: 1156–1163.

429. Yamaguchi H, Shiraishi M, Fukami K, Tanabe A, Ikeda-Matsuo Y, Naito Y, Sasaki Y. 2009. MARCKS Regulates Lamellipodia Formation Induced by IGF-I via Association with PIP_2 and Beta-Actin at Membrane Microdomains. Journal of Cellular Physiology 220: 748–755.

430. Yang L, Lin HK, Altuwaijri S, Xie SZ, Wang L, Chang C. 2003. APPL Suppresses Androgen Receptor Transactivation via Potentiating Akt Activity. Journal of Biological Chemistry 278: 16820–16827.

431. Yang S, Tang Y, Liu Y, Brown AJ, Schaks M, Ding B, Kramer DA, Mietkowska M, Ding L, Alekhina O, Billadeau DD, Chowdhury S, Wang J, Rottner K, Chen B. 2022. Arf GTPase Activates the WAVE Regulatory Complex Through a Distinct Binding Site. Science advances 8: eadd1412.

432. Yarar D, Surka MC, Leonard MC, Schmid SL. 2008. SNX9 Activities are Regulated by Multiple Phosphoinositides Through both PX and BAR Domains. Traffic 9: 133–146.

433. Yarar D, Waterman-Storer CM, Schmid SL. 2007. SNX9 Couples Actin Assembly to Phosphoinositide Signals and is required for Membrane Remodelling during Endocytosis. Developmental Cell 13: 43–56.

434. Ye K, Ahn J-Y. 2008. Nuclear Phosphoinositide Signalling. Frontiers in Bioscience-Landmark 13: 540–548.

435. Yoshida S, Hoppe AD, Araki N, Swanson JA. 2009. Sequential Signalling in Plasma Membrane Domains during Macropinosome Formation in Macrophages. Journal of Cell Science 122: 3250–3261.

436. Zagelbaum J, Schooley A, Zhao J, Schrank BR, Callen E, Zha S, Gottesman ME, Nussenzweig A, Rabadan R, Dekker J, Gautier J. 2022. Multiscale Reorganisation of the Genome Following DNA Damage Facilitates Chromosome Translocations via Nuclear Actin Polymerisation. Nature Structural & Molecular Biology 30: 99–106.

437. Zaniew M, Bokenkamp A, Kolbuc M, La Scola C, Baronio F, Niemirska A, Szczepanska M, Buerger J, La Manna A, Miklaszewska M, Rogowska-Kalisz A, Gellermann J, Zampetoglou A, Wasilewska A, Roszak M, Moczko J, Krzemien A, Runowski D, Siten G, Zaluska-Lesniewska I, Fonduli P, Zurrida F, Paglialonga F, Gucev Z, Paripovic D, Rus R, Said-Conti V, Sartz L, Chung WY, Park SJ, Lee JW, Park YH, Ahn YH, Sikora P, Stefanidis CJ, Tasic V, Konrad M, Anglani F, Addis M, Cheong HI, Ludwig M, Bockenhauer D. 2018. Long-term Renal Outcome in Children with OCRL Mutations: Retrospective Analysis of a Large International Cohort. Nephrology Dialysis Transplantation 33: 85–94.

438. Zhang X, Jefferson A, Auethavekiat V, Majerus P. 1995. The Protein Deficient in Lowe Syndrome is a Phosphatidylinositol-4,5-Bisphosphate 5-phosphatase. Proceedings of the National Academy of Sciences of the United States of America 92: 4853–4856.

439. Zhang X, Li X, Xu H. 2012. Phosphoinositide Isoforms Determine Compartment-Specific Ion Channel Activity. Proceedings of the National Academy of Sciences of the United States of America 109: 11384–11389.

440. Zhang Y, Zhang X-F, Fleming MR, Amiri A, El-Hassar L, Surguchev AA, Hyland C, Jenkins DP, Desai R, Brown MR, Gazula V-R, Waters MF, Large CH, Horvath TL, Navaratnam D, Vaccarino FM, Forscher P, Kaczmarek LK. 2016. Kv3.3 Channels Bind Hax-1 and Arp2/3 to Assemble a Stable Local Actin Network that Regulates Channel Gating. Cell 165: 434–448.

441. Zhou K, Takegawa K, Emr S, Firtel R. 1995. A Phosphatidylinositol (PI) Kinase Gene Family in *Dictyostelium discoideum* - Biological Roles of Putative Mammalian p110 and Yeast Vps34p PI3-Kinase Homologues during Growth and Development. Molecular and Cellular Biology 15: 5645–5656.

442. Zhou KM, Pandol S, Bokoch G, Traynor-Kaplan AE. 1998. Disruption of *Dictyostelium* PI3K Genes Reduces [P^{32}] Phosphatidylinositol 3,4-Bisphosphate and [P^{32}] Phosphatidylinositol Trisphosphate Levels, Alters F-actin Distribution and Impairs Pinocytosis. Journal of Cell Science 111: 283–294.

443. Zhou X, Wang L, Hasegawa H, Amin P, Han B-X, Kaneko S, He Y, Wang F. 2010. Deletion of PIK3C3/Vps34 in Sensory Neurons Causes Rapid Neurodegeneration by Disrupting the Endosomal but not the Autophagic Pathway. Proceedings of the National Academy of Sciences of the United States of America 107: 9424–9429.

444. Zhu G, Chen J, Liu J, Brunzelle JS, Huang B, Wakeham N, Terzyan S, Li X, Rao Z, Li G, Zhang XC. 2007. Structure of the APPL1 BAR-PH Domain and Characterisation of its Interaction with Rab5. Embo Journal 26: 3484–3493.

445. Zimmet A, Van Eeuwen T, Boczkowska M, Rebowski G, Murakami K, Dominguez R. 2020. Cryo-EM Structure of NPF-Bound Human Arp2/3 Complex and Activation Mechanism. Science Advances 6: eaaz7651.

446. Zoncu R, Perera RM, Balkin DM, Pirruccello M, Toomre D, De Camilli P. 2009. A Phosphoinositide Switch Controls the Maturation and Signalling Properties of APPL Endosomes. Cell 136: 1110–1121.

447. Zuchero JB, Belin B, Mullins RD. 2012. Actin Binding to WH2 Domains Regulates Nuclear Import of the Multi-Functional Actin Regulator, JMY. Molecular Biology of the Cell 23: 853–863.